Accession No.

SID 66-1638

PARAGLIDER LANDING SYSTEM TEST PROGRAM

Final Report

Contract NAS9-5706

December 1966

Prepared by

Paraglider Program

Approved by

N. F. Witte, Director
Flexible Wing Systems

NORTH AMERICAN AVIATION, INC.
SPACE and INFORMATION SYSTEMS DIVISION

NASA CR 9.222

FOREWORD

The Paraglider Landing System Test Program was conducted under Contract NAS9-5206 by the Space and Information Systems Division of North American Aviation, Inc., for the NASA Manned Spacecraft Center.

The objective of the program was to determine flight and landing characteristics of the Paraglider by conducting twelve manned flight demonstrations. This report presents the data obtained on these twelve manned flights and other associated test flights and concludes that the system has excellent flight and landing characteristics. The landing requires some specialized training; however, the tests determined that the learning rate is very rapid. The effects of wind and turbulence are discussed, and the ability to spot land the system has been demonstrated.

The hardware and prior data obtained under Contracts NAS9-1484, NAS9-136, NAS9-167 and NAS9-539 were utilized effectively. This prior effort is described in report SID 65-196.

NORTH AMERICAN AVIATION, INC. SPACE and INFORMATION SYSTEMS DIVISION

TECHNICAL REPORT INDEX/ABSTRACT

ACCESSION NUMBER		DOCUMENT SECURITY CLASSIFICATION	
		UNCLASSIFIED	

TITLE OF DOCUMENT	LIBRARY USE ONLY
PARAGLIDER LANDING SYSTEM TEST PROGRAM	
AUTHOR(S)	
CHRISTENSEN, N.R. * SNODGRASS, R.R.	

CODE	ORIGINATING AGENCY AND OTHER SOURCES	DOCUMENT NUMBER
	NAA S&ID	SID 65-1638

PUBLICATION DATE	CONTRACT NUMBER
11DEC65	NAS9-5206

DESCRIPTIVE TERMS

SPACECRAFT RECOVERY SYSTEM, PARAGLIDER SYSTEMS, PARAGLIDER CONTROL SYSTEMS

ABSTRACT

THE RESULTS OF THE PARAGLIDER LANDING SYSTEM TEST PROGRAM CONDUCTED IN THREE PHASES DURING THE PERIOD OF 1 MAY TO 6 NOVEMBER ARE REPORTED. MODIFICATIONS TO THE VEHICLE IN SUPPORT OF THE TEST PROGRAM ARE ALSO DOCUMENTED.

FORM 181-V REV 11-64
PUBLICATIONS USE ONLY

CONTENTS

ILLUSTRATIONS

TABLES

INTRODUCTION

This landing system research and development program utilized the existing tow test vehicle and Paraglider wings. A new Paraglider test bed was designed and fabricated. The new vehicle was used for operational flight training of the crew and for wing rigging verification. Upon initiation of the contract, the two test vehicles were removed from storage, and a thorough inspection of the vehicle structure and landing gear components was made. In addition, flight and data gathering instruments and associated AGE were calibrated.

The objectives of this flight test program were as follows:

1. Evaluate various flight maneuvers for landing
2. Evaluate flight characteristics in pitch, turns, and gusts
3. Evaluate trim control in pitch and roll
4. Evaluate performance of the control actuation system
5. Investigate wing flight characteristics throughout the mission profile particularly during preflare, flare, touchdown, and landing roll-out
6. Demonstrate navigational capability from tow release to touchdown
7. Demonstrate capability of performing predetermined spot landings

The Paraglider wing is composed of an inflatable frame with an attached sail. In operational configuration, the wing is stored in a container on the forward end of the spacecraft and is extracted, inflated, and deployed at subsonic speeds. The wing is attached to the spacecraft by five cables—three in the pitch plane and two in the roll plane. Control is achieved by differentially reeling in and/or out the two aft pitch cables or the two roll cables. The control system is powered by gaseous nitrogen pneumatic motors, which are actuated at a constant rate, in response to the vehicle hand and/or trim controller movement.

Certain vehicle modifications, to be described in detail in this report, were as follows:

1. A radar altimeter was added to provide the pilot with an accurate altitude indication so that flare maneuvers could be initiated.

2. Visual omnidirectional range (VOR) and distance measuring equipment (DME) were added for navigational capability, which would be used on two-man flights.

3. The landing gear system was modified to sustain a sink rate of 17.5 feet per second at touchdown.

4. The wing pressure makeup system was removed from the vehicle and wing.

5. The UHF communication system was replaced by a VHF system.

6. As a result of a NASA DEI Board decision, the A-4D seat replaced the F-86 seat.

The objectives of the program were completed during three phases of operation. Each phase consisted of a period of vehicle modification and thorough checkout followed by a period of concentrated flight testing at Edwards Air Force Base dry lakebed. During this time, four unmanned flights and twelve manned flights were completed, in addition to twelve flights of the Paraglider test bed (PTB).

To ensure adequate support for the Paraglider operational test program, a mobile telemeter receiving station was provided. This station provided real-time readout of flight safety data points. It also included capabilities of receiving, recording, and data play-back of all telemetry. Exclusive use of this equipment permitted immediate analysis of flight data in preparation of subsequent flights. In addition, a communications van was utilized for flight operations coordination and control.

A closed-circuit television camera mounted on an M45 tracker provided real-time observation of the flight characteristics as well as play-back capability for analysis. This mount also held three cameras with long focal-length lenses to provide additional data and documentary coverage.

A Sikorsky S-61 helicopter, owned and operated by Los Angeles Airways and under subcontract to NAA-S&ID, was used as the tow vehicle, and 1200 feet of nontwist cable was used as the tow line. A vertical liftoff procedure was employed—that is, the TTV was resting in a vertical position on the heat shield at liftoff.

MISSION DESCRIPTION

The TTV is a manned free-flight test vehicle, towed to altitude by a Sikorsky helicopter. Prior to liftoff, the TTV vehicle is rotated onto the heat shield and supported by the main landing gear and a launch wheel located at the upper vertical center line of the aft bulkhead. The launch wheel drops off as soon as the TTV is lifted off the ground. The Paraglider wing is fully inflated and rests on the upper vertical center line of the forward bulkhead, with the boom and keel ends on the ground.

The tow helicopter, attached to the TTV and Paraglider wing by a 1200-foot nortwist steel cable is positioned directly over and slightly forward of the TTV at an altitude of 1200 feet. The helicopter accelerates up and forward into the wind, lifting the TTV and Paraglider wing from the ground. The Paraglider wing is manually separated from the TTV by two 125-foot lines (one attached to each boom) until sufficient forward speed is attained to fill the Paraglider sail. The Paraglider wing assumes a pitch-up flight attitude, and climbout is initiated.

When the test altitude and correct position are reached, the helicopter initiates a descent sequence. When the proper descent rate of 1000 feet per minute is achieved, the pilot releases the tow cable from the TTV and flies the predetermined flight plan. On touchdown, he releases the Paraglider wing, and the landing run-out is completed.

TEST PHASE SUMMARY

PHASE I

During the three-week period of June 30, 1965 to July 17, 1965, 17 operations were performed. Of these operations, 14 utilized the Paraglider Test Bed (PTB) and three utilized the Tow Test Vehicle (TTV).

In general, it may be stated that the PTB operations satisfied the objectives. The cable rigging of all available wings was verified, and the flight operations crew, including the ground controller and helicopter crew, was given thorough training to increase assignment proficiency.

The operations using the TTV were unsuccessful. One flight aborted when a cable brushed against the wing apex fitting and broke off the pressure cap, causing a leak. The two others were also unsuccessful, one because the radar altimeter locked on the nose gear, and the other because the flare command was cancelled by a subsequent control maneuver given by the ground controller. Extensive damage to the vehicle resulted. All TTV flights were radio-command controlled.

PHASE II

Of the ten operations performed during the three-week period of 24 August 1965 to 11 September 1965, two utilized the PTB, and eight utilized the TTV—two radio-commanded and six manned. The primary purpose of the PTB flights was to familiarize the test operations crew and to verify a slight change in roll-line rigging to minimize the roll trim for steady-state flight. Of the eight TTV operations, there were two aborts. One was caused by premature release of the vehicle tow release circuitry, and the other by entanglement of the forward line on the radar altimeter antenna during liftoff.

A relatively high sink rate was obtained on one of the flights because of a head-on wind shear or gust encountered immediately prior to the flare maneuver. However, the test phase was considered successful in that five flights produced sink rates of between 11 and 19 feet per second.

The eight manned operations performed during the three-week period of 20 October 1965 to 5 November 1965 used the TTV. Three of these flights employed ballast to simulate the weight of the second pilot.

During this phase, five flights attained a minimum sink rate at touchdown of 10 to 19 feet per second, and three flights attained sink rates of 21 to 25 feet per second. Only minor damage to the vehicle was experienced at the higher sink rates.

Ability to land at a predetermined landing spot was also demonstrated.

A chronological summary of the flight operations activity is given in Tables 1, 2, and 3.

Table 1. Phase I Flight Operations Chronological Summary

Date	Flight	Vehicle	Wing No.	Sail Type	Weight (lb)		Release Altitude (feet above ground level)	Sink Rate at Touchdown	Flight Time	Comments
					Vehicle	Wing				
30 June 1965	Para-P-001	PTB*	Z19	High Lobe	3295	462.5	-	-	-	Abort — damaged wing on liftoff
30 June 1965	Para-P-002	PTB	Z04	High Lobe	3295	-	-	-	-	Abort — marginal helicopter performance due to high ambient temperatures and zero winds
1 July 1965	Para-P-002	PTB	Z04	High Lobe	3295	500.27	8000	-	4 min. 23 sec	Seven-to-8 left turn required for straight glide, flared high, minor vehicle damage
1 July 1965	Para-P-003	PTB	Z04	High Lobe	3295	500.27	8650	-	4 min. 47 sec	Good flight — release glide and landing OK
2 July 1965	Para-P-004	PTB	Z19	High Lobe	3295	462.5	6900	-	4 min. 5 sec	Good flight — landed 50 yards from communications van
2 July 1965	Para-R-005	ITV** No. 002	Z04	High Lobe	3295	462.5	7800	-	4 min. 11 sec	Vehicle flared 50 to 75 feet high, resulting in major damage
6 July 1965	Para-P-006	PTB	Z07	High Lobe	3295	507.04	6800	-	3 min. 52 sec	Good flight — flared approximately 5 feet high
7 July 1965	Para-P-007	PTB	Z04B	T evil	3295	475.0	7000	-	3 min. 2 sec	Flight OK — assumed pitch-down position during most of flight
7 July 1965	Para-P-008	PTB	Z07	High Lobe	3295	507.04	4800	-	3 min. 43 sec	Good flight — flare and landing good
7 July 1965	Para-P-009	PTB	Z07	High Lobe	3295	507.04	6590	-	3 min. 44 sec	Good flight — landed crosswind
8 July 1965	Para-P-010	PTB	Z07	High Lobe	3295	507.04	-	-	-	Abort — several strands of 1200-foot steel tow cable broken
8 July 1965	Para-P-010	PTB	Z07	High Lobe	3295	507.04	6000	-	3 min. 33 sec	Flared high — vehicle damage and minor wing damage
9 July 1965	Para-P-011	PTB	Z07	High Lobe	3295	507.04	-	-	-	Abort — tow cable release connector was separated on liftoff
9 July 1965	Para-P-011	PTB	Z07	High Lobe	3295	507.04	-	-	-	Abort — helicopter could not position for liftoff due to winds at 1200 feet
9 July 1965	Para-P-013	PTB	Z07	High Lobe	3295	507.04	4000	-	3 min. 51 sec	Good release and glide but flared late
10 July 1965	Para-R-012	ITV No. 001	Z04	High Lobe	3295	500.27	-	-	-	Abort — tow cable broke off open full forcing causing wing to lose pressure
12 July 1965	Para-R-013	ITV No. 001	Z04	High Lobe	3295	500.27	-	-	-	Abort — faulty release mechanism, prevented bridle release
13 July 1965	Para-R-014	ITV No. 001	Z04	High Lobe	3295	500.27	7850	-	3 min. 40 sec	No flare — major vehicle damage pitch up command caused flare command
15 July 1965	Para-P-015	PTB	Z07	High Lobe	3295	507.04	7000	-	4 min. 24 sec	Did not achieve flare attitude — pitch sprocket key sheared causing minor vehicle damage
16 July 1965	Para-P-016	PTB	Z07	High Lobe	3295	507.04	4500	-	3 min. 43 sec	Good flight — release glide and preflare good excellent landing
16 July 1965	Para-P-017	PTB	Z07	High Lobe	3295	507.04	-	-	-	Abort — tow cable release connector separated

*Paraglider Test Bed
**Tow Test Vehicle

P — PTB Flight
R — Radio-Command Flight
M — Manned Flight

Table 2. Phase II Flight Operations Chronological Summary

Date	Flight	Vehicle	Wing No.	Sail Type	Weight (lb)		Release Altitude (feet above ground level)	Sink Rate at Touchdown	Flight Time	Comments
					Vehicle	Wing				
24 Aug 1965	Para-P-018	PTB*	204	High Lobe	3295	500.27	6400		3 min. 34 sec	Good flight — trimmed to the left requiring right-turn input, flare late
24 Aug 1965	Para-P-019	PTB	207	High Lobe	3295	507.04	6800	-	3 min. 37 sec	Flared high — pitch motor chain broke during flare maneuver
26 Aug 1965	Para-R-020	TTV** No. 002	204	High Lobe	3395	500.27	7780	11.0 ft/sec	5 min. 44 sec	Good flight — flare slightly high
28 Aug 1965	Para-R-021	TTV No. 001	204	High Lobe	3394	500.27	7500	13.0 ft/sec	5 min. 49 sec	Good flight — landing very good
2 Sept 1965	Para-M-022	TTV No. 002	204	High Lobe	3395	500.27	7530	13.0 ft/sec	4 min. 0 sec	Good flight — slight left yaw on landing
6 Sept 1965	Para-M-023	TTV No. 002	204	High Lobe	3395	500.27	-	-	-	Abort — tow cable connector disconnected on liftoff
6 Sept 1965	Para-M-023	TTV No. 002	204	High Lobe	3395	500.27	6800	17.0 ft/sec	4 min. 30 sec	Flared high — did not achieve full pitch down in preflare causing minor vehicle damage
9 Sept 1965	Para-M-024	TTV No. 001	204	High Lobe	3395	500.27	4600	28.5 ft/sec	4 min. 36 sec	Flared 30 feet high — major damage to landing gear
11 Sept 1965	Para-M-025	TTV No. 002	204	High Lobe	3395	500.27	-	-	-	Abort — forward line caught on radar antenna
11 Sept 1965	Para-M-025	TTV No. 002	204	High Lobe	3395	500.27	8200	11.5 ft/sec	4 min. 19 sec	Good flight and landing — wing impacted vehicle on touchdown, ruptured, and broke right TTV (canopy)

*Paraglider Test Bed
**Tow Test Vehicle

Table 3. Phase III Flight Operations Chronological Summary

Date	Flight	Vehicle	Wing No.	Sail Type	Weight (lb)		Release Altitude (feet above ground level)	Sink Rate at Touchdown	Flight Time	Comments
					Vehicle	Wing				
20 Oct 1965	Para-M-026	TTV* No. 002	204	High Lobe	3385	500.27	9,500	21.0 ft/sec	5 min. 11 sec	Good flight — flared high, indicated airspeed boom bent and probe broken off the end of the boom
22 Oct 1965	Para-M-027	TTV No. 001	204	High Lobe	3385	500.27	10,500	10.5 ft/sec	5 min. 4 sec	Good flight and landing
26 Oct 1965	Para-M-028	TTV No. 002	204	High Lobe	3565	500.27	10,200	10.0 ft/sec	6 min. 48 sec	Good flight and landing
28 Oct 1965	Para-M-029	TTV No. 001	204	High Lobe	3385	500.27	10,300	15.5 ft/sec	5 min. 8 sec	Good flight — flared approximately 15 feet high
30 Oct 1965	Para-M-030	TTV No. 002	204	High Lobe	3565	500.27	10,000	4.2 ft/sec	5 min. 33 sec	Good flight — left main gear wheel bent on liftoff, flared late
2 Nov 1965	Para-M-031	TTV No. 002	204	High Lobe	3565	500.27	9,250	25.2 ft/sec.	4 min. 36 sec	Hard landing — slight damage to nose gear, VHF antenna broken off, missed spot landing by 100 feet
4 Nov 1965	Para-M-032	TTV No. 001	204	High Lobe	3385	500.27	9,450	10.0 to 10.5 ft/sec	6 min. 43 sec	Flared approximately 20 feet high, missed spot landing by 1000 feet
5 Nov 1965	Para-M-033	TTV No. 001	204	High Lobe	3385	500.27	10,250	- sec	4 min. 43 sec	Flared approximately 10 feet high, missed spot landing by 180 feet, left wheel bent on touchdown

*Tow Test Vehicle

TOW TEST VEHICLE

STRUCTURAL DESCRIPTION

The primary structure of the Tow Test Vehicle (TTV) consists of riveted aluminum skin and bulkheads. The cylindrical portion of the forward and aft bulkheads are of welded aluminum structure. Longitudinal intercostals provide support for the nose gear and forward cable. The conical portion is designed to duplicate the cabin bulkhead locations of the Gemini spacecraft. Removable plexiglass hatches are installed on each side of an upper center-line structural box to provide pilot visibility. The aft bulkhead is fabricated from 3/16-inch-thick, low-carbon steel with welded flanges and stiffeners. Skin panels are 1/8-inch-thick aluminum, riveted to the frames. Access door panels are 1/8-inch-thick aluminum attached with screws.

The following modifications to the TTV have been accomplished subsequent to the publishing of report.*

Landing Gear

In order to increase the structural integrity of those areas where damage had occurred during previous hard landings, the landing gear was modified to minimize damage at sink rates in excess of 17.5 feet per second.

The rod-end bearings at each end of the main gear parallel link were changed to bearings made from maraging steel. The rated load increased from 26,000 to 50,000 pounds. The jam nuts were removed from the bearings at the wheel end to allow increased angular motion of the link assembly without binding the bearings.

Flat steel straps were added to the forward and aft sides of the parallel link to provide redundancy and to relieve the parallel link at high loads. Any failure in the parallel link would have allowed the main gear strut to contact the landing surface and trip the vehicle.

The nose gear was installed in the 17-degree nose-down position, reducing the possibility of contacting the nose wheels first in a nose low attitude at landing.

---

*Final Report of Paraglider Research and Development Program. NAA-S&ID, SID 65-195 (19 February 1965)

Foot rests were installed forward of the brake pedals, precluding the pilot's inadvertently applying the brakes due to the inertia of the pilot's feet and legs at initial touchdown.

Vehicle Structure

No modifications were required to the basic structure. Changes were incorporated only to accommodate system changes (Figure 1). Structural repair, when required, duplicated the integrity that existed before damage occurred.

A wing guard was installed at the top of the aft bulkhead to prevent the wing from contacting the pitch pulleys during liftoff.

A bracket was installed on the aft bulkhead to receive a launch wheel to facilitate vertical positioning and subsequent liftoff. When the vehicle was lifted, the launch wheel fell free and was recovered. (See Figure 2 vehicle/wing position for liftoff.)

A solenoid-actuated pitot boom release mechanism was installed aft of the forward bulkhead. The boom is folded down at launch to protect the wing. After liftoff, the pilot actuates a switch on the center console to erect the boom.

Pilot's Seats

An F-86 ejection seat was installed in lieu of the Gemini seat. However, during a subsequent design review meeting, it was decided to incorporate a seat that had an integrated parachute harness. As a result of this decision, an A-4D seat was used for all manned flights. Minor modifications were required to the seats to provide pilot's access to man/seat manual separation handles. F-100 seat cushions were installed in lieu of the survival pack. NB-5 26-foot conical parachutes were provided.

PARAGLIDER WINGS (FRAMES/SAIL)

The wings used on this flight test program were originally fabricated and used on the Paraglider program, contract NAS9-1484.

A total of four wings were available in the required TTV configuration capable of fulfilling the requirements of this flight test program. Of the four wings available, three had high-lobe sails with 45-degree sweep. The other wing had a low-lobe "T"-sail with a 52.5-degree sweep and a wedge-shaped keel stand of approximately 45 inches at the aft end. Figure 3 shows sketches of the wings.

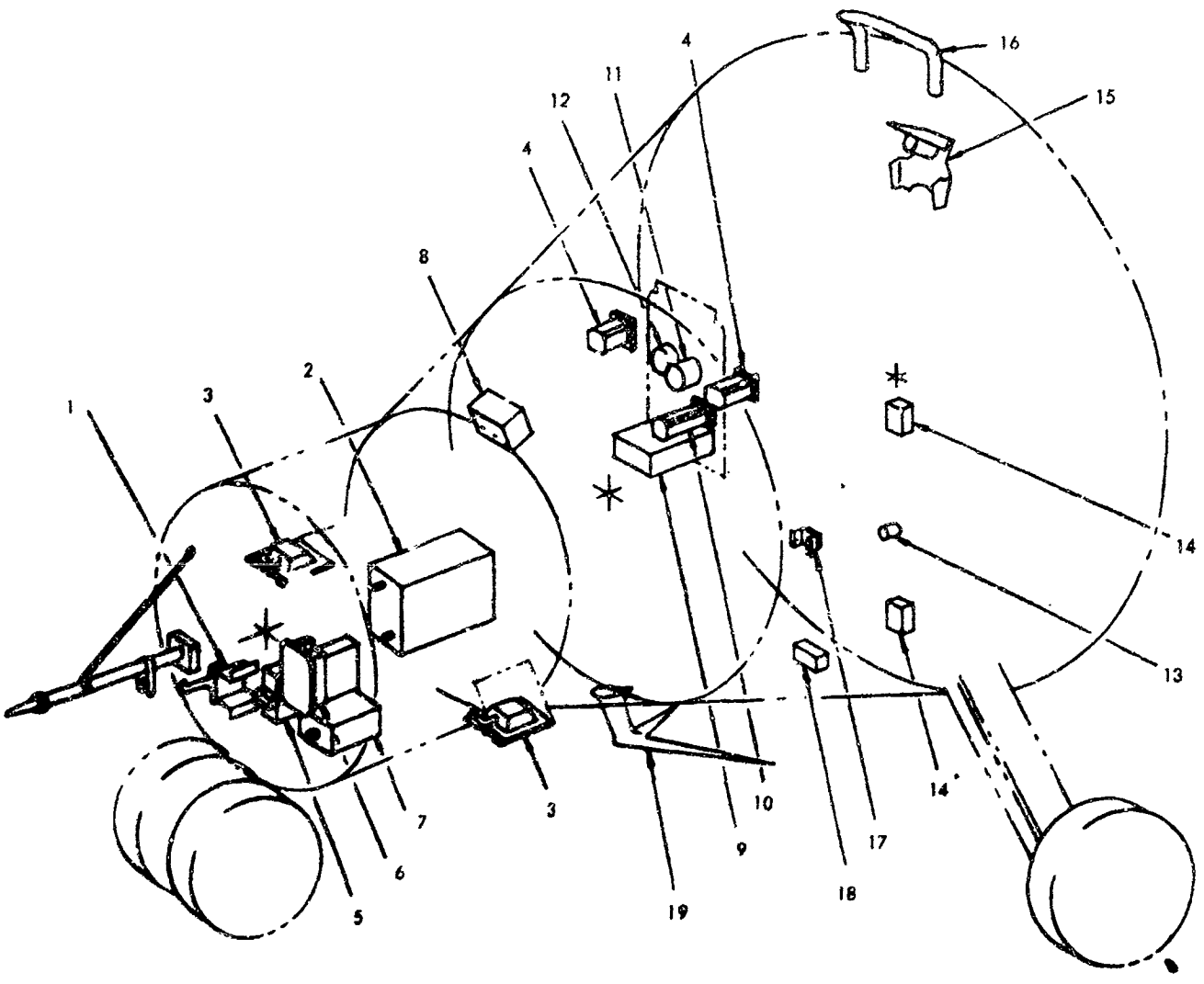

LEGEND:

1. PITOT BOOM RELEASE MECHANISM
2. RADAR ALTIMETER RECEIVER/TRANSMITTER
3. RADAR ALTIMETER ANTENNA
4. RADAR ALTIMETER INDICATOR
5. DME RF UNIT
6. RADAR ALTIMETER INVERTER
7. DME POWER UNIT
8. MODULATOR - COMMUNICATIONS POWER UNIT
9. MARK 12 OMNI/VHF TRANSCEIVER
10. OMNI INDICATOR
11. DME INDICATOR
12. DME STATION SELECTOR SWITCH
13. TRI-AXIS ACCELEROMETER
14. AMPLIFIER - TELEMETRY
15. LAUNCH WHEEL BRACKET
16. WING GUARD
17. FLARE LINE IMPACT RELAY
18. AUDIO TONE
19. OMNI/VHF ANTENNA

Figure 1. Towed Test Vehicle Component Composite

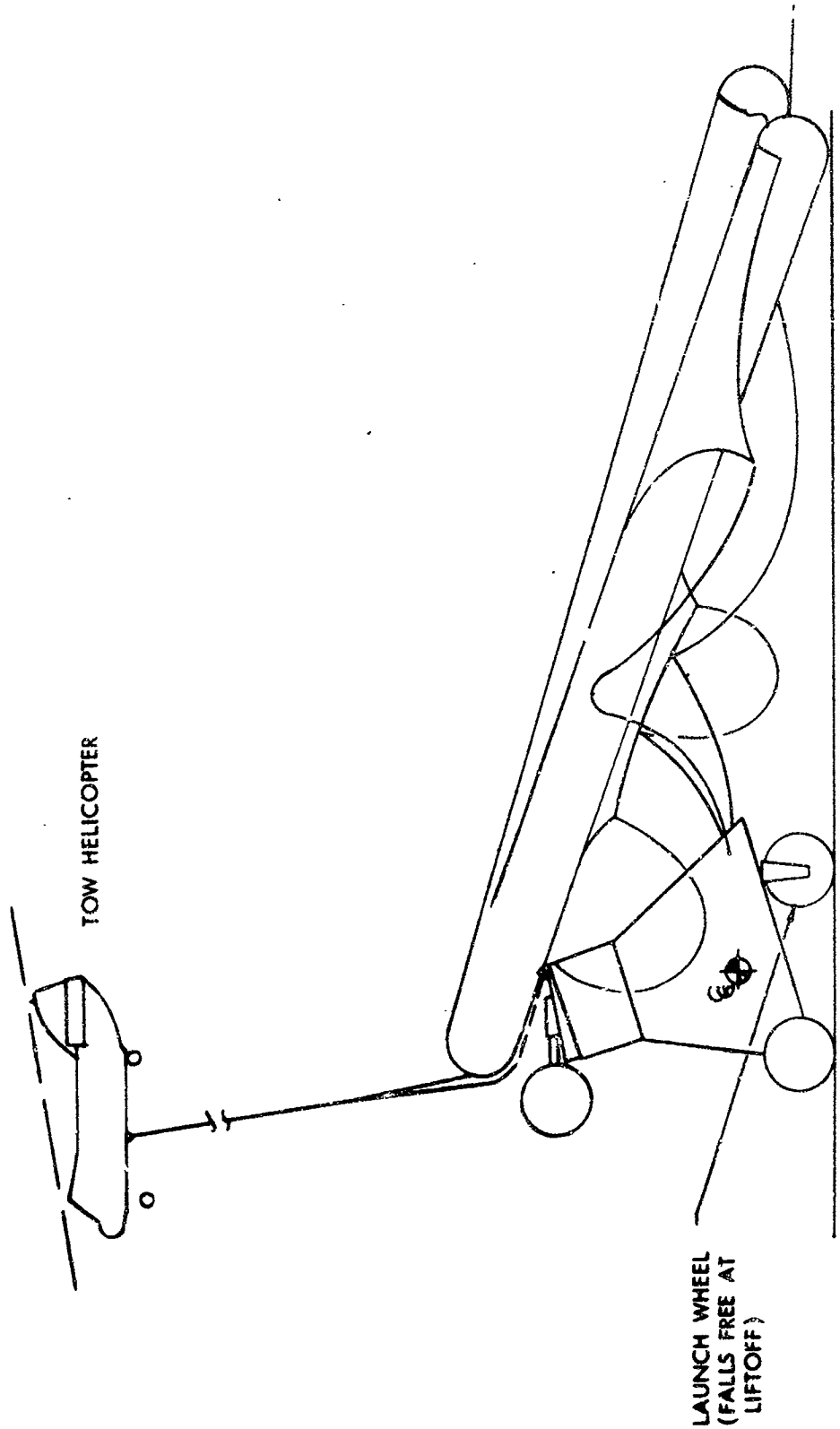

Figure 2. Towed Test Vehicle Vertical Takeoff Technique

MATERIAL

SAIL - 4.5 OZ POLYESTER FABRIC (FORTREL)
6.5 OZ DACRON (CALENDERED) FABRIC

FRAME - COATED DACRON FABRIC TYPE I
COATED DACRON FABRIC TYPE II

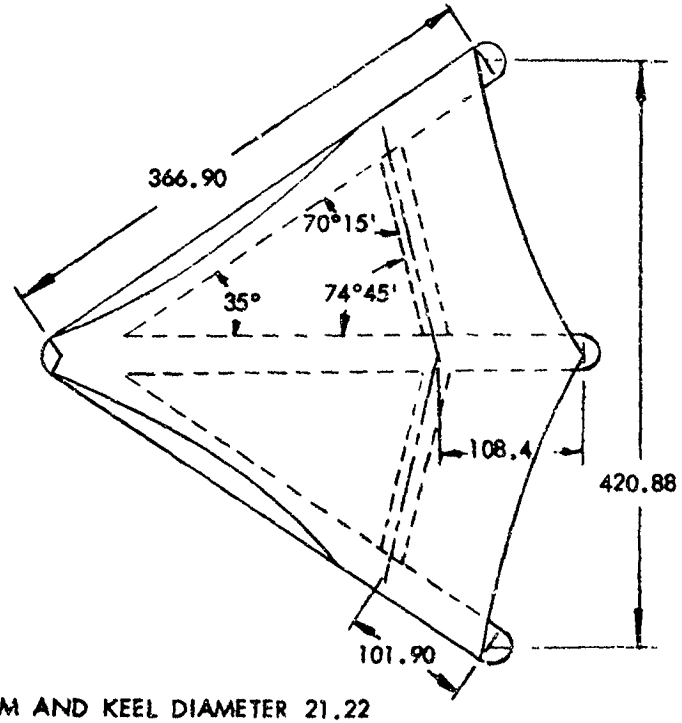

BOOM AND KEEL DIAMETER 21.22
SPREADER BAR DIAMETER 15.52

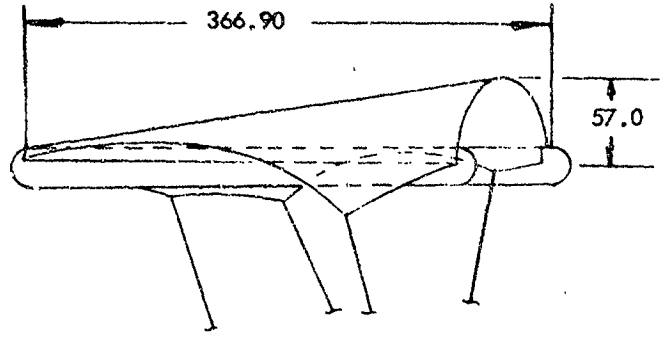

HIGH LOBE SAIL

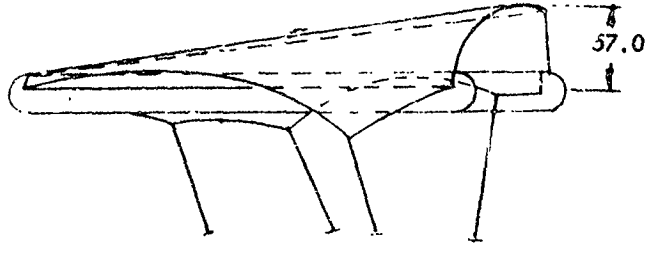

"T" SAIL

Figure 3. Prototype Wings

The wing working pressure of 15.7 $^{+1.25}_{-0.00}$ psig was established. Wing employment during the test program was as follows:

Wing No.	PTB	Radio Command-TTV	Manned-TTV	Total Flights
204	3	4	12	19
206B	1	0	0	1
207	7	0	0	7
210	1	0	0	1

Frames

Prior to the first flight test phase of this program, samples representative of the wing fabric and bonds were tested to determine the effect of age on the material and bonds. The results of these tests indicated no degradation of strength for either test. Each frame was proof-pressure-tested to 21.0 psig to verify the frame structural integrity. Prior to each flight, the wing to be used was thoroughly inspected and proof-pressure tested to 21.0 psig, if required. Proof-pressure testing was not performed prior to Paraglider test bed (PTB) flights unless the wing had encountered damage or an exceedingly hard landing on a previous flight. Proof-pressure testing of the wing to be used was required prior to each radio-command TTV or manned TTV flight.

During this program, only slight modifications were made to the wings such as scuff protection pads on the booms, exposed cordless cord, webbing on the bottom of the wing, and the addition of tabs to the lower apex shroud to provide for stowing the tow bridle during liftoff.

Flight Damage

All flight damage incurred on this program was classified in one of the following categories:

(A) OK to use: Possible to have damage or defects that would have no effect on the serviceability or integrity of the wing

(B) Minor defects: Defects that could be adequately repaired on the test site using cold bonding methods per NAA Specification MA0105-025 for frame repairs, and patching or restitching of sail defects

(C) Major defects: Frame defects that would have to be repaired using the "hot-bond" method per NAA Specification MA0208-2020, or sail defects that would have to be returned to the vendor for repair

During the flight test phases, "OK to use" and "minor defects" type of damage often resulted from the wing sliding on the ground after landing. Major defects were encountered twice—the first was encountered during Phase I when wing No. 210 impacted the PTB vehicle during liftoff and suffered a 3-inch cut in the left-hand spreader bar. The cut was patched per NAA Specification MA0208-2020. The second major damage was encountered during Phase II. At touchdown, the wing (204) fell onto the vehicle, rupturing the left-hand boom and spreader bar intersection. It was necessary to replace the spreader bar/boom intersection and a portion of the left-hand boom to facilitate adequate repair. In each case, the wing involved was proof pressure-tested to 25.0 psig after completion of the repairs.

After each available wing had been flown on the PTB, a decision was made, based on suspected slightly superior performance, to use wing number 204 for the initial TTV flights. Subsequent experience showed that the schedule could be met by using the same wing for all flights.

FLIGHT CONTROL SYSTEM

The flight control system consists of a rotary pneumatic actuator Paraglider control actuator (PCA), which is electronically controlled and/or actuated through the attitude control package (ACE) and the Paraglider control electronics (PCE) via the trim controls and/or hand controller. Command inputs from the trim controller or hand controller are summed in the ACE package with the feedback signal. The error signal operates a low hysteresis switch, which generates the rate command signal. The rate command and rate feedback signals are summed in the PCE, and the resulting rate error signal actuates a pair of "and" gates, which turn on the torque motor drivers.

The torque motors position the pneumatic poppet valves and thus control the speed and duration of the actuator movement. The control range is ±12.89 inches in pitch and ±15 inches in roll. The control rate is 9±3 inches per second for pitch and roll. The electrical limits are established at ±18 inches in pitch and roll, and the mechanical stops are established ±22 inches on both actuators.

The trim controls have the same authority as the hand controller for control movement of the actuators in a closed-loop system. In open-loop control, the trim controllers are not in the circuit; the hand controller is the only signal input source in this mode of operation. No open loop flights were made.

The useable gas mass available on each flight was approximately 20 pounds; the mass used for a flight was seven pounds. The leakage rate on the actuator was 0.05 pounds per hour; the allowable leakage rate per specification was 0.05 pounds per minute. Motor efficiency was better than predicted

for the cable loads encountered during flight. The predicted gas usage was higher than the actual usage per flight because of the low leakage rate, apparently low cable loads, higher efficiencies on the motor-gear train, and the low number of pitch maneuvers during the flight. Table 4 contains the control data for flight Phases II and III.

System and/or component malfunctions during the flight phases were limited to a gain change in the torque motors on PCA 00001. The gain change on the torque motors was due to a magnetic structure change and resulted in a decreased force output. The motors were not capable of controlling the poppet valves under high-pressure, nominal-flow conditions. The resultant malfunction was an oscillating actuator during a commanded maneuver. System response was decreased slightly but was not noticeable to the pilots.

Radar Altimeter System

The radar altimeter system was composed of a receiver-transmitter (HG7091), two indicators (DHG 206A4), and two antennas (DLG 80A1) manufactured by Honeywell Aeronautical Division. The system was a light-weight, high-resolution, short-pulse radar system that automatically located terrain returns and provided a continuous, selective, precision leading-edge track of the signal. The altitude was displayed in both cockpits by the height indicators.

A manually set, low-level warning index was provided on both indicators. The L/H indicator was preset to the desired flare altitude and provided the pilot with a warning light and an audio tone in the head set when the altitude decreased to the preset value. The audio tone was also transmitted on VHF. During radio command flights, this transmitted audio tone was used to flare the vehicle from the ground control station; or, when armed by ground control, a completely automatic flare would occur when altitude decreased to the index setting.

The right-hand indicator low-level warning index was set to the minimum safe flare altitude during manned flights and provided a semi-automatic flare system by cancelling the pitch trim, returning the control system to the position of the hand controller. This function was selected by an arming switch on the left-hand instrument panel at the discretion of the pilot. Refer to Table 4 for the flare altitude settings of the indexes.

The addition of this system to the TTV's satisfied a requirement for an accurate altitude reference for flare during the landing maneuver on radio command, as well as manned flights. A Flight-Tronics inverter (PC-14) was added to supply the 115-volt, 400-cycle power requirements of the radar altimeter system.

Table 4. Control Data for Phases II and III

Flight	Mass at Release	Mass at Touchdown	Mass in Flare Vessel	Total Mass	Mass Used	Percent Used	Cable Rate		Cable Travel		Pressure*		Radar Altimeter		Wing Pressure	Batteries		Flight Time (hr/min/sec)
							Pitch	Roll	Pitch	Roll	Main	Flare	Left	Right		Voltage*	Ampere	
020	34.1	32.9	1.9	20.9	2.7	12.8	8 to 9	7	86	66	2525 2280	2490 2250	119	-	19 4 14 1	29.9 to 28.9 14.1 to 14.2 28.5 to 27.6	10.0 to 12.5 5.0 to 10.0	9:45:9
021	38.6	36.0	1.6	23.2	2.6	10.9	7 to 8	7	102	77	2525 2140	2700 2400	117	-	19.24 14.0	30.0 to 28.5 14.5 to 14.5 28.0 to 27.5	10.0 to 14.0 5.0 to 8.0	9:49:4
022	36.0	28.4	1.7	20.4	7.2	35.2	8 to 9	7	45	312	2550 1960	2600 2460	117	100	19.7 15.0	30.0 to 30.0 15.0 to 15.0 27.5 to 27.0	15.0 to 17.0 6.0 to 9.0	4:4
025	37.1	29.1	1.7	21.1	8.0	38.8	8 to 9	7	31	171	2700 2200	3600 2975	119	104	19.0 15.0	30.0 to 30.0 15.0 to 15.0 27.1 to 28.2	15.0 to 17.0 6.0 to 10.0	4:19
026	37.7	29.8	1.8	21.9	7.8	35.7	7 to 8	7	126	380	3620 2000	2700 2600	120	107	18.7 15.5	31.0 to 31.0 19.2 to 15.9 - -	14.0 to 17.0 6.0 to 9.0	4:36
025	35.7	30.5	1.8	20.0	5.6	27.8	8 to 9	7	120	372	2700 2190	2700 2610	119	105	19.7 14.7	29.8 to 29.5 15.5 to 15.4 29.0 to 28.0	10.0 to 13.5 6.0 to 9.0	4:18:9
026	38.6	32.1	2.0	23.0	6.5	28.2	9 to 10	7	29	654	2690 2700	2900 2900	118	95	18.0 15.5	30.0 to 30.0 15.0 to 15.0 28.5 to 28.0	12.5 to 17.0 6.0 to 10.0	5:10:9
027	41.0	36.5	2.0	24.0	4.4	17.8	11 to 12	9 to 10	101	287	2880 2200	3000 2960	114	95	18.0 15.0	30.0 to 30.5 15.0 to 15.0 27.0 to 28.1	17.0 to 19.0 6.0 to 9.0	4:5:9
028	38.8	35.5	1.9	23.7	3.1	13.1	9 to 10	7	42	217	2800 2400	2950 2850	119	95	17.0 14.7	29.5 to 29.5 14.5 to 14.5 28.0 to 27.8	9.0 5.5 to 9.0	4:48:1
029	35.6	28.6	2.0	20.8	7.1	34.1	11 to 12	9 to 10	78	317	2730 2015	2920 2950	112	85	18.4 14.0	30.5 to 30.8 14.7 to 14.7 27.7 to 27.9	15.0 6.0 to 8.5	5:2
030	39.2	30.3	1.9	24.1	8.7	36.1	9 to 10	6 sec	76	743	2800 2125	2900 2850	112	89	17.0 14.0	29.5 to 29.0 14.1 to 14.5 28.3 to 28.0	12.0 5.5 to 9.0	5:13:2
031	31.4	25.7	1.8	16.2	5.5	34.0	9 to 10	6 sec	152	492	2200 1700	2600 2550	112	85	19.5 13.5	30.5 to 30.5 15.0 to 15.0 28.8 to 28.5	12.0 5.5 to 9.0	4:34:9
032	36.6	28.4	1.9	21.9	7.9	36.8	11 to 12	9 to 10	77	468	2600 1780	2840 2890	108	85	19.8 14.0	30.1 to 30.2 14.4 to 14.0 27.4 to 28.2	15.0 to 20.0 5.5 to 9.0	4:43
033	36.2	34.0	1.9	23.1	3.3	14.3	11 to 12	9 to 10	56	201	2550 2230	2800 2850	104	85	19.8 14.0	30.6 to 30.2 14.8 to 14.2 27.5 to 28.9	18.0 to 22.0 5.5 to 9.0	4:53

PCA 00001 ⇕ = 0.09 lb/hr
PCA 00002 ⇔ = 1.1 lb/hr
PCA 00004 ⇔ = 2.2 lb/hr
PCA 00005 ⇕ = 0.14 lb/hr

*Top number listed for each flight is for liftoff; bottom number is for touchdown.

System Performance

The system locked onto the nose gear on the initial test flight. This condition was corrected by installing a small reflector between the transmitter antenna and the nose gear. System operation proved to be satisfactory for all subsequent flights.

ELECTRICAL POWER

The electrical power system supplied power to the pneumatic, flight control, instrumentation, communications/navigation, radar altimeter, and pyrotechnic systems for operation of the TTV. The electrical system utilizes two separate power sources. A 28 volt, 25 ampere-hour nickel-cadmium battery unit was used for the primary power source, and a 28-volt, 12.5-ampere-hour, nickel-cadmium battery was used for secondary power. Redundant power sources were used to initiate the pyrotechnic devices. The sources were 15-volt, 2 ampere-hour, nickel-cadmium batteries.

Bus loads and battery voltages during and after TTV flights are covered in Table 4. The average "on-time" for the flights was one hour. Additional system description can be obtained from report SID 65-196.

The following changes increased the load requirements on the electrical power system.

1. The UHF communication system was removed, and a VHF communication/navigation system including DME was installed.

2. A radar altimeter was installed, requiring the addition of a PC14 inverter to supply 115-volt, 400-cps, 1000-ampere-hour power.

System Performance

The electrical system was adequate to handle the additional loads and performed satisfactorily on all TTV flights.

TELEMETER INSTRUMENTATION

The instrumentation system consisted of a FM/FM system, multiplexing, sensors, signal conditioners, and associated equipment. For the most part, this system was the same as that referred to in SID 65-196. The differences were some deletions of parameters and reassignment of channels and the addition of parameters, such as altitude and sink rate from the radar altimeter, pitch and roll line positions, a normal acceleration, flare indicators

from radar altimeter, and a lead line and tow release continuity. For details of channel assignments, ranges, and hardware for the parameters used, refer to Table 5.

The telemetry system operated satisfactorily with a minimum loss of data. Loss of data from the attitude system was traced to the adverse attitude of the vehicle at liftoff. This was corrected on later flights by delaying activation of the system until after liftoff in the tow position and delaying movement of the vehicle for a specified period of time after deactivation of the system.

The line loads were not recorded during Phase I and III. Data obtained during Phase II indicated that the available load cells were of too great a range to provide accurate load data in the 0- to 2000-pound range.

Radio Command

The radio command system (Airborne) used an R. S. Electronics receiver Model 1801 and Model 2621A Coder De-modulator that were mounted on a shelf assembly with the associated electrical circuitry and switching.

The radio command system used radio frequency of 424 mc. The following is a list of the code channels and their assigned functions:

1. Roll left
2. Roll right
3. Pitch up
4. Pitch down
5. Flare command
6. Spare
7. Arm flare and horizon camera "ON"
8. Jettison wing
9. Tow release
10. Coding signal (actuated with each command)

The radio command (ground) used two stations—one mobile van as the primary control, and the other as a stand-by back-up located in the telemeter

Table 5. Tow Test Vehicles No. 001 and 002 Instrumentation List

Measurement No.	Change No.	Measurement	Range	Instrument	Converter	Patching
Time code generator	1 (2, 5)	Time code generator	Binary	V20-7[illegible]400	None	2D to 12C (TB4-8)
T310	2 (0)	Internal boom p essure	0 to 10 psig	Edcliff 11[illegible]96	None	2F to 12D (TB4-8)
T311 T313	3 (3, 9)	Flight control supply pressure or PCA inlet pressure	0 to 4000 psig	Bourns 50420-0.40-102	None	2G to 12F (TB5-9)
T1007	3 (3, 9)	Normal acceleration	±20 g	Humphrey LA34-2020-1	None	Same channel as T311 after radar flare
T1003	4 (5, 4)	Pitch line position	7, 5 vrms, 400 cps	Flight control	Dc amplifier D6006-2PA C13AR16	3B to 12F (TB2-8)
T1001	5 (7, 15)	Sink rate (radar)	0 to 50 ft/sec	Radar altimeter	PM 1048 (special)	5B to 12G (TB3-1)
T1002	6 (10, 5)	Altitude (radar)	0 to 512 ft	Radar altimeter	PM 1048 (special)	5E to 12H (TB3-2)
T204	7 (14, 5)	Pitot-static pressure (indicated airspeed)	0 to 6, 1 psid	Scetmxn 2017-6, 1-PDS	None	2M to 12J (TB4-10)
T1005	8 (22, 0)	Roll line position	7, 5 vrms, 400 cps	Flight control	Dc amplifier D6006-2PA C13AR17	3C to 12K (TB2-9)
T401	9 (10, 0)	Pitch drum rate	0 to 5 vdc	Flight control	None	4N to 12L (TB1-5)
T211	11 (52, 5)	Pitch attitude	±40 deg	American gyro VG-1[illegible]- 1-21920	Dc amplifier D6006-2P C13AR11	4L to 12M (TB1-4)
T212	12 (70, 0)	Roll attitude	±40 deg	American gyro VG-1[illegible]- 1-21920	Dc amplifier D6006-2P C13AR12	4K to 12N (TB1-5)
T101*	40 (10-1)	Forward keel line load	0 to 5000 lb	V20-750150-11	MCS-101 C13AR1	15A, B, C, D, and E. GND to 7A
T102*	40 (10-3)	Diagonal keel line load	0 to 5000 lb	V20-750150-11	MCS-101 C13AR2	15A, B, C, D, and E. GND to 7A
T103*	40 (10-5)	Aft keel line load	0 to 3000 lb	V20-750150-11	MCS-101 C13AR3	15A, B, C, D, and E. GND to 7A
T104*	40 (10-4)	Left room line load	0 to 4000 lb	V20-750150	MCS-101 C13AR4	15A, B, C, D, and E. GND to 7A
T105*	40 (10-5)	Right room line load	0 to 4000 lb	V20-750150	MCS-101 C13AR5	15A, B, C, D, and E. GND to 7A
T201	40 (10-6)	Normal acceleration	-1 to +5 g	Humphrey LA39-0608-1	None	1L to 15F (TB5-4)
T202	40 (10-7)	Lateral acceleration	±1 g	Humphrey LA39-0608-1	None	1M to 15G (TB5-5)
T203	40 (10-8)	Longitudinal acceleration	-1 to +4 g	Humphrey LA39-0608-1	None	1K to 15H (TB4-6)
T205	40 (10-9)	Static pressure	0 to 15 psia	Fucliff 11[illegible]95	None	2H to 15J (TB5-1)
T208	40 (10-10)	Pitch rate	±60 deg/sec	Humphrey RGO2-1806-1	None	1F to 15K (TB5-2)
T209	40 (10-11)	Roll rate	±60 deg/sec	Humphrey RGO2-1806-1	None	2A to 15L (TB5-7)
T210	40 (10-12)	Yaw rate	±60 deg/sec	Humphrey RGO2-1806-1	None	1J to 15M (TB5-1)
T401	40 (10-13)	Electrical load primary No. 1	0-25 amp	Electrical shunt	Dc amplifier PM 1048 C13AR7	2C to 15N (N/TB)
T402	40 (10-14)	Electrical load primary No. 2	0-25 amp	Electrical shunt	Dc amplifier PM 1048 C13AR8	2F to 15P (N/TB)
T303	40 (10-15)	Electrical load secondary	0-25 amp	Electrical shunt	Dc amplifier PM 1048 C13AR9	2K to 14A (N/TB)
T304	40 (10-16)	Electrical load pyro No. 1	0-25 amp	Electrical shunt	Dc amplifier PM 1048 C13AR10	1A to 14B (N/TB)
T305	40 (10-17)	Electrical load pyro No. 2	0-25 amp	Electrical shunt	Dc amplifier PM 1048 C13AR11	1D to 14C (N/TB)
T133	40 (10-18)	Tow cable separator	ON-OFF	Electrical shunt	V20-750220	4D to 14D (TB1-1)
T402	40 (10-19)	Roll dream rate	0 to 5 vdc	Flight control	None	4J to 14E (TB)
T403	40 (10-20)	Pitch command	7, 5 vrms, 400 cps	Flight control	Dc amplifier D6006-2PA C13AR14	3D to 14C (TB1-8)
T405	40 (10-21)	Roll command	7, 5 vrms, 400 cps	Flight control	Dc amplifier D6006-2PA C13AR15	3A to 14G (TB1-9)
T503	40 (10-23)	PCA inlet GN_2 temperature	+65 to +160 F	Gulton L-712	V20-750220	4F to 14H (TB2-1)
T504	40 (10-24)	Flight control supply GN_2 temp	+65 to 160F	Gulton L-712	V20-750220	3K to 14J (TB2-5)
T1004	40 (10-74)	Flags indicator (radar)	0 to 28 vdc	Radar altimeter	None	5C to 6C, 6A to 14K (TB1-10)

*These parameters were used in Phases I and II of this program but were deleted in Phase III.

Table 5. Tow Test Vehicles No. 001 and 002 Instrumentation List (Cont)

Measurement No.	Change No.	Measurement	Range	Instrument	Converter	Patching
T1006	40 (10-25)	Flare indicator (lead line)	0 to 28 vdc	Electrical	None	3F to 8N, 9L to 14L (TB3-9)
T1008	40 (10-26)	Tow release continuity	0 to 5 vdc	Instrumentation	None	2B to 14M (TB4-7)
Calibration	40 (10-27)	5-v calibration	+5 vdc	V12-751020	None	7P to 14N (TB7-8)
Calibration	40 (10-28)	0-v calibration	0 vdc	V12-751020	None	2J to 14P (TB7-4)

*These parameters were used in Phases I and II of this program but were deleted in Phase III.

trailer. Both stations used a Babcock Model ARW-66 transmitter and a BCC25 Coder Modulator in conjunction with associated electrical wiring and switching assembly. The radio command system used for Phases I and II of this program was removed for the Phase III manned portion.

The system performed satisfactorily and experienced no malfunctions.

Cockpit Display

During Phases I and II of this program, the cockpit instruments were for all practical purposes as shown in SID 65-196. However, for Phase III it was determined that a regrouping of these instruments would be advisable from a pilot's human factor standpoint and better photo-recording of priority instruments.

For detailed arrangement of cockpit display as used during Phase III, reference Figure 4.

PYROTECHNIC SYSTEM

The pyrotechnic system was redundant, having two Gould CL5200B 15-volt, 2-ampere-hour, nickel-cadmium batteries. Each battery supplied power to an electrical bus. At pyrotechnic circuitry switch actuation, primary and secondary bus firing voltage were presented at the pyrotechnic device simultaneously.

All pyrotechnic devices were fused and employed shielded wire. The shields and all ground returns were terminated at a single point. Bridge wires of the pyrotechnics were shorted to ground prior to firing through the closed contacts of their firing relays or switches.

Pyrotechnic Subsystems

The wing tangent release and wing ballast release subsystems were deleted due to the use of the test vehicle vertical liftoff concept. Active pyrotechnic subsystems and their function are as follows:

TTV Towline Release - Separation of the test vehicle from the tow cable and towing aircraft

TTV Wing Ground Release - Separation of the Paraglider wing from the test vehicle subsequent to landing during ground roll out phase. Separation points were on the flight control cables above the test vehicle moldline.

1. ROLL LINE POSITION INDICATOR
2. AIRSPEED INDICATOR
3. FLARE COMMAND INDICATOR
4. PITCH LINE POSITION INDICATOR
5. TIME CODE GENERATOR LIGHTS
6. PITCH LINE POSITION INDICATOR
7. RADAR ALTIMETER INDICATOR
8. BATTERY VOLTAGE INDICATOR
9. DISTANCE MEASURING EQUIPMENT (DME) INDICATOR
10. DISTANCE MEASURING EQUIPMENT (DME) INDICATOR
11. RADAR ALTIMETER INDICATOR
12. VOLTAGE SELECTOR SWITCH
13. RATE OF DESCENT INDICATOR
14. VEHICLE ATTITUDE INDICATOR
15. BAROMETRIC ALTIMETER INDICATOR
16. AUTOMATIC FLARE SWITCH
17. OMNI INDICATOR
18. INTERCOMMUNICATION AND COMMUNICATION SWITCH
19. BAROMETRIC ALTIMETER INDICATOR
20. ELAPSED-TIME CLOCK
21. TOW RELEASE CONTINUITY INDICATOR
22. RATE OF DESCENT INDICATOR
23. HEADING SLEW SWITCH
24. F/C SUPPLY PRESSURE INDICATOR
25. WING PRESSURE INDICATOR
26. FLARE BOTTLE PRESSURE INDICATOR
27. ELAPSED-TIME CLOCK
28. FLIGHT SAFETY WARNING LIGHTS
29. COMMUNICATIONS TRANSMITTER (VHF/NAVIGATION RECEIVER)
30. TRIM CONTROL
31. PITOT BOOM RELEASE SWITCH

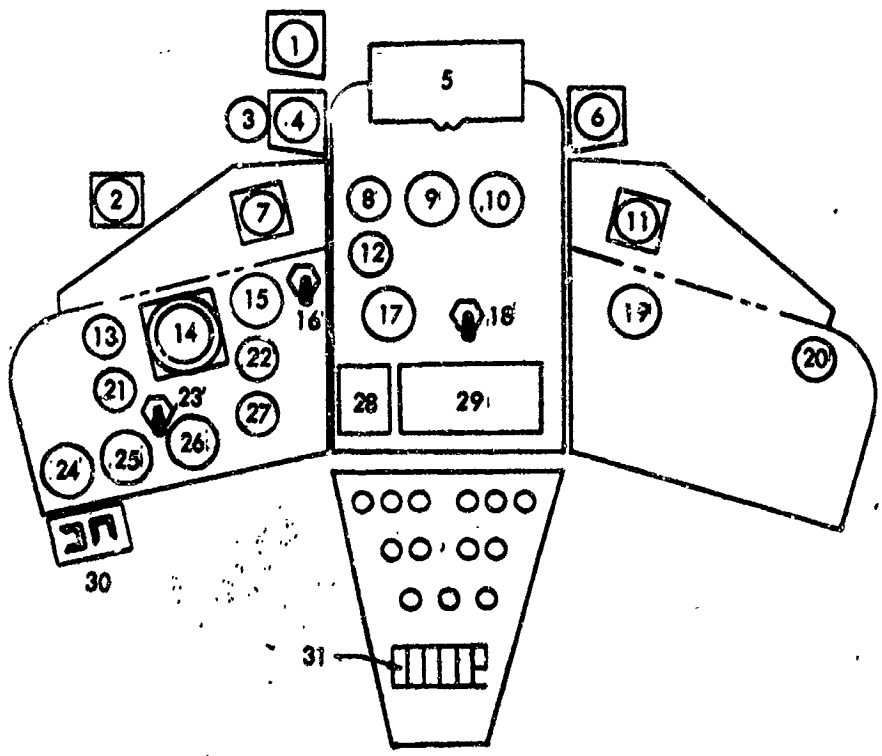

Figure 4. Towed Test Vehicle Cockpit Display (Two-Pilot Configuration)

TTV Emergency Wing Jettison - Airborne separation of Paraglider wing from the test vehicle, accomplished by severing flight control cables. Separation points were below the moldline.

Design requirements for pyrotechnic components and subsystems are as set forth in SID 65-196, "Final Report Paraglider Research and Development Program," dated 19 February 1965.

System Performance

There were no pyrotechnic system malfunctions with respect to electrical system or pyrotechnic device failure. One mechanical failure occurred during a PTB flight in Phase I when towline release was initiated. This was due to improper refurbishment of the release mechanism. A change in checkout procedure eliminated any further problems.

COMMUNICATIONS AND NAVIGATIONAL EQUIPMENT

During this program, the Collins UHF equipment described in SID 65-196 was removed and replaced by a Narco Mark 12 VHF transceiver and navigation receiver used in conjunction with a Narco VOA-4 Omni/localizer converter and a Narco distance-measuring equipment (DME) UDI-2AR interrogator. This change was necessary to give the navigational capability and to make use of available ground support in the Edwards Air Force Base area.

The Narco Mark 12 equipment comprises a VHF communications transceiver and a VHF navigation receiver in a panel-mounted unit and a remote-mounted modulator power unit. The VHF transceiver for communications has 360 crystal control channels. This program used 123.35 megacycles as the primary operational test frequency and 123.5 megacycles as the secondary backup frequency. The VHF navigation receiver portion has a 100-channel capability to provide VOR navigation capability.

The Narco VOA4 Omni/localizer converter uses the Omni signal derived from the navigation receiver of the Mark 12 equipment and converts it into a visual signal in the form of a vertical "left-right" indication by the indicator instrument needle. In addition, the indicator has a "TO-OFF-FROM" flag signal.

The Narco UDI-2AR DME interrogator is comprised of two units designed to present, by means of an indicator marked in nautical miles, the distance between an aircraft and a ground station. It operates on the basic principle of measuring the time required for radio signals to travel round trip between an aircraft and ground station. It is crystal-controlled and

operates at the UHF frequencies matched to the VHF VOR frequencies. Therefore, the channel selector is marked in the VHF frequency ranges VOR 108.0 through 117.9 megacycles.

No malfunctions were experienced in the communications and navigational systems. Due to the limited altitudes available with the vehicle used for towing the TTV, the distance measuring equipment system received a minimal operational check.

PARAGLIDER TEST BED

The basic structure of the Paraglider Test Bed (PTB), Figure 5, consisted of boilerplate and tooling tubing welded together to form a sturdy test platform. Two steel skids welded to the structure provide a landing surface. The flight control cable pulleys were positioned to simulate TTV control cable geometry. The PTB was ballasted to provide accurate horizontal center-of-gravity location, but vertical center of gravity location, but vertical center of gravity was not stringently maintained to simulate the TTV. Ballasting provided simulation of TTV gross weight. The PTB was originally a static tooling article, fabricated on contract NAS9-1484 and modified to function as a flight test vehicle. All flight control cables were 1/4-inch-diameter steel, of a fixed length and having wing attachment fittings to mate the TTV wing fittings.

Pitch and roll flight control motors were Lear rotary actuators of 700-inch-pound torque with electrical power requirements of 24-vdc at 120 amperes maximum. The clutch system was a Lear magnetic particle type and was used for braking as well as driving the flight control drums. The reduction gear box (planetary system) was modified from a Jack and Heintz a-c engine starter and provided a gear reduction of approximately 576:1. Sprocket chain drive (std 3/8 pitch) provided the mechanical link between gear box and drum. The drum diameter for both pitch and roll was 7 inches and provided a control line rate of approximately 7.5 inches per second.

Power for the vehicle was supplied by 24-vdc "Gould" nickel-cadmium batteries rated at 12 ampere hours.

The pitch trim control system consisted of an AiResearch linear actuator used to position mechanically the "pitch neutral" and "end limit" switch mounting plate to ±40 degrees of rotation. The rate of pitch trim control was less than 15 degrees per second in order for the pitch flight control system to follow the trim adjustment. The purpose of the trim system is to determine the optimum "pitch neutral" wing position for performance.

The radio command system consisted of an R&S receiver/decoder and single antenna to receive coded command signals to the vehicle.

An on-board 16-mm movie camera (8 frames/sec) was installed on the Paraglider Test Bed to provide recorded data of radio command signal inputs versus pitch system control operation.

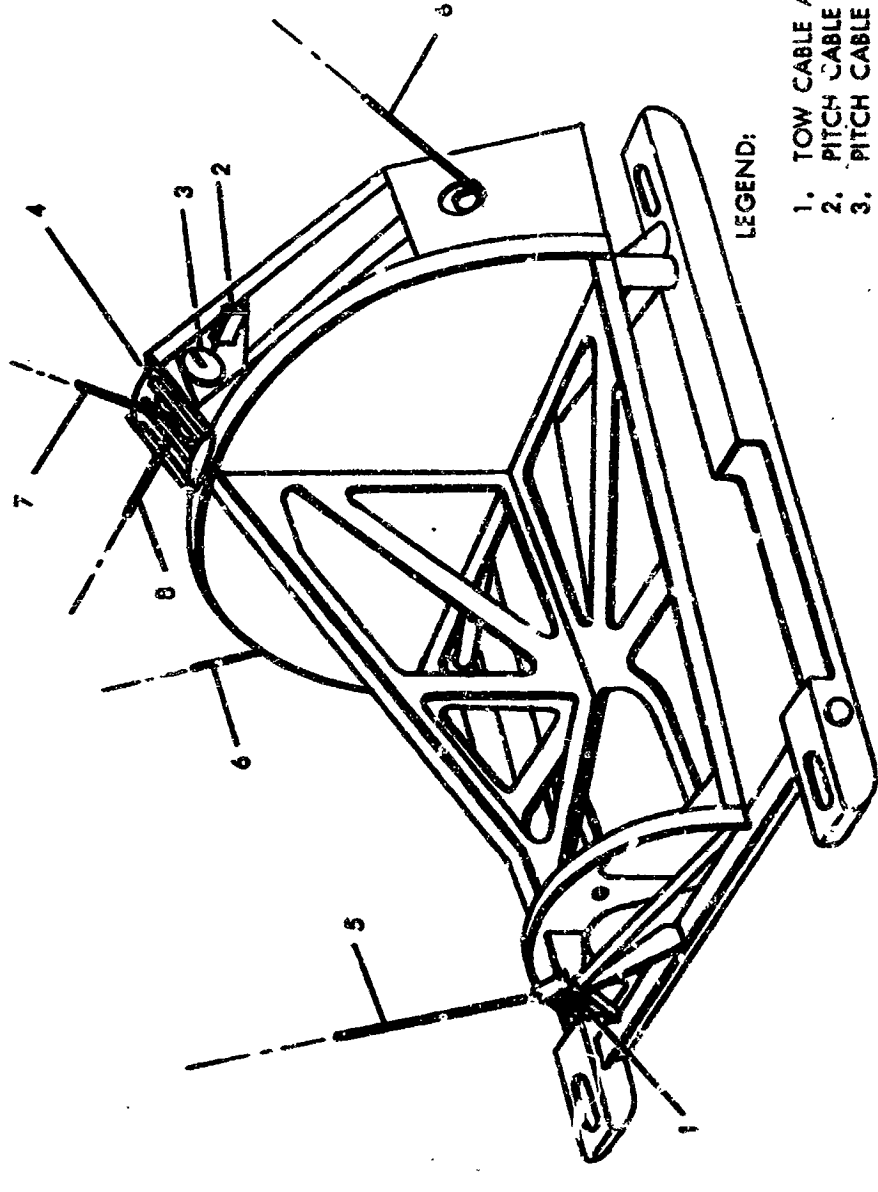

Figure 5. Paraglider Test Bed Configuration

TELEMETRY RECEPTION AND RECORDING

The telemetry van contained two F/M receivers covering the VHF telemetry band from 215 to 260 megacycles. Incoming telemetering signals were received via a nondirectional, broad-band antenna and the two F/M receivers. The receiver outputs, the composite audio signals, were mixed with a 100-kilocycle reference signal and recorded on magnetic tape by either of two one-inch tape recorders. A Panadaptor and telemetering indicator permit a degree of visual analysis of the composite telemetry signal.

REAL-TIME TELEMETRY DATA PRESENTATION

Telemetry receiver outputs were routed to a bank of 18 subcarrier discriminators, which separate the composite signal into its individual data channels. These data channels, which generally represent individual measurements, were shown on specially prepared meters, calibrated in terms of the actual parameter values. Up to five measurements were viewed in this manner. Data channels were also shown on either of two direct-writing oscillographs. A PAM or PDM decommutator permits documentation of wavetrains corresponding to a variety of IRIG standards. The outputs of this device may be presented in similar fashion as the continuous channels from the discriminators. All IRIG standard subcarrier frequencies were accommodated by the telemetry van.

POST-TEST PLAYBACK AND PRESENTATION

These functions were performed using the same equipment used in presenting real-time telemetry data. One notable exception was the use of playback compensation system to minimize the effects of tape recorder wow and flutter on the data. Whereas the data source for real-time presentation was the telemetry receiver, the source was a previously recorded magnetic tape for posttest playback. Discrimination, decommutation, and presentation methods were the same in both cases.

COMMUNICATIONS

The telemetry van includes equipment for voice communications in both the VHF and UHF bands. Two VHF transceivers, one operating on battery power for emergency communications in the event of power failure, cover the frequencies from 108 to 138 megacycles. An aircraft-type UHF transceiver provides coverage on all normally used channels. Nondirectional antennas are used with all equipment.

RADIO COMMAND

A radio command transmitter and encoder were used as a back-up system in the event of failure of the primary command source. This transmitter operated on a frequency of 424 megacycles.

PHOTO INSTRUMENTATION

During this program, three cameras were installed in the vehicle: one showing the cockpit instrument panel, another covering the spreader bar area of the wing, and the third directed out of the nose of the vehicle showing the horizon. During the third phase of the program, the spreader bar camera was deleted, and this camera was mounted on top of the right-hand seat. The camera was directed forward through the canopy windshield area, giving an additional view of the horizon.

In addition to the on-board photo coverage, ground coverage was supplied by three photographic cameras and a television camera mounted on a M45 gun mount. This supplied tracking coverage of liftoff, flight, and landing. The television camera used a zoom lens and a tape recorder, which provided immediate playback of the operation. The photographic cameras were two Mitchels--one with a 400-mm lens, the other with 1000-mm lens--and one Milliken camera operating at 400 frames per second with a 400-mm lens. The Milliken was operating at vehicle touchdown only.

AERODYNAMICS

FLIGHT DATA

Analysis of the data obtained during the three phases of the Paraglider program has been made in an attempt to verify predicted and test data obtained previously or to arrive at new flight relationships. Previous data were reported in NAA report number SID 65-196. A review has shown considerable data from the on-board telemetry system, which appears to have functioned very well during the program. Nike radar tracking data is somewhat unreliable; in several cases it was not available, and in others it is so bad as to be completely unusable, especially during Phase III.

Analysis has shown that there is little steady-state data where an absence of either turning or pitching has resulted in equilibrium flight at a time when Nike tracking and on-board gyros were functioning.

Nike radar tracking data was received as an IBM printout. Space position data results in several parameters with and without winds, including sink rates, speeds, dynamic pressure, and direction. The track of the radar was electrically centered, and a curve-smoothing subroutine does not allow for any discontinuities within the track. The output of the tracking data is input into a data reduction program which takes into consideration all accelerations and variables while aerodynamic coefficients are computed. These data include flight path angles and rate of change of angles, bank angle, lift and drag coefficients, and lift/drag ratio.

During analysis of the data, extremely high lift to drag ratios were noted during a pitch-down maneuver. Investigation of the calculation method revealed that in the calculation of drag:

$$D = -m\dot{v} - W \sin \gamma$$

The rate of change of speed with time ($\dot{V}$) became fairly large, approaching 10 to 12 fps^2, and with a mass of 120 slugs, the drag approaches zero, resulting in a large L/D. This magnitude of acceleration appears unlikely and is probably due to the curve-smoothing technique within the tracking program.

Investigation of the Nike radar tracking data was undertaken during Phase II to resolve the problem of high lift to drag ratios during pitch-down maneuvers. The data reduction program used a seven-point differentiation

method, which smoothed the data over a s n-second interval when computed at a rate of one per second. Different run rates of two per second and ten per second were tried. The two-per-second computations rate gave improved results in analysis of the rate of sink but exaggerated the effect of the dv/dt term and resulted in erratic lift-to-drag variations. The ten-per-second rate appears to be beyond the accuracy of the tracker and resulted in variations in rates above the response capabilities of the vehicle. The data reduction program was then modified to remove the -mv̇ term from the drag equation, so that D = -Wsinα. This modification resulted in a somewhat less erratic lift-to-drag variation but left some doubt as to the alignment of the answer; therefore, both values were plotted and are presented in the enclosures for comparative purposes.

The tracking data of Flight 005 indicates some of the dynamics associated with the flight. The major portion of this flight was at a pitch line setting $\ell_1/\ell_k = 0.56$. The oscillation and variations in sink rate and dynamic pressure (Figure 6) are mostly due to turns.

The data from telemetry indicates preflare was fully in 26 seconds before touchdown. The preflare setting was held in 18 seconds before touchdown (Figure 7). Note that flare was $0.54\ell_1/\ell_k$ and line travel was completed after touchdown. Figures 6 and 7 indicate the effects of bank angle, where the recovery from a turn has the same effect as a partial flare by reducing speed and sink rate. Exact timing between Nike radar and telemetry data was difficult. Countdown to release was the major timing factor and can be in error by a few seconds. Nike radar also was very doubtful as the vehicle approaches the ground, and touchdown cannot be determined. This was corrected during Phases II and III by addition of PAR-set-timing to both telemetry and Nike radar.

Since the major portion of Flight 005 was at one line setting, the aerodynamics data were plotted as a function of bank angle for correlation purposes (Figure 8). The expected effect of increased lift coefficient and decreased lift to drag at high bank angle was not apparent. There was very little steady-state data. The acceleration effect on lift to drag, as mentioned above, was apparent.

Time histories of flight parameters (Figures 9 and 10) indicate the many maneuvers associated with Flight 014. The telemetry traces of pitch and roll line position (Figure 9) and the accompanying Nike radar histories of sink rates and bank angles indicate the excellent vehicle control response. These traces also show the lack of steady-state data associated with periods of no control inputs. These data present a reasonable variation of lift

FOLDOUT FRAME 1

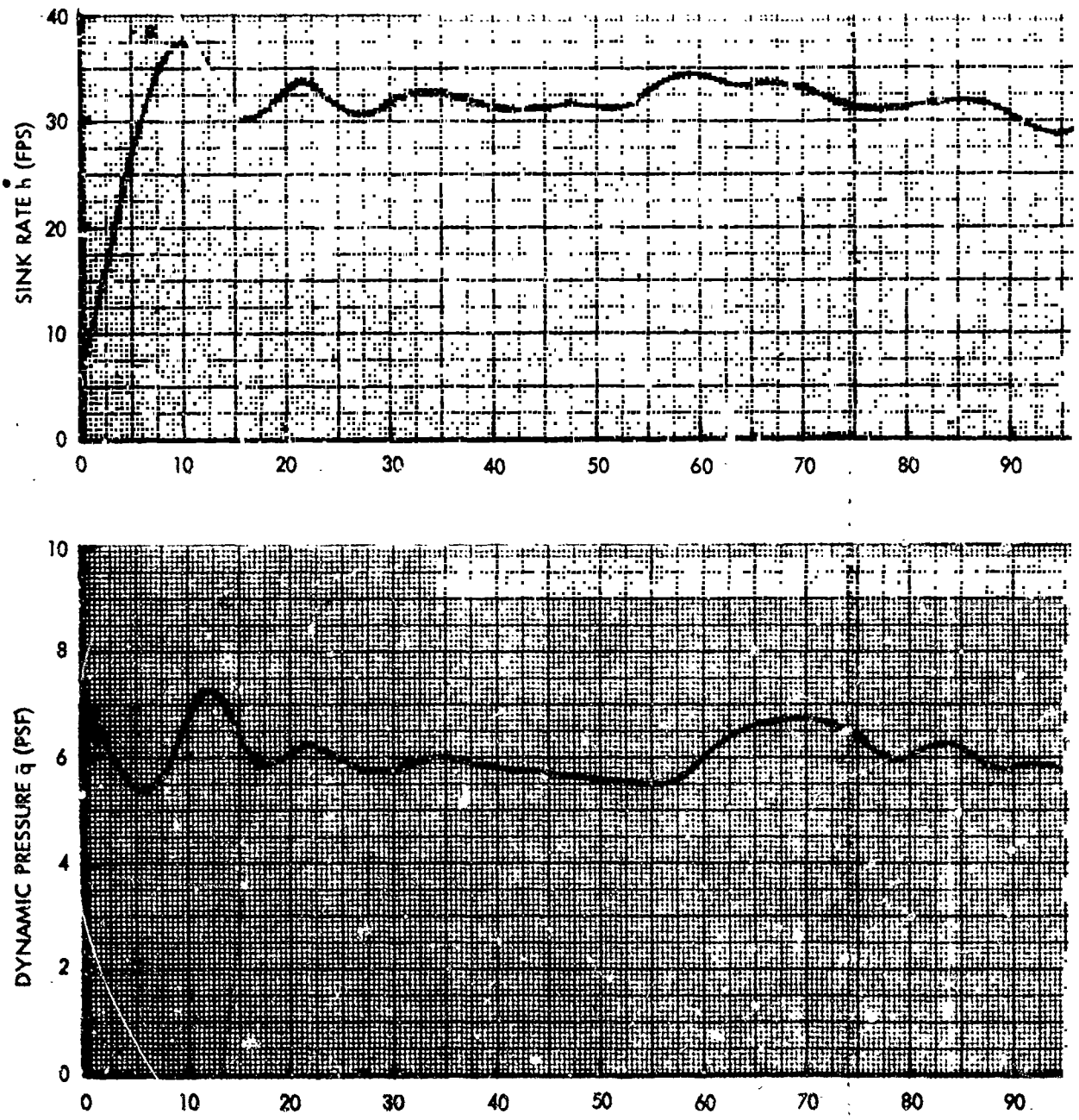

FOLDOUT FRAME 2

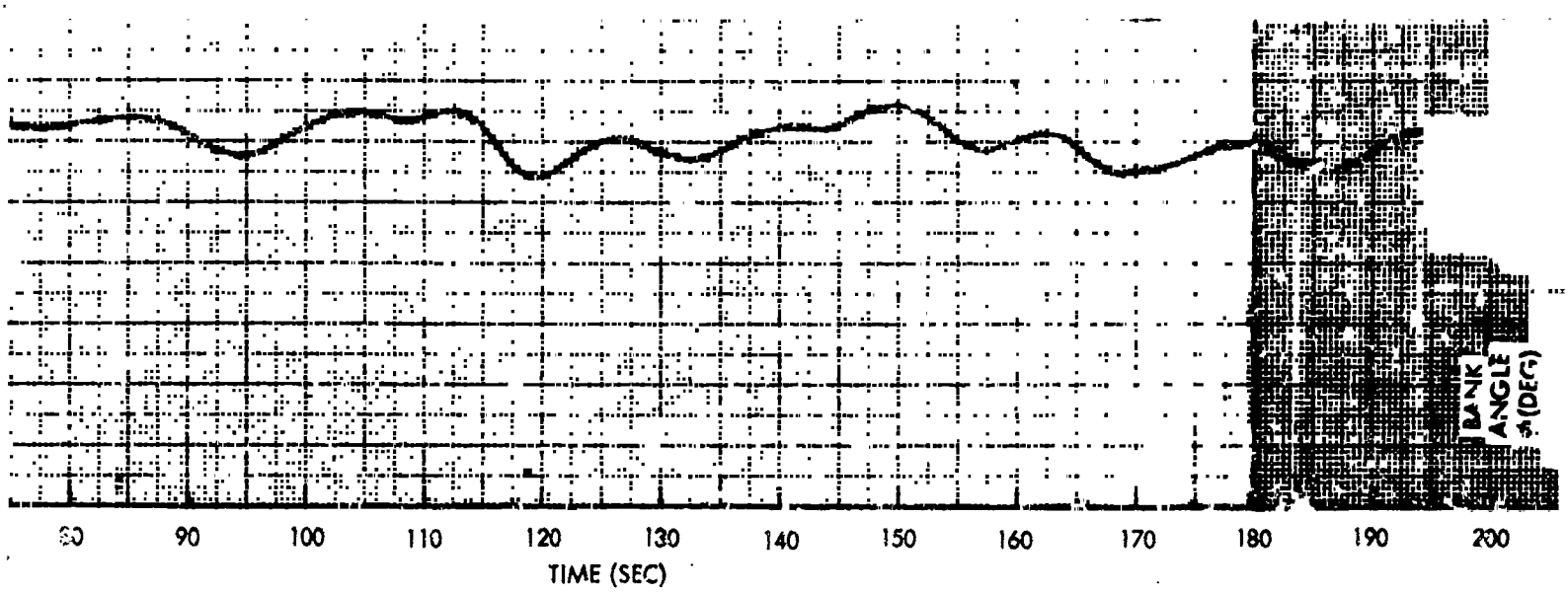

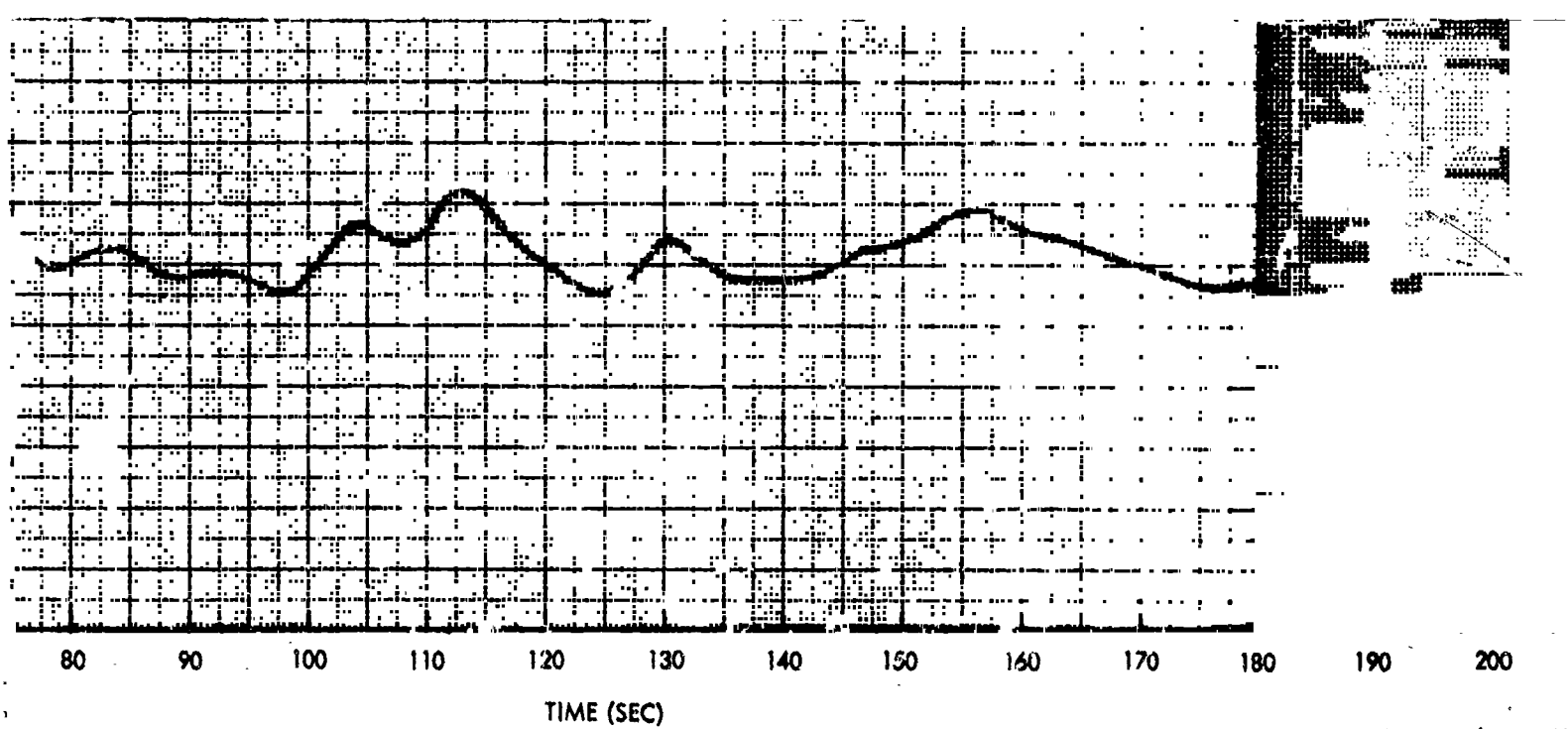

Figure 6. Nik

FOLDOUT FRAME 3

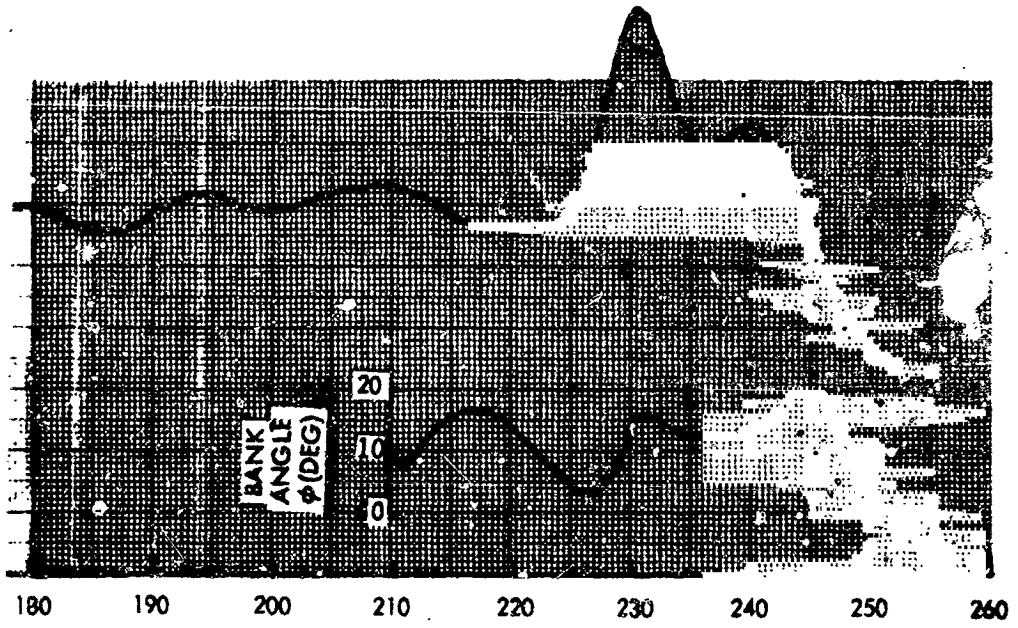

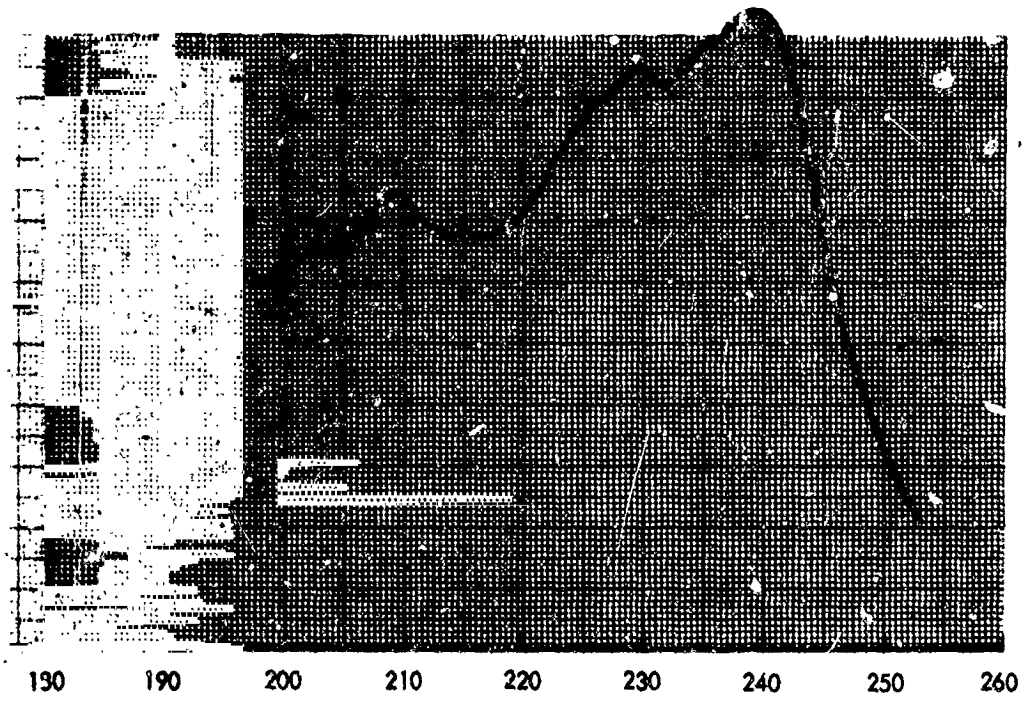

Figure 6. Nike Radar Tracking Data, Flight 005

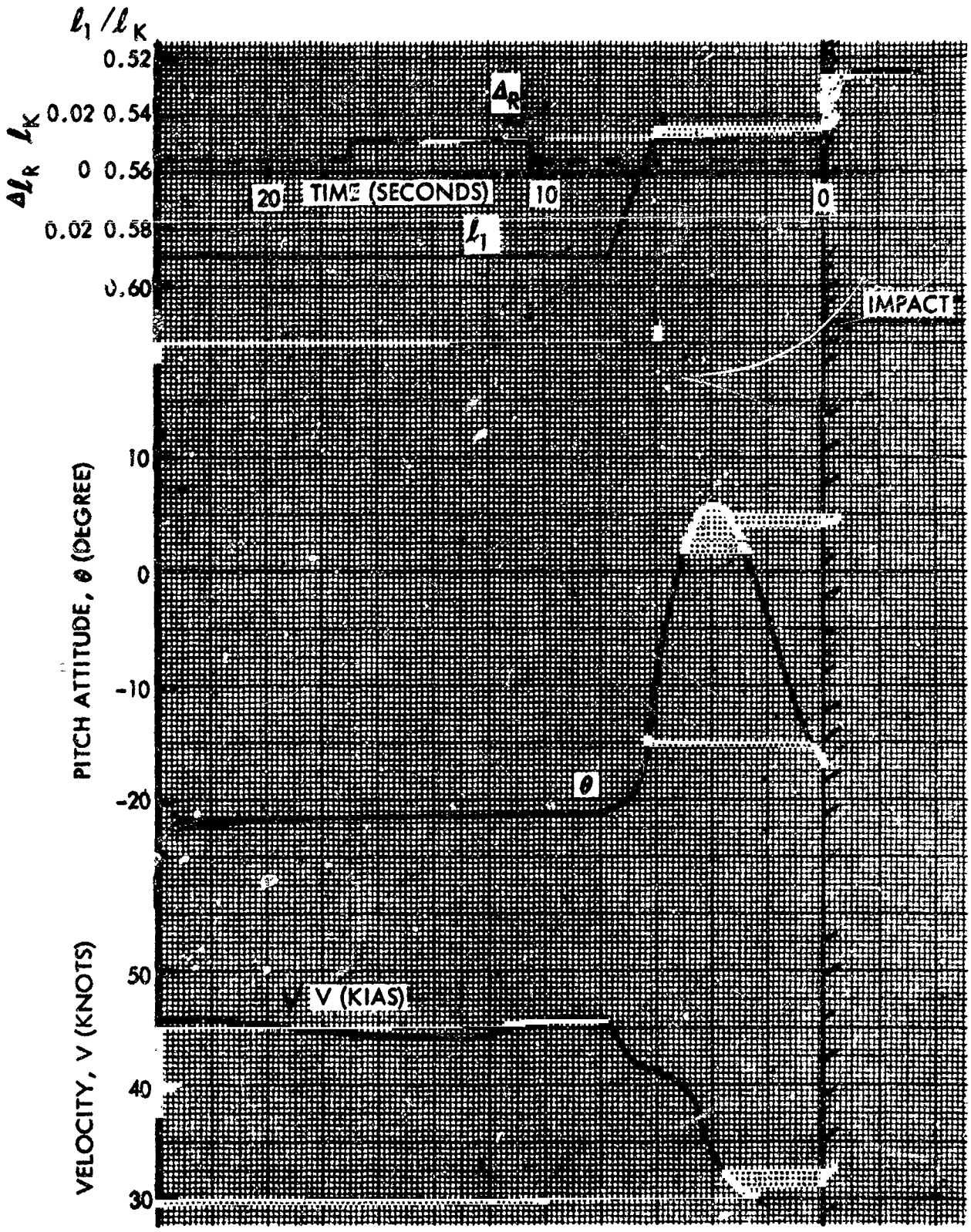

Figure 7. Flare Data, Flight 005

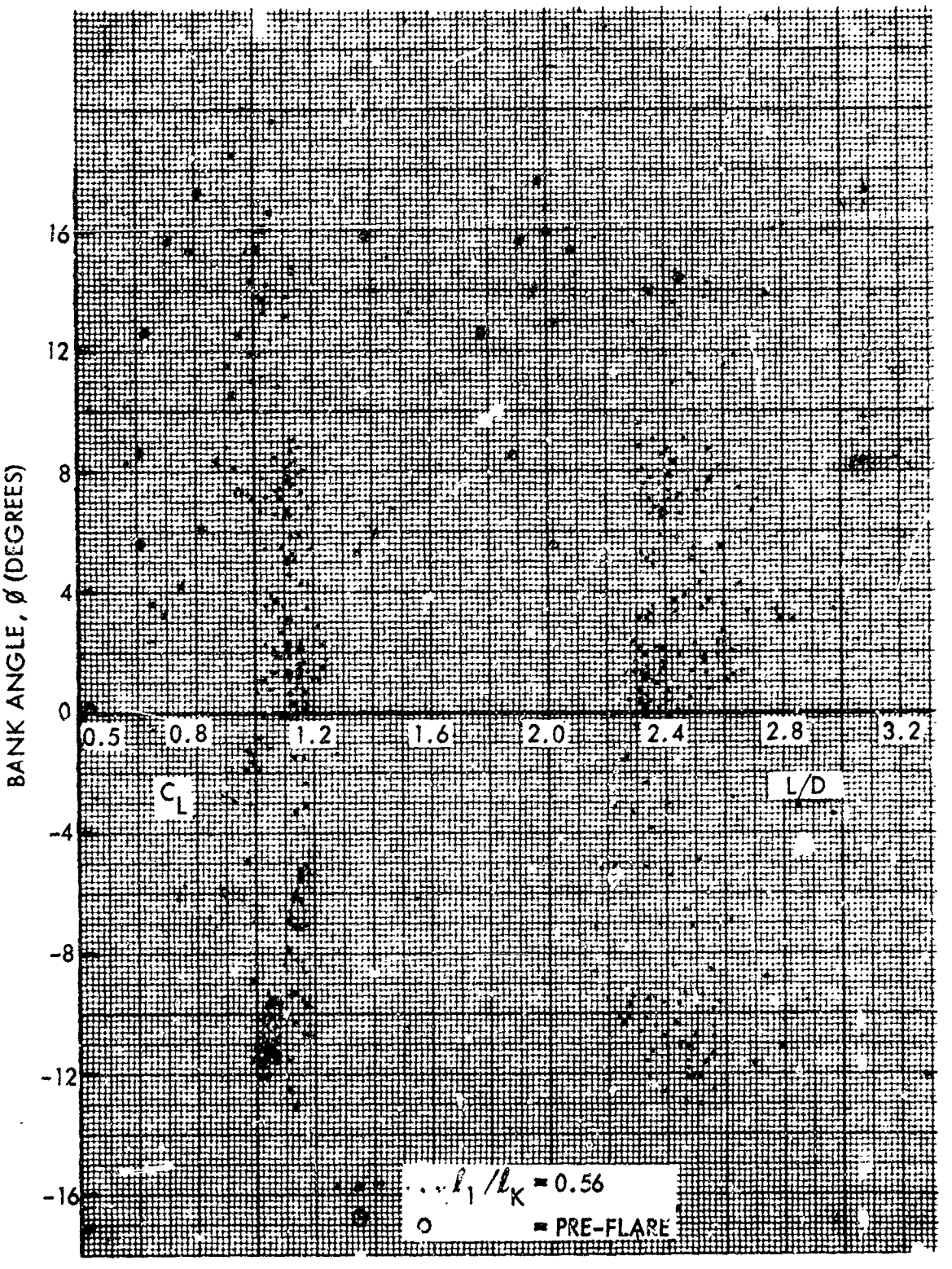

Figure 8. Effect of Bank Angle, Flight 005

FOLDOUT FRAME 1

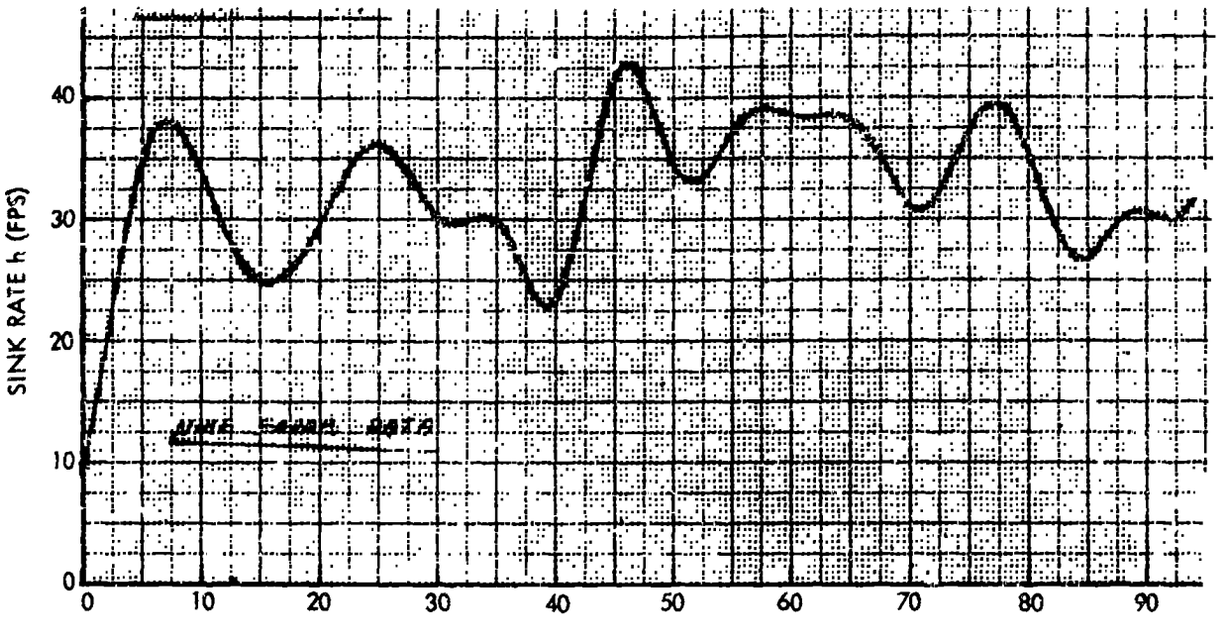

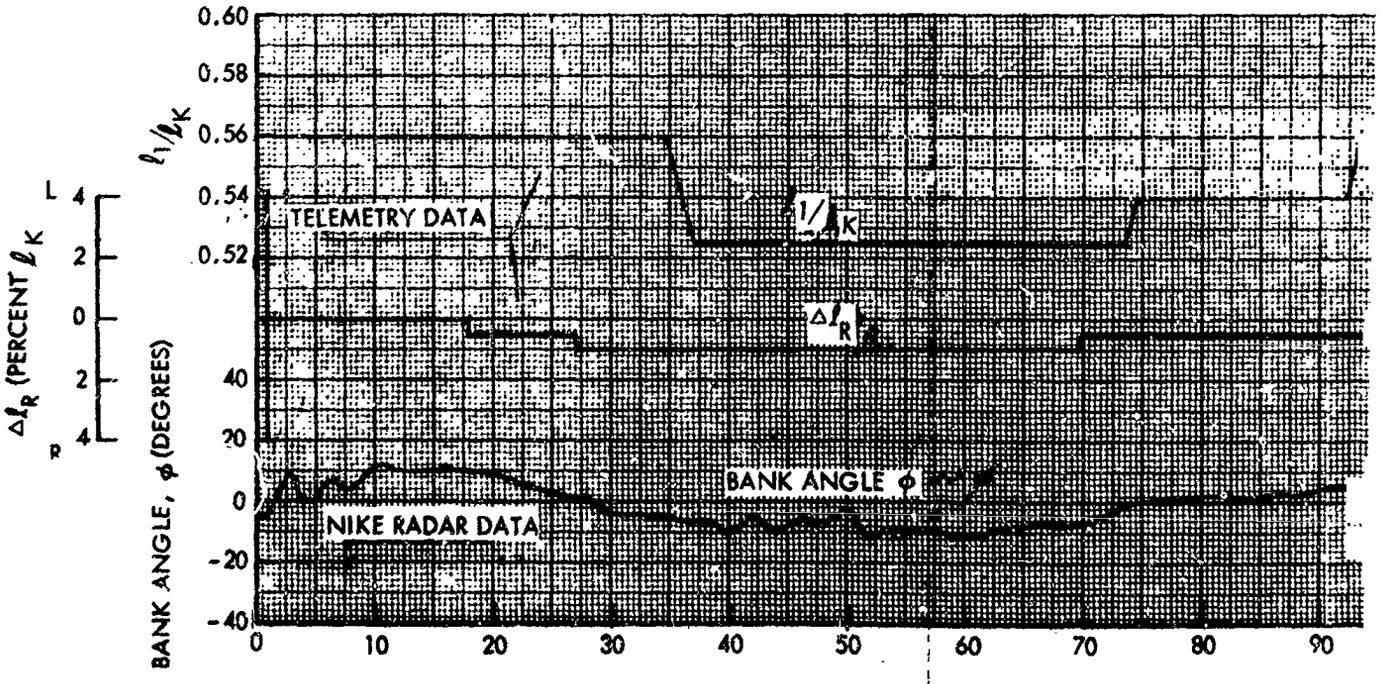

FOLDOUT FRAME 2

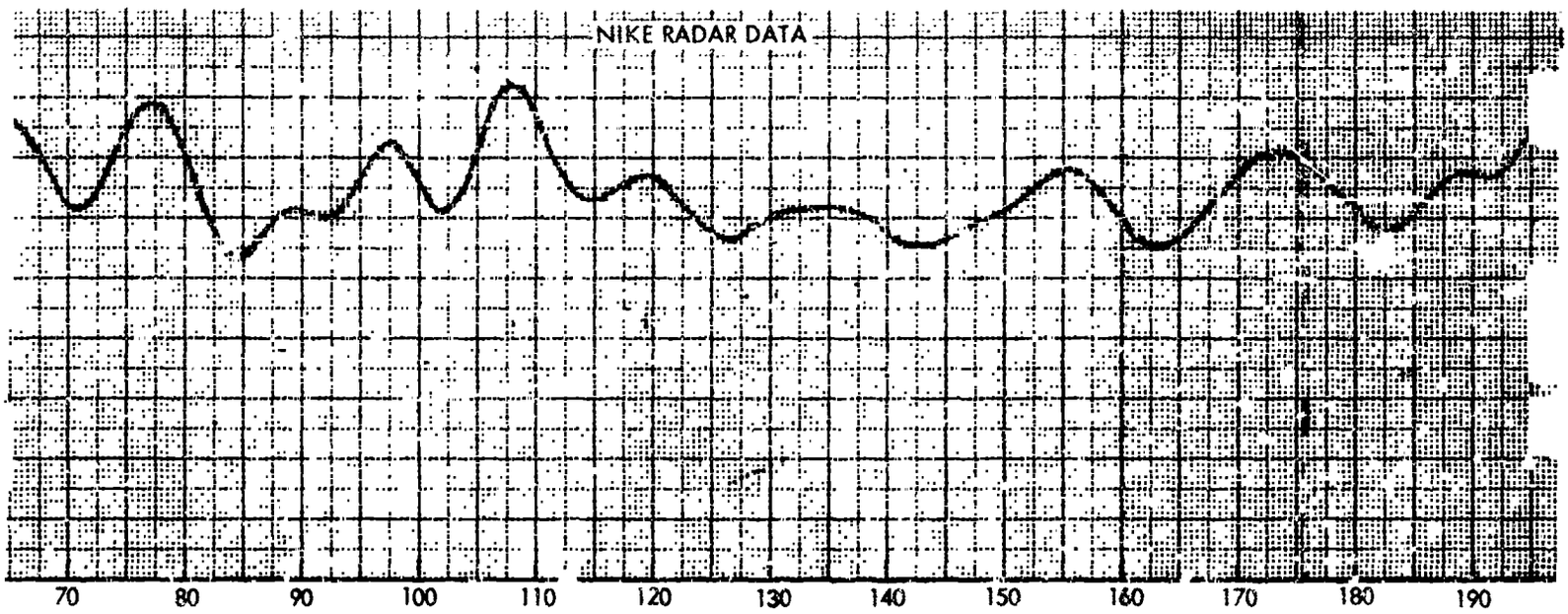

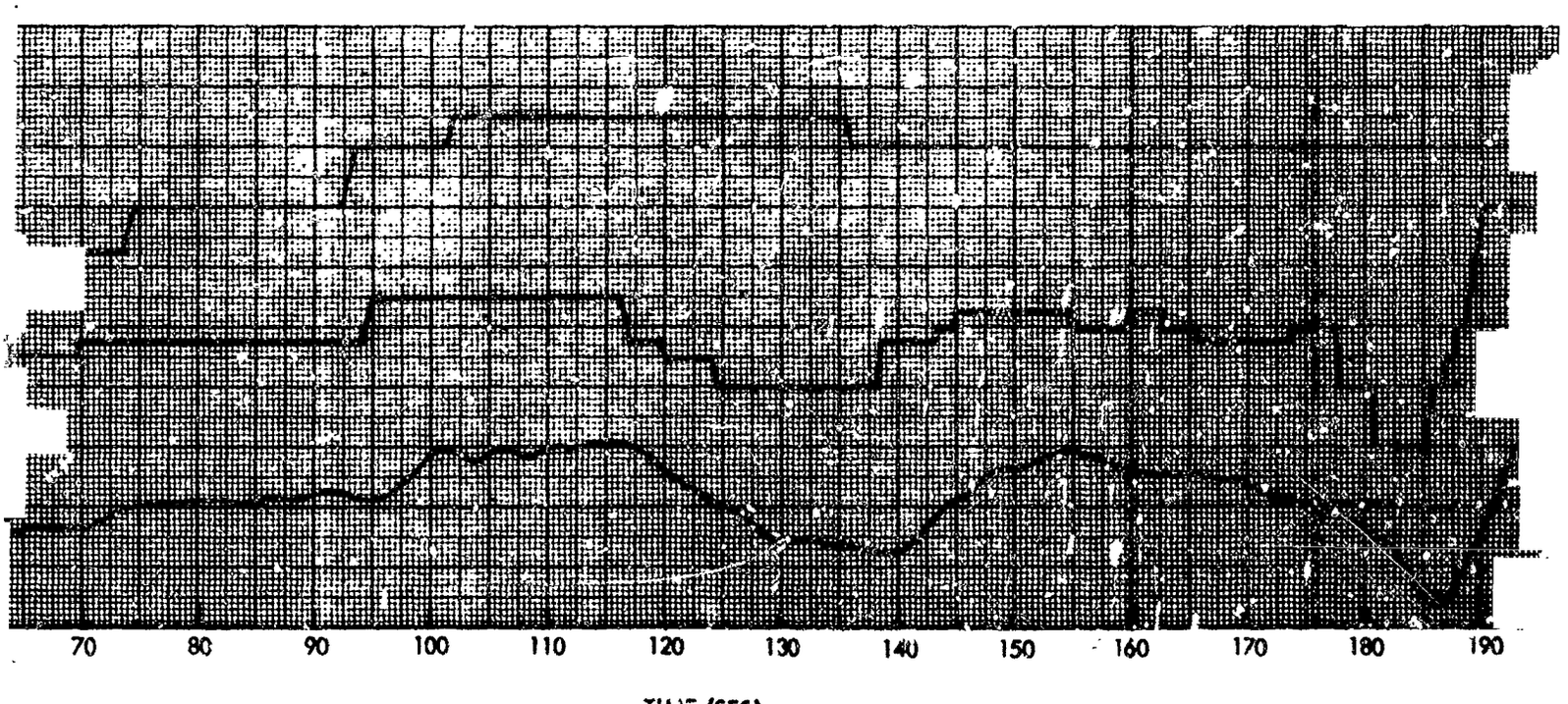

Figure 9. Towed Test Vehicle

FOLDOUT FRAME 3

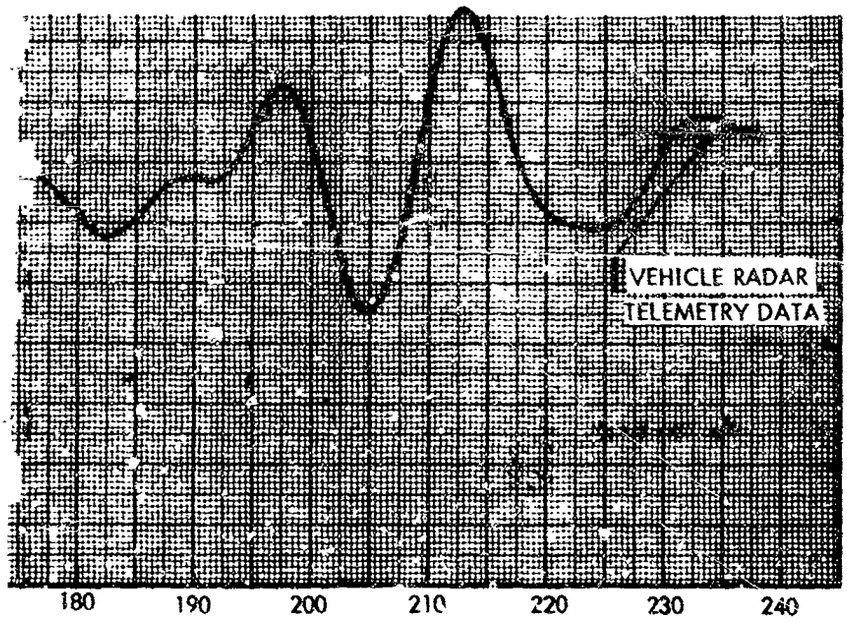

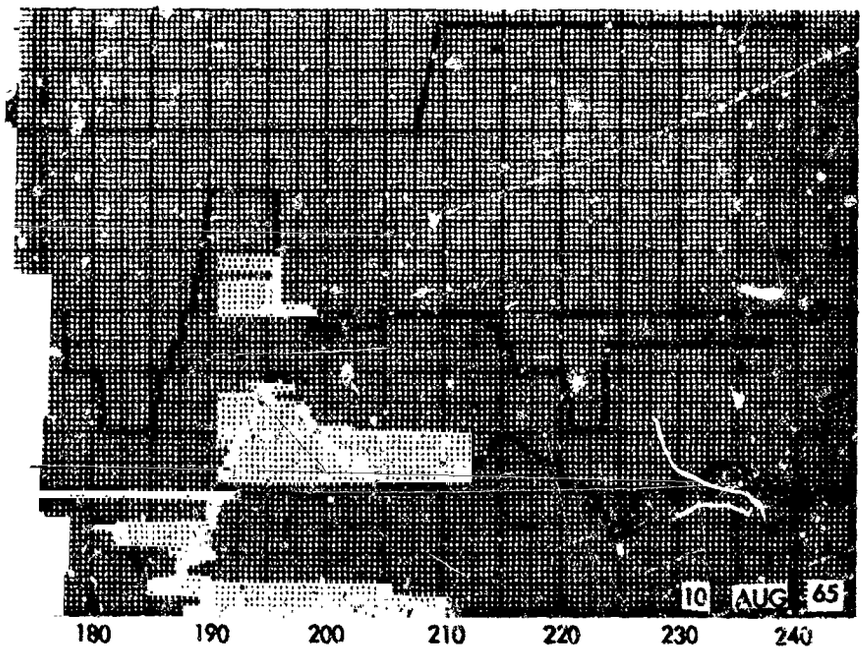

owed Test Vehicle Flight Data, Sink Rate Line Position and Bank Angle

FOLDOUT FRAME

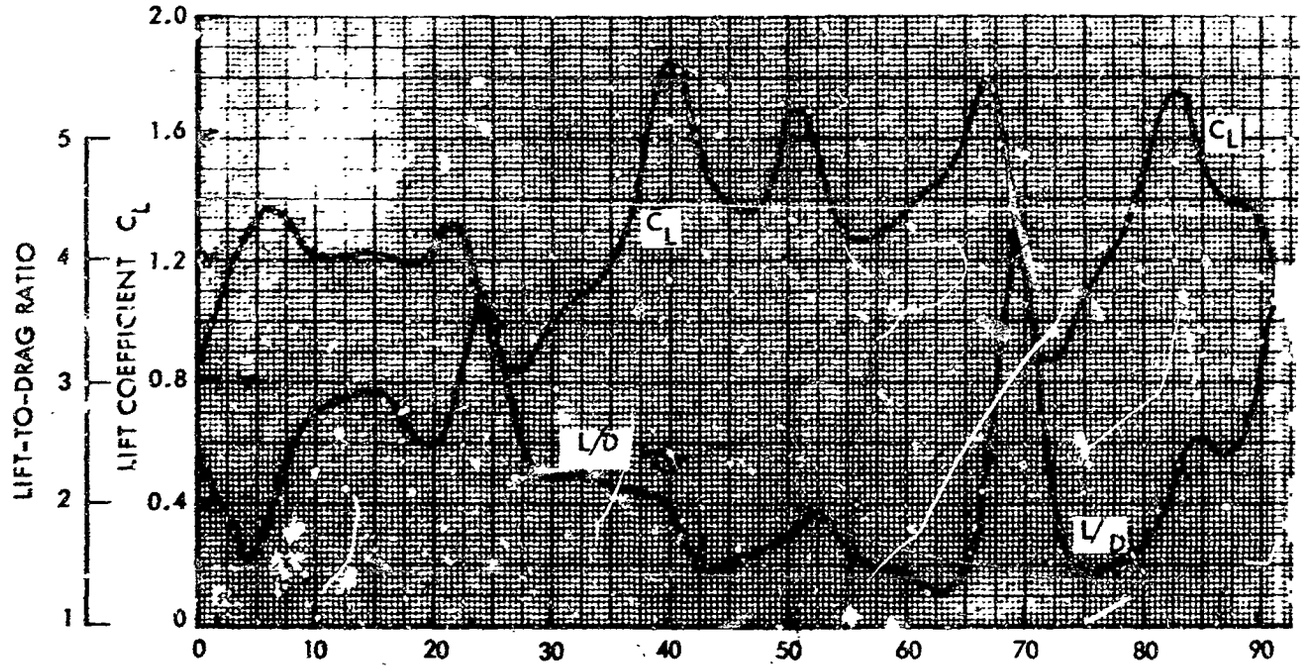

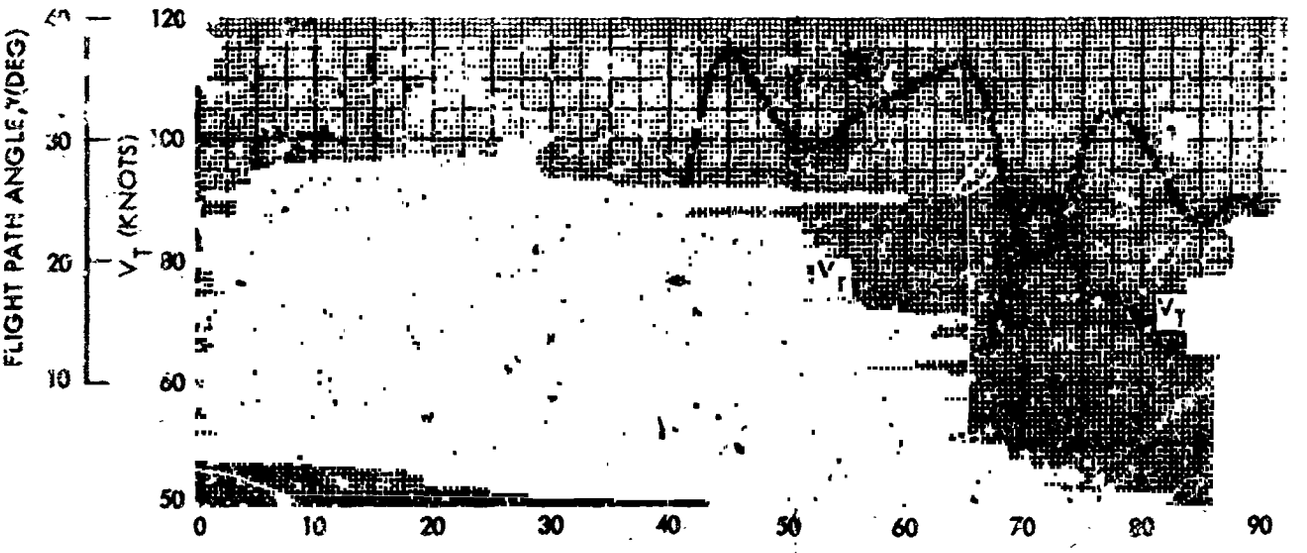

FOLDOUT FRAME 2

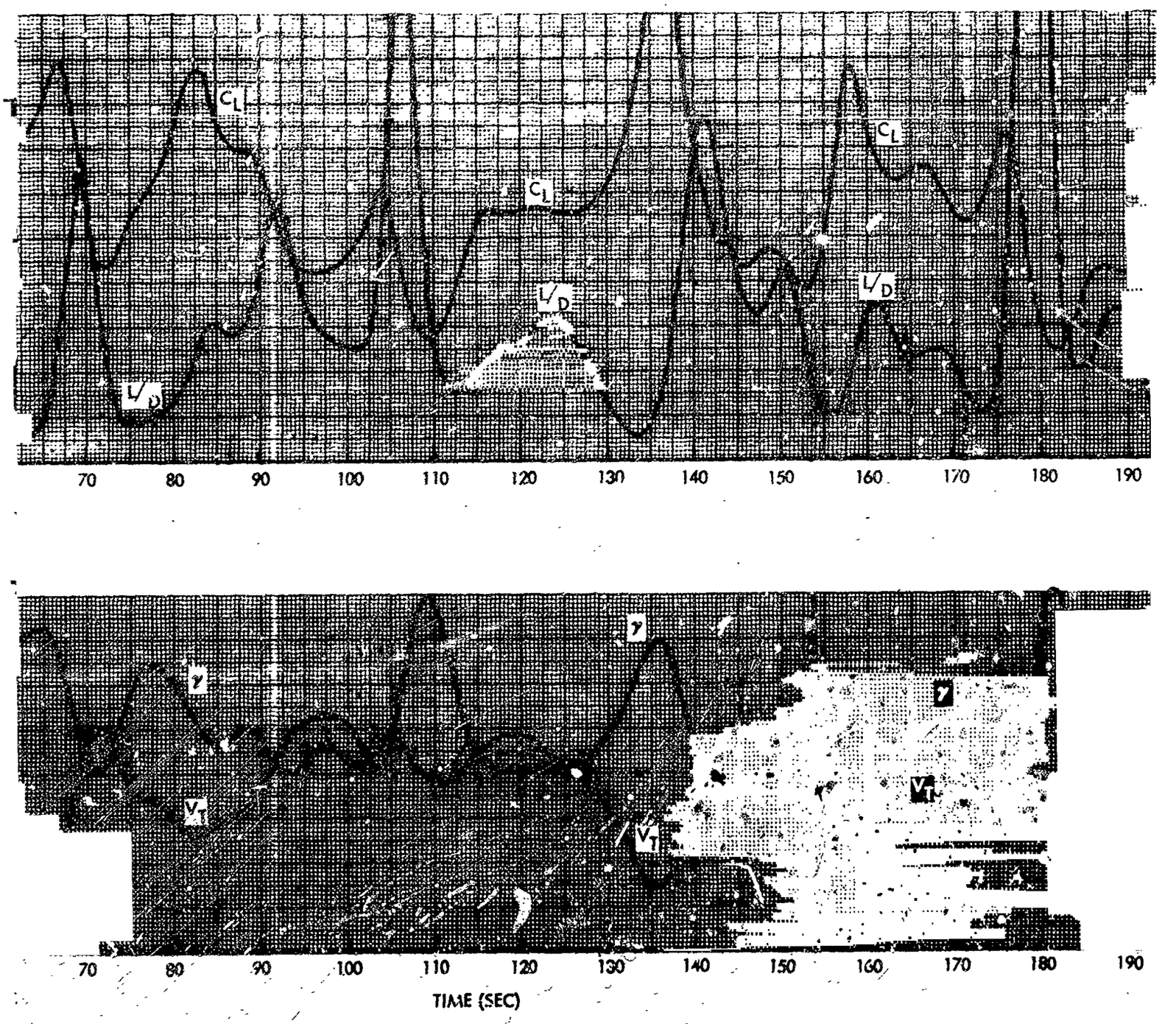

Figure 10. Nike Radar

FOLDOUT FRAME 3

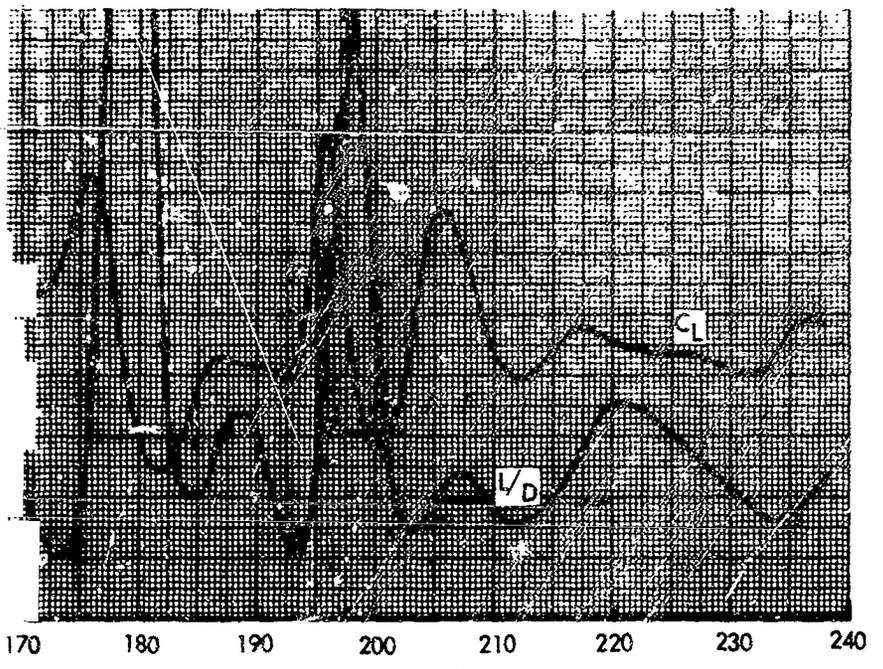

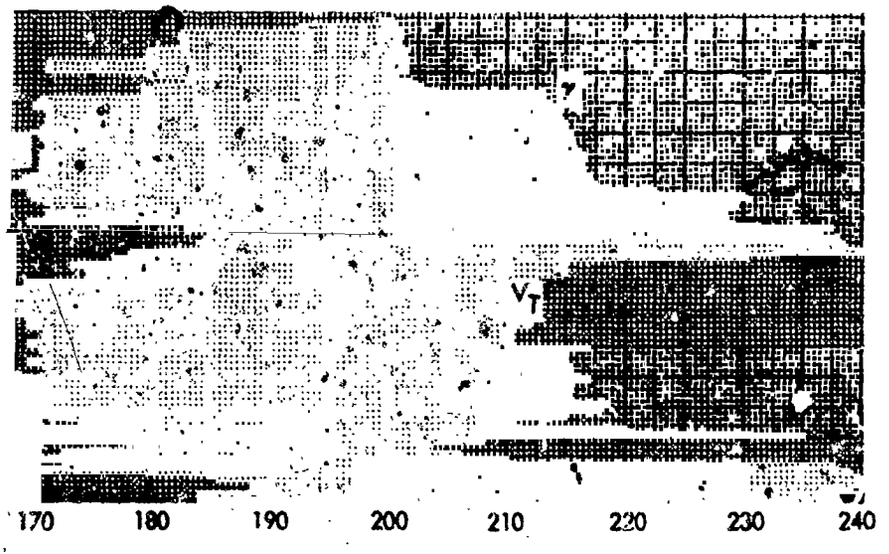

e 10. Nike Radar Aerodynamic Data, Flight 014

coefficient with pitch line position and indicate three dynamic oscillations following the pitch-up maneuvers at 35 seconds. This does not appear to be a stall oscillation, since the lift coefficient reaches a maximum of only 1.84, where wind tunnel predicts a maximum of about 2.0.

Comparison of the lift-to-drag ratio with the speed variation shows the high L/D at any time when there was a steep slope in the speed curve during an acceleration. During deceleration, the L/D was also lowered; but the effect was not as apparent, since the drag approaches the weight instead of zero.

Determination of aerodynamic data based on flight test results involved a process of elimination of the data scatter by a selected point method. Near-equilibrium stabilized data were selected at a particular time during the flight. A presentation of selected points of L/D and lift coefficient (Figure 11) indicates the variations and the amount of scatter. The size of the symbol represents the range of scatter at the selected points. The fairing of the curve appears somewhat optimistic until a comparison was made with the wind tunnel data (Figure 12) and the large excursions of data when individual points are presented.

The drag estimate from the December 1964 flights* was also included for reference. These data (Figure 12) were used as a basis for the flare computations presented later in this report. Figure 13 presents the drag polars and the data scatter of Figure 12 presented in a different form.

Further data were taken from the selected points to determine longitudinal control effectiveness (Figure 14) and to compare data predictions. Variation in sink rate from that calculated from test data is probably due to altitude and turning effects.

The TTV performance with a high-lobe sail was updated based on the estimated aerodynamics and estimated combined rigging derived from the flight test data as analyzed at the conclusion of Phase I. The present best estimate of TTV aerodynamics and performance presented in Figures 15 and 16 are compared to results obtained from half-scale wind tunnel test data.

The flare data were revised based on the best estimate of aerodynamics from the flight test data and are presented in Table 6. A line setting of $0.59\,\ell_1/\ell_k$ was recommended for preflare.

The longitudinal control effectiveness over the flight control range, as measured by the available lift coefficient, is below that which was predicted.

*Reference SID 65-196.

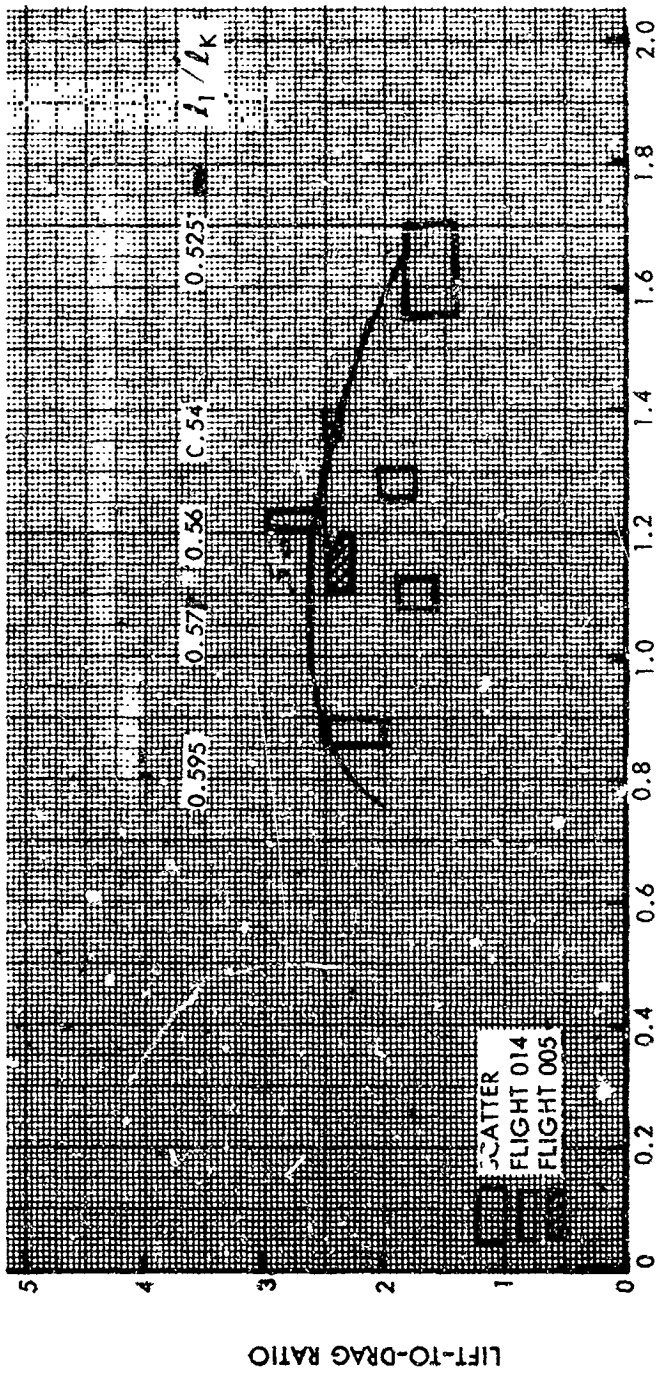

Figure 11. Selected Test Points: Lift-to-Drag Ratio Versus Lift Coefficient

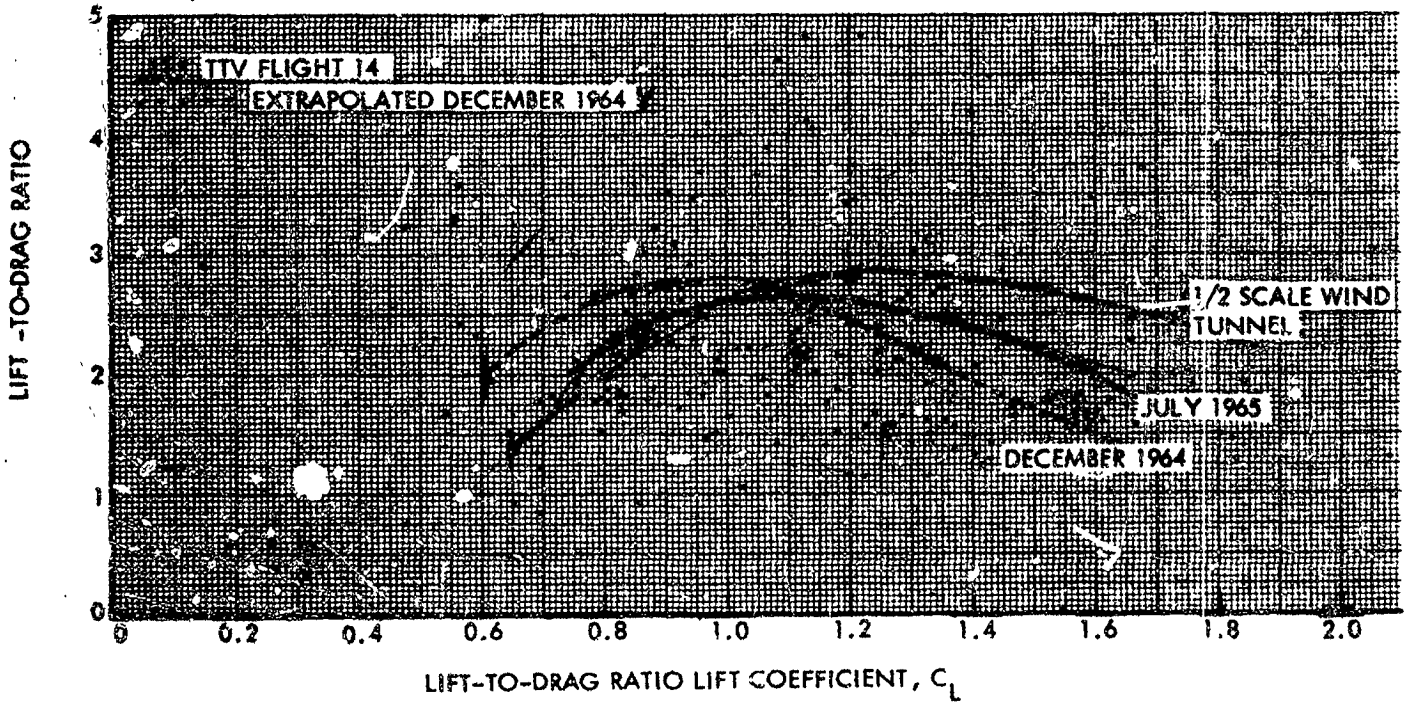

Figure 12. Aerodynamic Data: Lift-to-Drag Ratio Versus Lift Coefficient, Flight 014

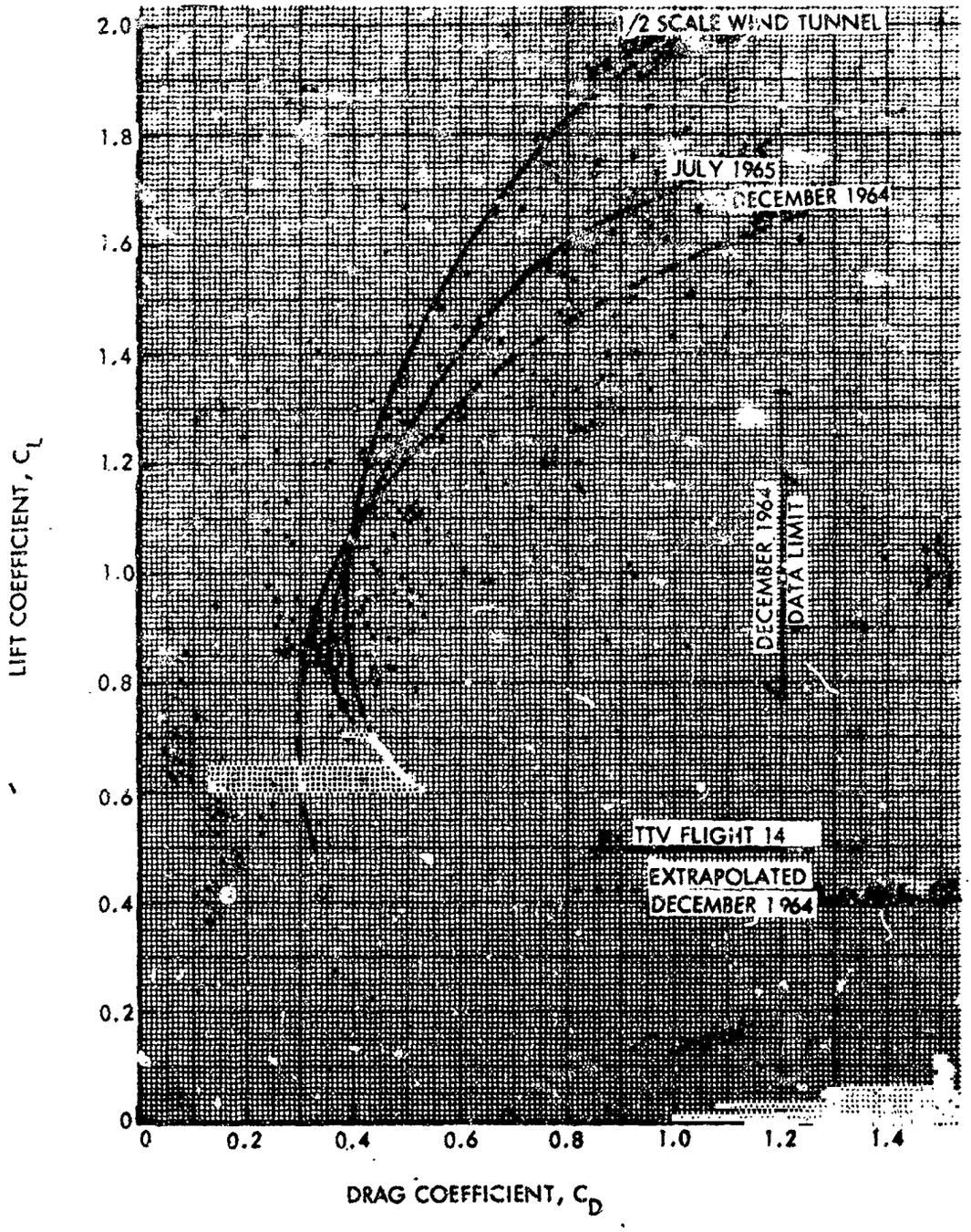

Figure 13. Aerodynamic Data: Drag Polar, Flight 014

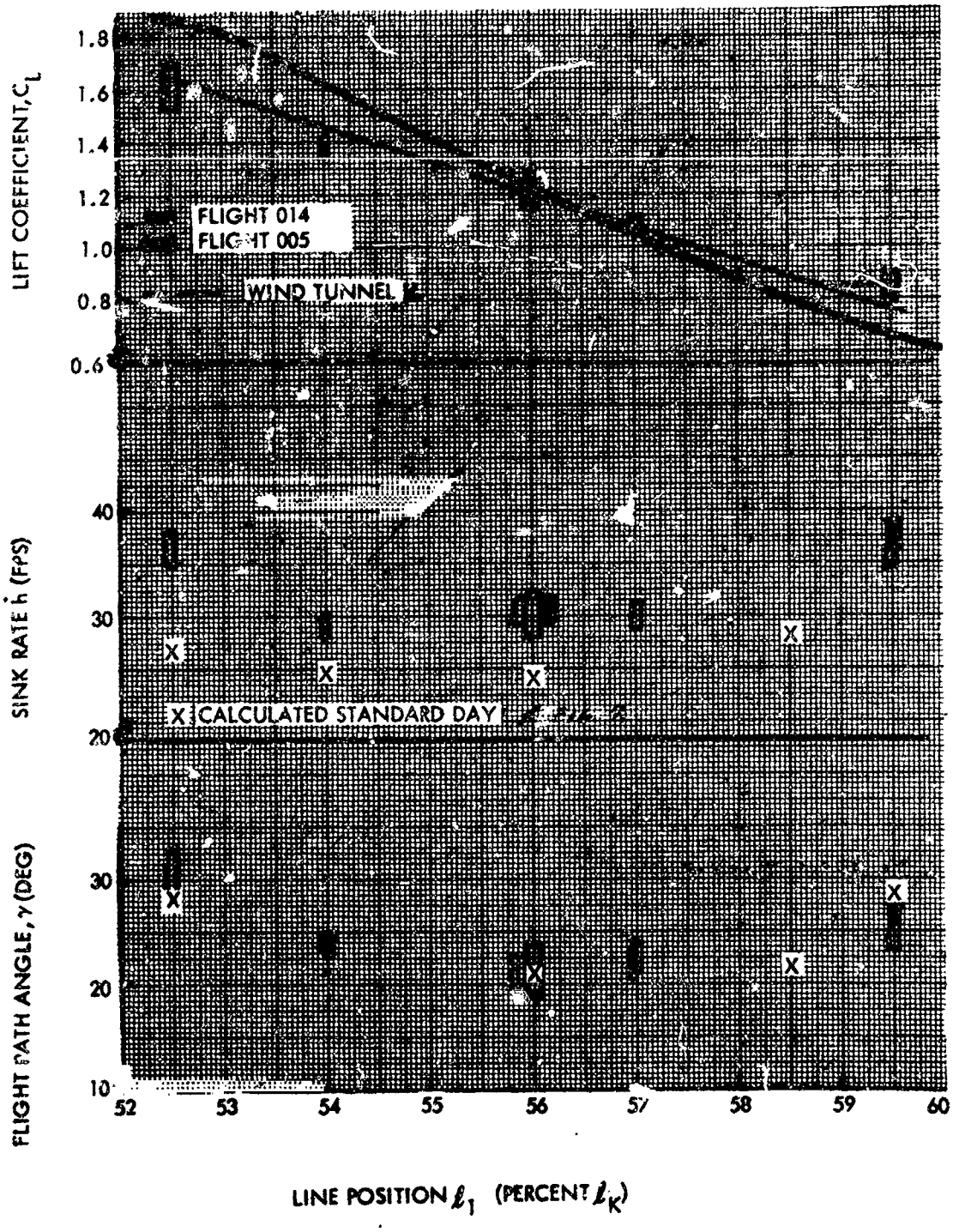

Figure 14. Selected Test Points: Lift Coefficient, Sink Rate, and Flight Path Angle Versus Line Position

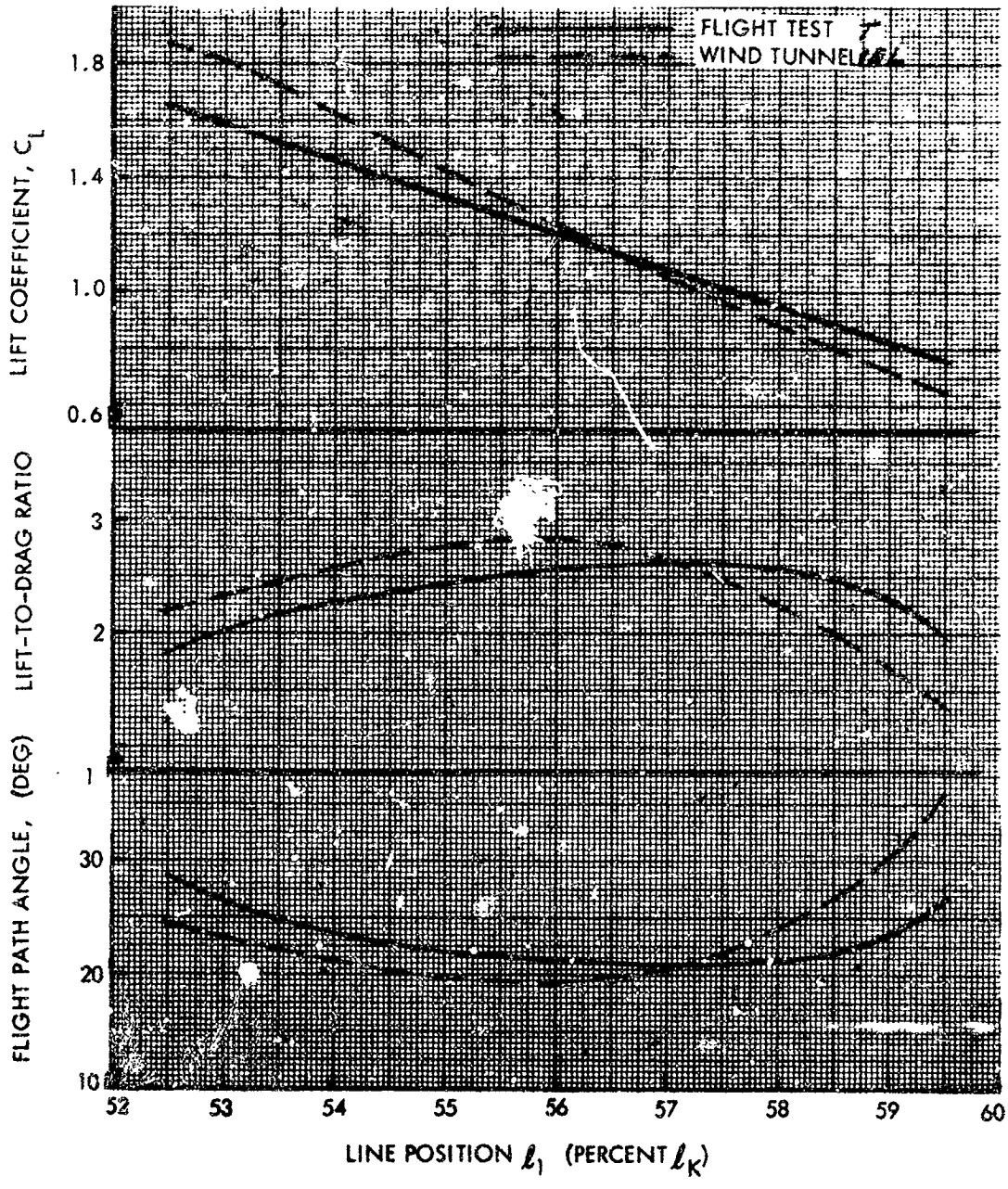

Figure 15. Aerodynamic Data: Lift Coefficient, Lift-to-Drag Ratio, and Flight Path Angle Versus Line Position

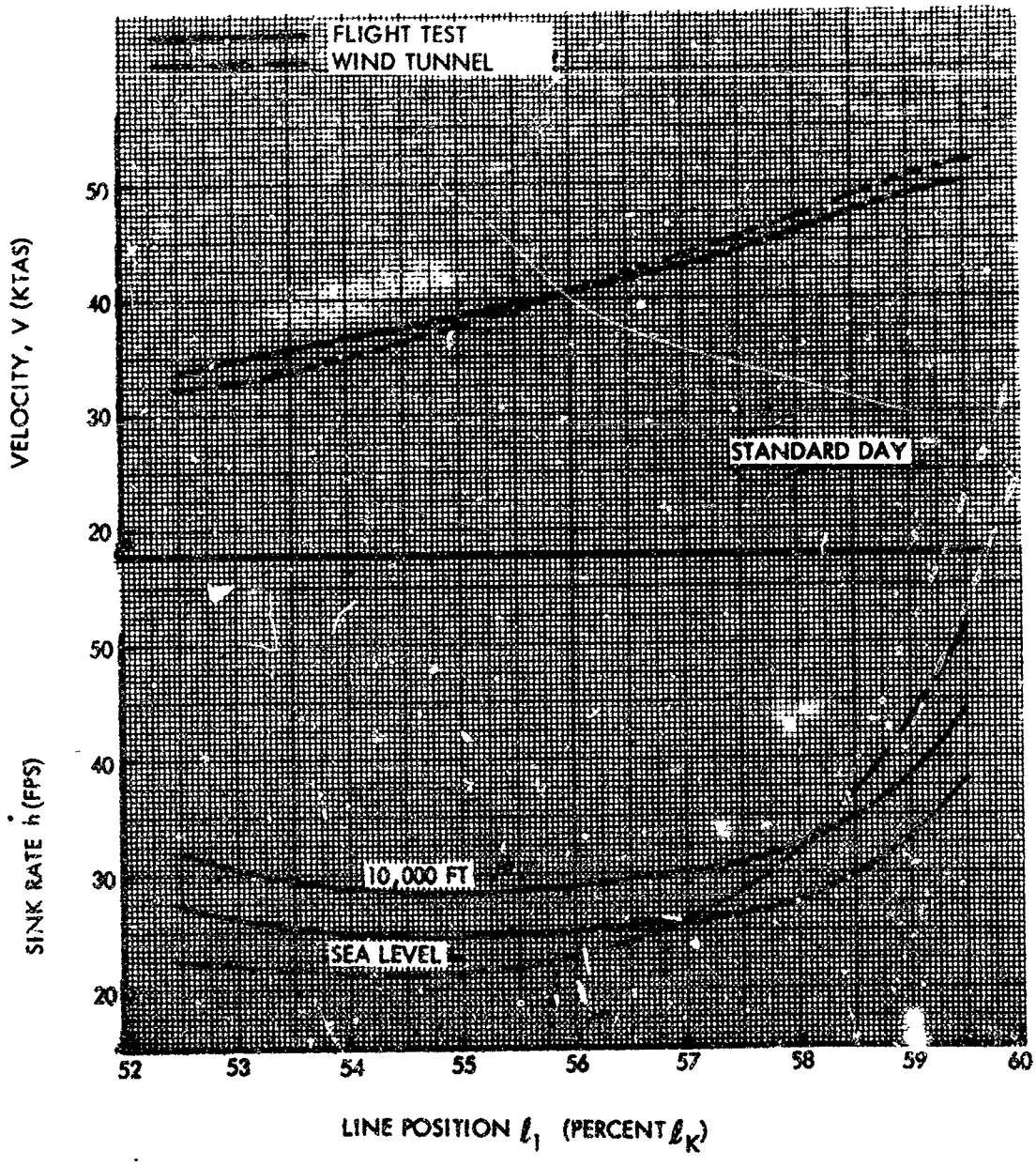

Figure 16. Estimated Performance for High Lobe Wing

Table 6. Recommended Flare Data

Preflare			at $\dot{h}$ = -10 fps		at $\dot{h}$ = -17.5 fps	
l_l/l_k	C_L	$\dot{h}$	Δn	Δt	Δh	Δt
0.59	0.82	36	10.9	±0.15	37.6	±0.52
0.595	0.76	39	13.9	±0.18	39	±0.50

$\dot{h}$ is the sink rate

Δh is the altitude differential at which the vehicle is at or below a given sink rate, e.g., $\dot{h}$ = -10 fps.

Δt is the allowable lead or delay time required to land within given sink rate limits.

Analysis of sink-rate data from Phase I was made by two methods in three different conditions. Where Nike radar tracking was available, a minimum sink rate was determined from tracking data. Analysis of film data with landscape background was used to determine sink rates associated with the flare and landing. These data (Table 7) are presented together with the lift coefficient at preflare, as determined from Nike radar tracking and the line travel for flare. During the first PTB flights, full pitch-down was not achieved because of an opposing load and insufficient time of control input. The Nike radar minimum sink rates were taken at the point along the flight path where the tracker recorder minimums. The two columns, taken from film, recorded both a touchdown sink rate and, in the case of an early flare command in which the flare was high, the minimum sink rate.

Analysis of the data from Phases I and II shows a lack of steady-state data for higher lift coefficients and for steady-state turns at any condition. The data from the PTB flights was of little value without Nike radar, since the on-board film gave uncertain line positions and times.

A time history of selected events for Flight 020 is presented in Figure 17. Nike radar was available for tracking in this flight. The on-board attitude gyros were not used. A comparison of Nike radar sink rates to telemetry sink rates, from the vehicle radar altimeter, indicates fairly good agreement (Figure 17, Sheet 1). The vehicle radar does not function over 5000 feet above ground level and therefore is missing in the first portion of the plot. Following the flare in the air, sink rates become fairly large and the telemetry trace drops. A review of the sink rate calibration shows one amplifier becoming saturated and output decreasing as input increases above a certain level. It is important to note this, because some of the later preflares also give doubtful readings. Another significant factor to mention here is noted by the bank angle (ϕ) change associated with the trim shift for the flare in the air.

The aerodynamic data obtained from this flight were above average, because there were short periods wherein flight approached equilibrium at different line settings (Figure 17, Sheet 2). The flare in the air produced the expected unusable aero data, and the tracker interference eliminated a turn. The effect of the acceleration term is apparent when comparing the L/D traces with the associated speeds. Selected points from the L/D, speed, and turn rate (Figure 17, Sheet 3) traces are used for later correlations.

Comparative data for Flight 022 are presented (Figure 18) even though the quality of the data from the tracker are unusable in most areas. It appears that the tracker was searching most of the time. This was the first

Table 7. Phase I Summary of Sink Rate Data

Flight	C_L Preflare	Line**	Travel**	Nike-Radar $\dot{h}$ min (ft/sec)	Film $\dot{h}$ min* (ft/sec)	Touchdown ($\dot{h}$*) (ft/sec)
002	≈0.9	No film		22	17	17
003	≈0.9	-2.0	+14.0	15	14	16
004	No tracking	-4.0	+13.0	No tracking	9	27
005	0.8 to 0.9	-11.0	+7.3	16	16	30
006	0.8 to 0.9	-6.0	+15.0	13	15	15
007	≈0.6	-11.0	Late flare****	6	No flare	32
008	No tracking	-13.0	+16.0	No tracking	12	12
009	No tracking	-13.0	+17.0	No tracking	5 Gust	5
010	No tracking	-13.0	+15.0	No tracking	10	20
011	No tracking	No film		No tracking	17	17
014	0.8 to 0.85	-12.8	No flare	23	No flare	38
015	No tracking	-10.0	No flare	No tracking	No flare	34
016	No tracking	-9.3	+11.0	No tracking	10	10

C_L = lift coefficient

*From film analyses (sink rate)
**Preflare — inches below pitch neutral of line length to keel length (l_1/l_k) = 0.56
***Flare — inches above pitch neutral
****Initialed at 50 to 60 feet

FOLDOUT FRAME

FOLDOUT FRAME 2

FOLDOUT FR

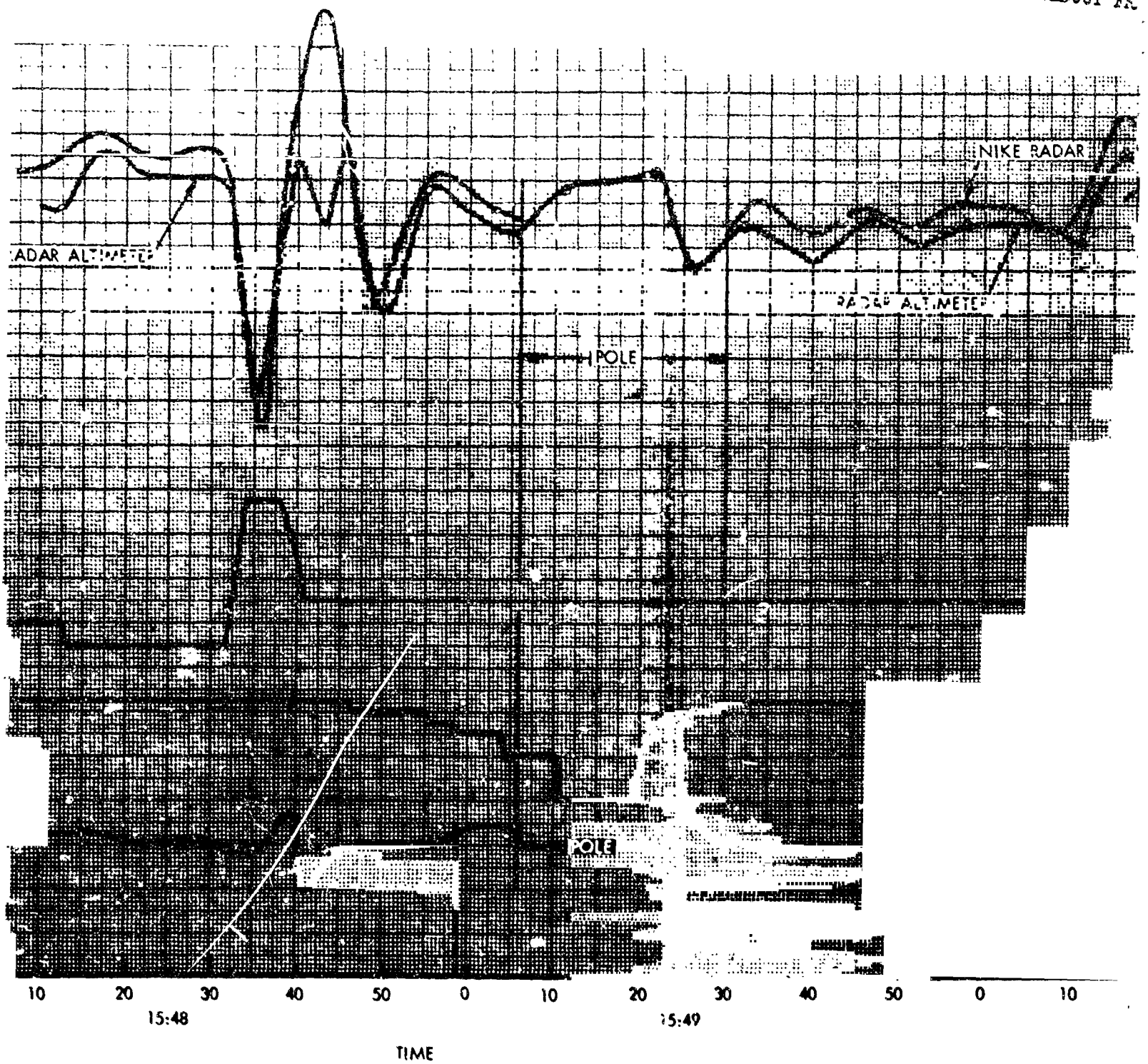

Figure 17. Flight 020 Time Histo

FOLDOUT FRAME 3

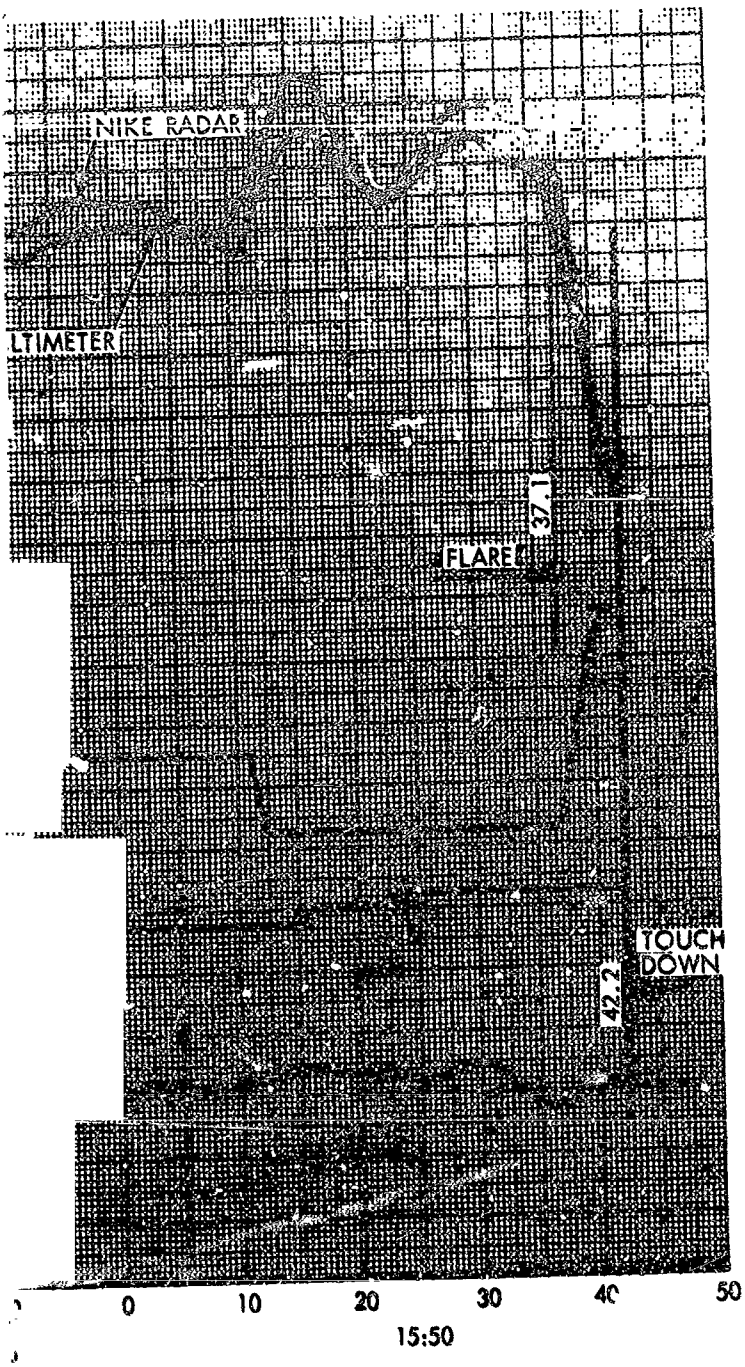

light 020 Time Histories (Sheet 1 of 3)

FOLDOUT FRAME 1

FOLDOUT FRAME 2

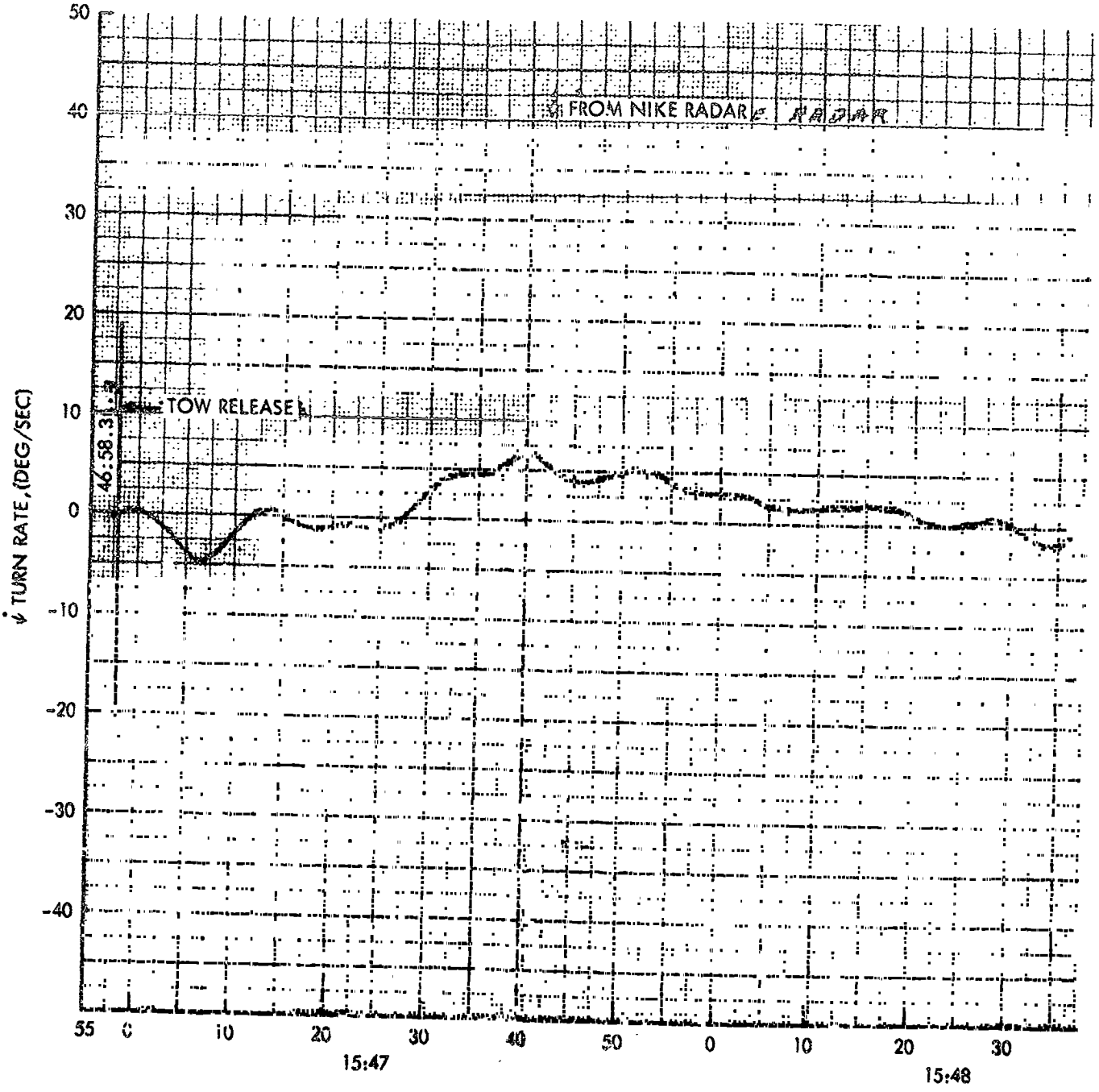

FOLDOUT FRAME 2

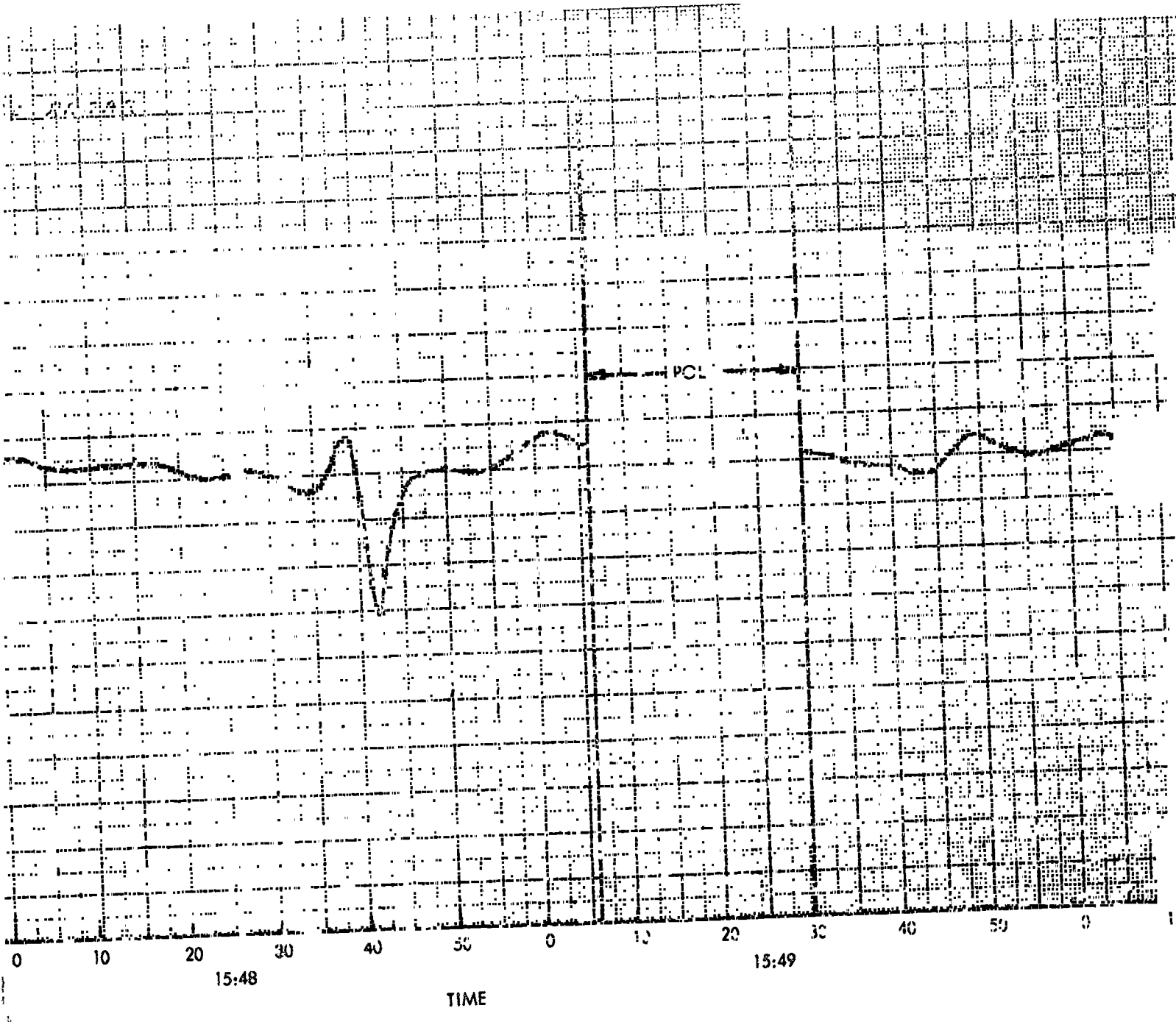

Figure 17. Flight 020 Time

FALLOUT FRAME 3

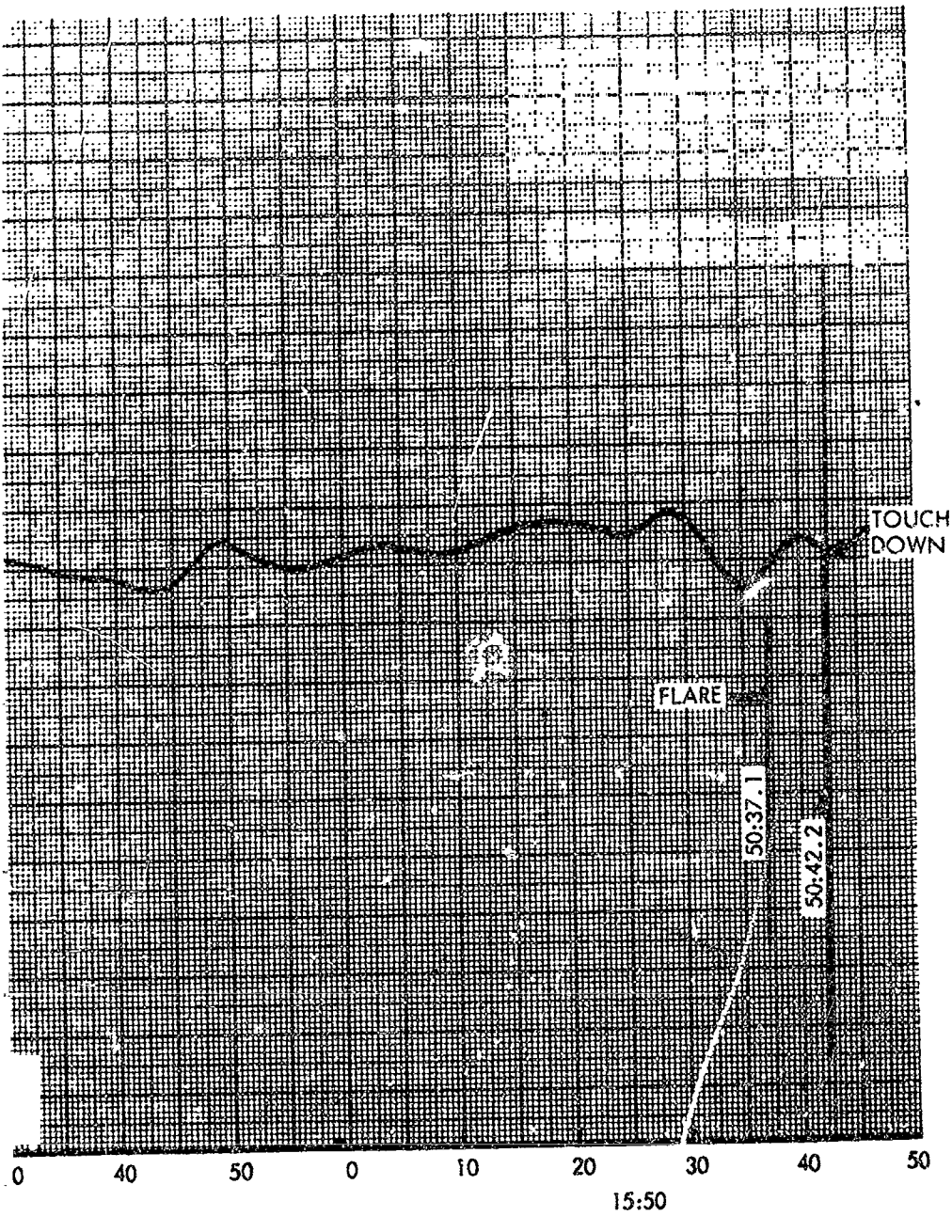

Figure 17. Flight 020 Time Histories (Sheet 2 of 3)

FOLDOUT FRAME /

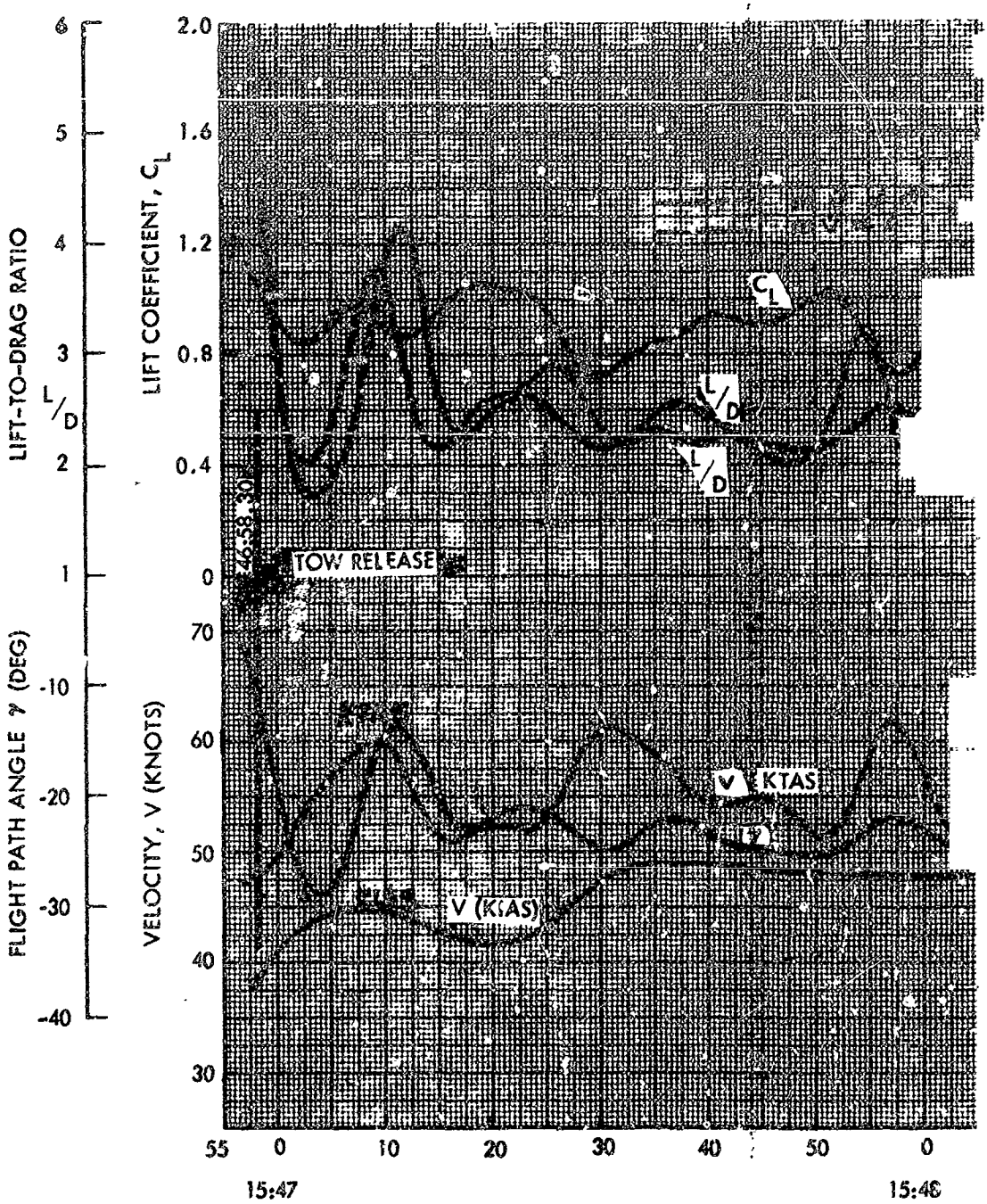

FOLDOUT FRAME 2

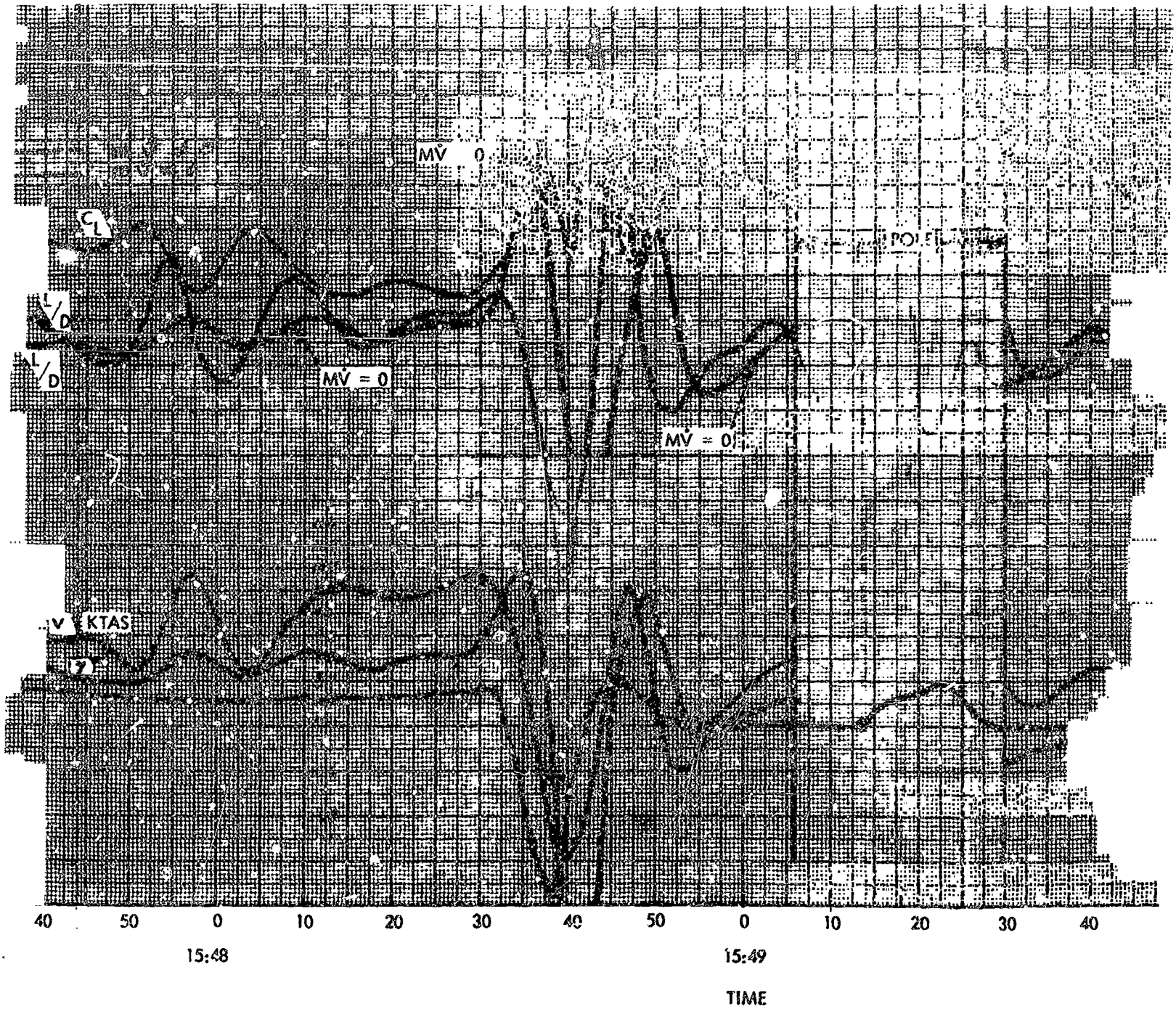

Figure 17.

FOLDOUT FRAME 3

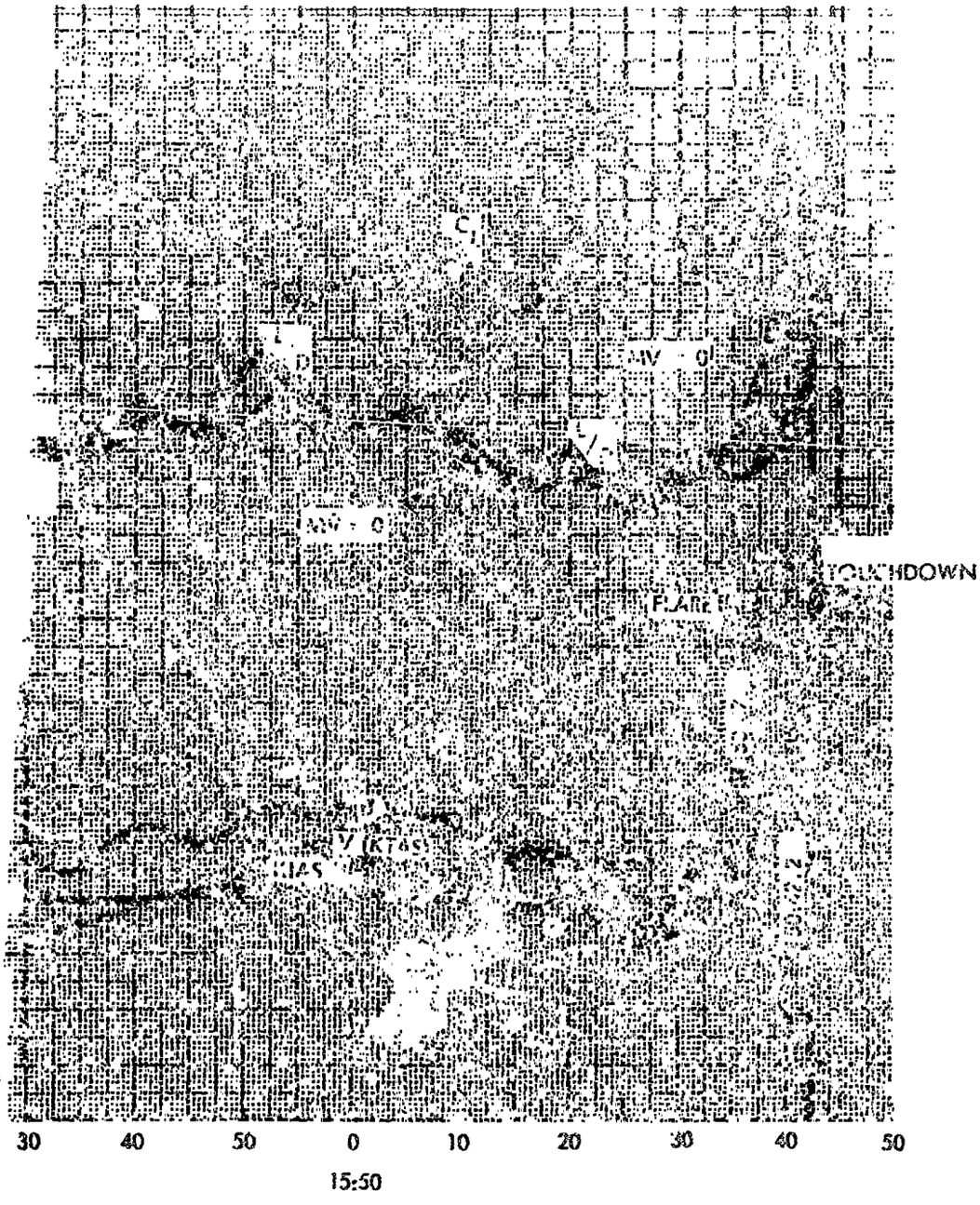

Figure 17. Flight 020 Time Histories (Sheet 3 of 3)

POLAROID FRAME 1

FOLDOUT FRAME

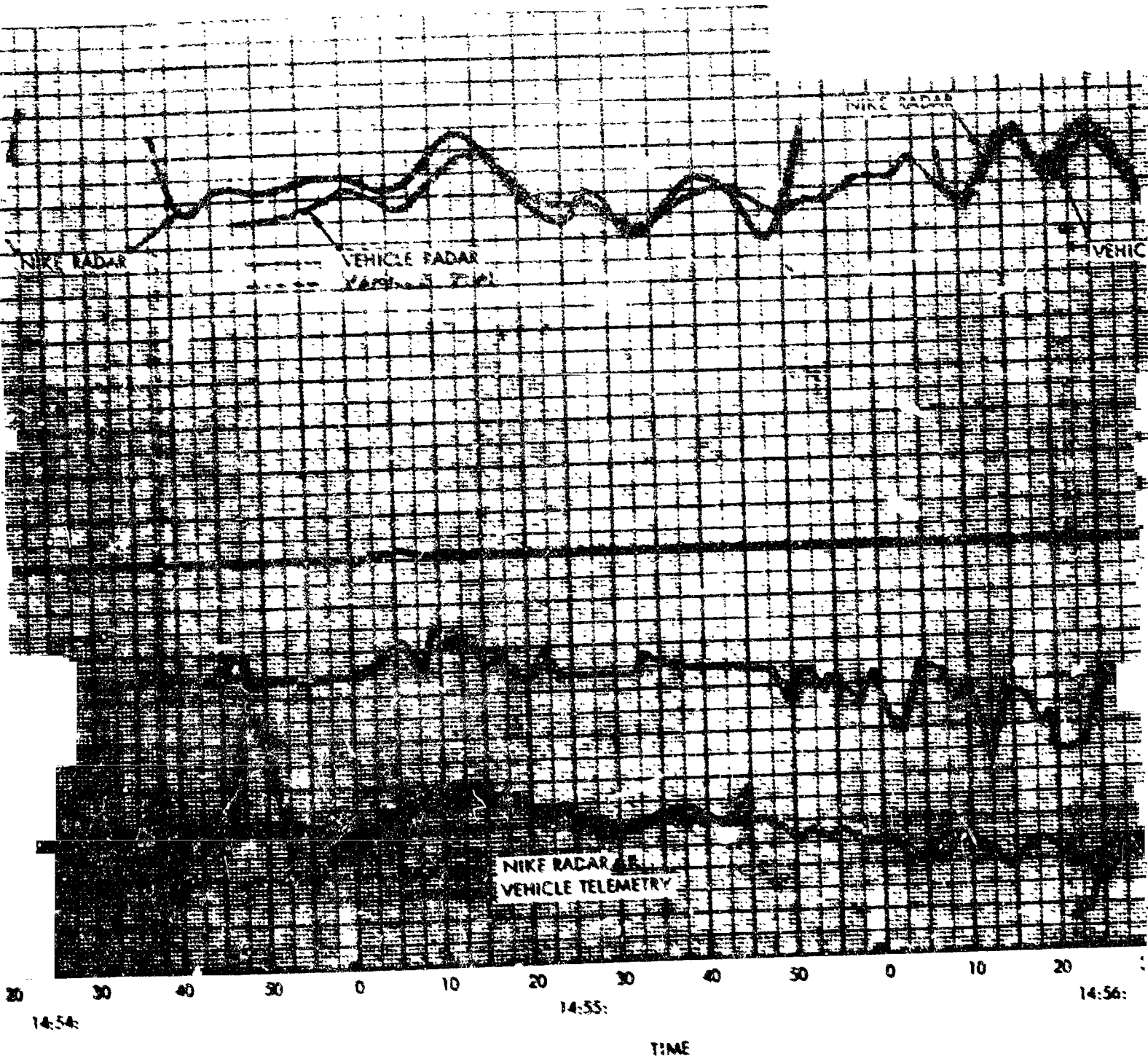

FOLDOUT FRAME 5

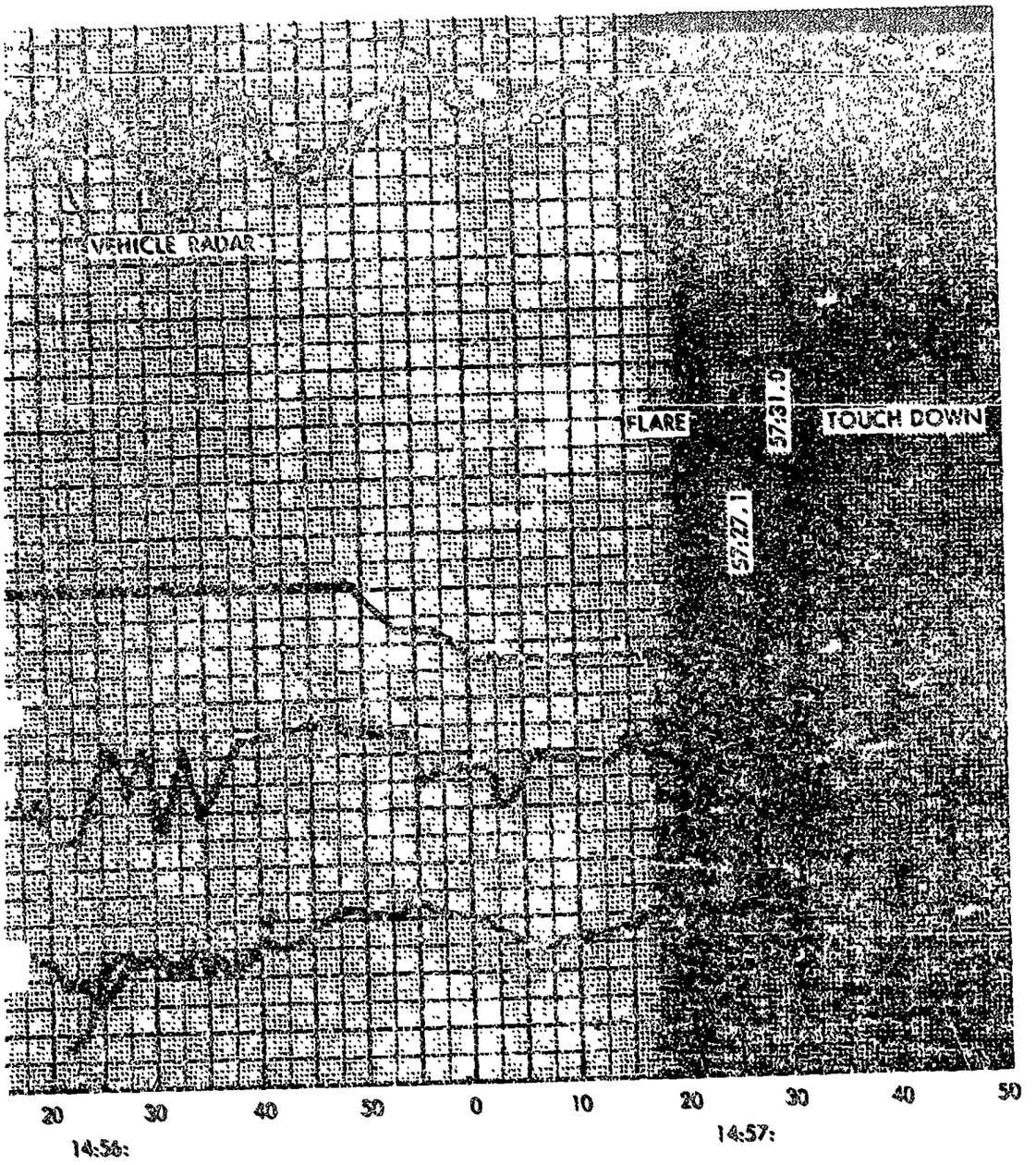

Figure 18. Flight 022 Time Histories (Sheet 1 of 2)

LIFT-TO-DRAG RATIO
LIFT COEFFICIENT, C_L
VELOCITY, V (KNOTS)
V
6
5
4
3
2
1
2.0
1.6
1.2
0.8
0.4
0
70
60
50
40
30
C_L
L/D
TOW RELEASE
V (KTAS)
MV ≠ 0
MV = 0
20
30
40
50
0
10
20
30
40
14:53:
14:54:

FOLDOUT FRAME 2

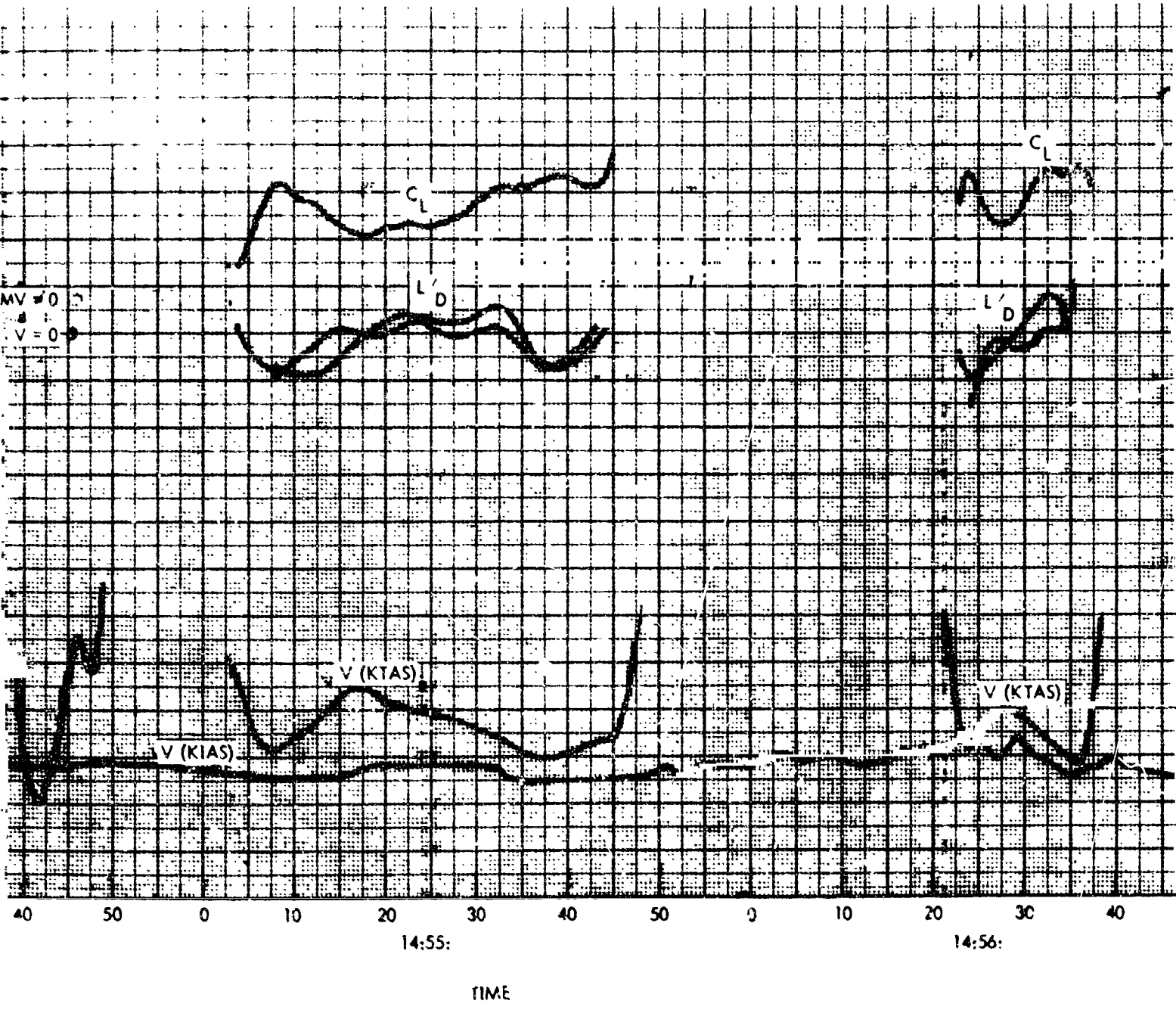

Figure 18. F

FOLDOUT FRAME 3

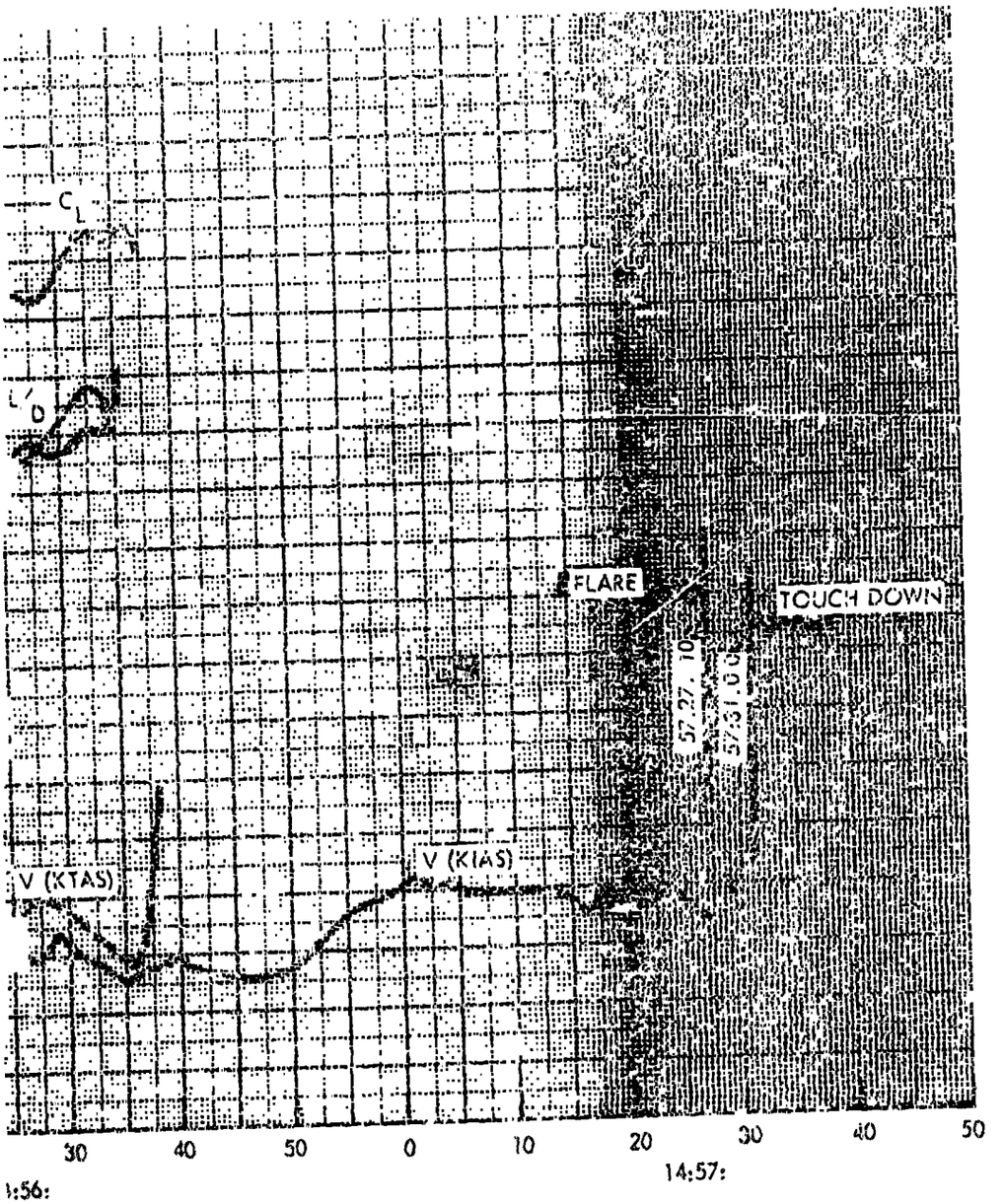

Figure 18. Flight 022 Time Histories (Sheet 2 of 2)

manned flight and was mostly navigation and roll response, both of which were very good. Small portions of L/D and speeds are available for correlation. Nike radar and telemetry gyros were not available for Flights 21 and 23 and, therefore, are not presented for data.

Flight 024 was the first flight of the second pilot, and an attempt to obtain data was hampered by Nike radar interference. Some usable data were obtained and is presented for comparative purposes in Figure 19. Once again, the Nike radar and telemetry sink rates and bank angles show close agreement (Figure 19, Sheet 1). The aero data (Figure 19, Sheet 2) variations are as expected. The differences in airspeed display the expected variations.

The angle data presented in Figure 19, Sheet 3, give a comparison of the turn rates from the two data sources, telemetry and Nike radar. The seven-point, curve-smoothing routine at one per second tends to change the Nike radar data so that the minor oscillations on telemetry data are missing. An analysis of the flight path angle and the vehicle attitude was made to determine angle of attack. The resulting wing angles were high over the flight range. The incidence angle was investigated to determine if it had changed. Measurement of wing angles were made from films of several flights and the incidence angle appeared to be in the correct range of from 30 to 35 degrees. Further investigation revealed that the probable error is in the attitude gyro.

The Nike radar sink rates compare very well with vehicle radar for Flight 025 (Figure 20, Sheet 1). The vehicle roll response when comparing bank angle to roll line position indicates the good roll effectiveness and, as on previous flights, the lag in system responses. Aerodynamic data (Figure 20, Sheet 2) display the lack of steady-state conditions. Again, the yaw rate comparison (Figure 20, Sheet 3) shows the smoothing tendency of the Nike radar data program.

The effect of elimination of the $-m\dot{v}$ term from the drag equation is apparent when Figure 21 is compared to Figure 12. The extreme peaks in L/D are avoided by this calculation method. The Phase I drag estimate still falls within the present scatter of data.

Data from the several flights were taken at selected points where steady state conditions were approached. These data were used for correlation purposes and presented in Figures 12, 13, 14, 22 and 23. Figures 11 and 22 present the best flight test data available on lift-to-drag ratios. There is a lack of data at the higher lift coefficients. The July 1965 Phase I data curve is fairly good for the present data. It may be a little high at the peak and somehwat low at low angle of attack, but for the present it will continue to be used for performance basis.

FOLDOUT FRAME 1

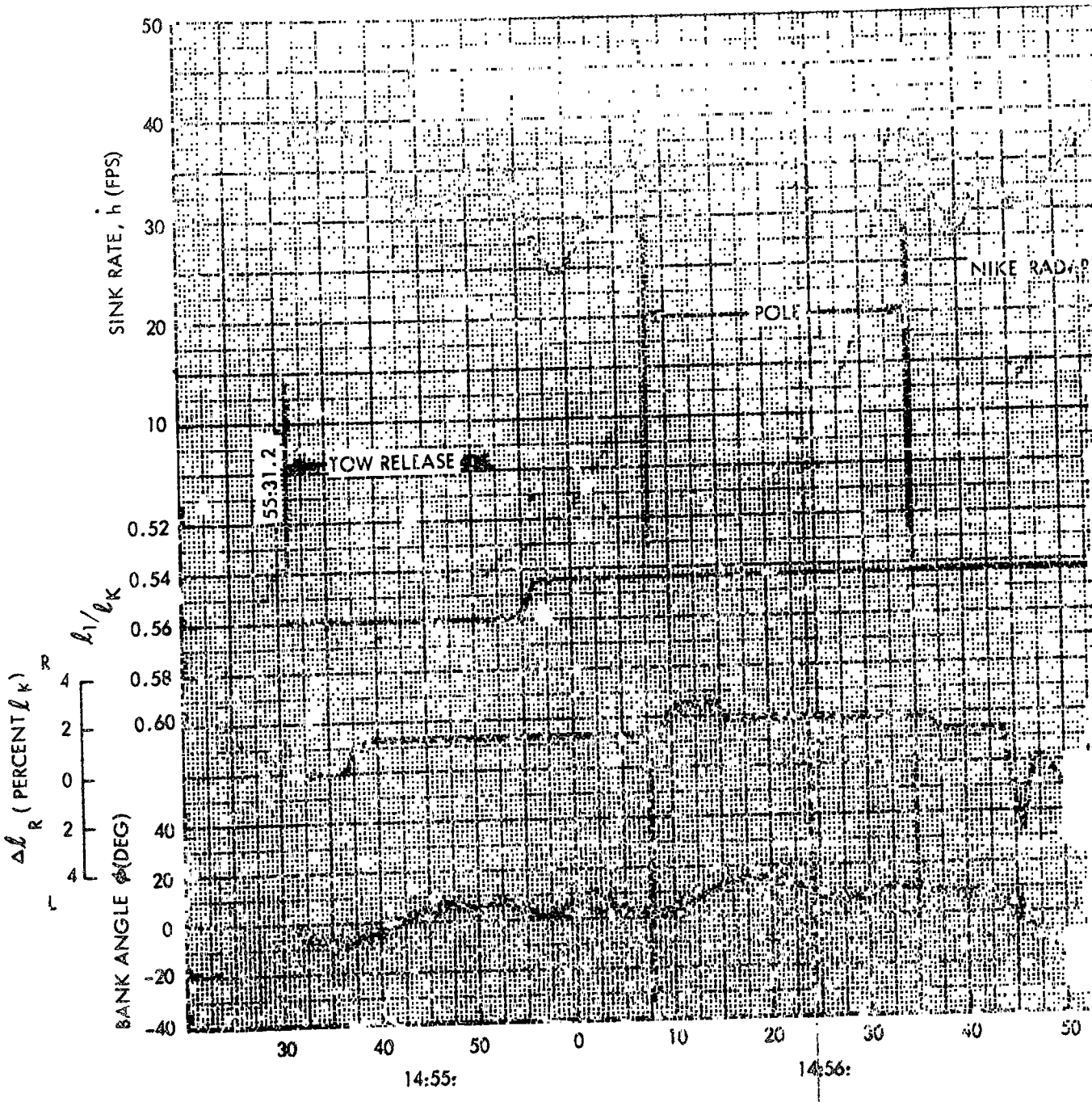

NC

FOLDOUT FRAME 2

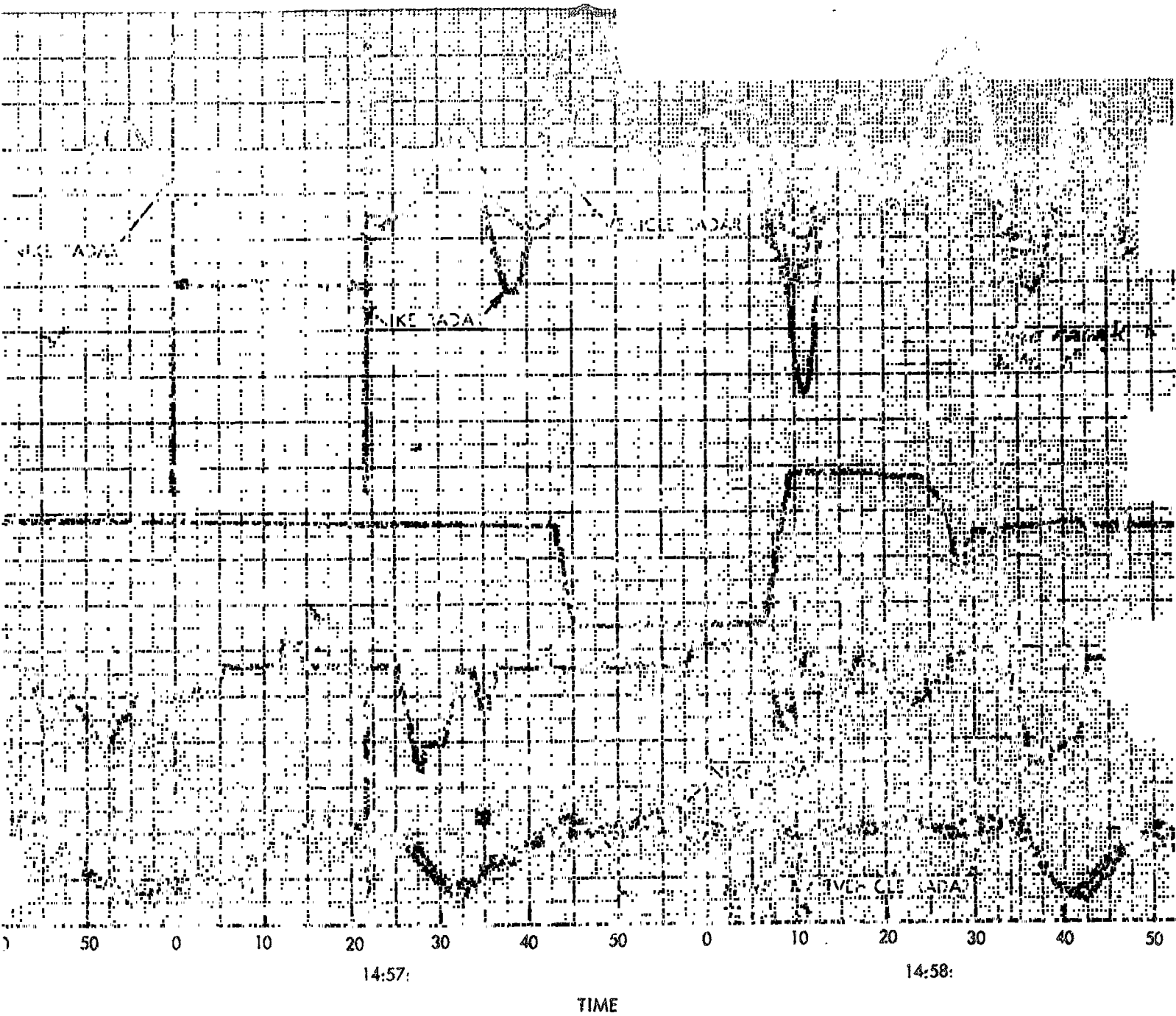

FOLDOUT FRAME 3

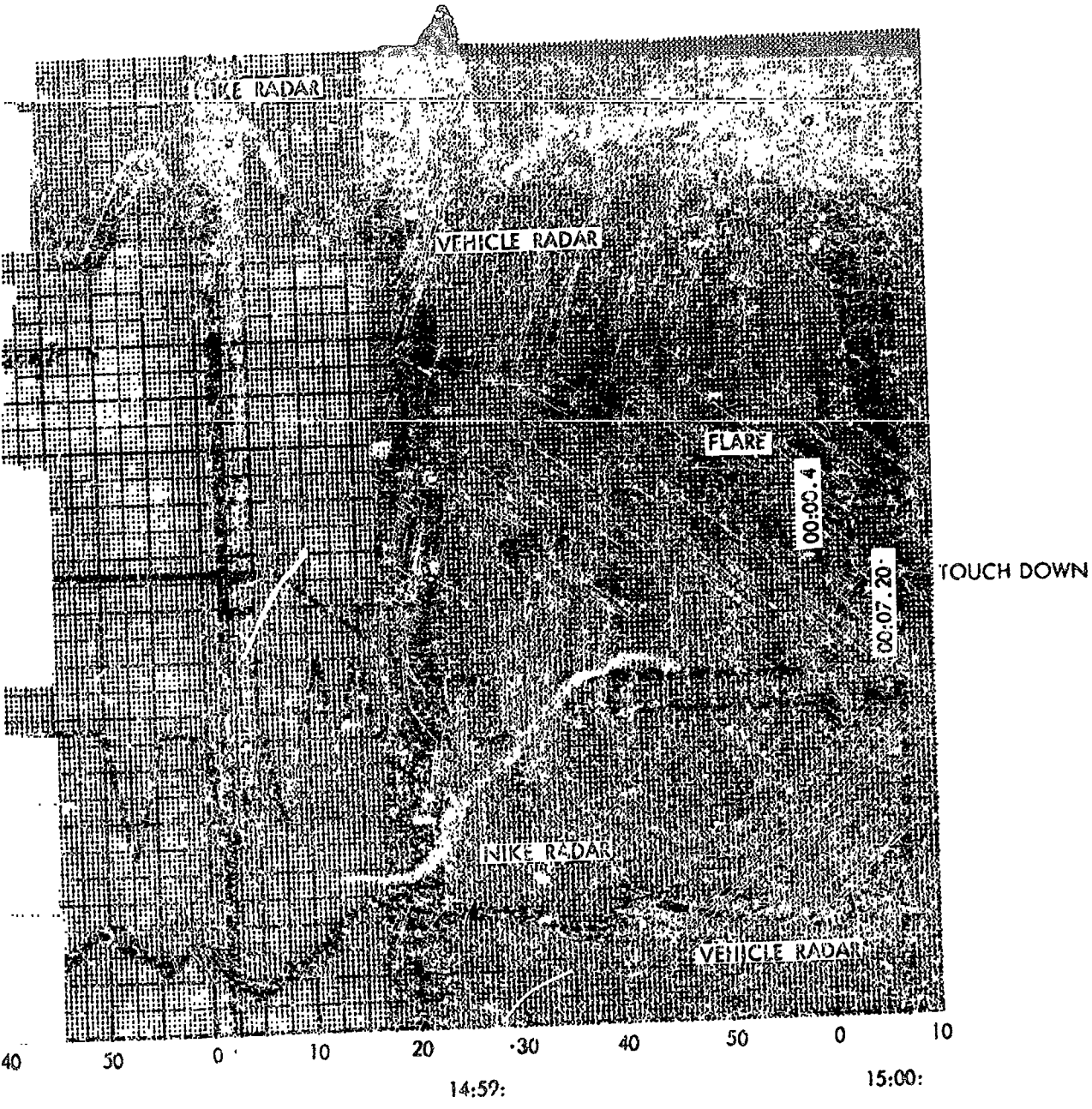

Figure 19. Flight 024 Time Histories (Sheet 1 of 3)

SID 65-1638

FOLDOUT FRAME 1

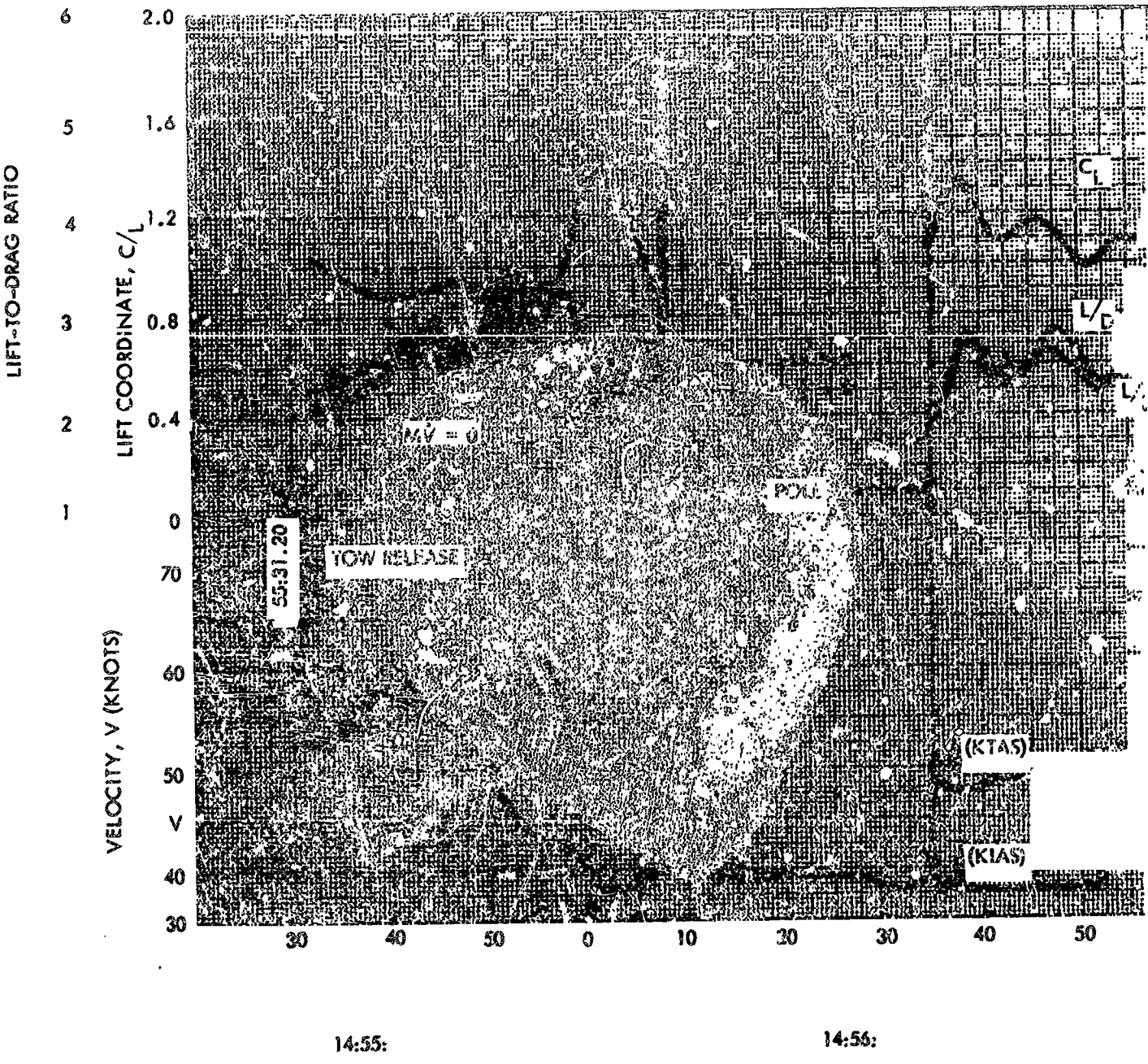

FOLDOUT FRAME 2

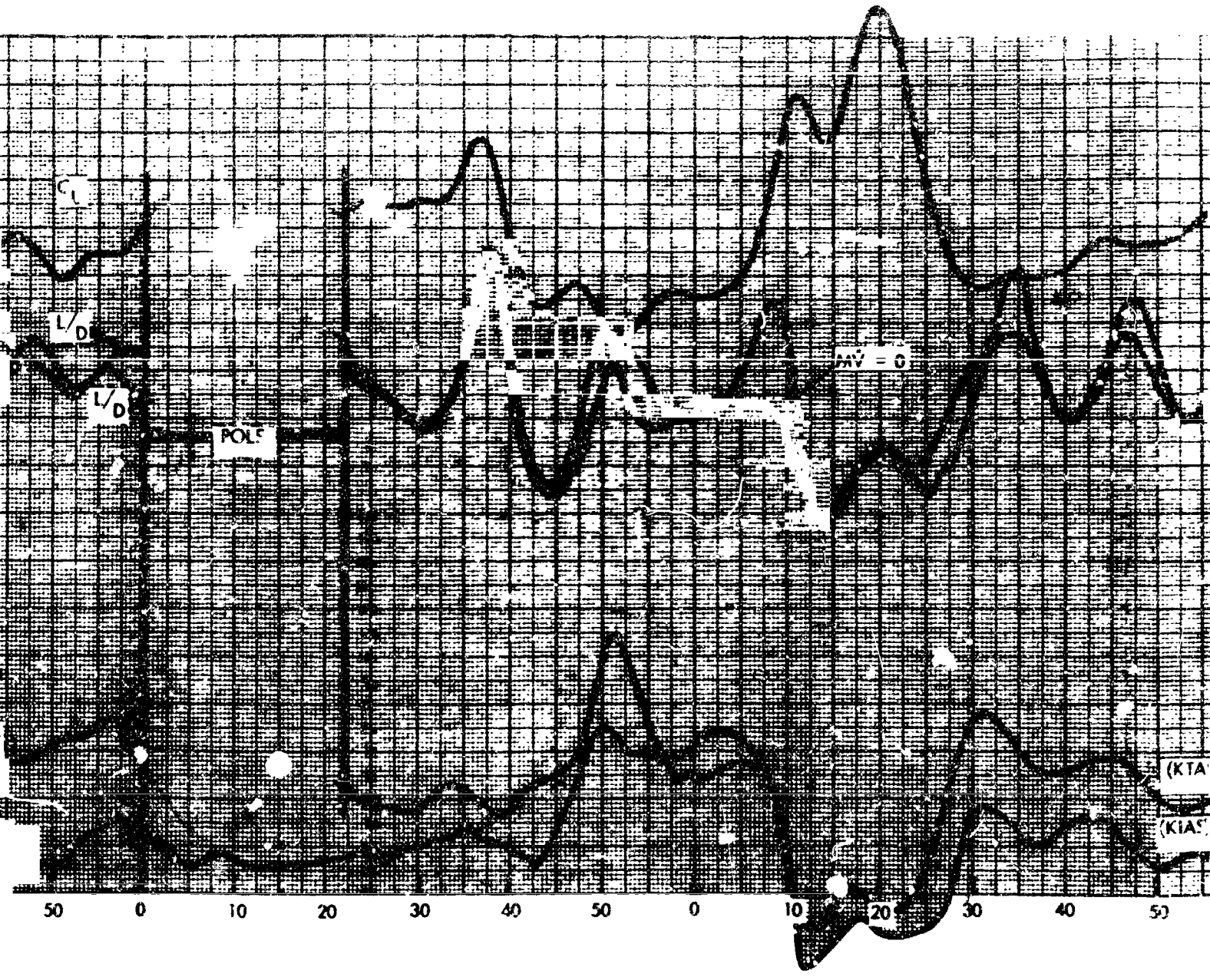

14:57:

14:58:

TIME

FOLDOUT FRAME 2

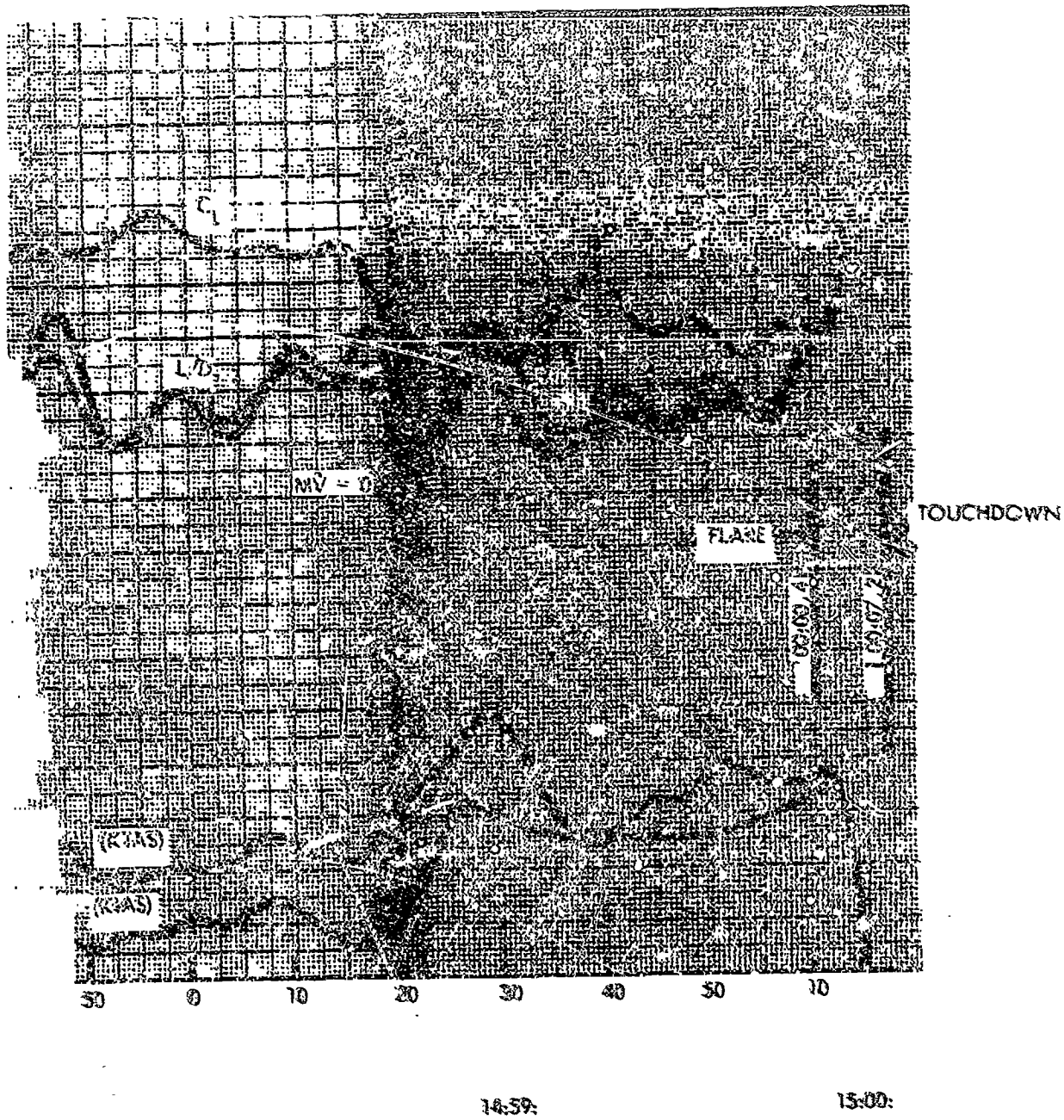

Figure 19. Flight 024 Time Histories (Sheet 2 of 3)

FOLDOUT FRAME 1

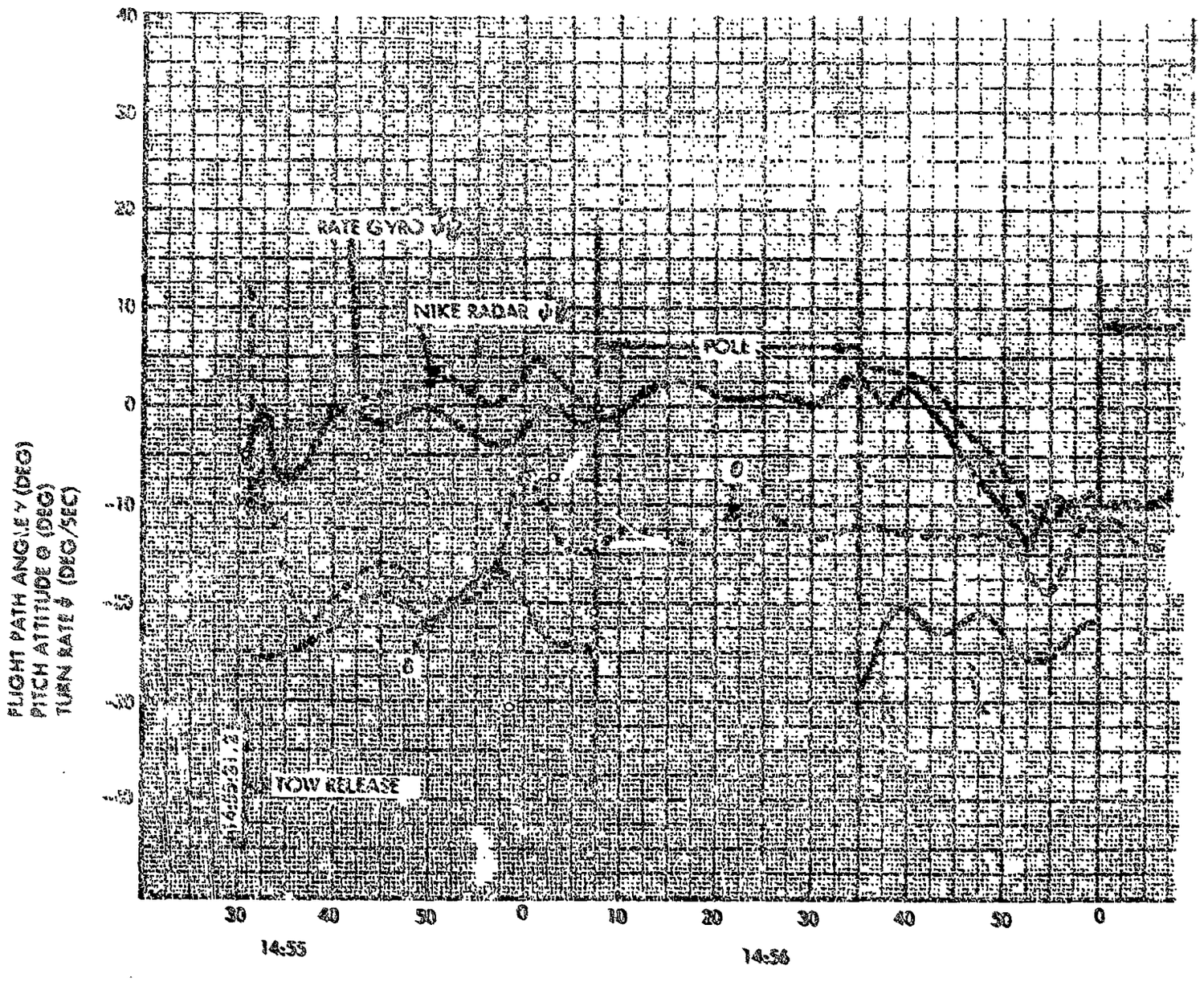

FOLDOUT FRAME 2

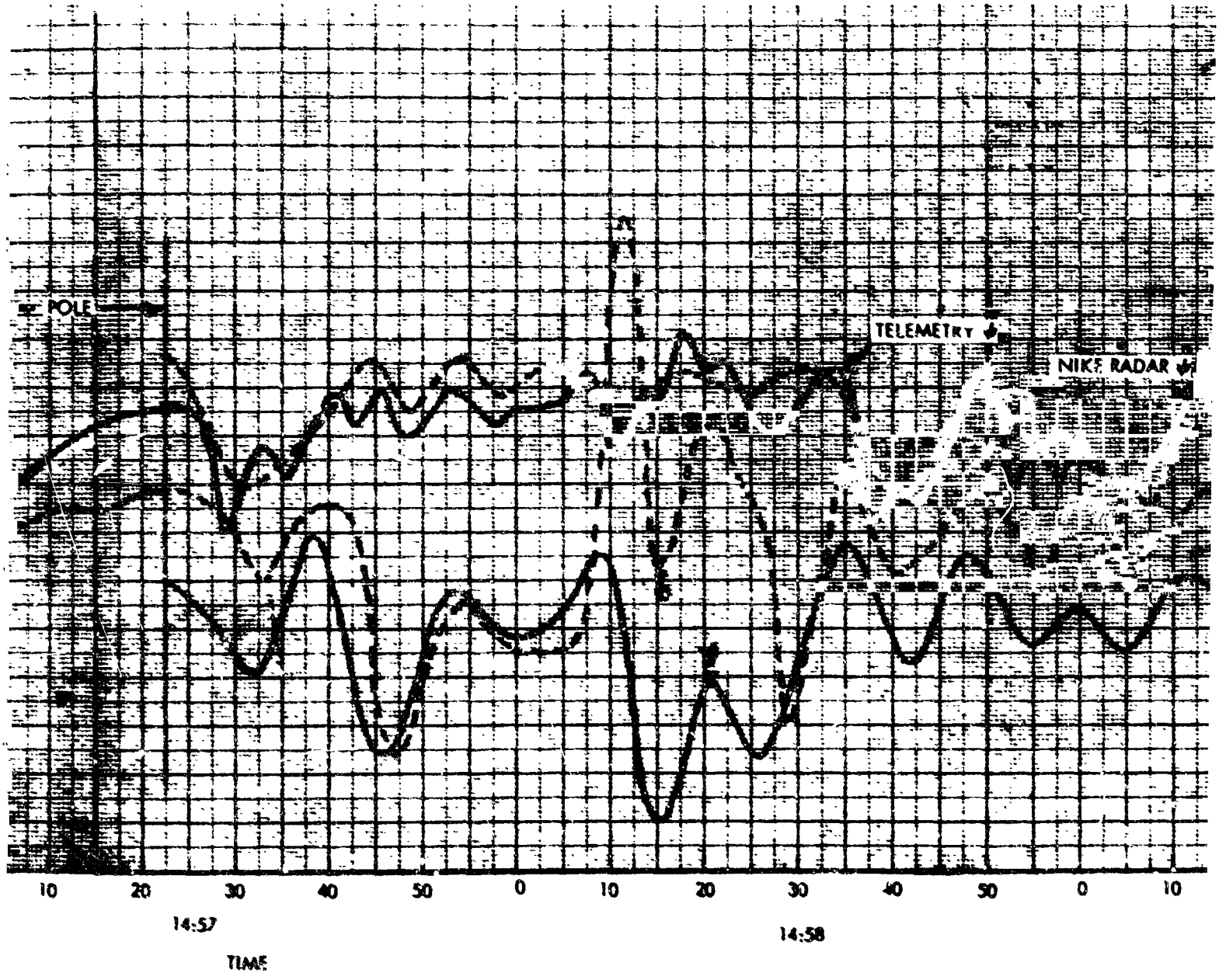

Figure 1

FOLDOUT FRAME 3

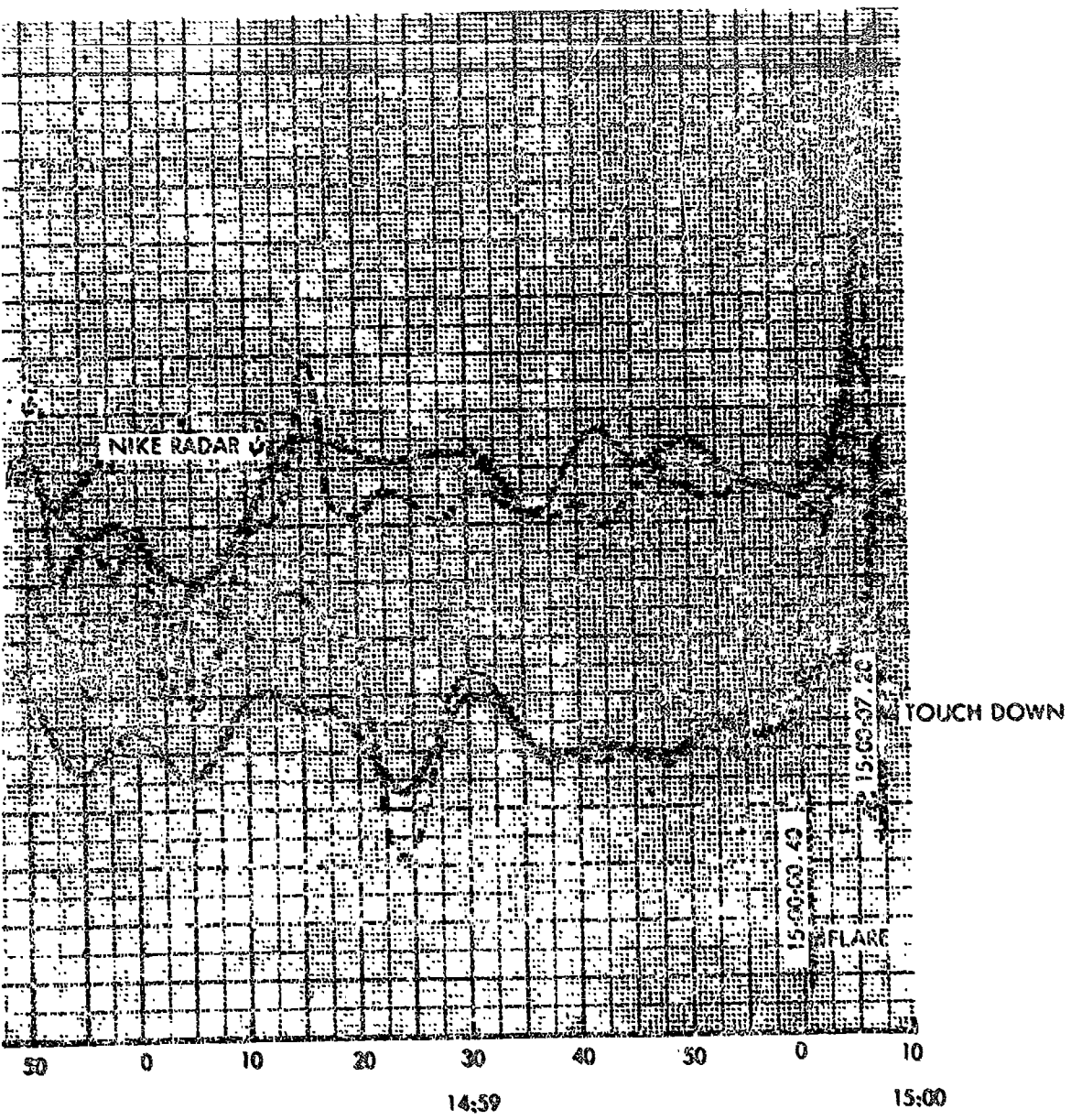

Figure 19. Flight 024 Time Histories (Sheet 3 of 3)

FOLDOUT FRAME 1

FOLDOUT FRAME 2

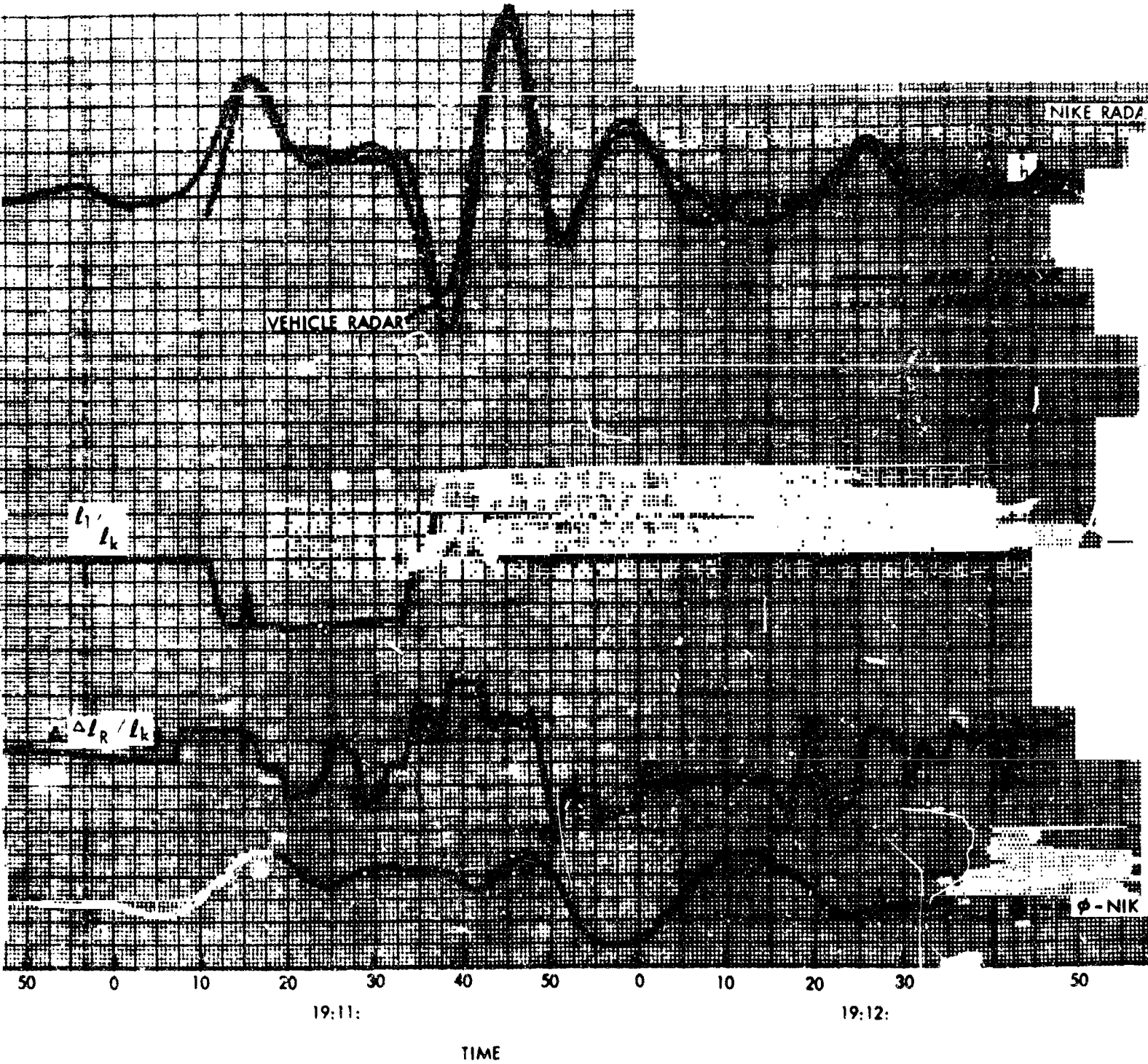

Figure 4

FOLDOUT FRAME 3

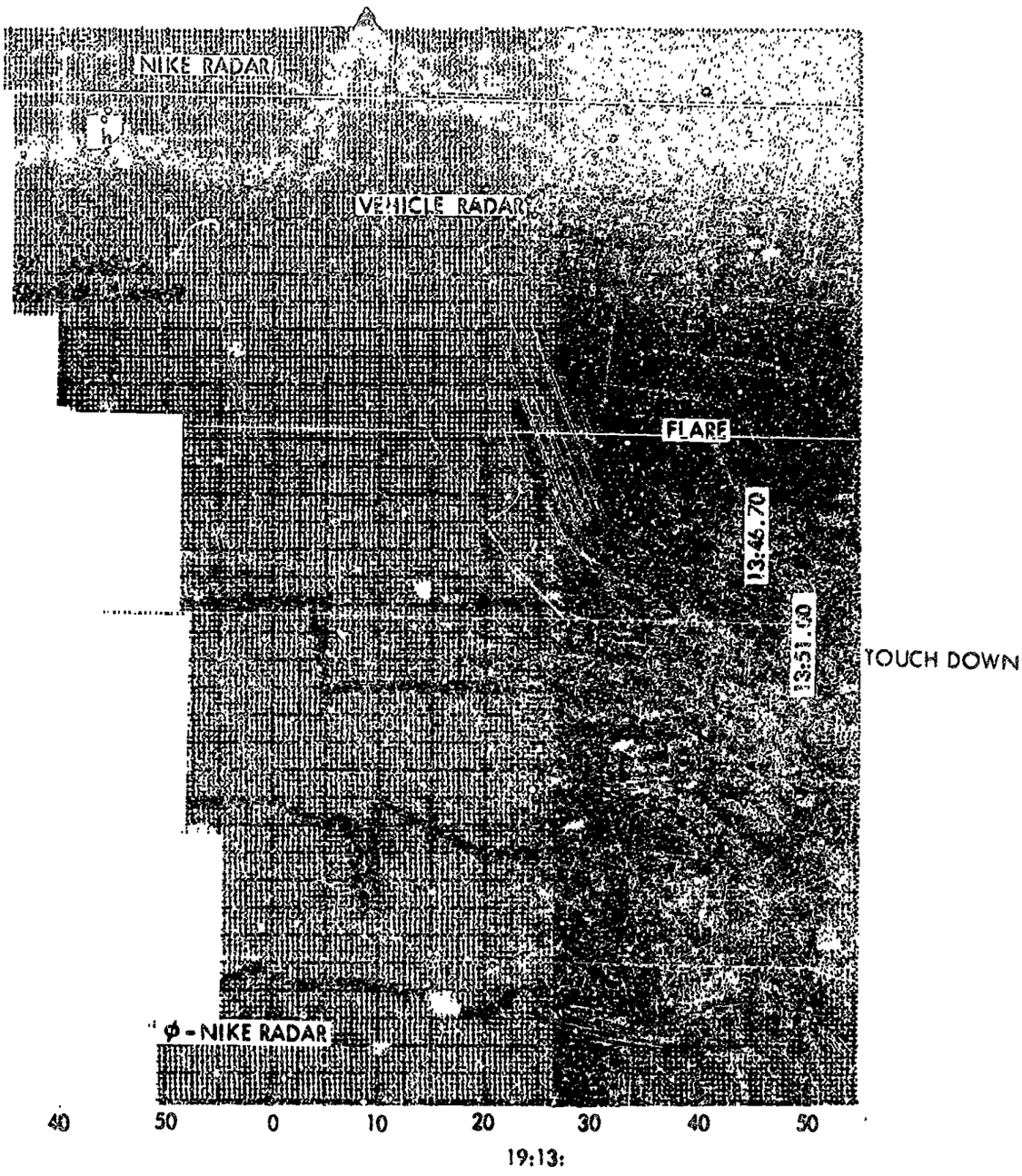

Figure 20. Flight 025 Time Histories (Sheet 1 of 3)

FOLDOUT FRAME 1

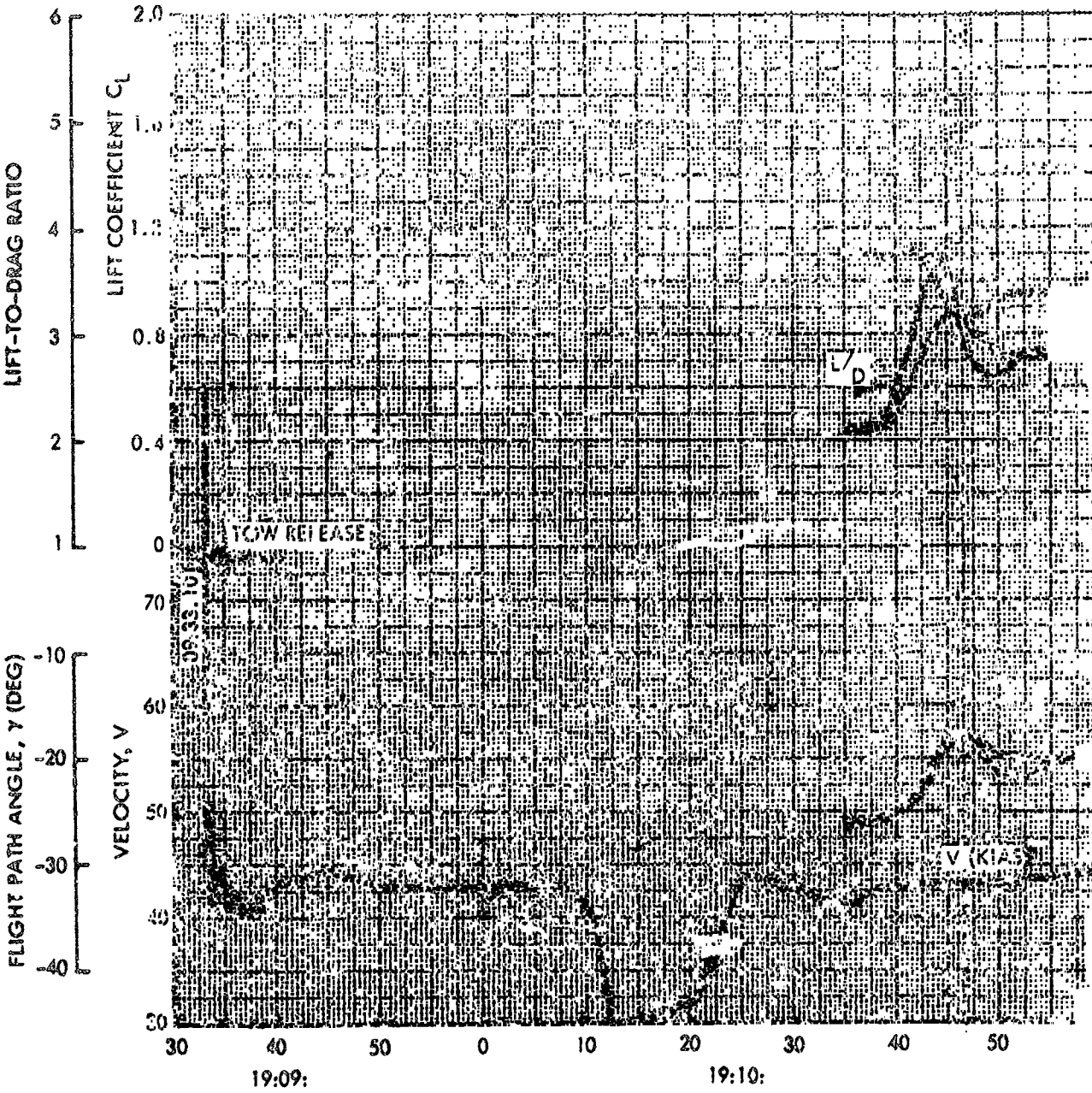

BLOWOUT FRAME 2

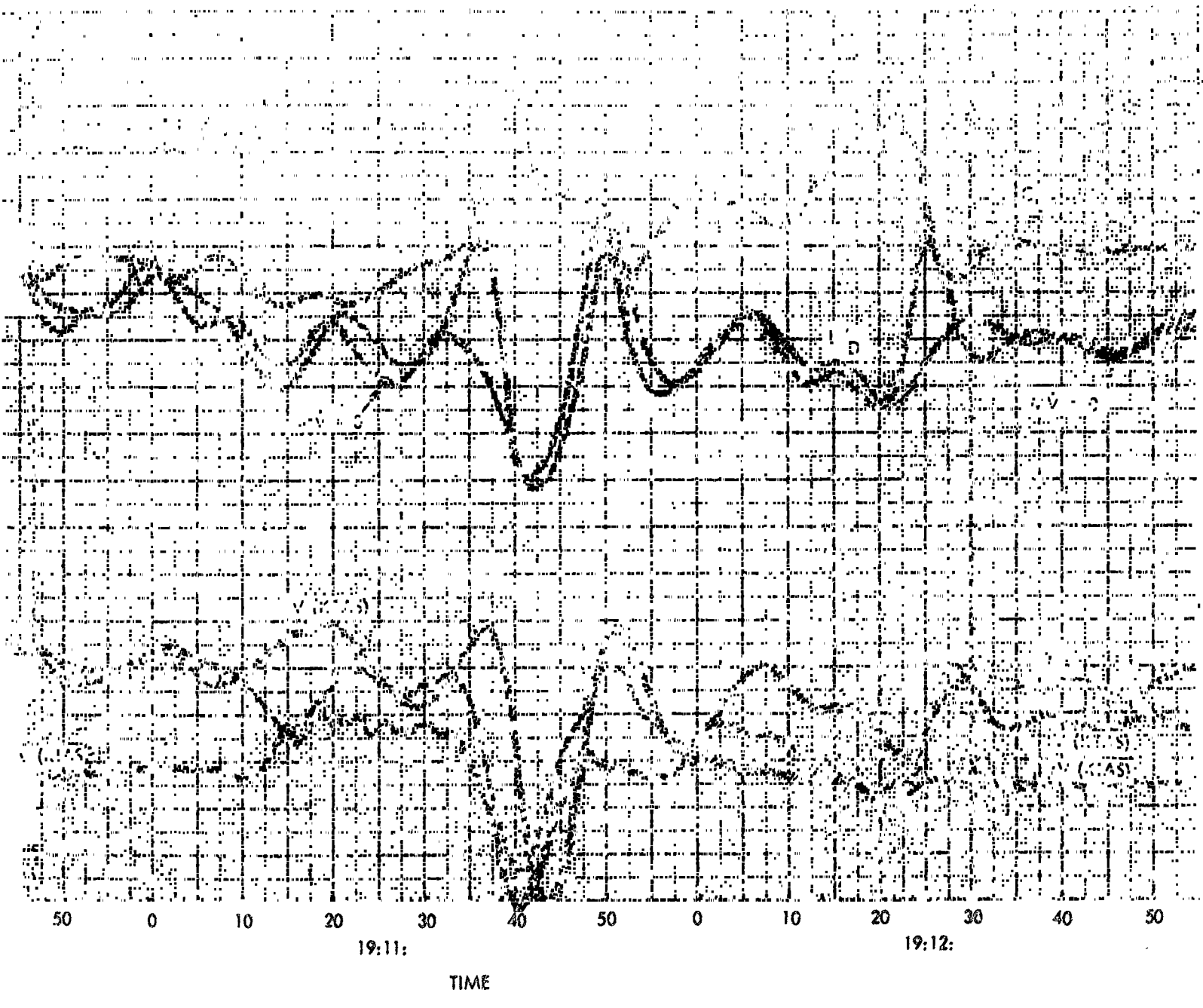

Figure 20. F

FOLDOUT FRAME 3

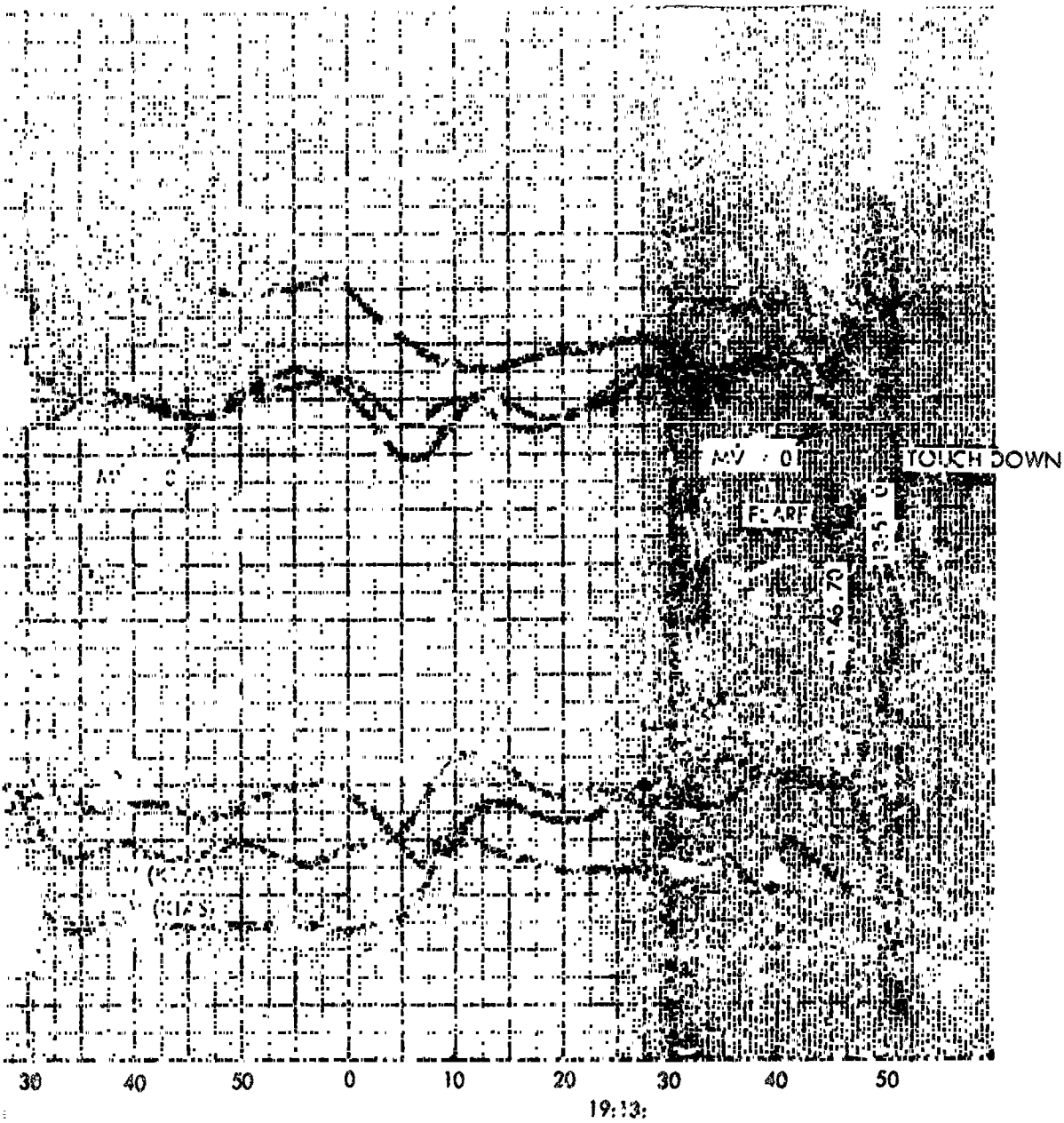

Figure 20. Flight 025 Time Histories (Sheet 2 of 3)

FOLDOUT FRAME 1

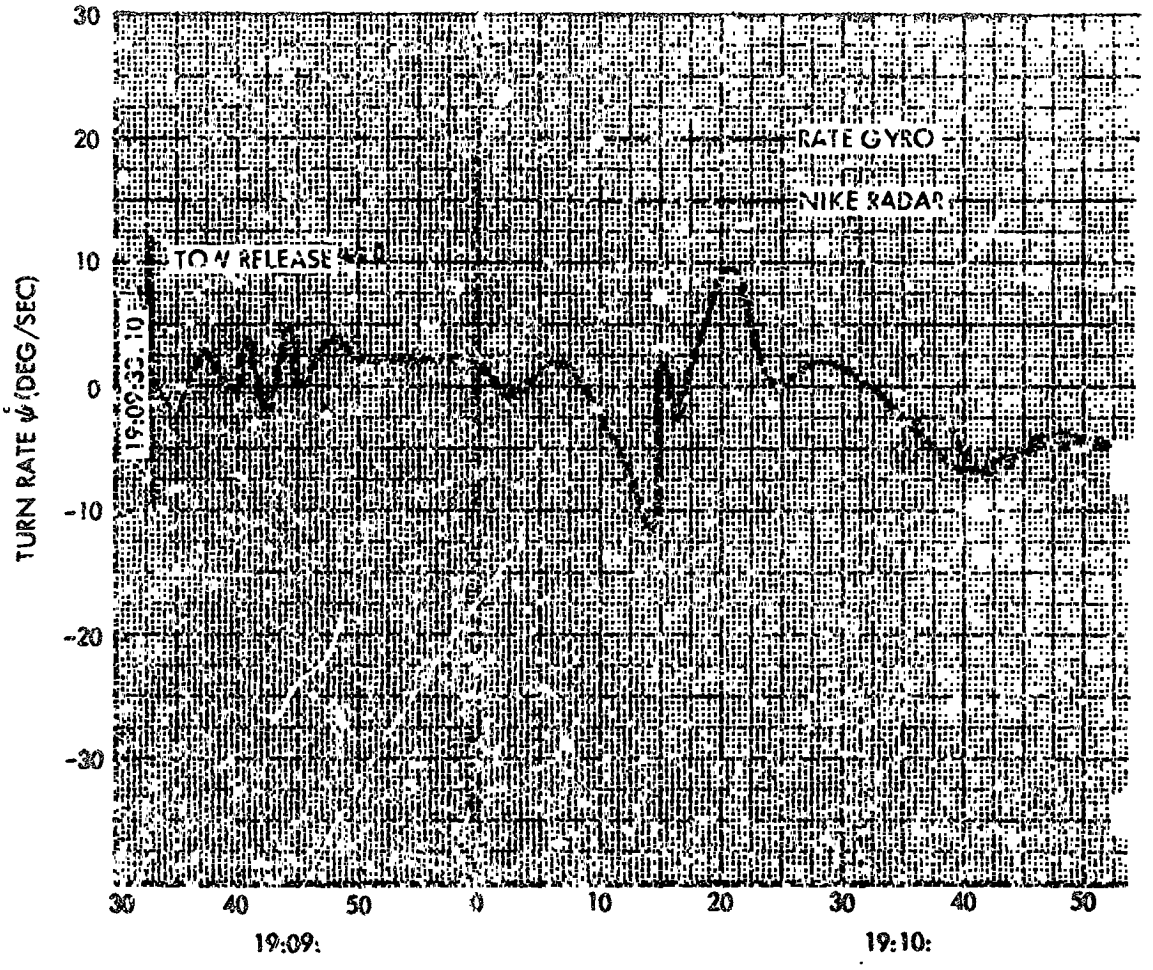

FOLDOUT FRAME 2

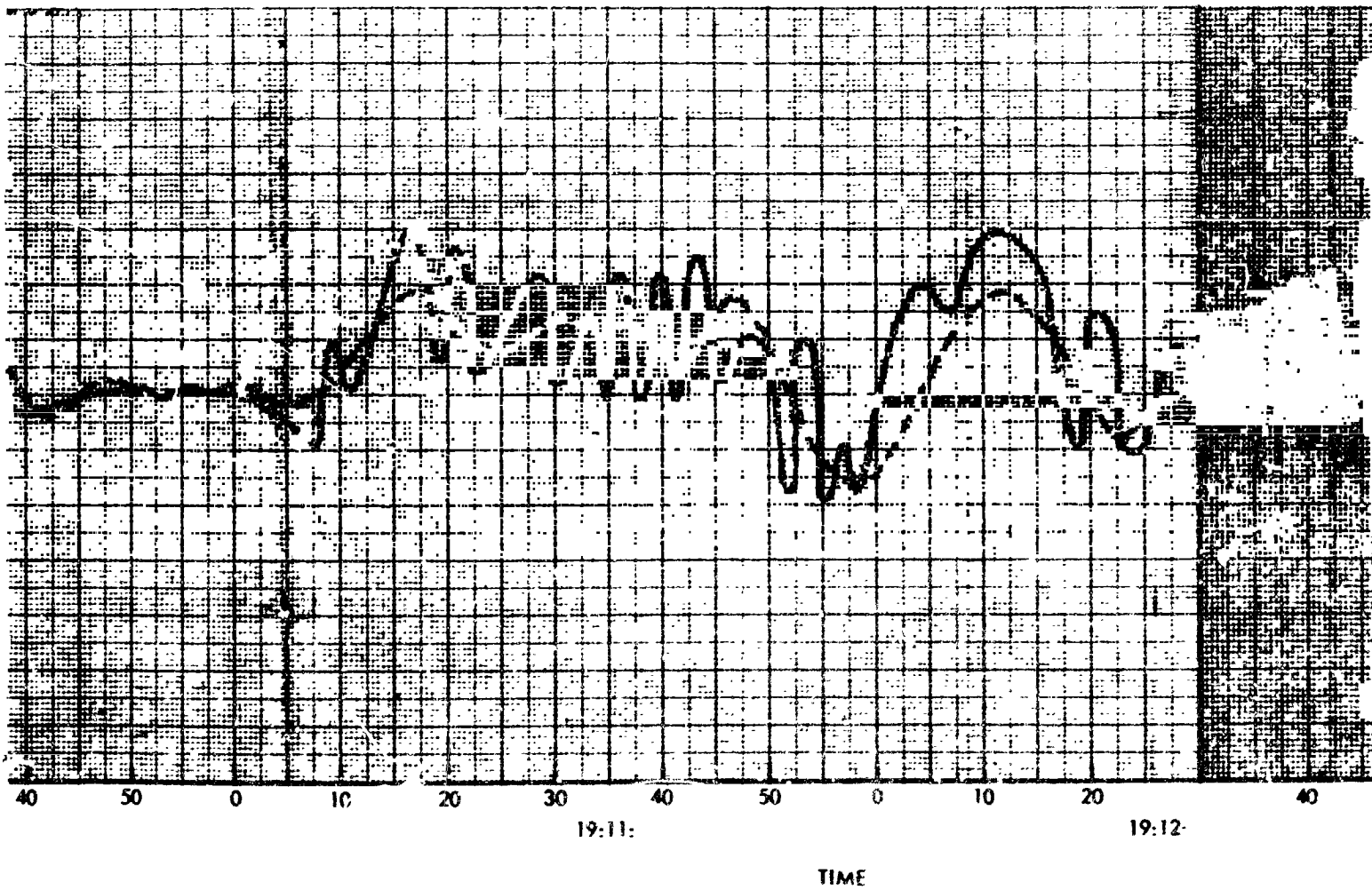

WITHOUT FRAME 3

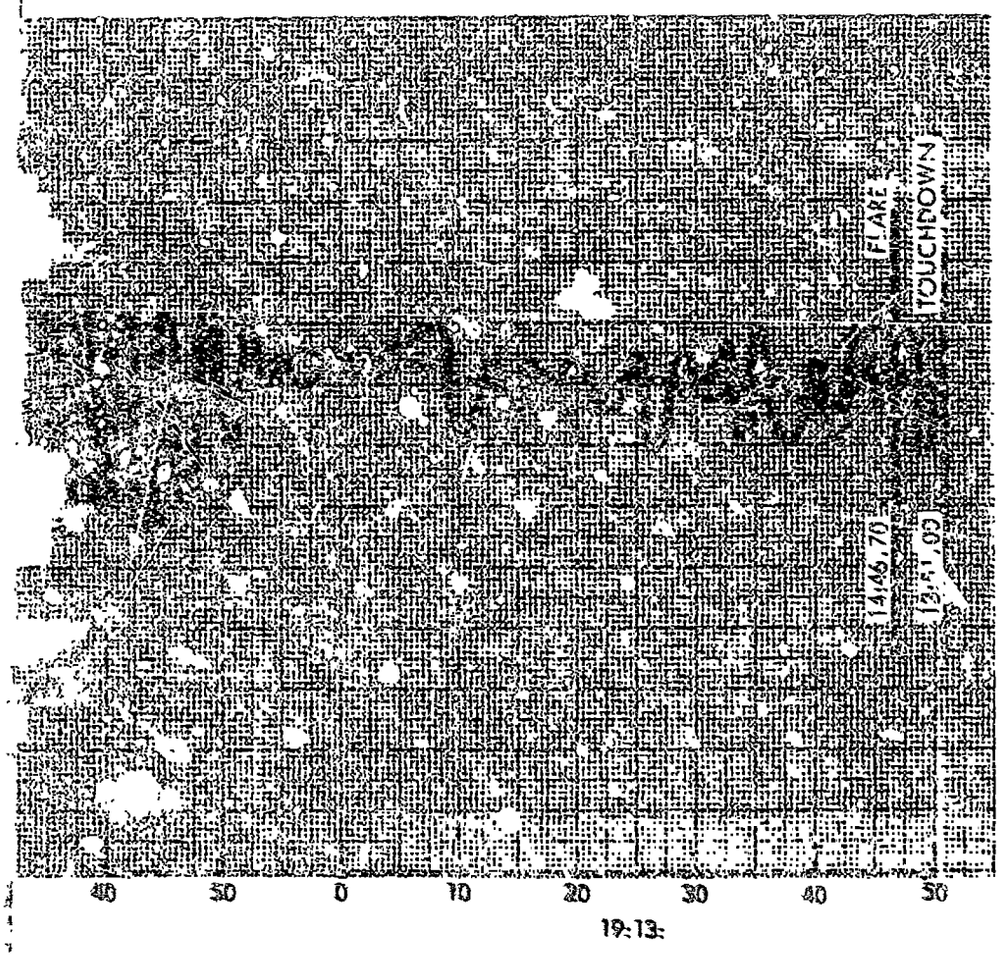

Figure 20. Flight 025 Time Histories (Sheet 3 of 3)

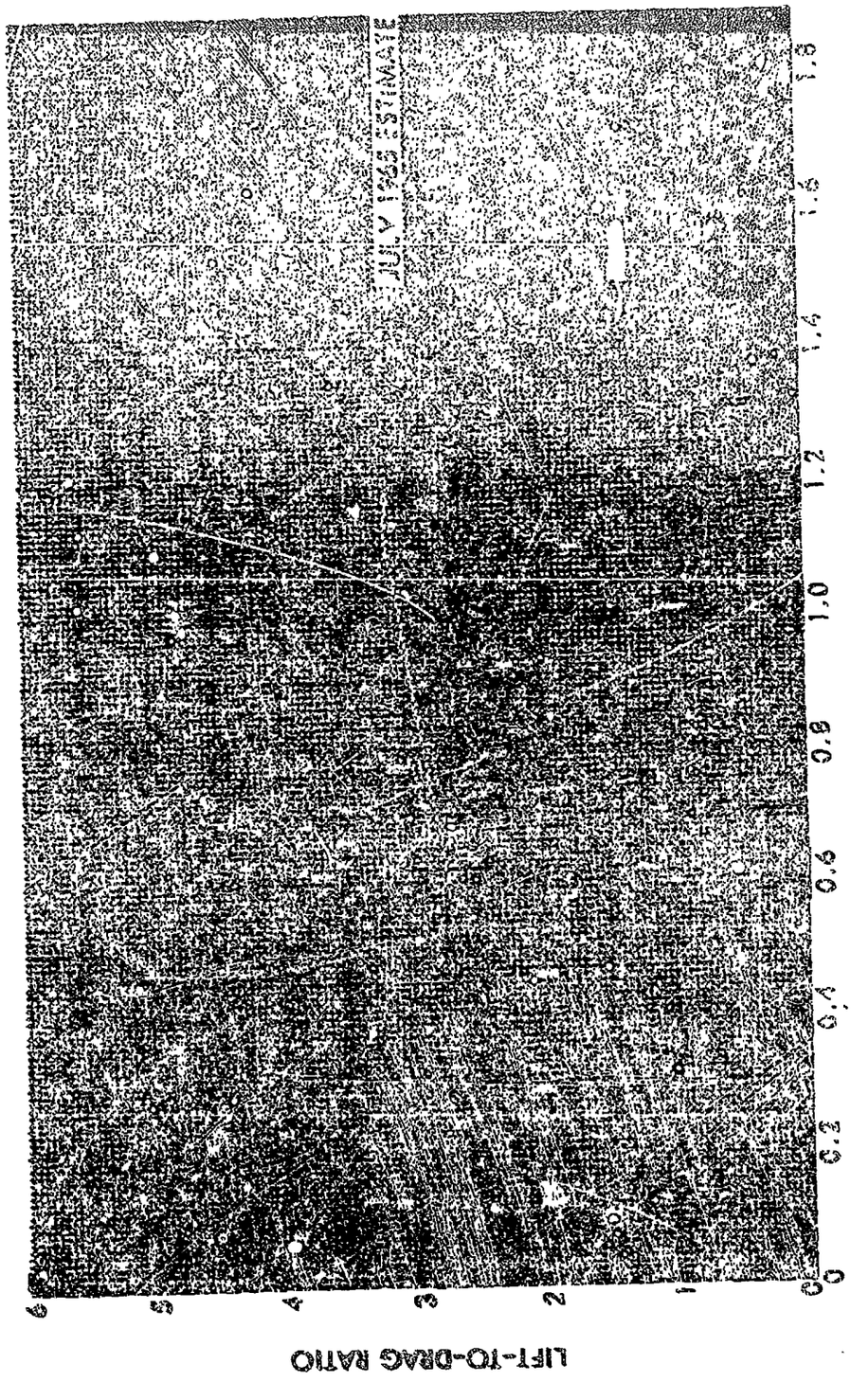

Figure 21. Flight Test Lift-to-Drag Ratio Variations for Flight 025

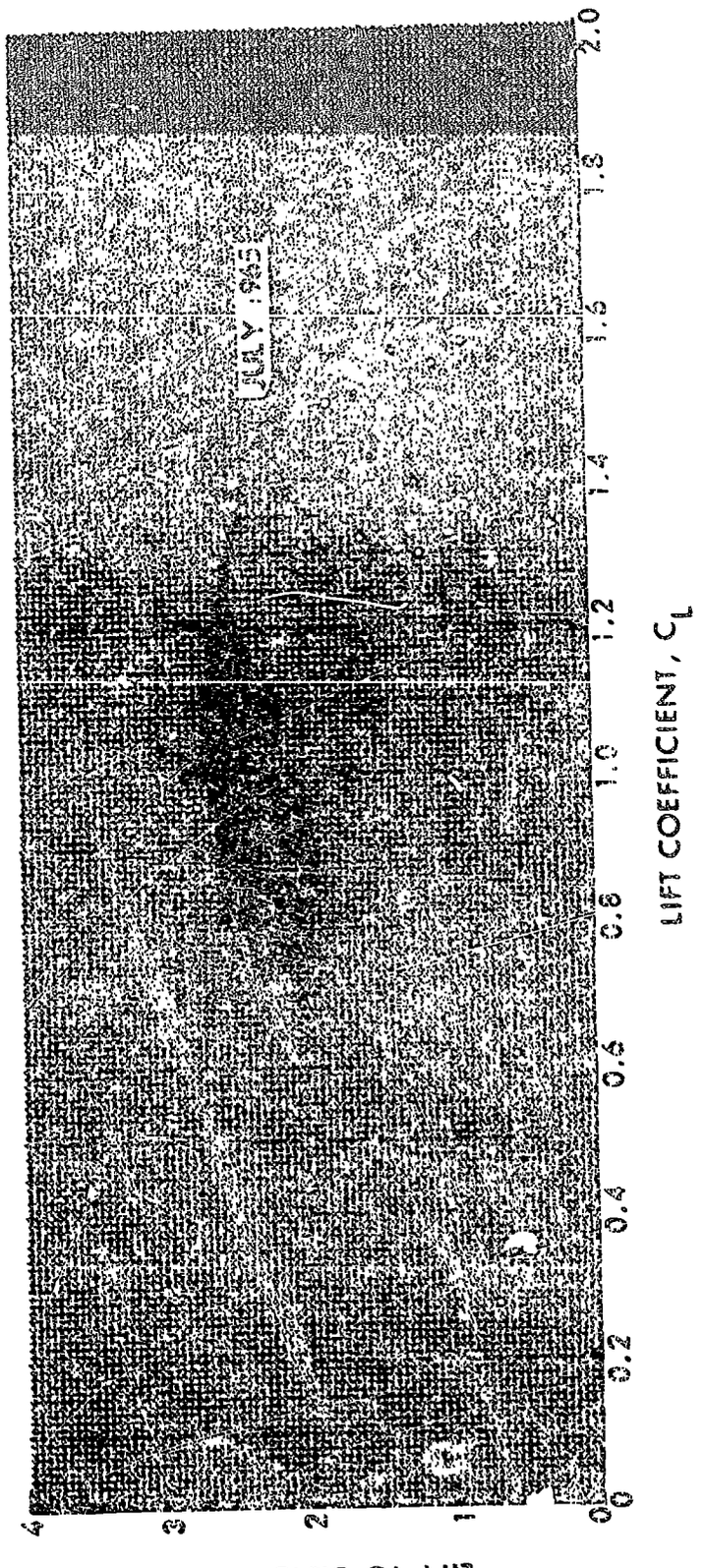

Figure 22. Lift-to-Drag Ratios From Selected Points

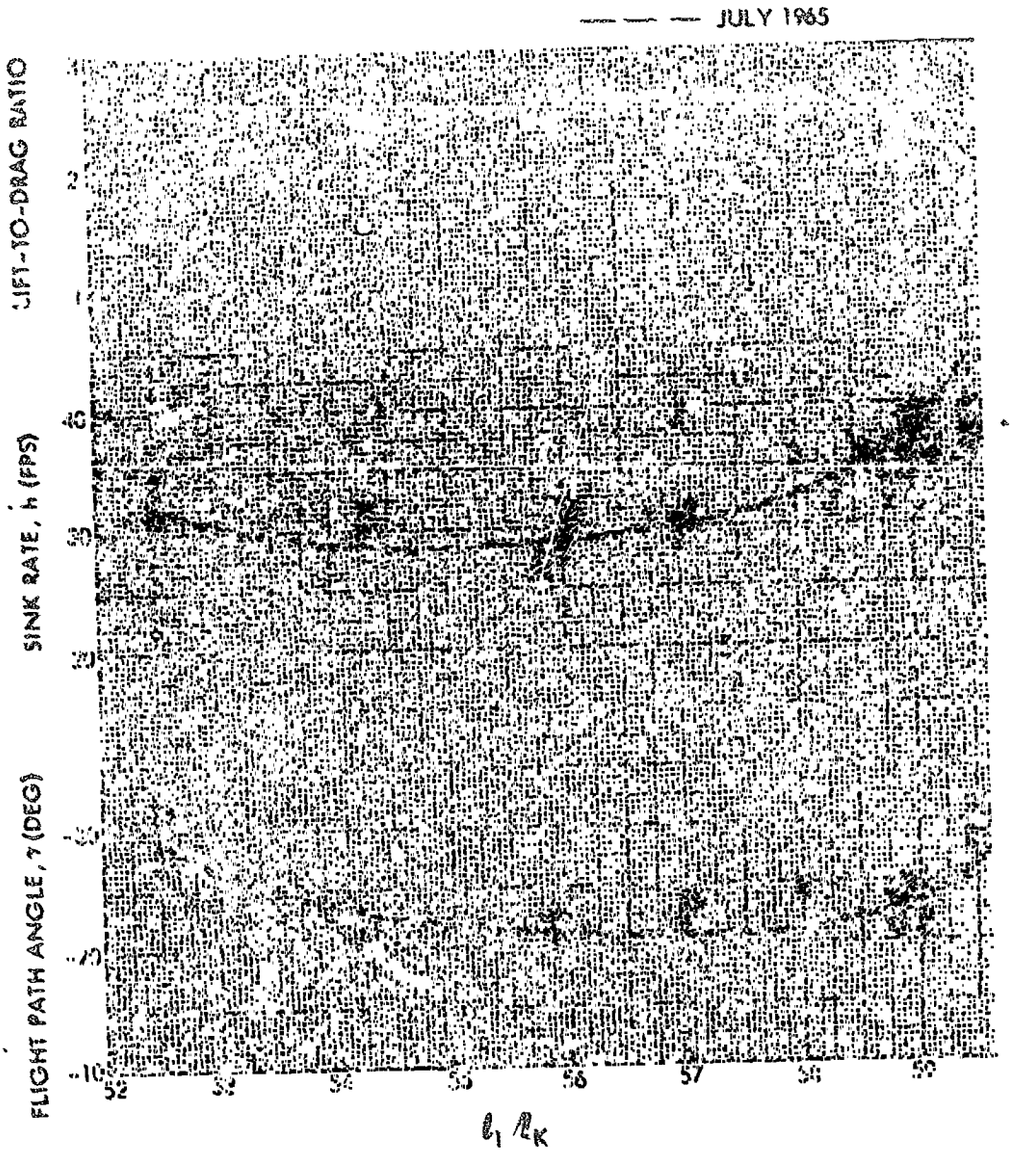

Figure 23. Phase II Selected Test Points

Aerodynamic and performance data from the selected points are plotted as a function of longitudinal control in Figures 23 and 24. These data are in close agreement with that presented in Figures 15 and 16; therefore, the vehicle predicted characteristics were not revised.

The true airspeed (KTAS) was taken from the Nike radar tracking data and compared to the indicated airspeed (KIAS). Altitude, time, temperature, and pressure were known, so that the KTAS could be converted to calibrated airspeed (KCAS). The difference between calibrated and indicated speeds is usually mostly instrument error and position error (that error associated with static pressure-port location). Previous test data indicated the airspeed error to be ten percent. Phase II test data indicate the error may be 3 to 4 knots, or approximately 7 percent, with the vehicle instrument reading low.

A comparison was made from on-board film of the radar altimeter and the pressure altimeter. The pressure instrument has a tendency to stick and then jump. The pressure altimeter tended to lag behind the radar altimeter from 15 to 40 feet, with a fairly consistent mean of about 25 feet. This is for the present instruments and static port locations.

Data from Flight 26 are presented in Figure 25. Due to high winds aloft and the track over the south lake bed, it was necessary to fly at a maximum range condition. Therefore, the largest majority of the flight was at a pitch line setting of $0.56\,\ell_1/\ell_k$. Nike radar was operative for this flight, and the data are presented along with the telemetered data for correlative purposes. The sink rate data from Nike radar compare very well with that from telemetry. The airspeed data trend compares well, considering there is a difference of true and indicated airspeeds. A large departure in airspeeds is apparent at about time 16:19, indicating a lack of good wind data at low altitudes. Also, of major consequence are the large changes in airspeed during the last 30 seconds of flight, which is associated with the shear layers, gusts, and atmospheric inversion layers over the test area during this time period.

Nike radar tracker did not function satisfactorily for data purposes during the remainder of Phase III testing. Therefore, only that data obtained from the on-board telemetry system is presented in Figures 26 through 32. Of general interest during this phase was the damping of the dutch roll oscillations at tow release. In Figure 30, Sheet 2, the turn rate indicates a towed dutch roll with a definite damping about 15 seconds after tow release. Damping data are also presented as turn rates in Figures 26 and 28.

The flares in the air and those for landing are presented as a later part of the report, but are also presented here as a part of the data for continuity. A larger portion of the preflare is also presented here, and the

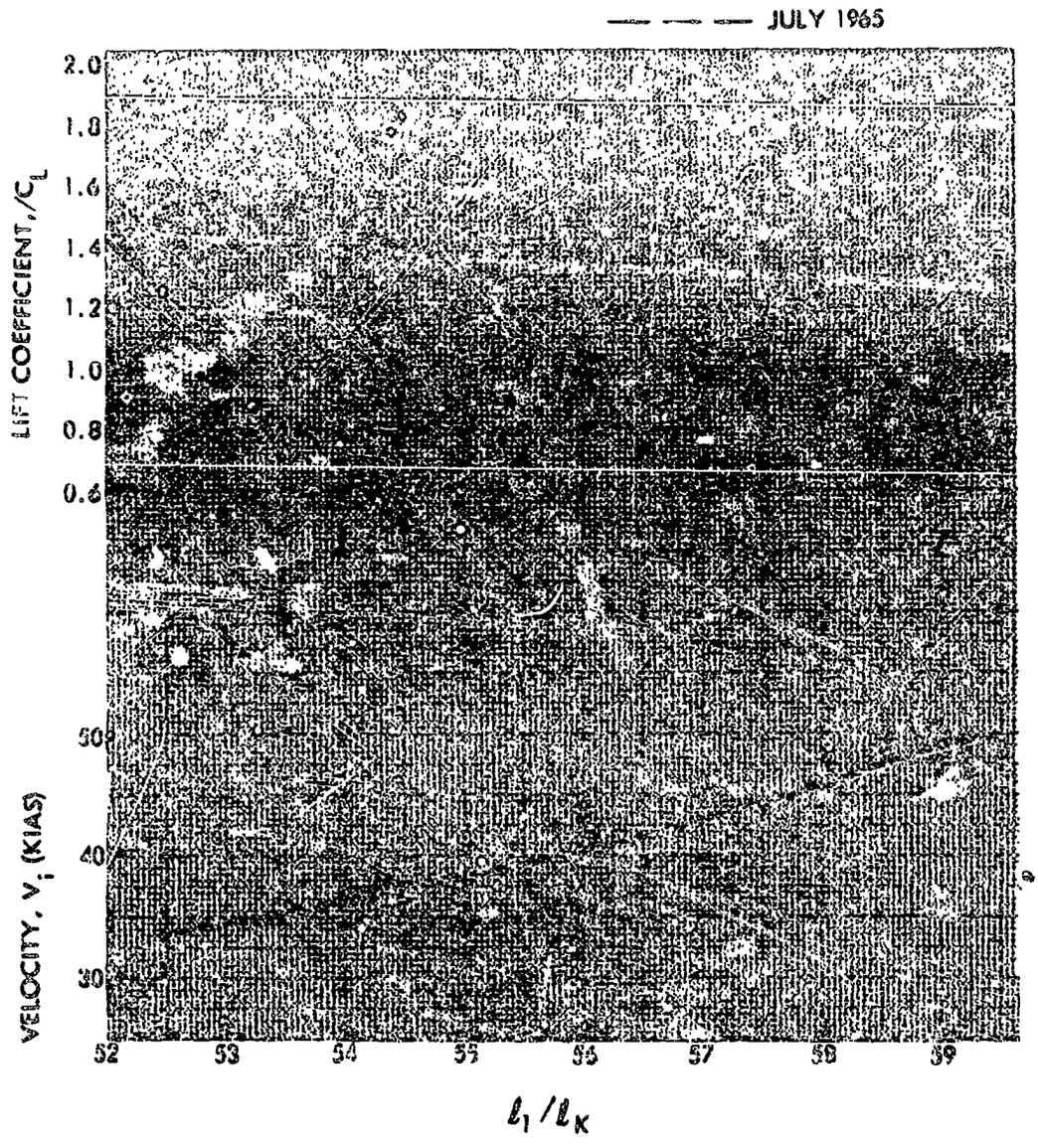

Figure 24. Selected Points of Longitudinal Aerodynamics

FOLDOUT FRAME

FOLDOUT FRAME

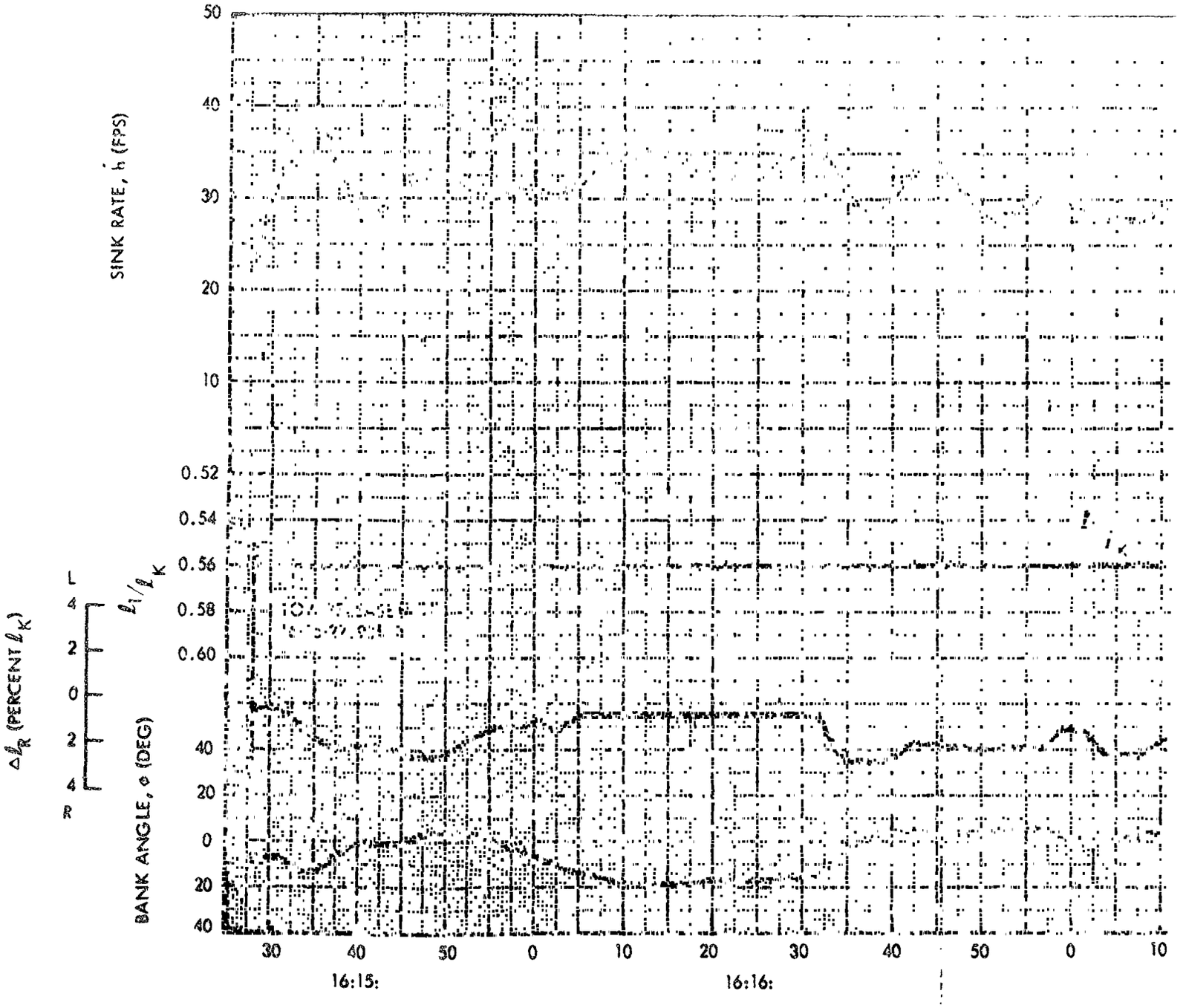

FOLDOUT FRAME 2

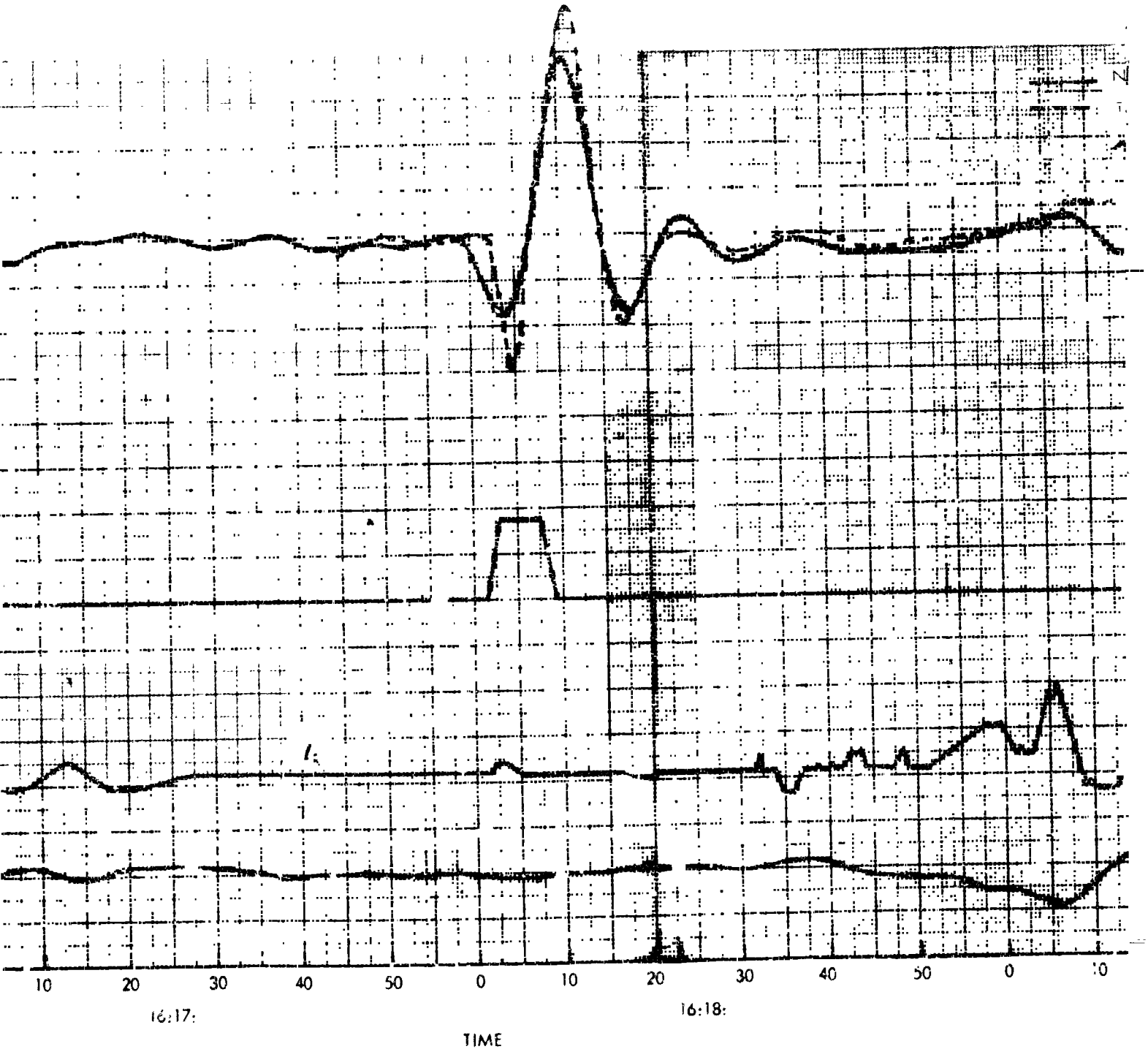

FOLDOUT FRAME 3

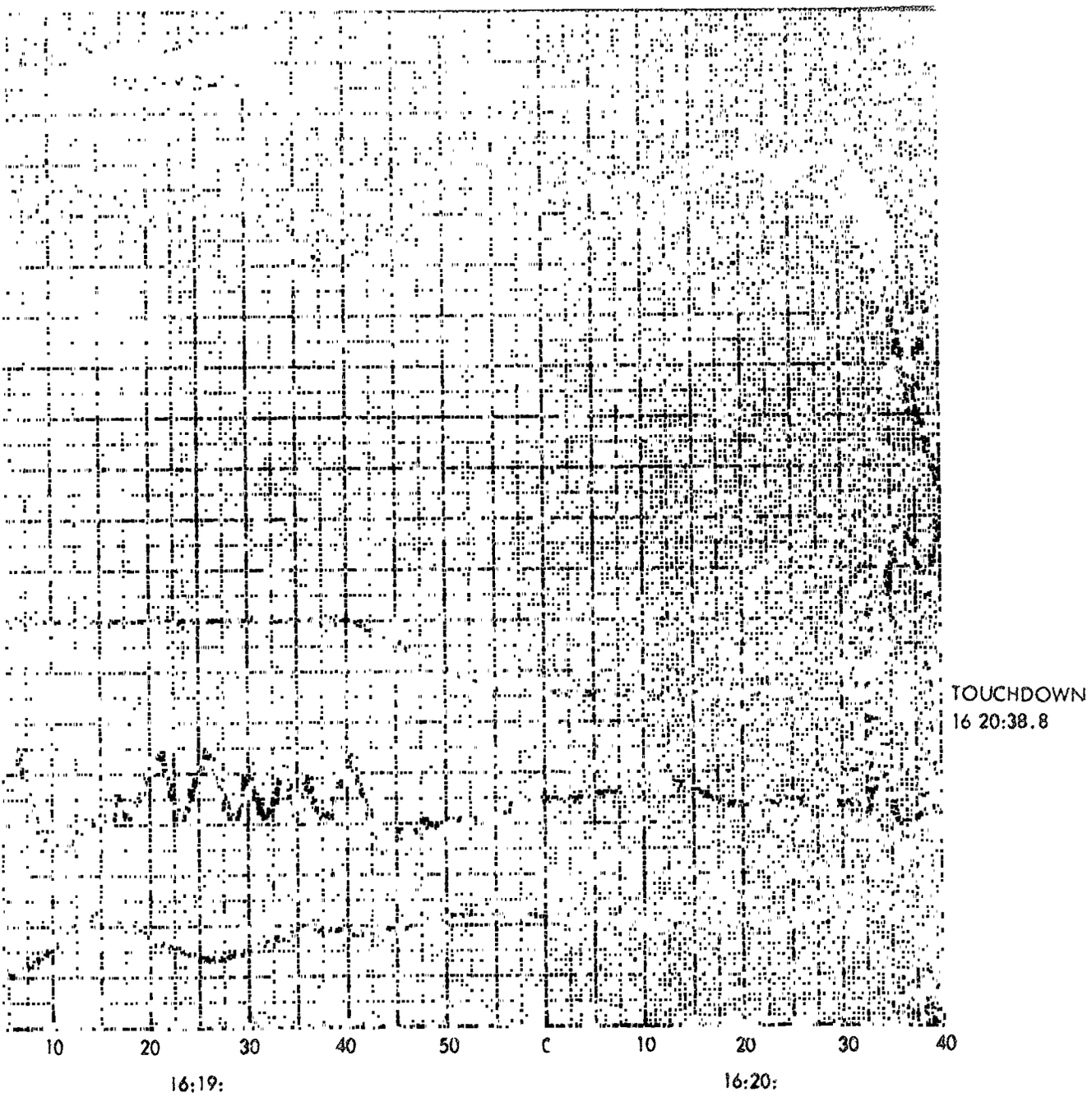

Figure 25. Flight 026 Time Histories (Sheet 1 of 2)

FOLDOUT FRAME

FOLDOUT FRAME

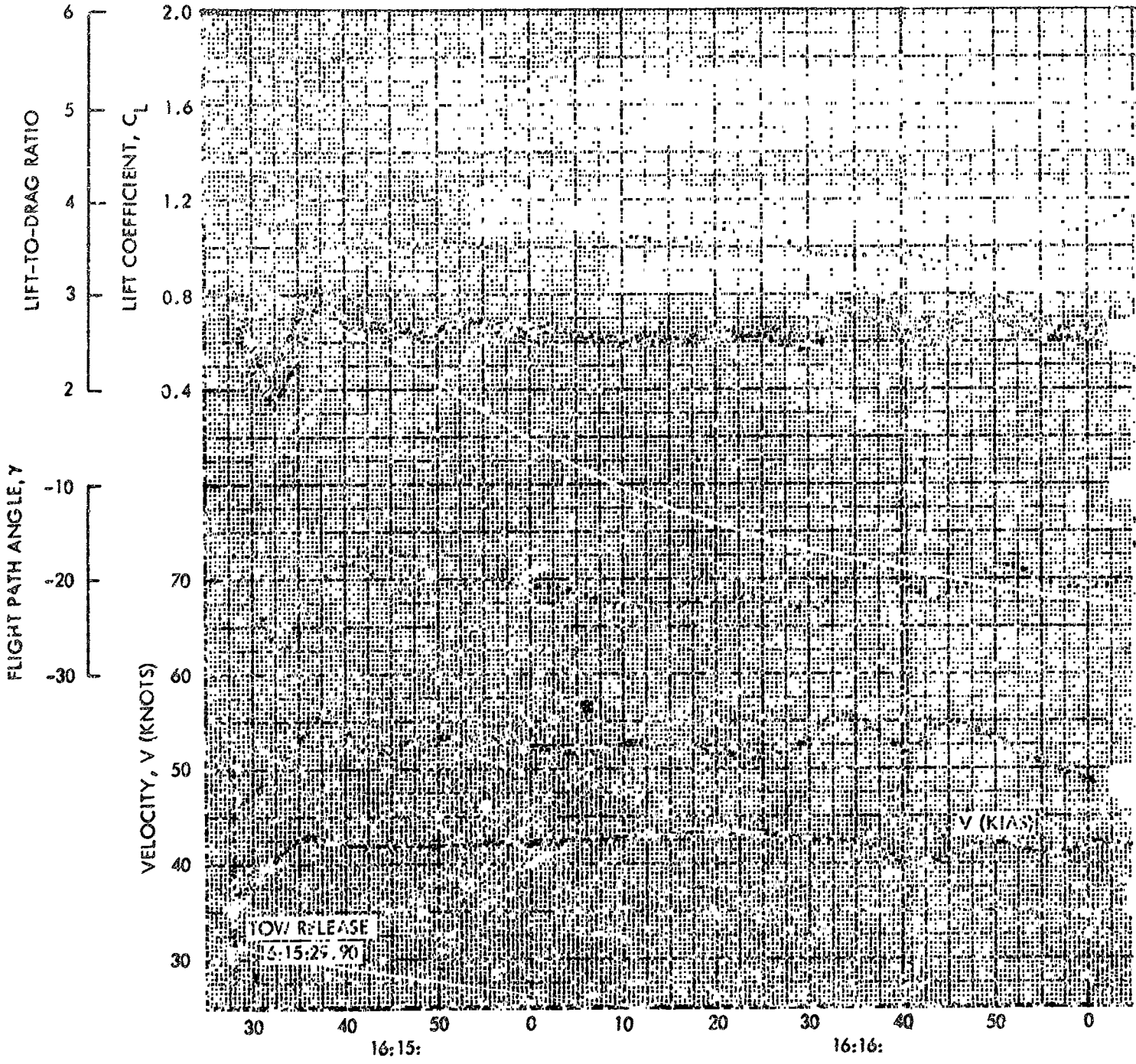

FOLDOUT FRAME 2

AME 1

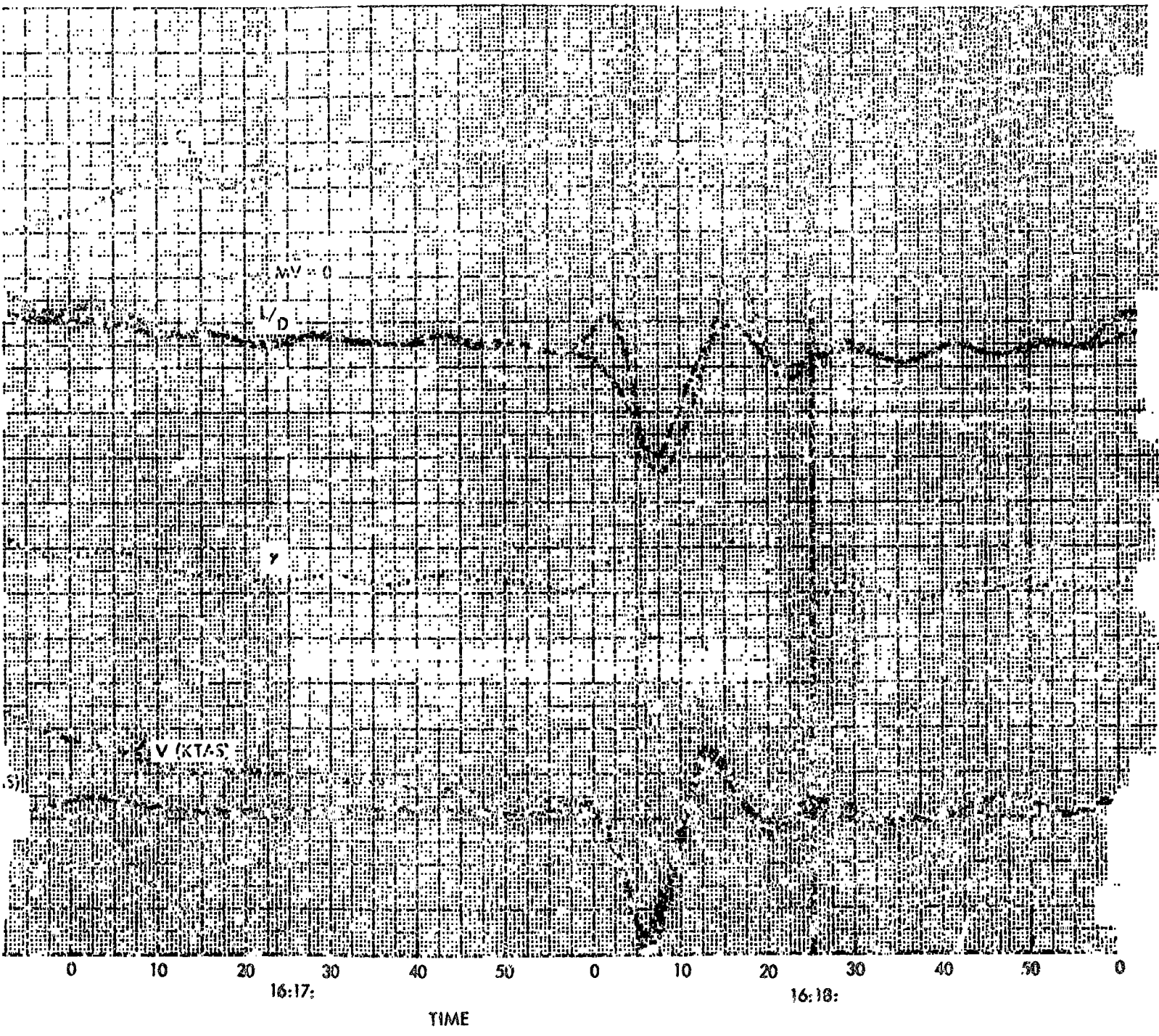

FOLDOUT FRAME 3

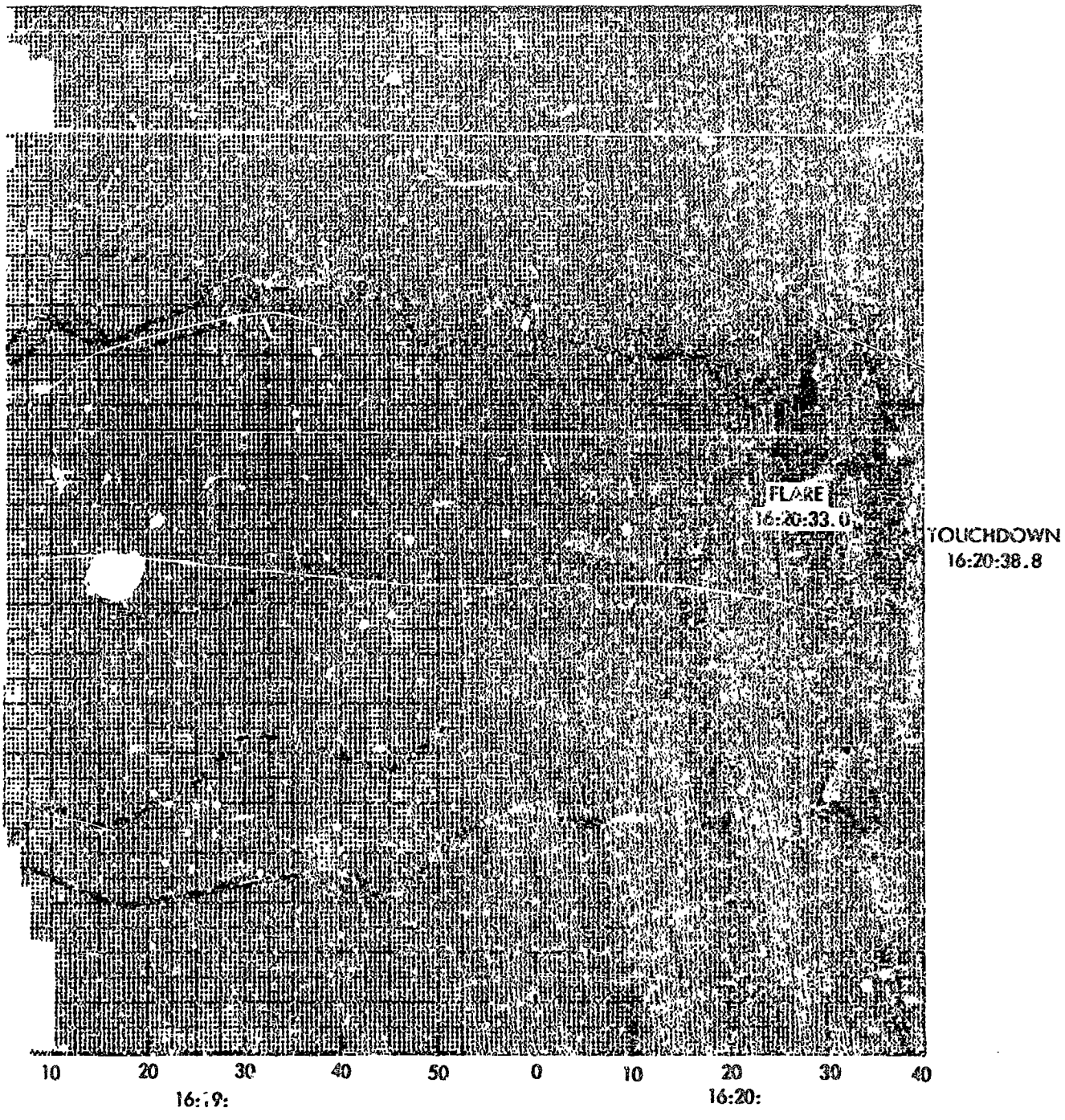

Figure 25. Flight 026 Time Histories (Sheet 2 of 2)

FOLDOUT FRAME 1

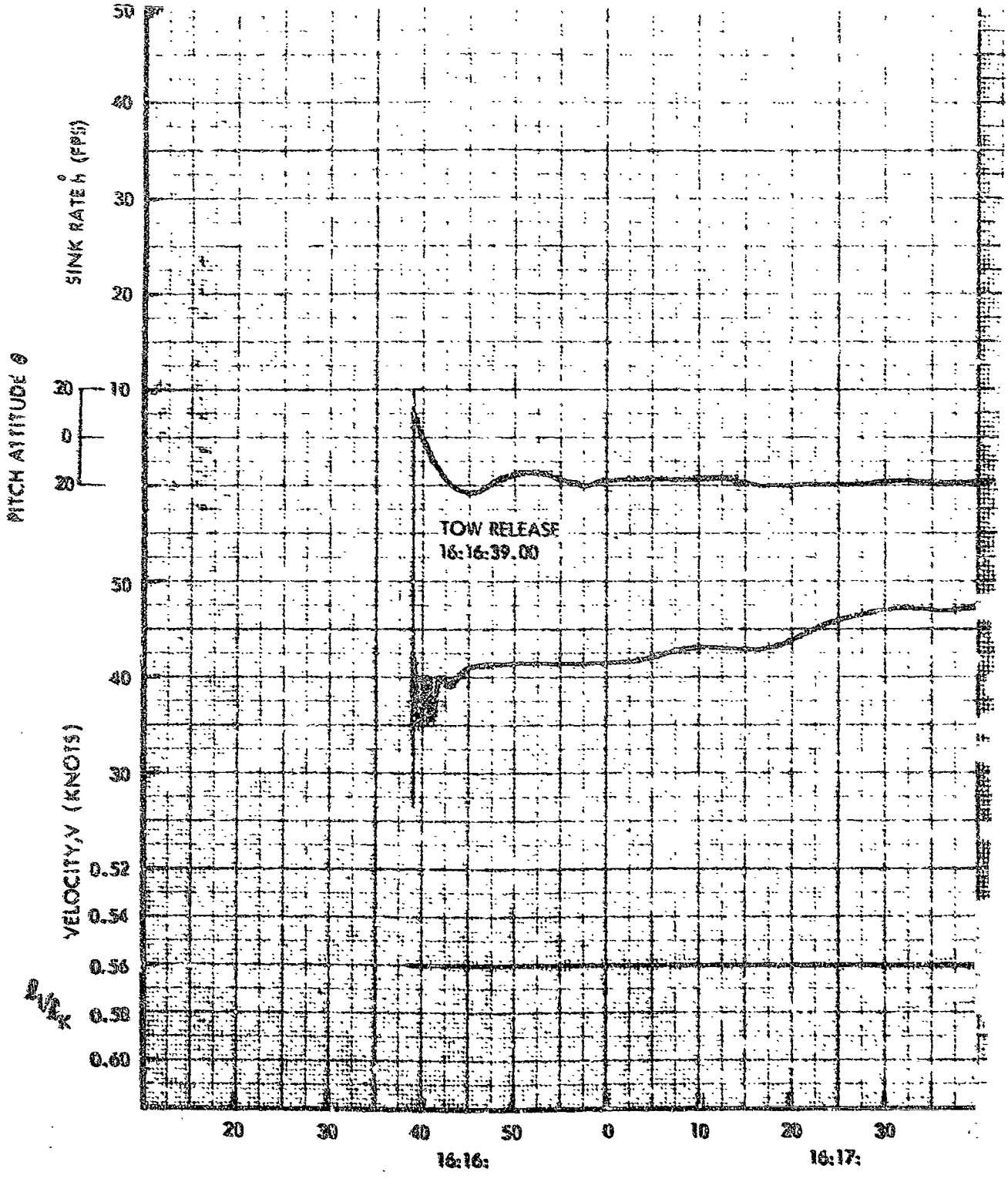

FOLDOUT FRAME 2

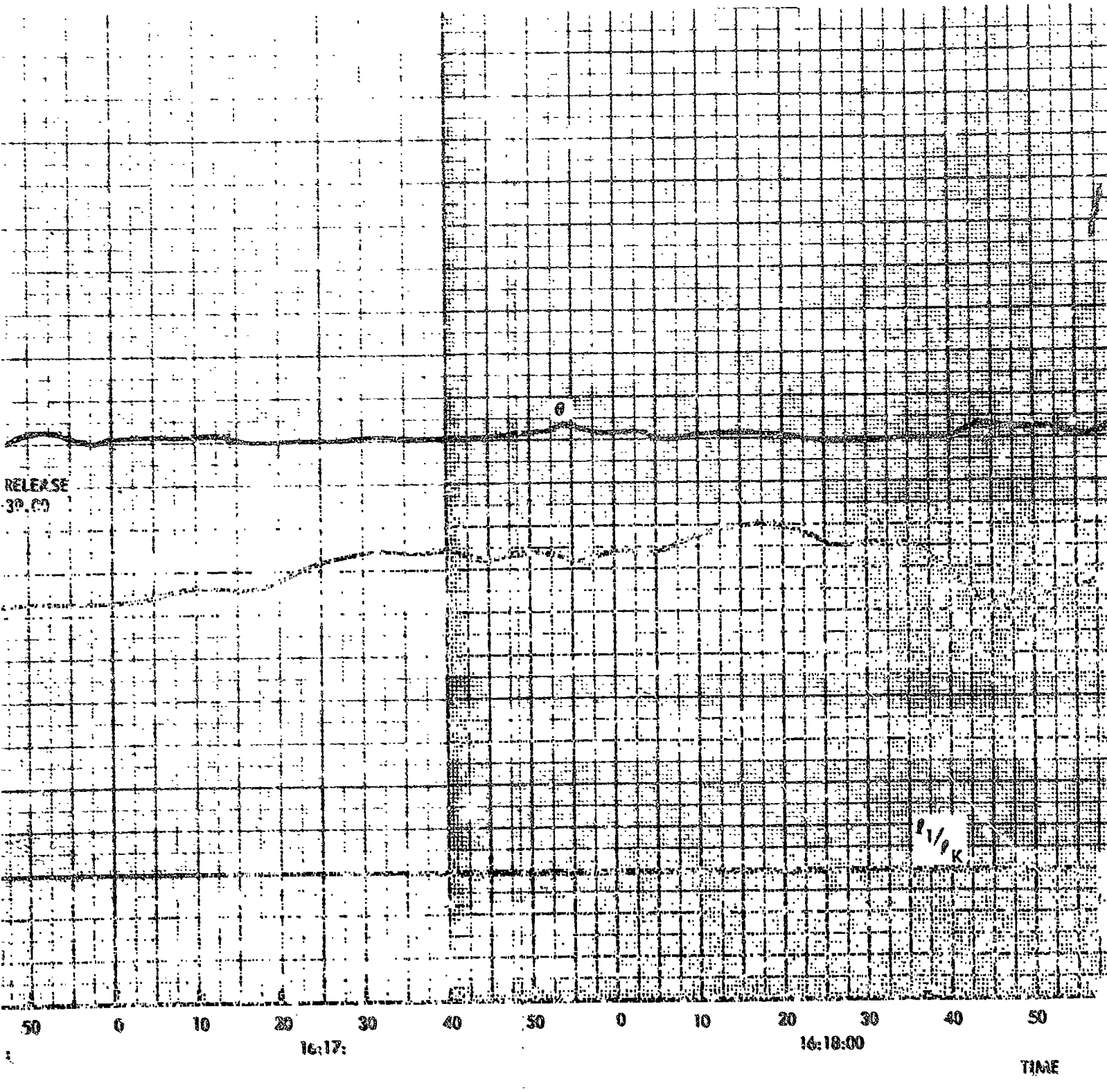

FOLDOUT FRAME 96

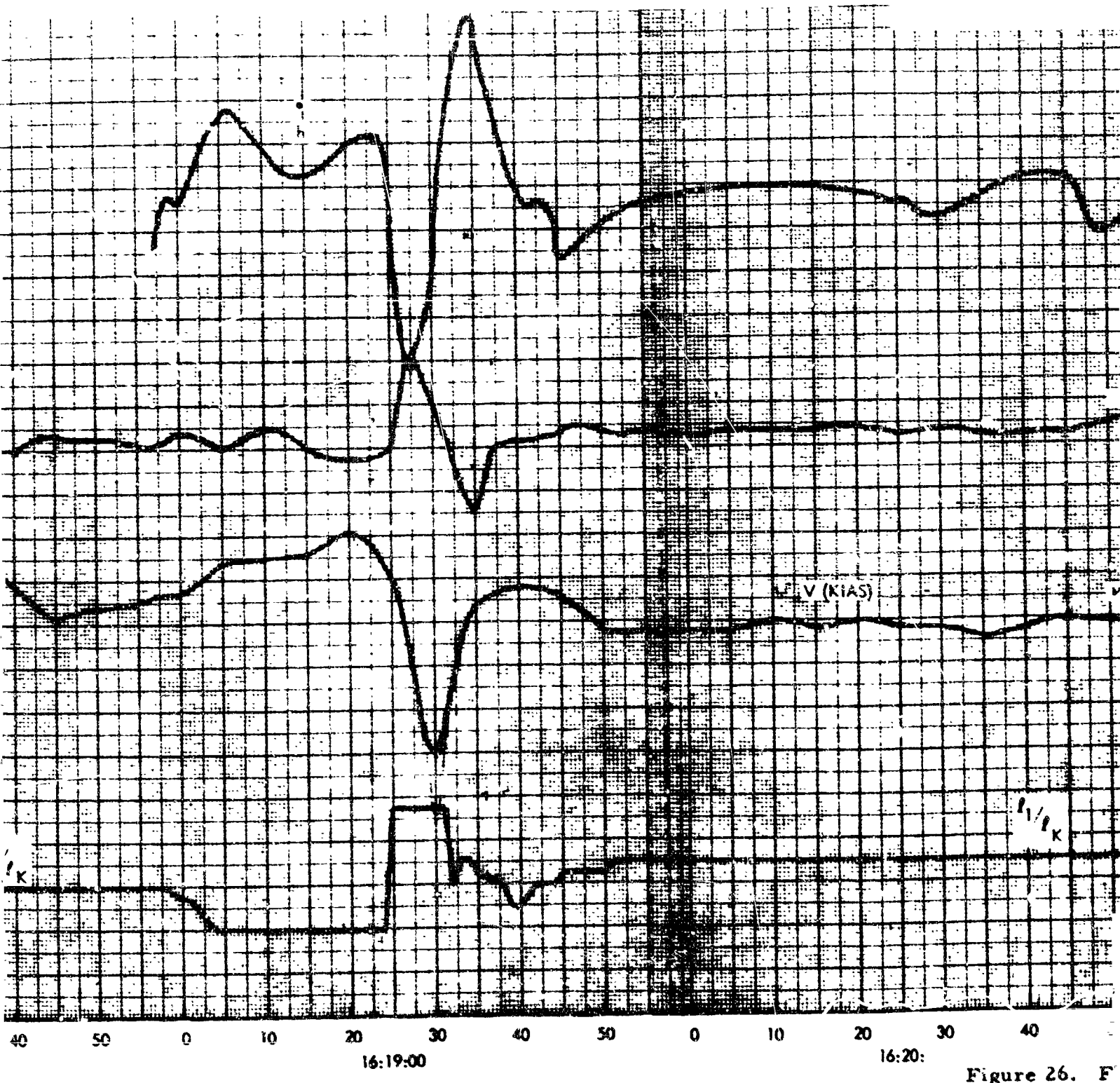

Figure 26. F

FOLDOUT FRAME 4

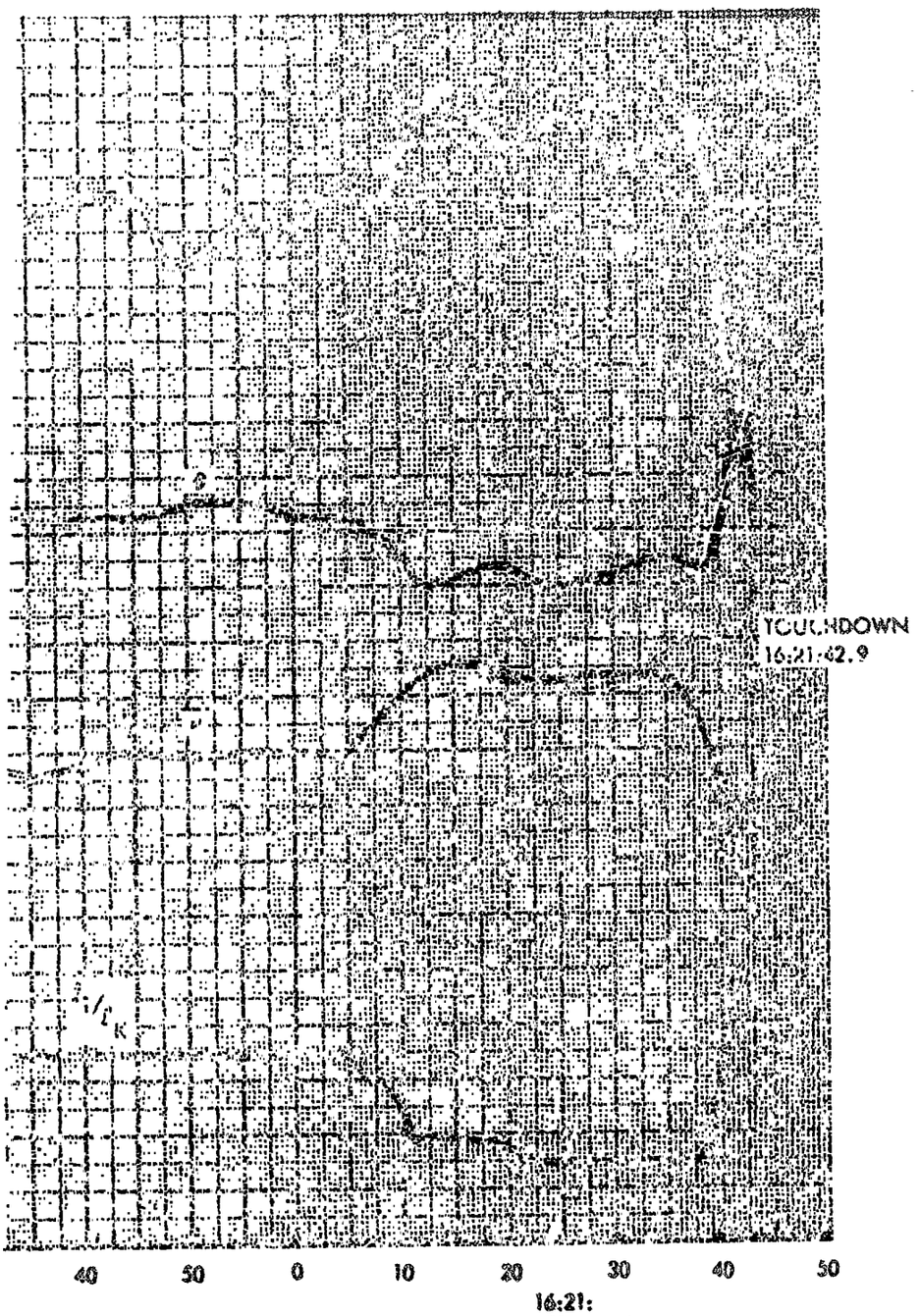

Figure 26. Flight 027 Time Histories (Sheet 1 of 4)

FOLDOUT FRAME 1

FOLDOUT FRAME

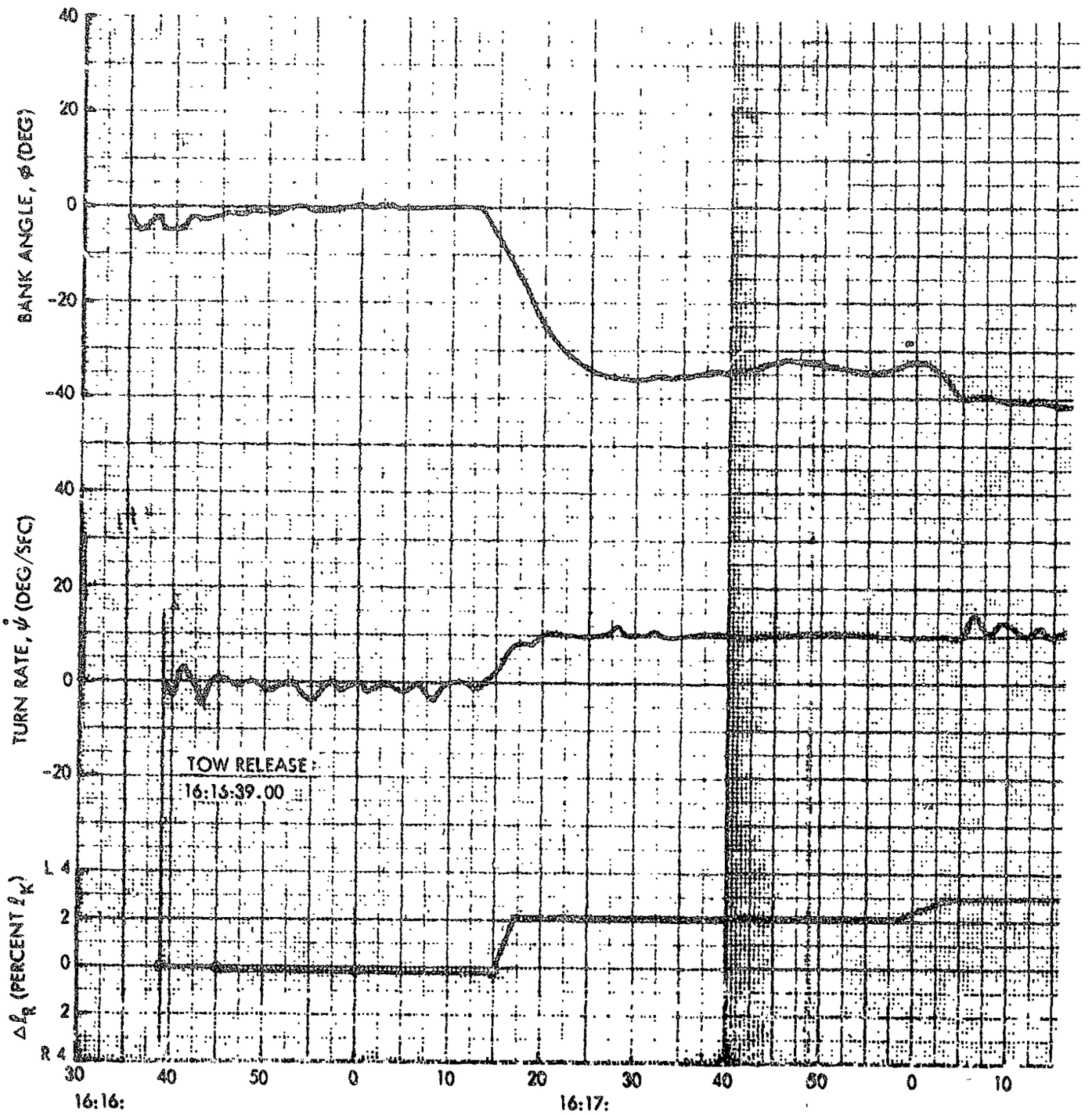

FOLDOUT FRAME 2

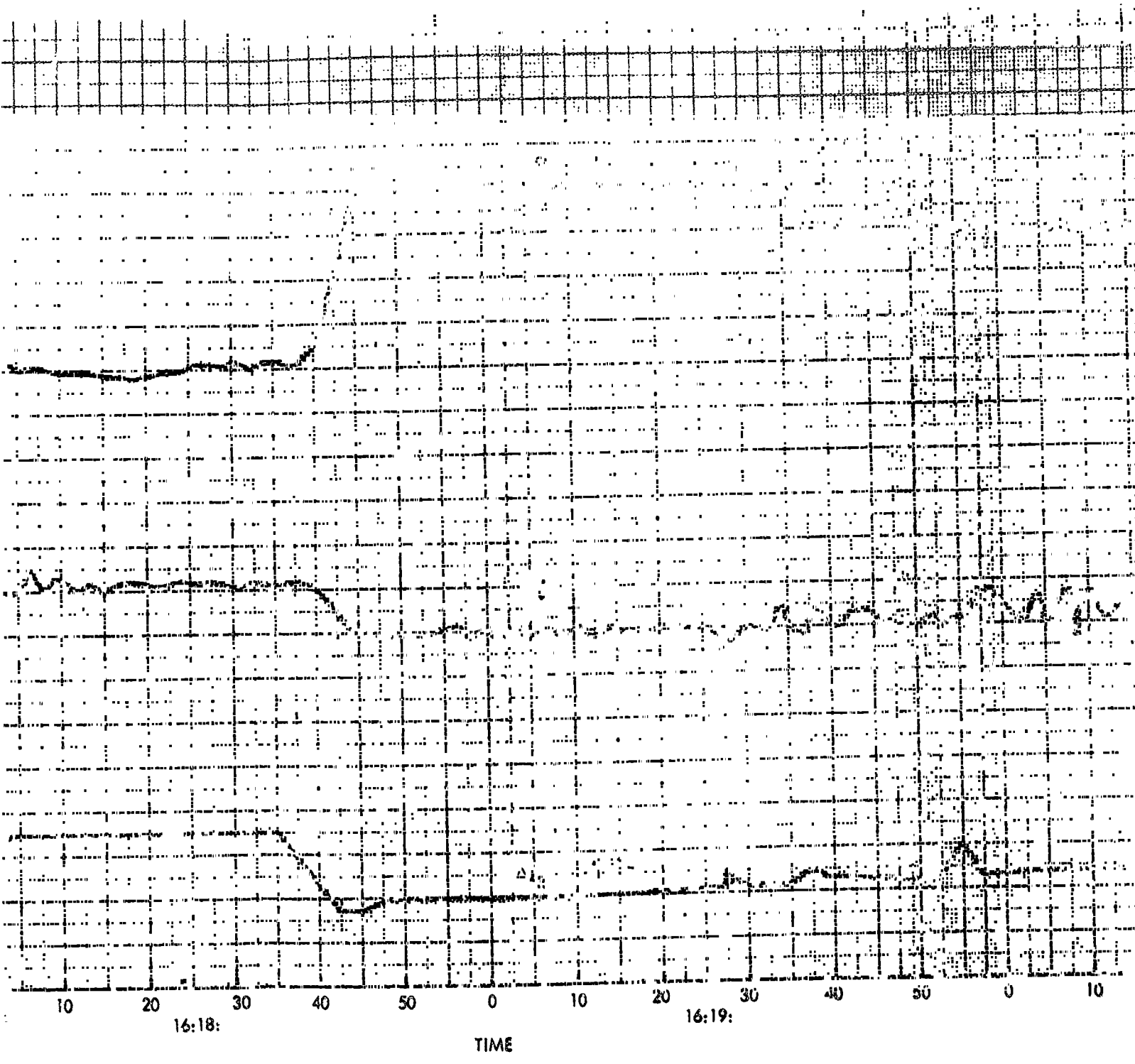

FOLDOUT FRAME 3

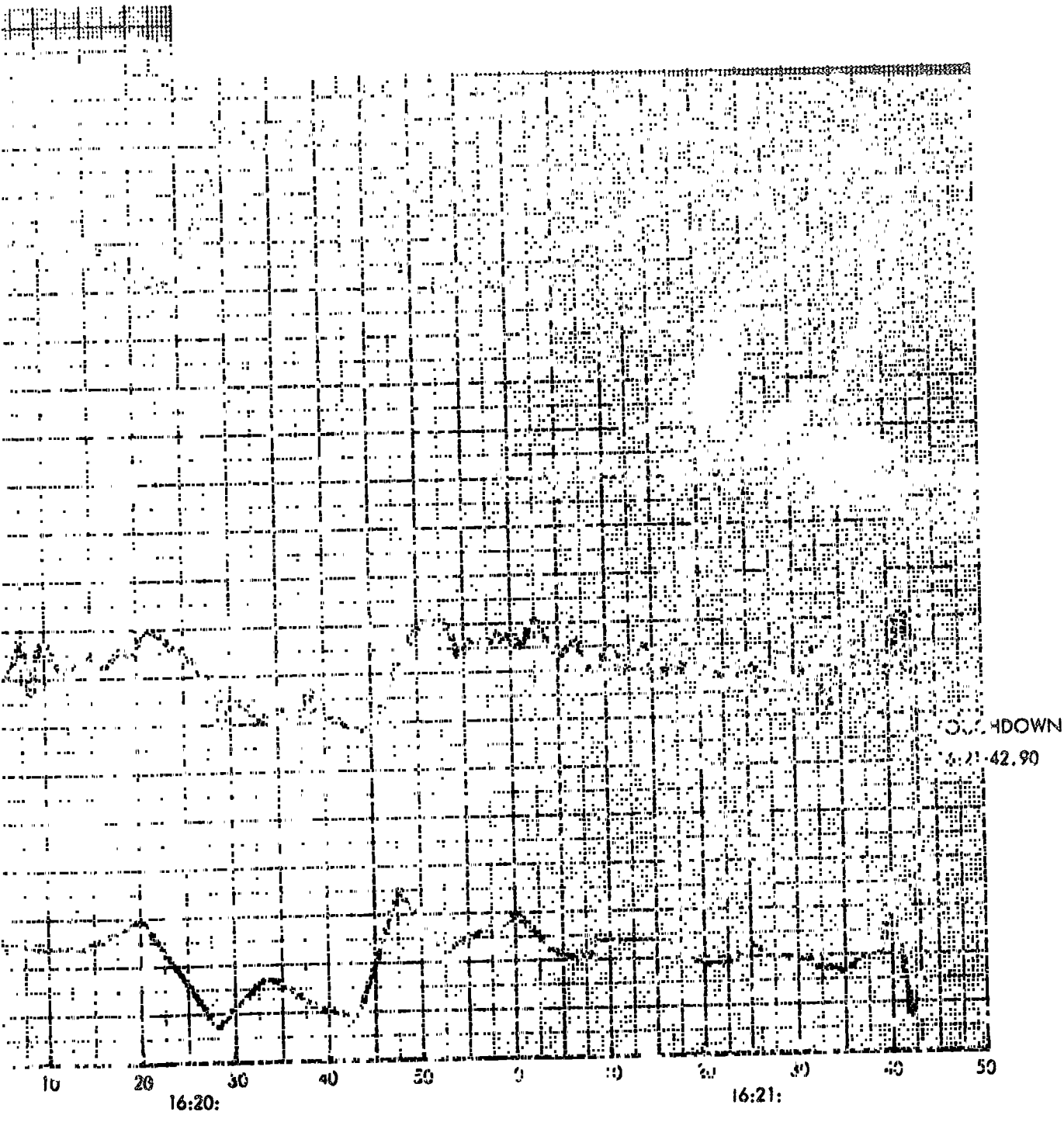

Figure 26. Flight 027 Time Histories (Sheet 2 of 2)

FOLDOUT FRAME /

FOLDOUT

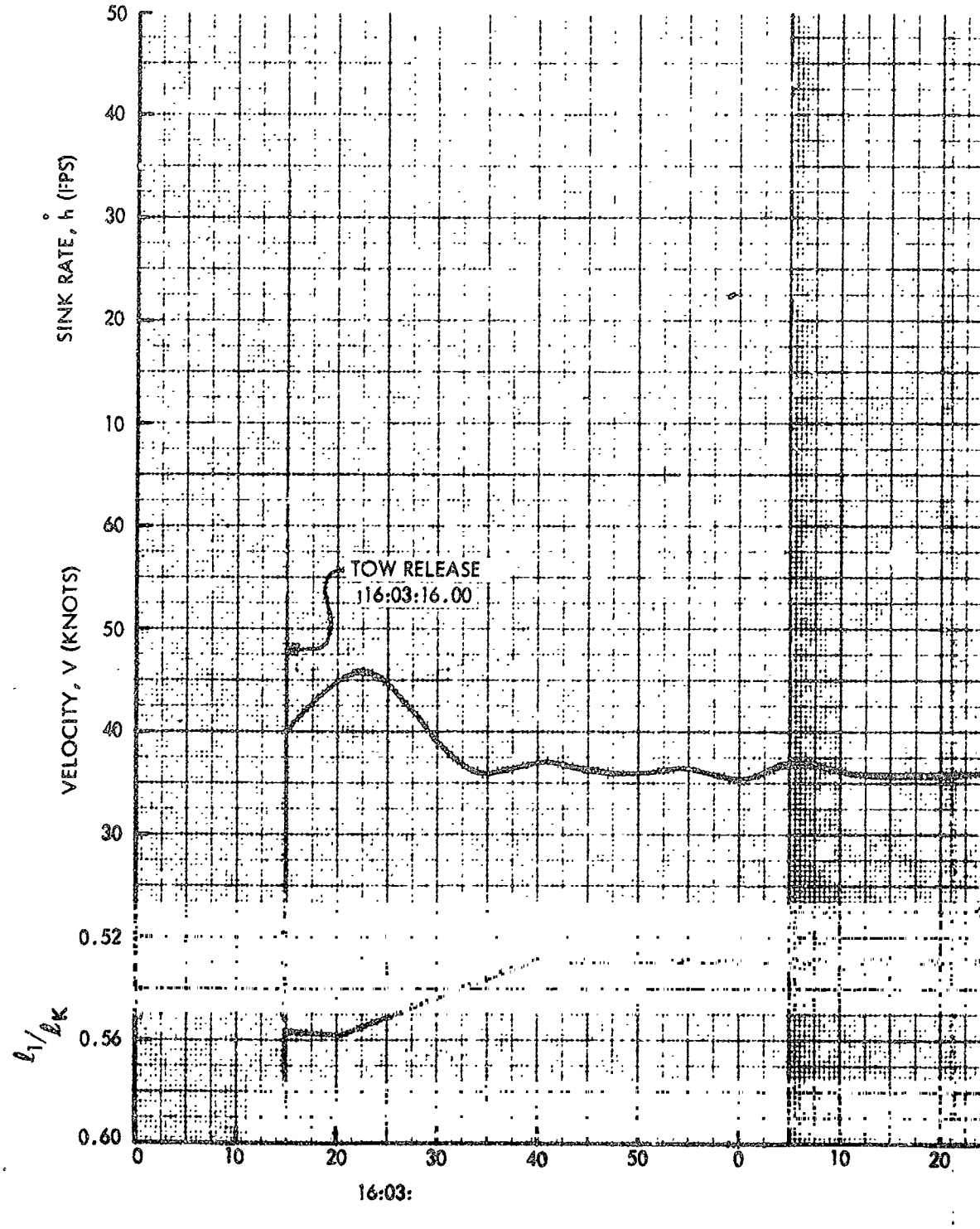

FOLDOUT FRAME 2

FOLDOUT FRAME

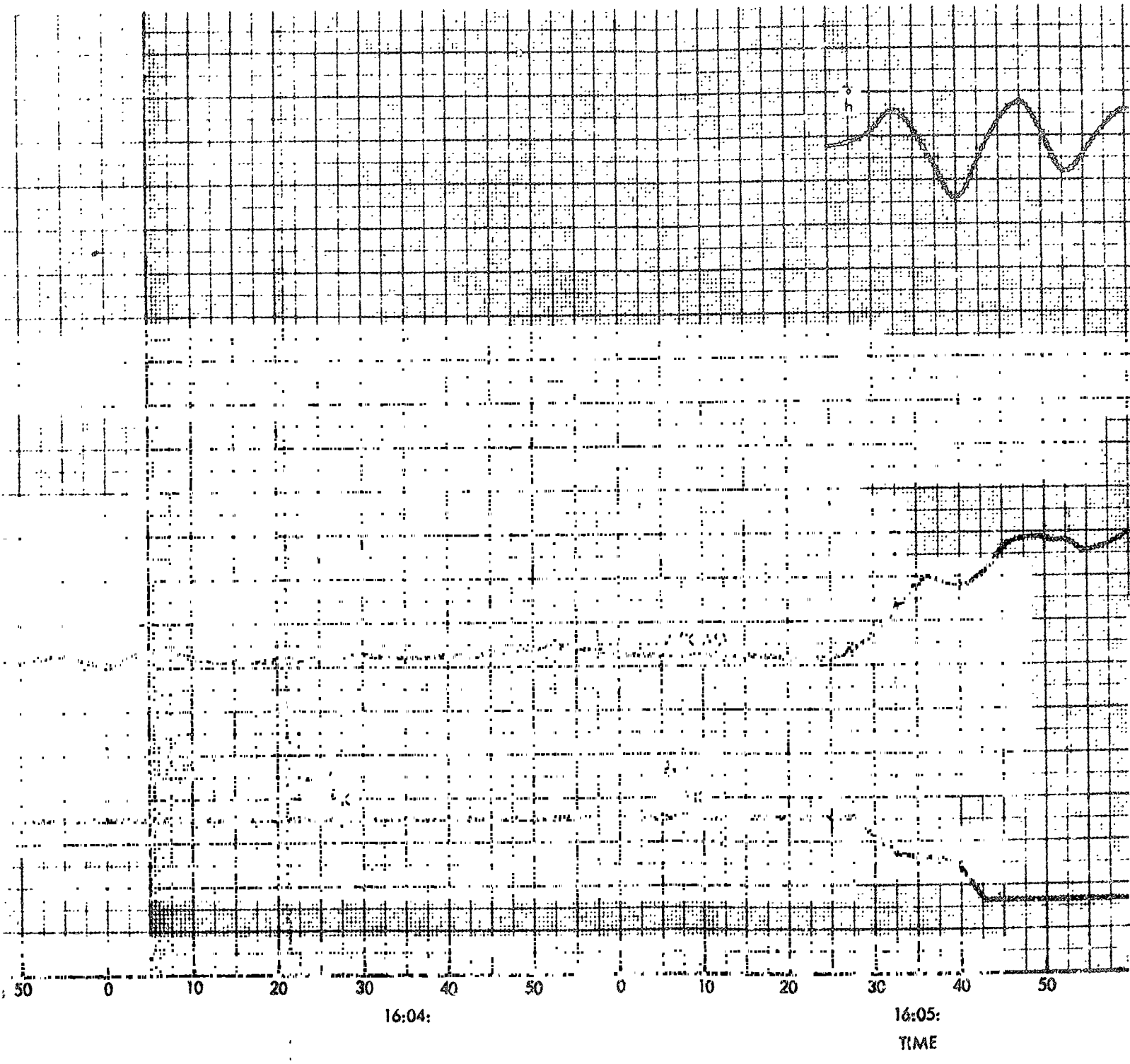

FOLDOUT FRAME 3

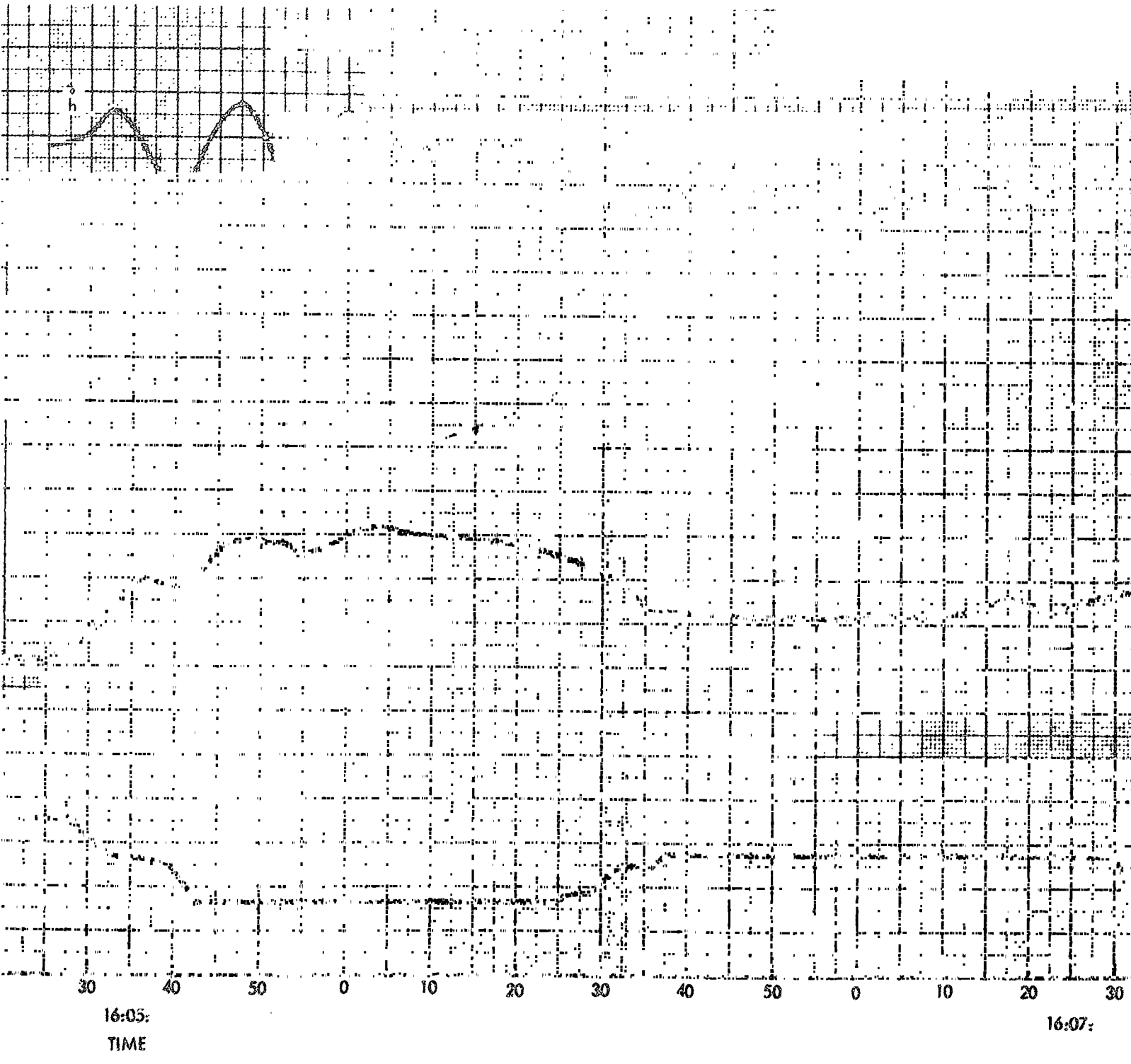

Figure 27. Flight

FOLDOUT FRAME 4

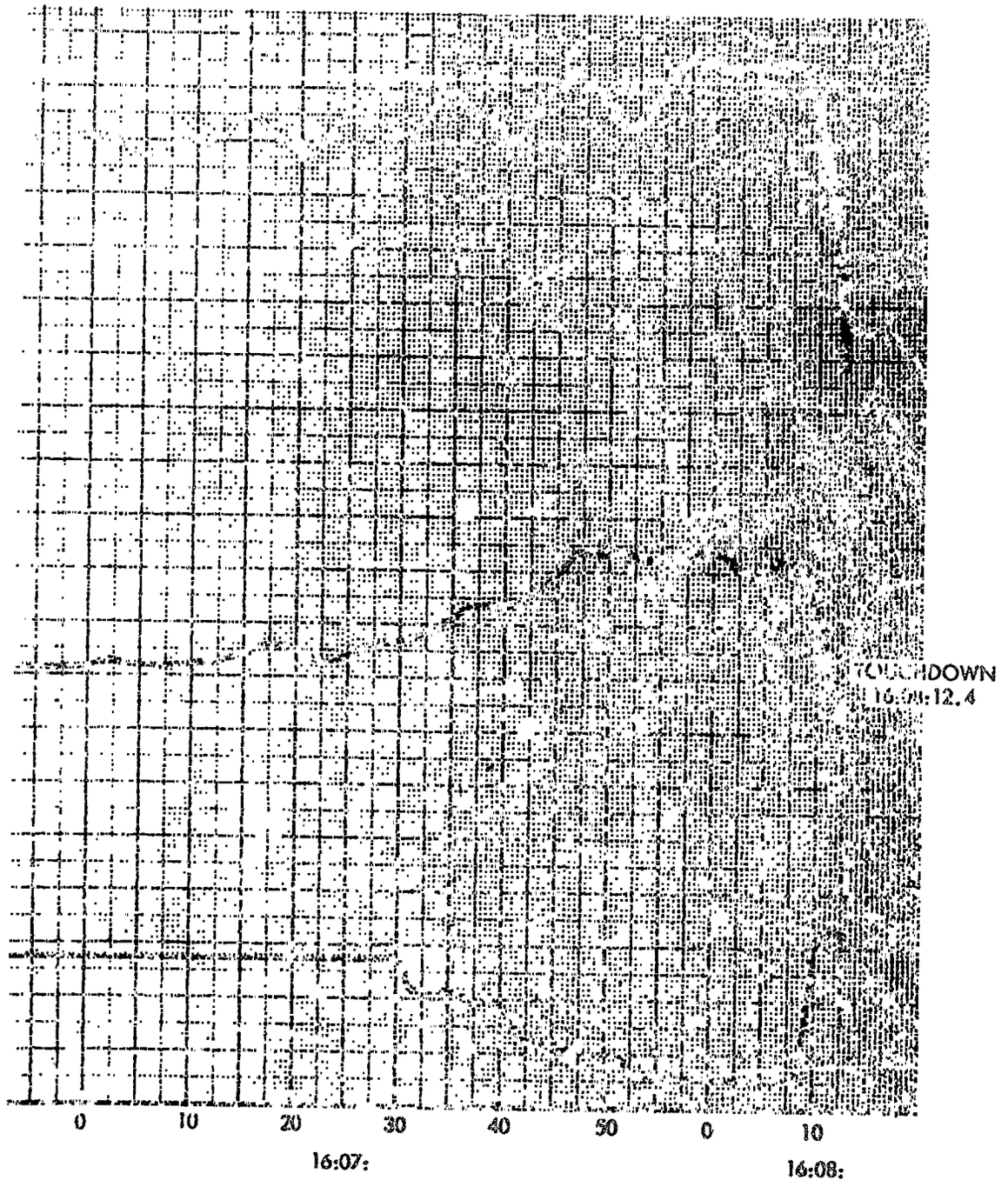

Figure 27. Flight 023 Time Histories (Sheet 1 of 2)

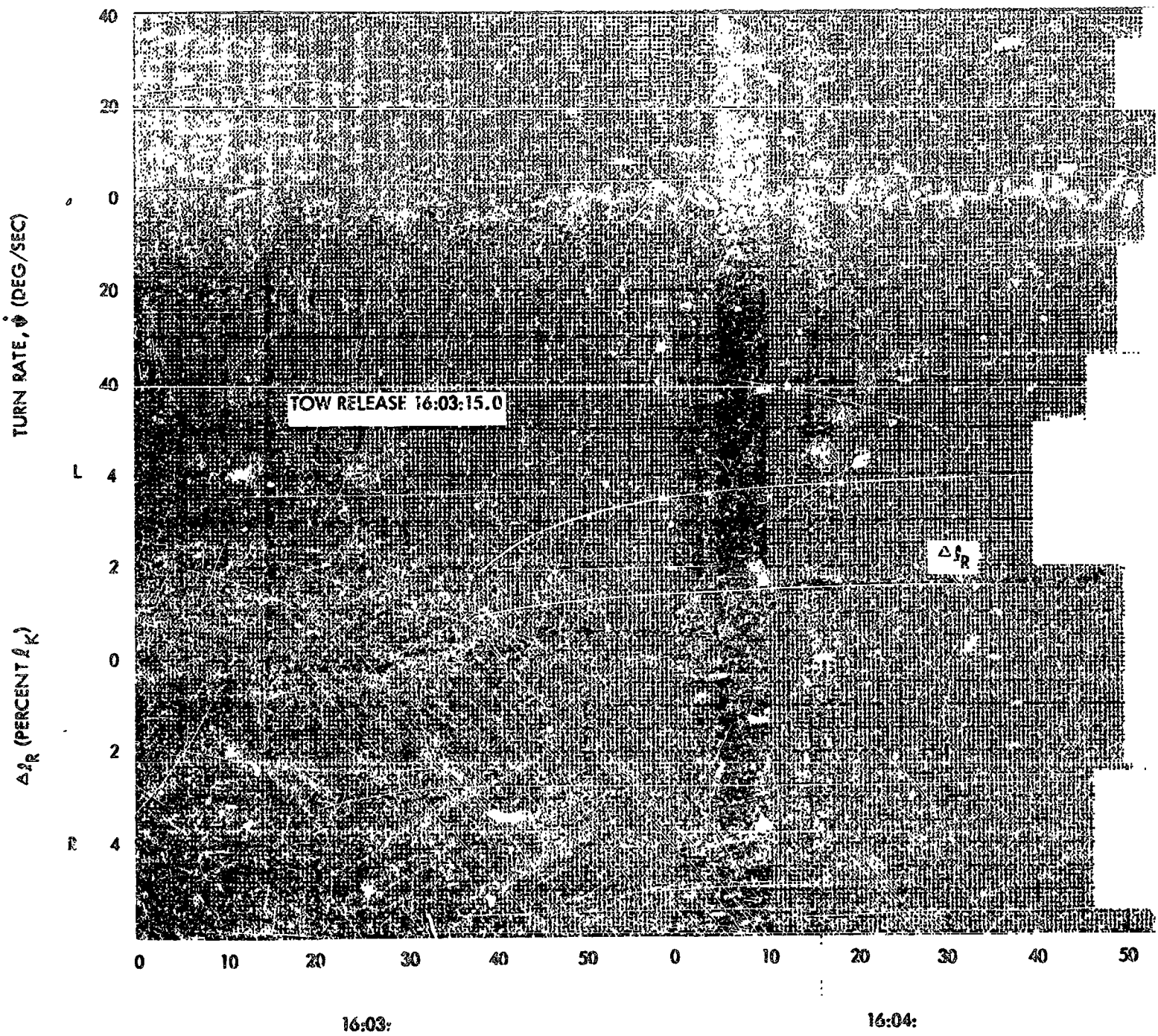

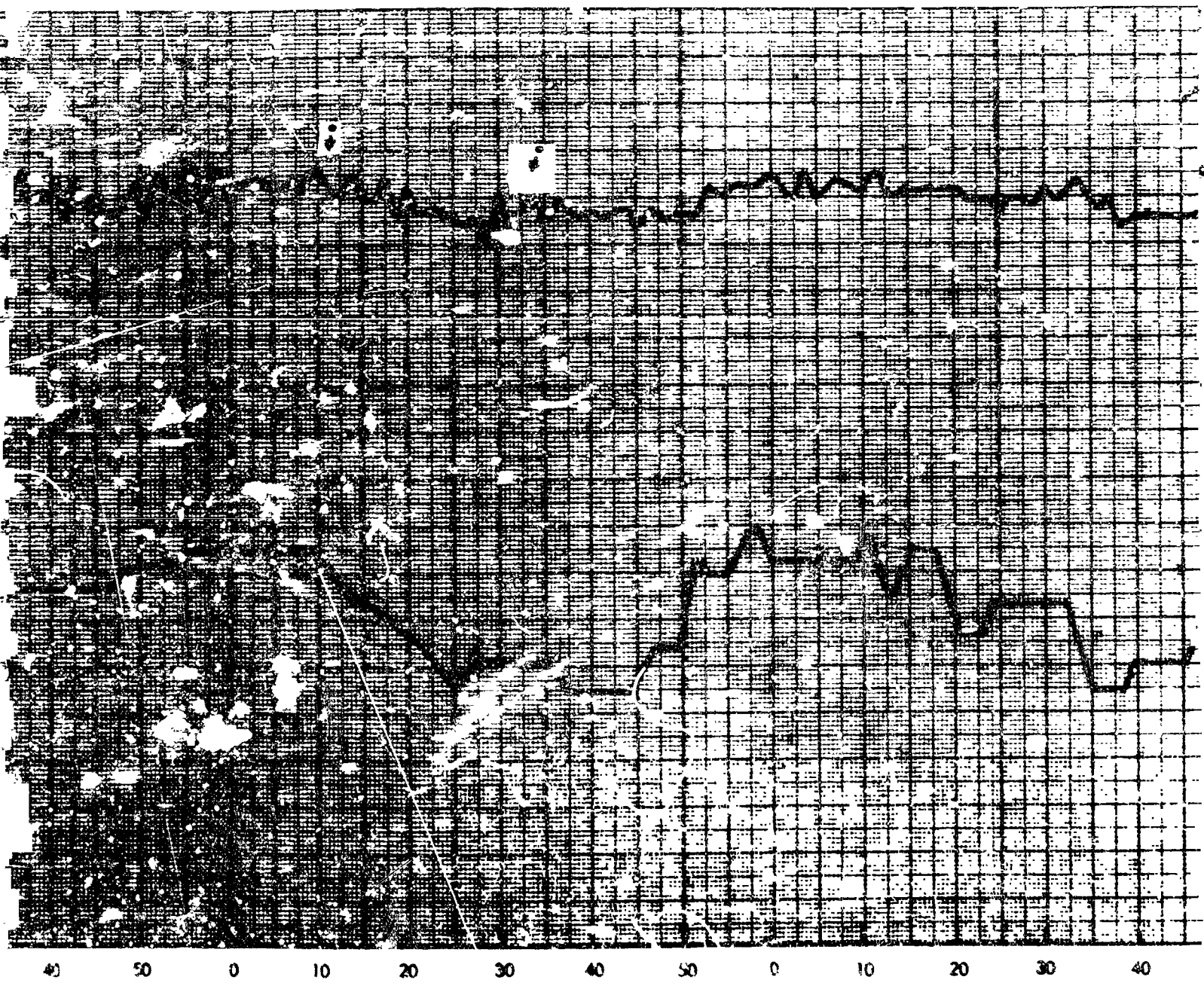
40
50
0
10
20
30
40
50
0
10
20
30
40
16:05:
TIME

FOLDOUT FRAME 3

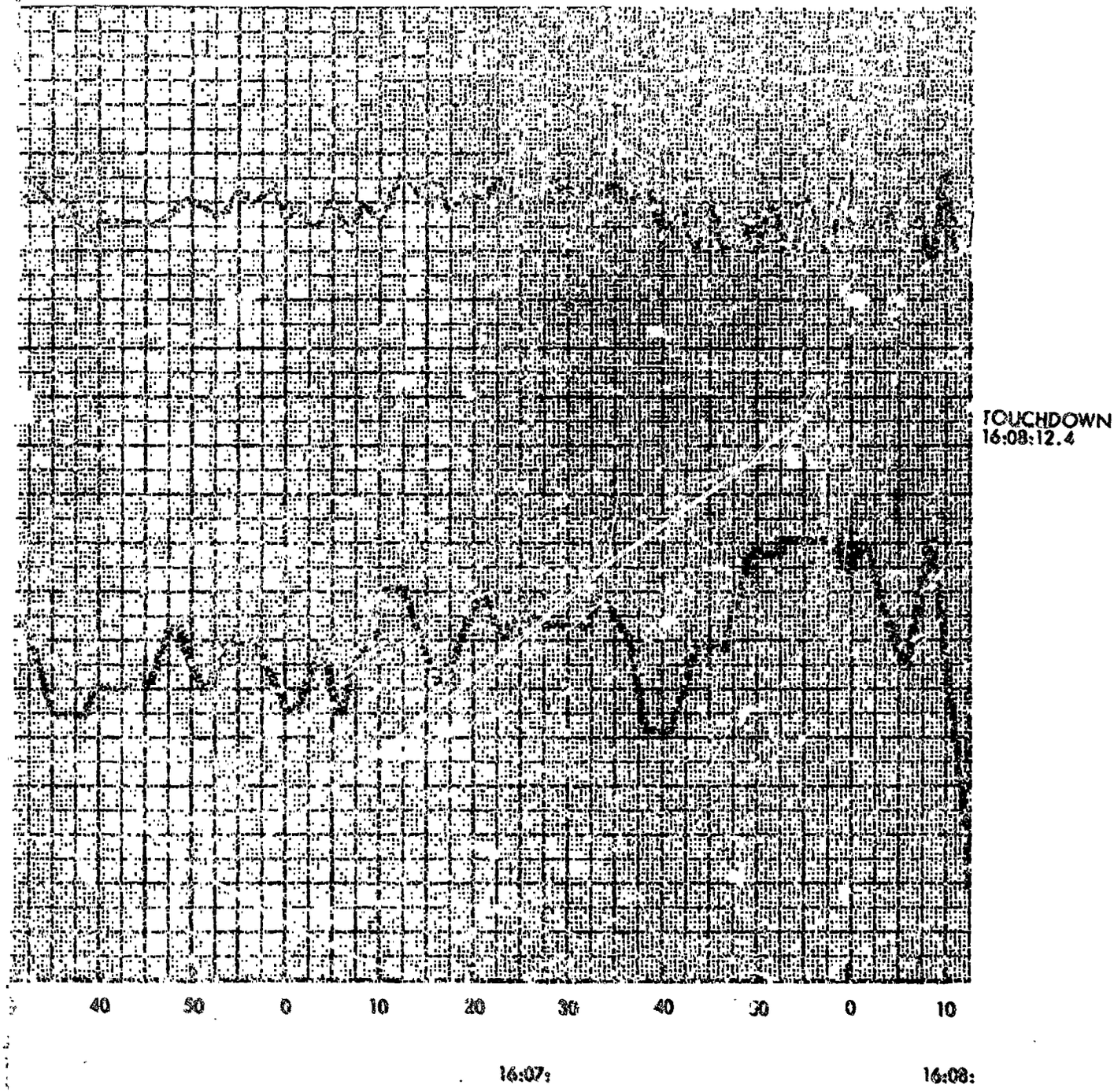

Figure 27. Flight 028 Time Histories (Sheet 2 of 2)

FOLDOUT FRAME

FOLDOUT FRAME

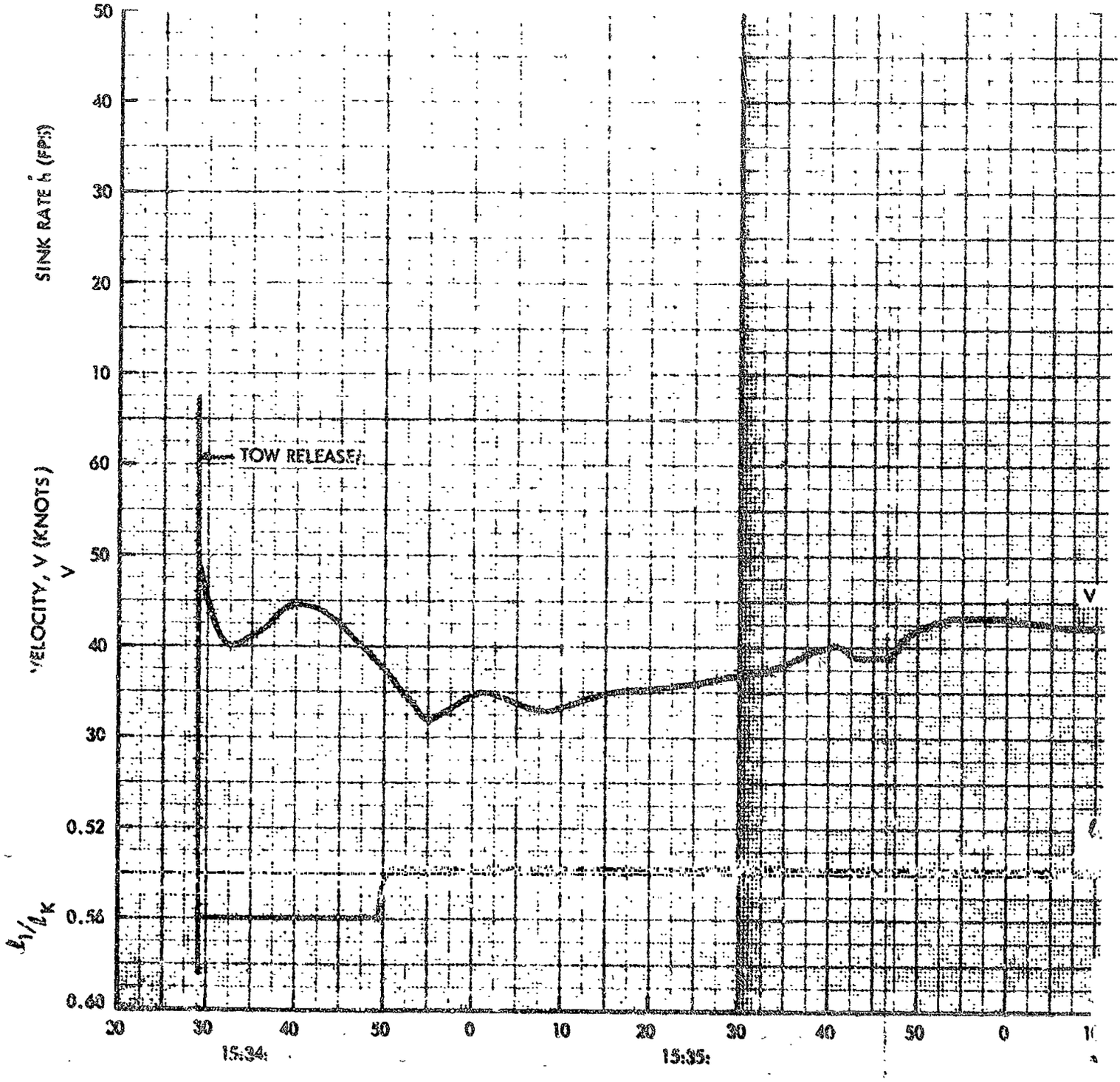

1

FOLDOUT FRAME 2

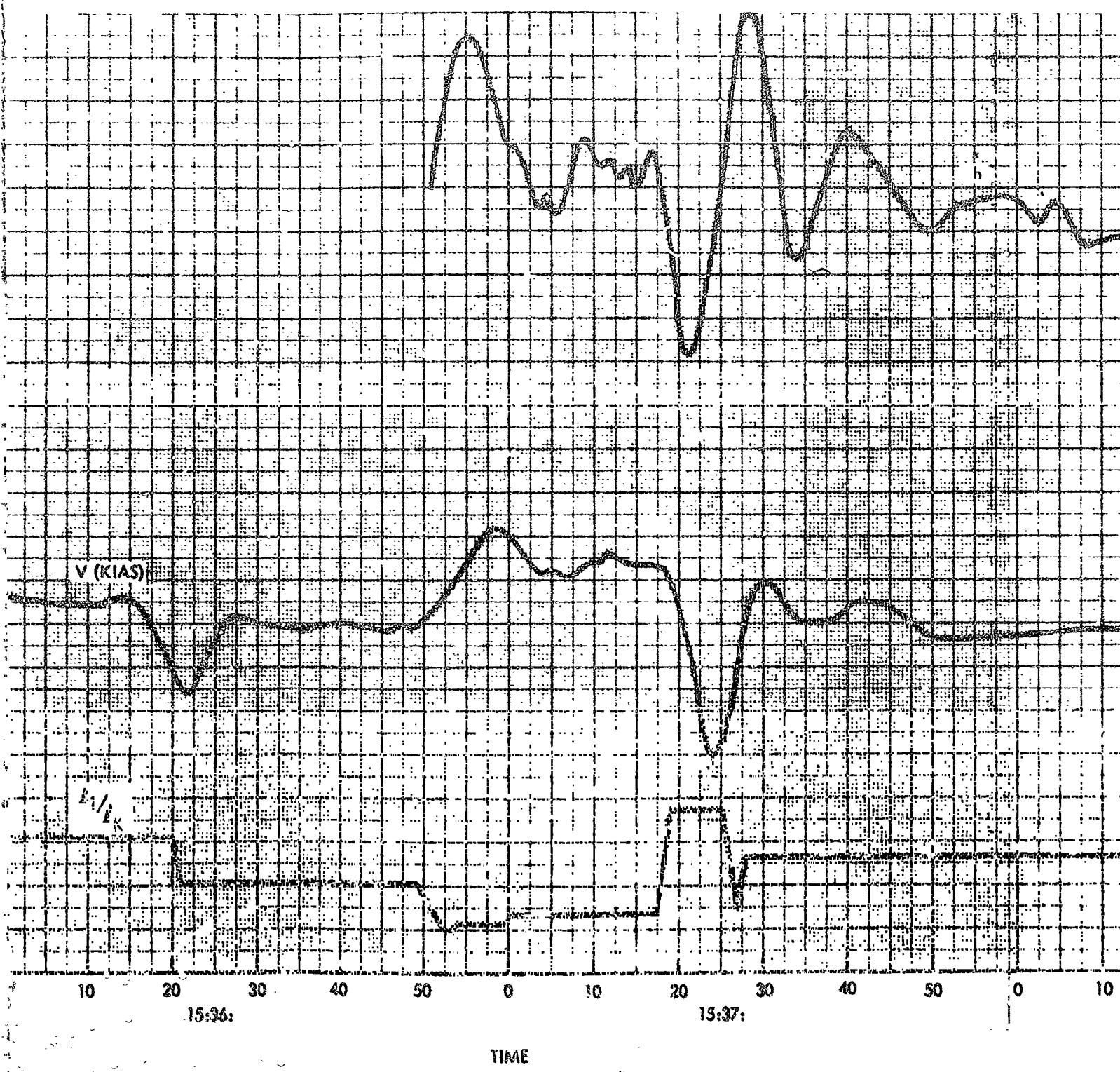

FOLDOUT FRAME 3

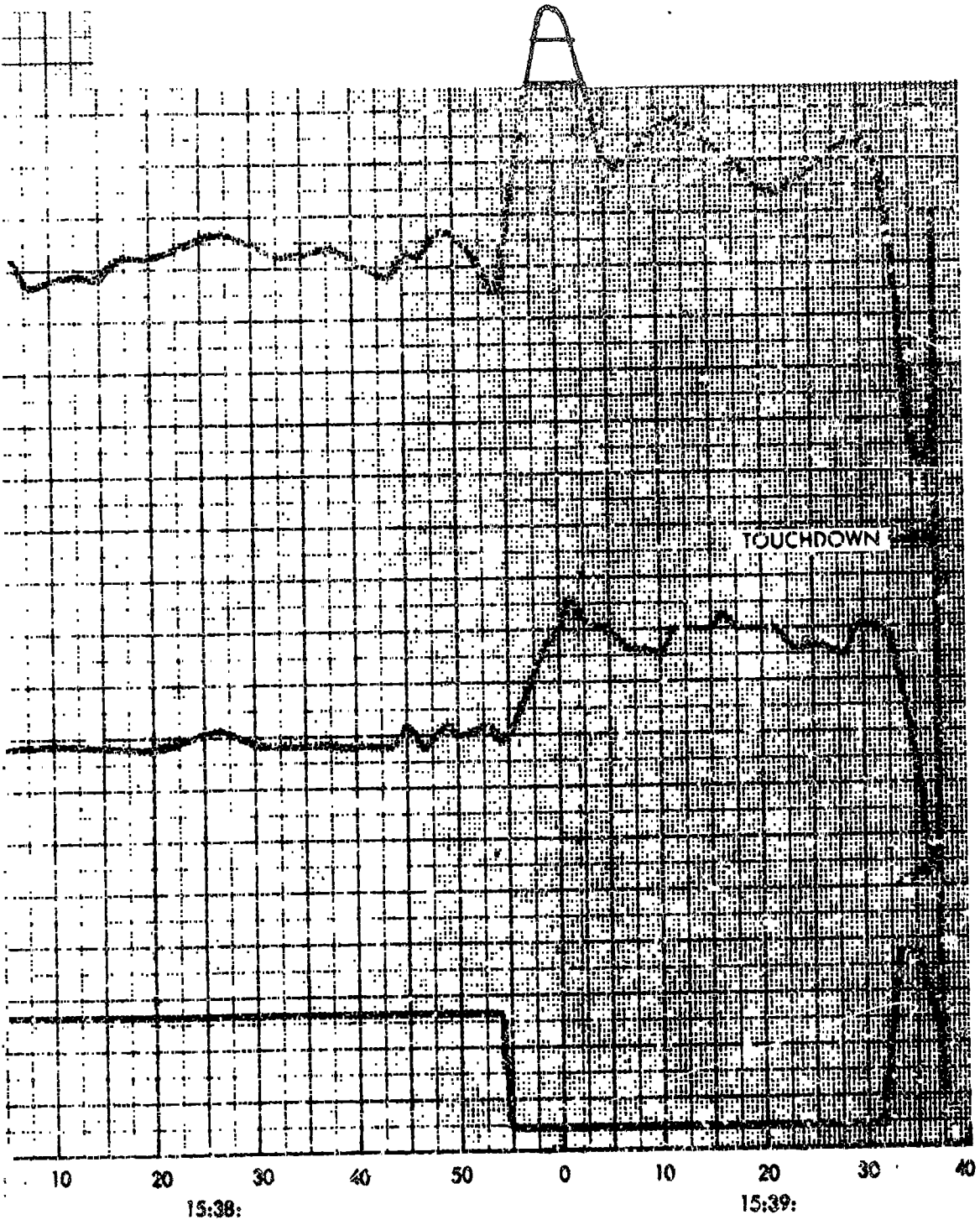

Figure 28. Flight 029 Time Histories (Sheet 1 of 2)

FOLDOUT FRAME

FOLDOUT FRAME

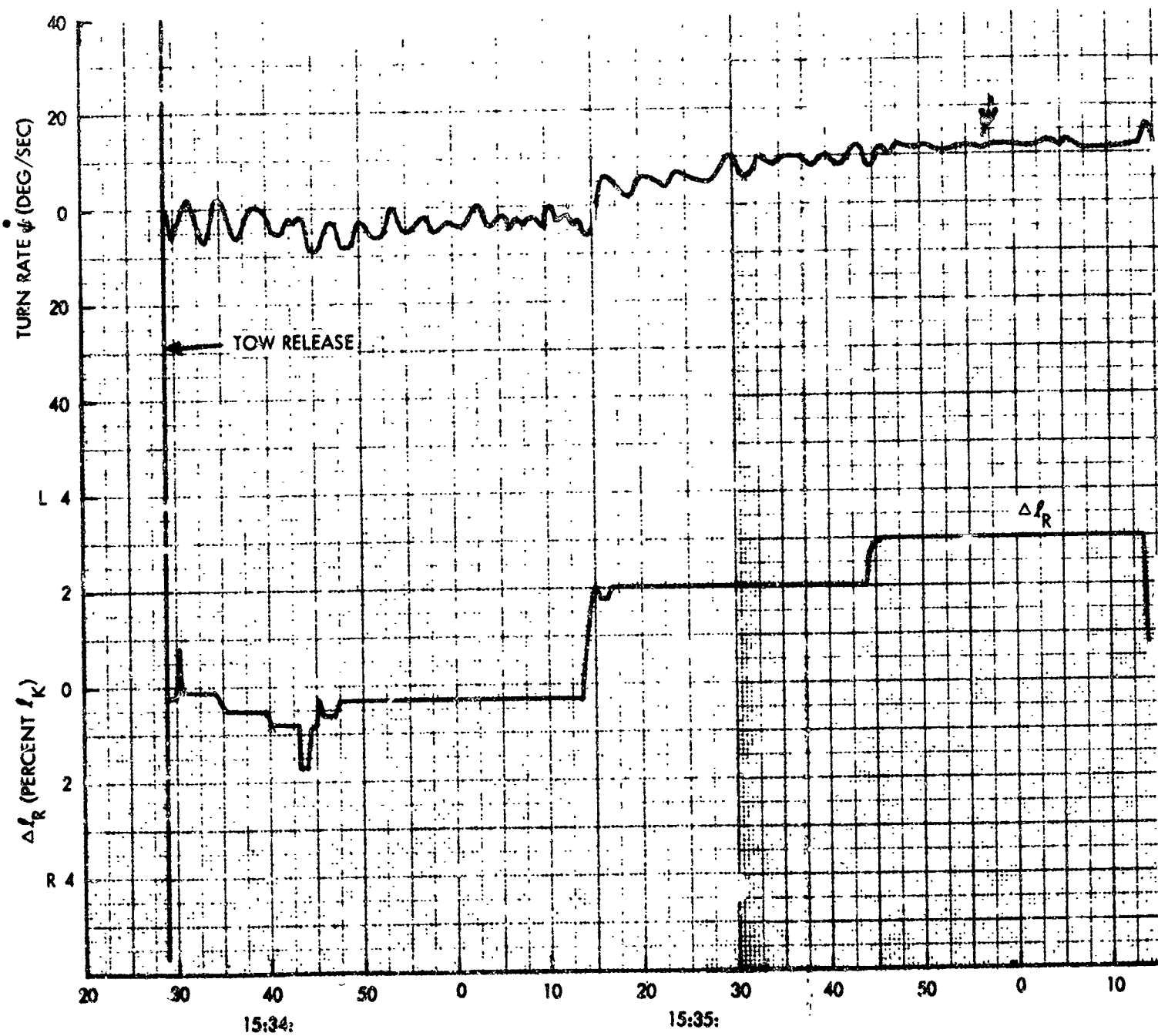

NORT

FOLDOUT FRAME 2

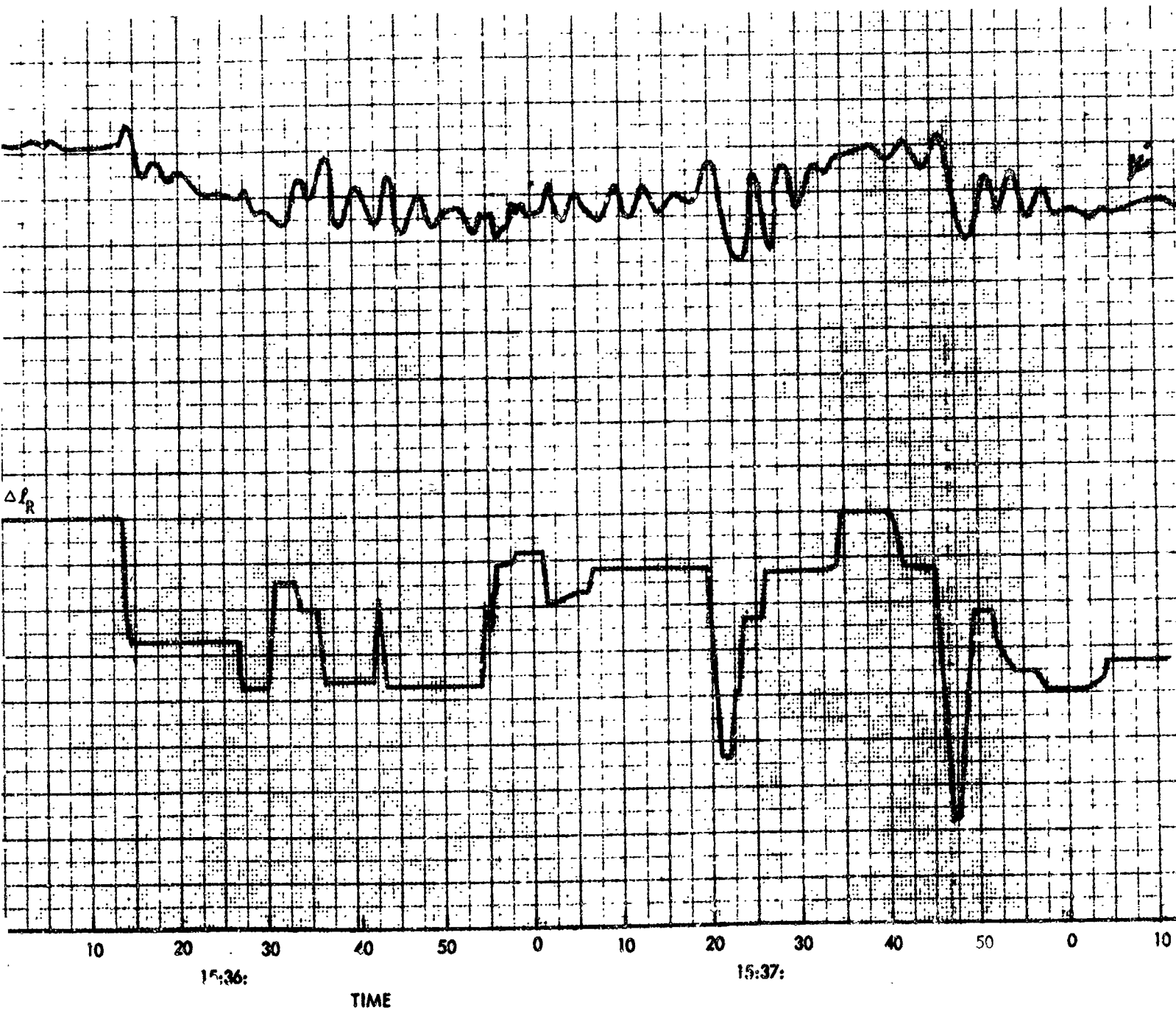

FOLDOUT FRAME 3

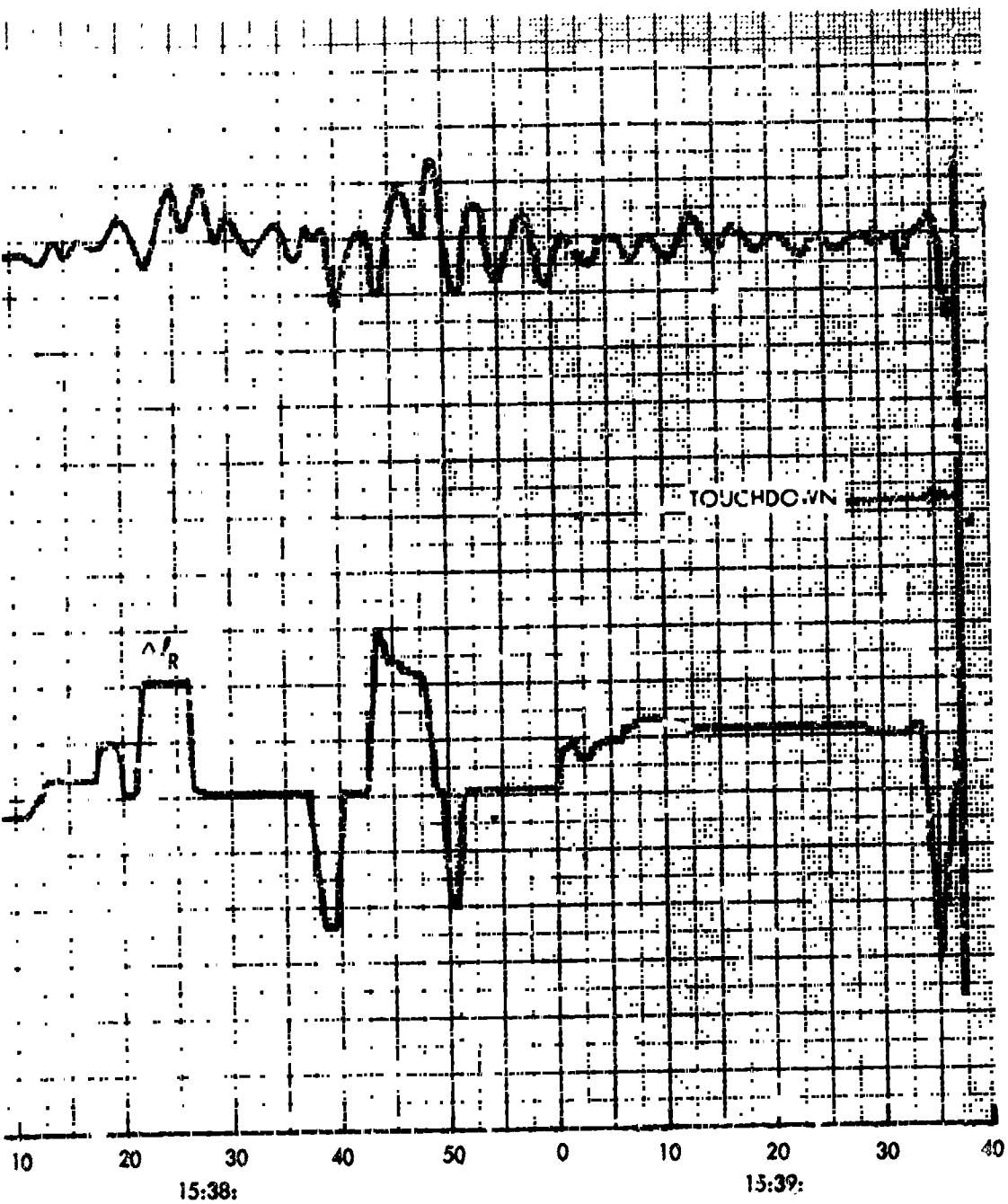

Figure 28. Flight 029 Time Histories (Sheet 2 of 2)

FOLDOUT FRAME

FOLDOUT FRAME

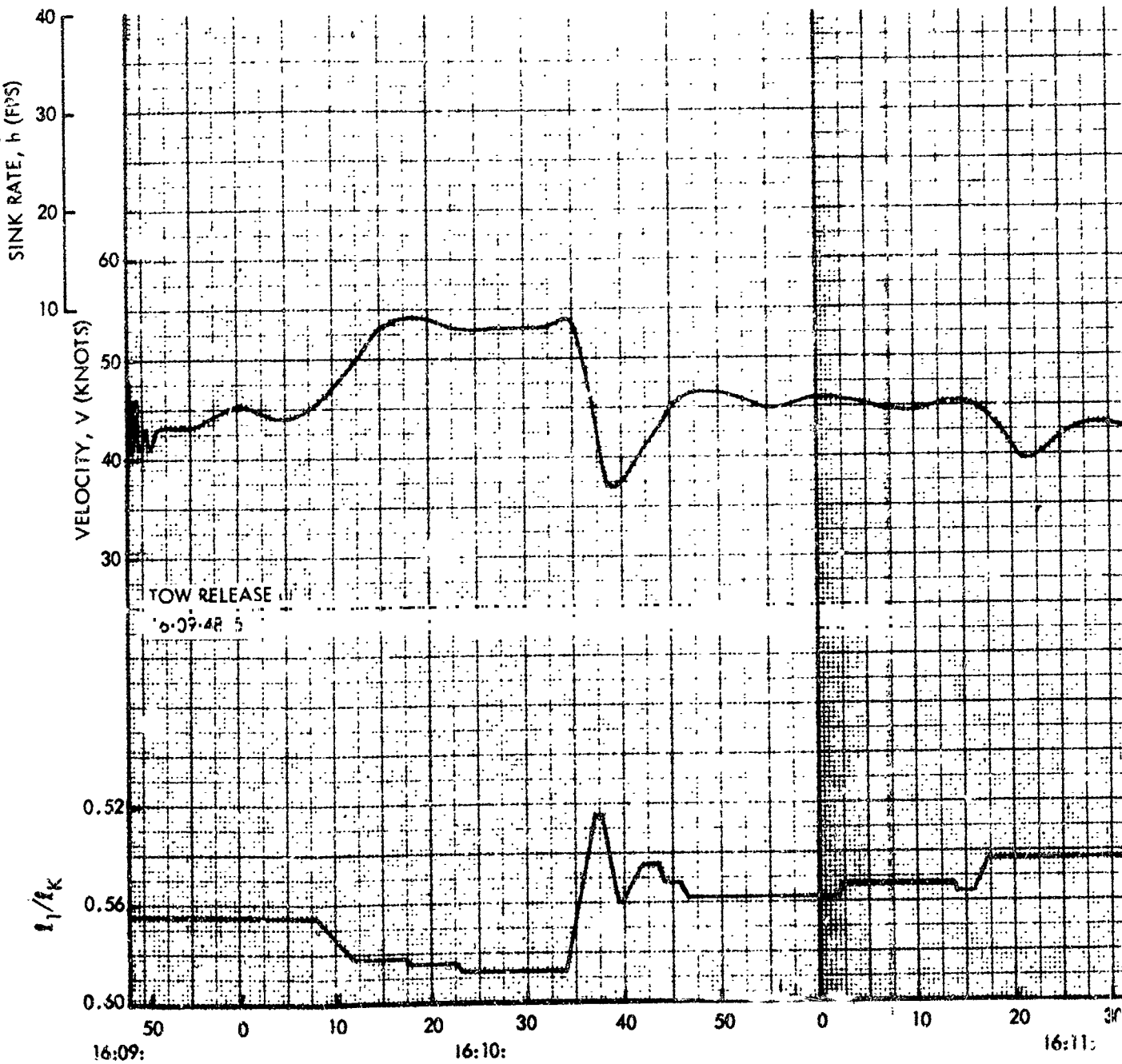

FOLDOUT FRAME 2

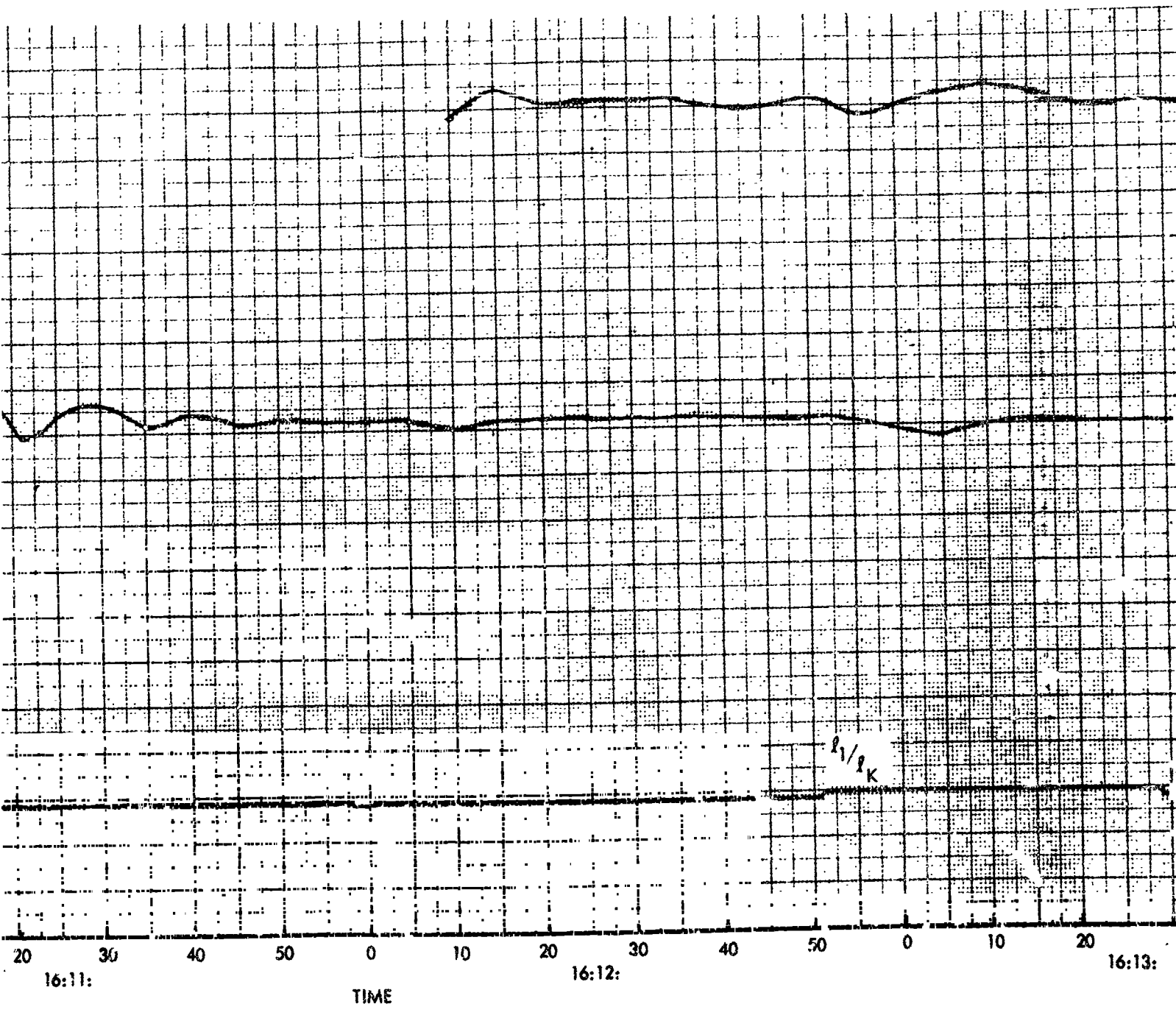

FOLDOUT FRAME 3

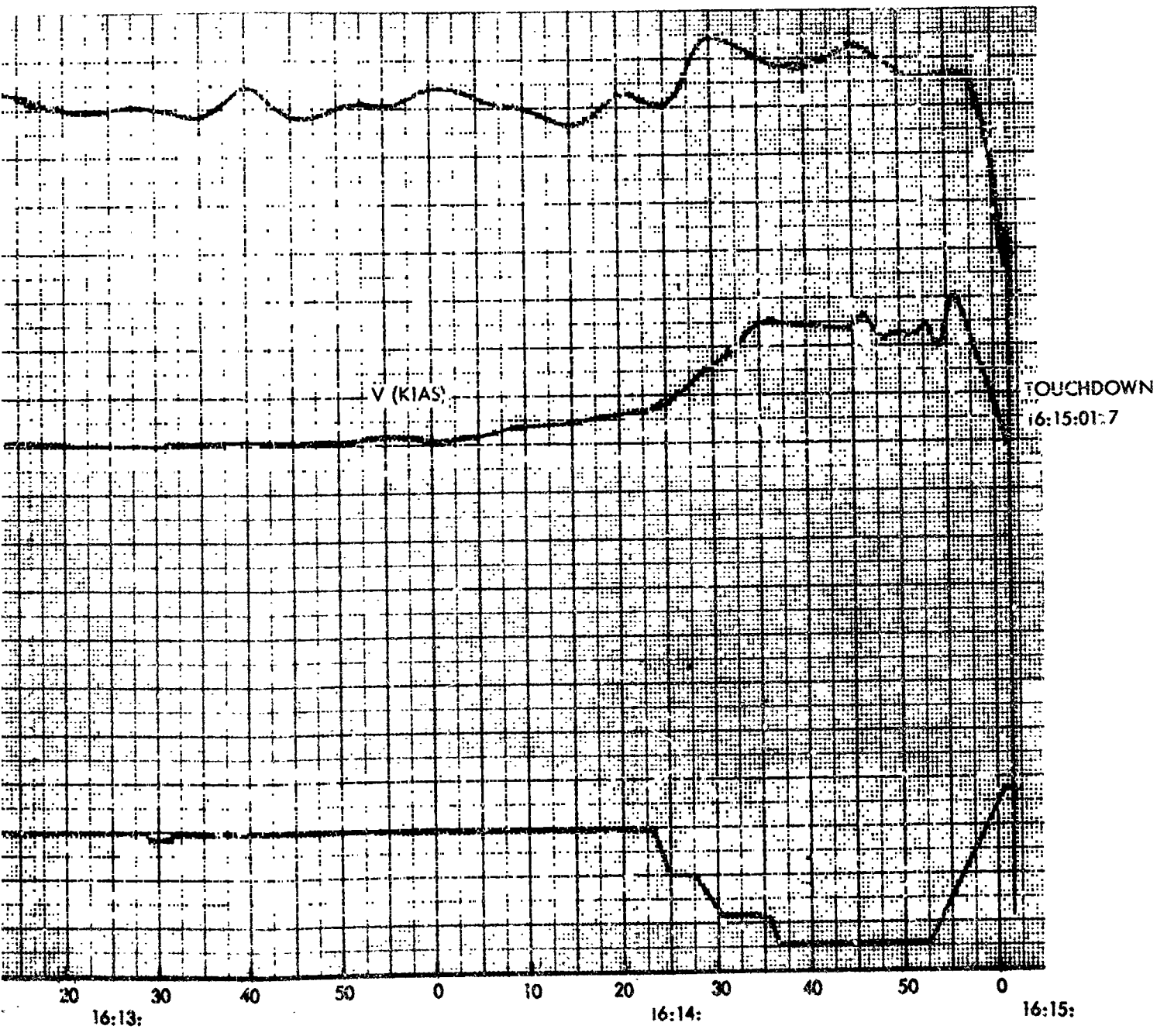

Figure 39. Flight 030 Time Histories (Sheet 1 of 2)

FOLDOUT FRAME 1

FOLDOUT FRAME

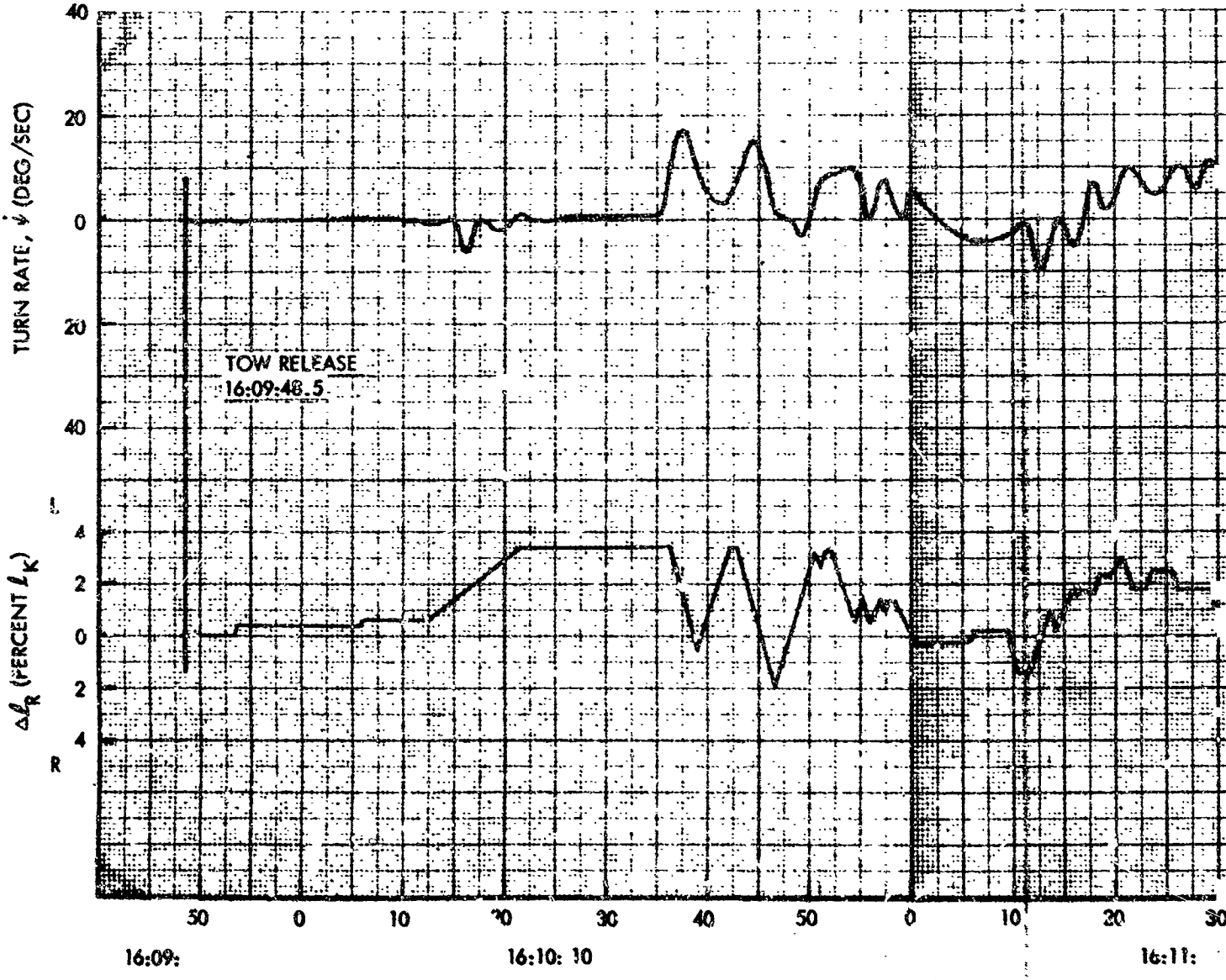

FOLDOUT FRAME 2

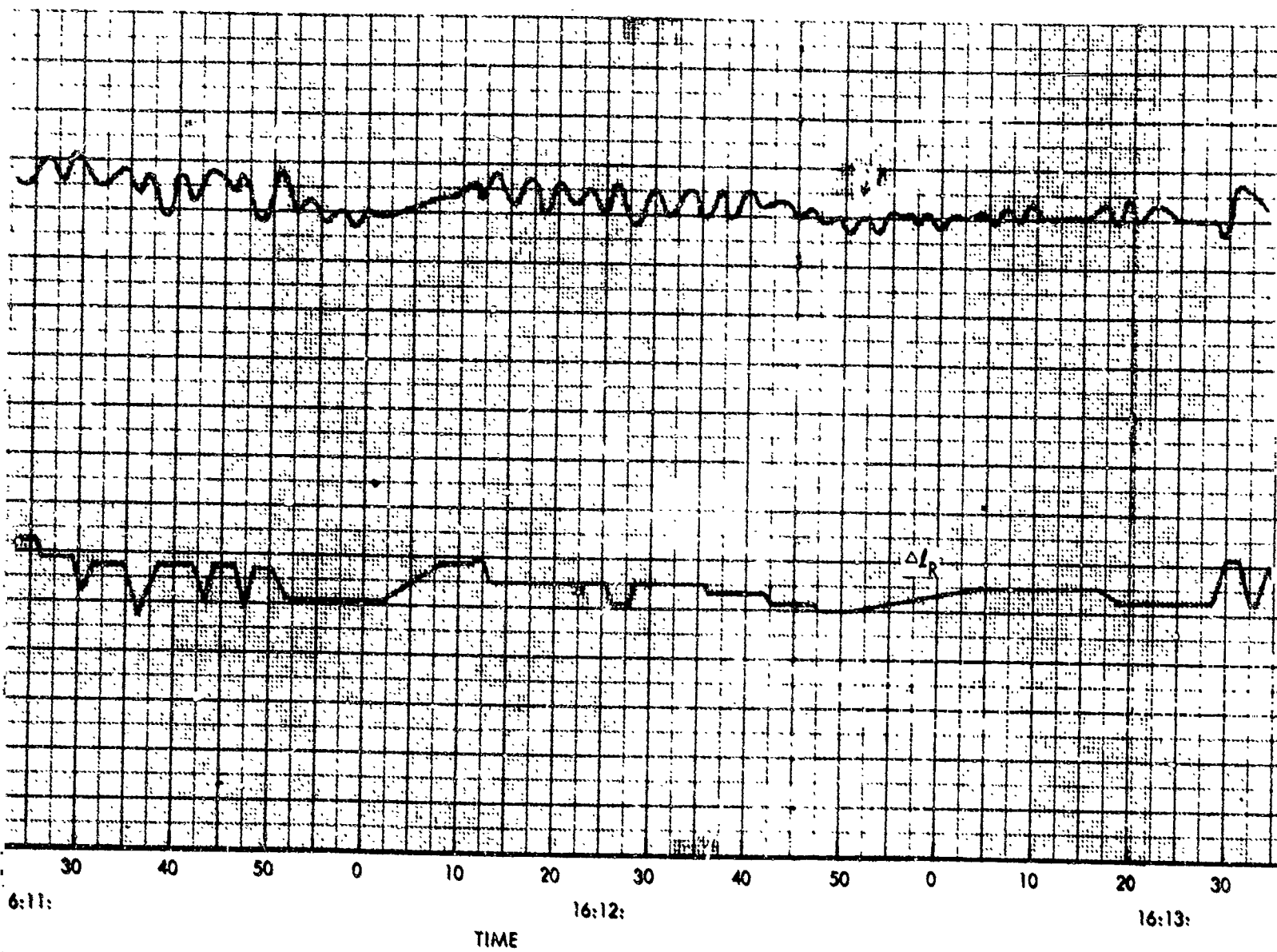

FOLDOUT FRAME 3

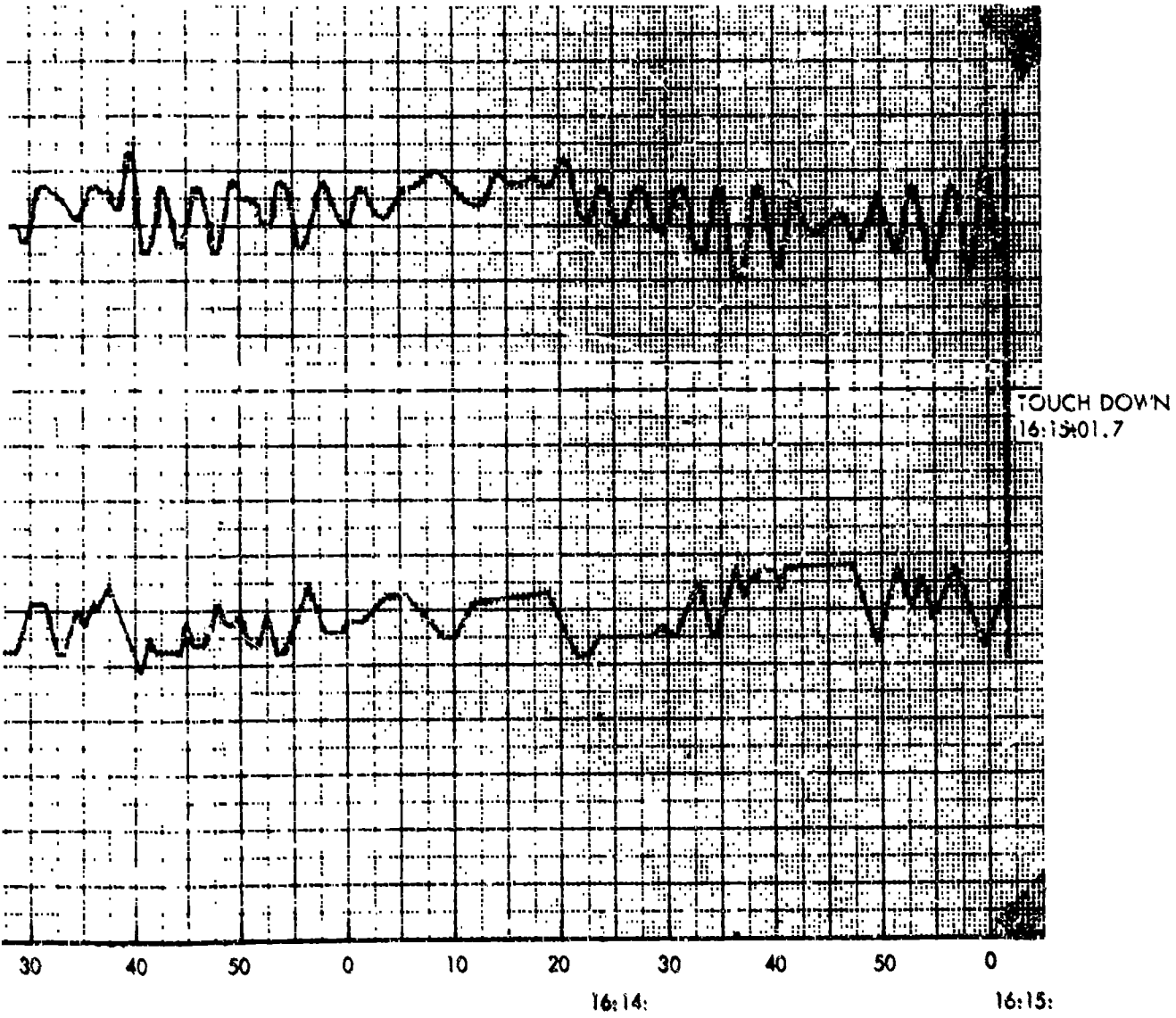

Figure 39. Flight 030 Time Histories (Sheet 2 of 2)

FOLDOUT FRAME 1

FOL FRAME

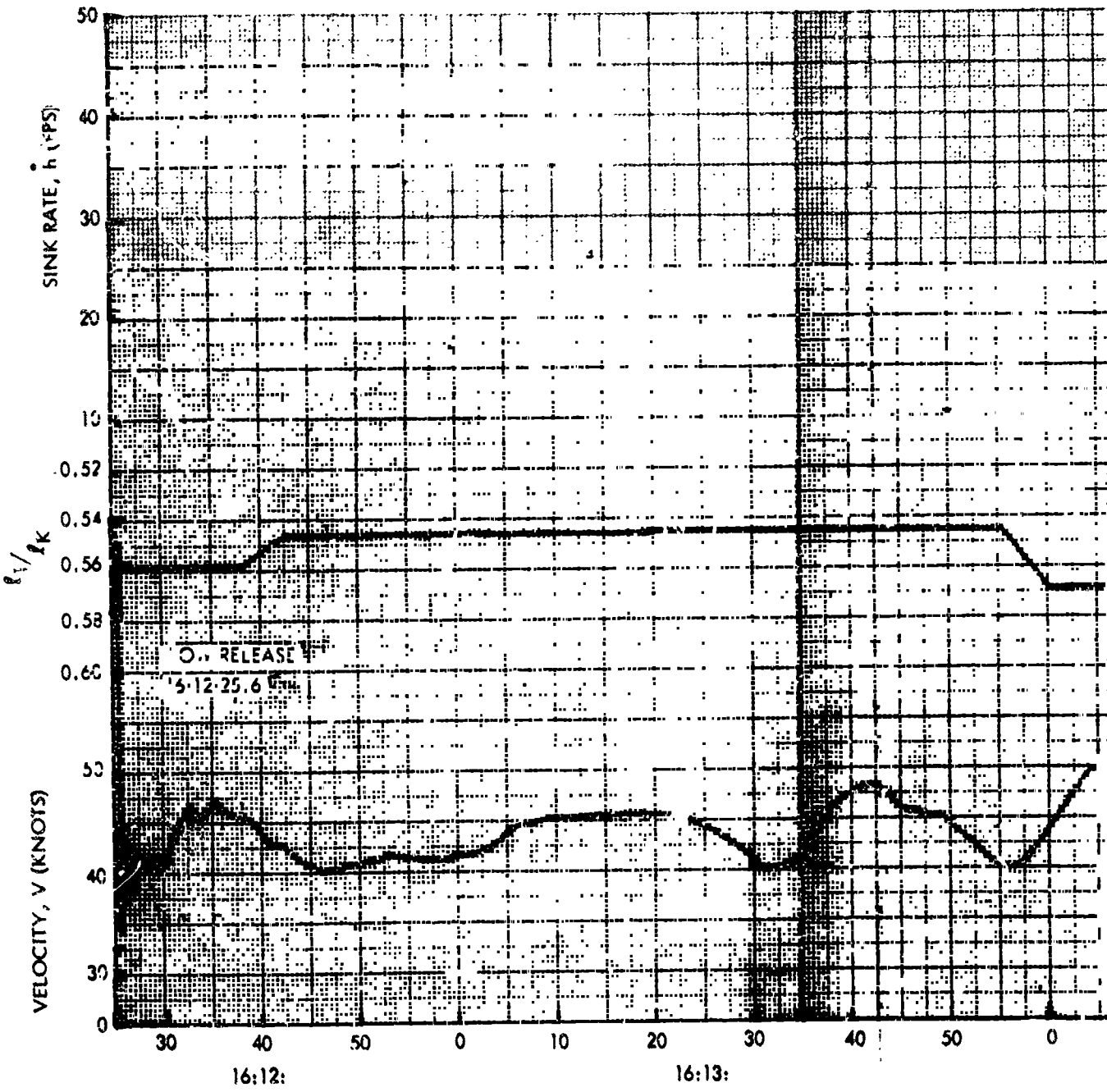

NO

FOLDOUT FRAME 2

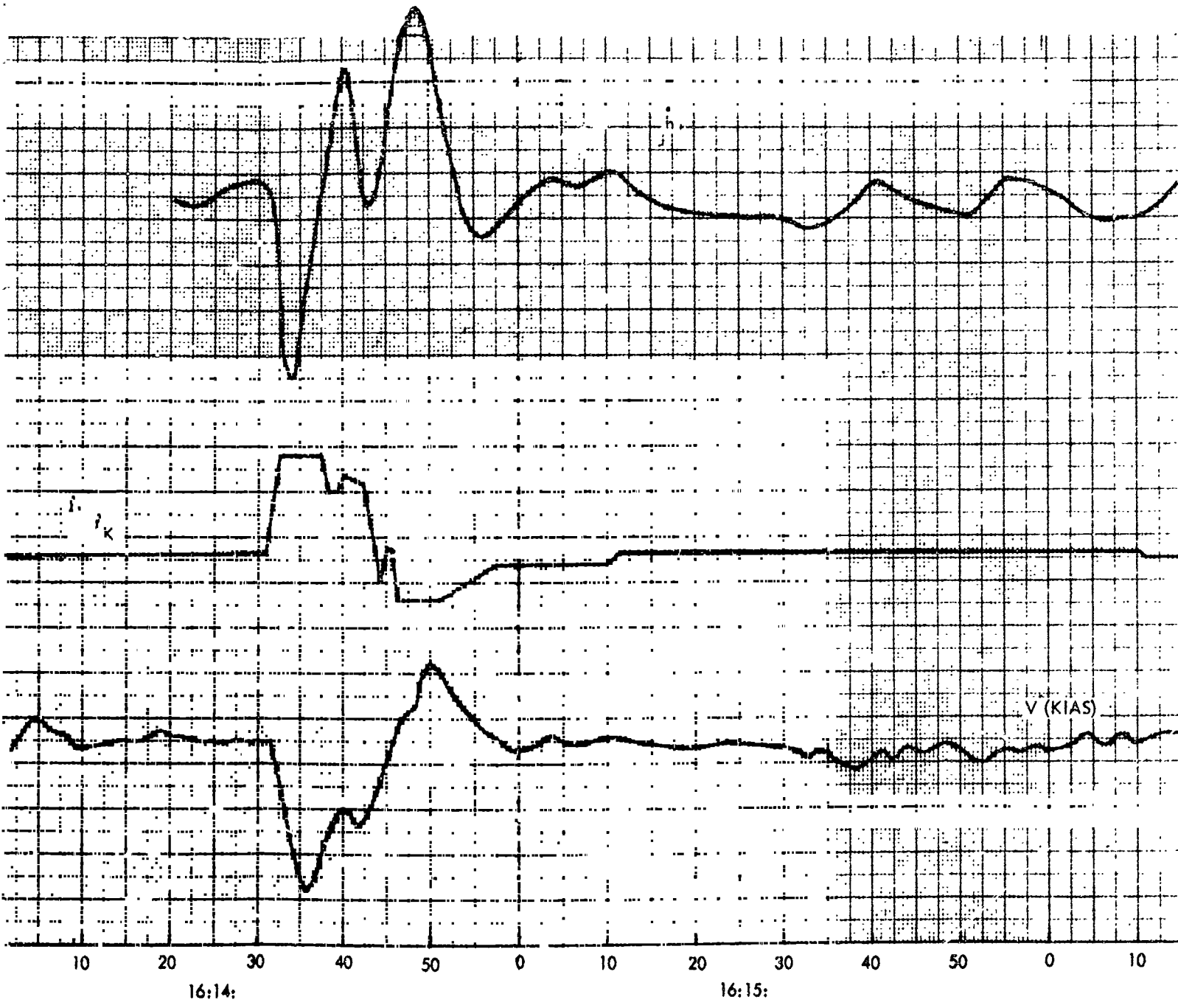

FOLDOUT FRAME 3

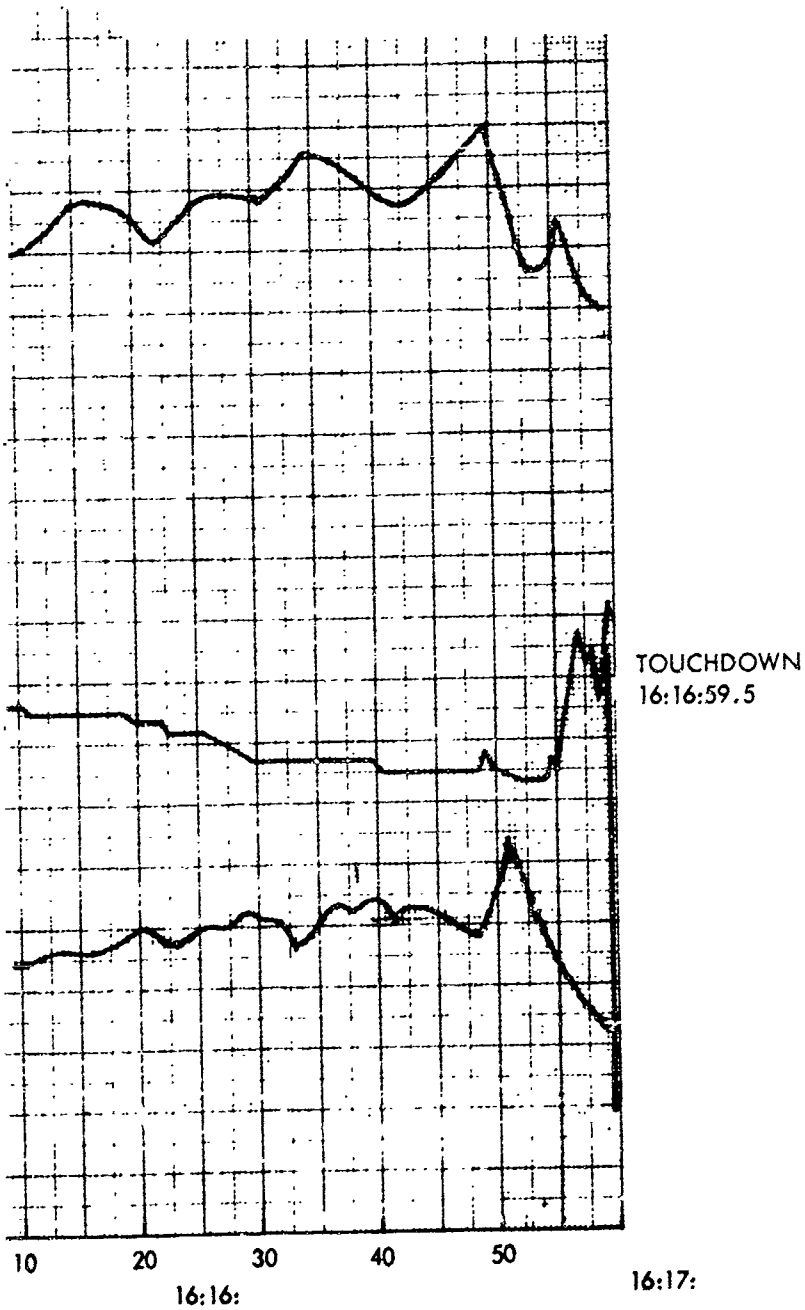

Figure 30. Flight 031 Time Histories (Sheet 1 of 2)

FOLDOUT FRAME 1

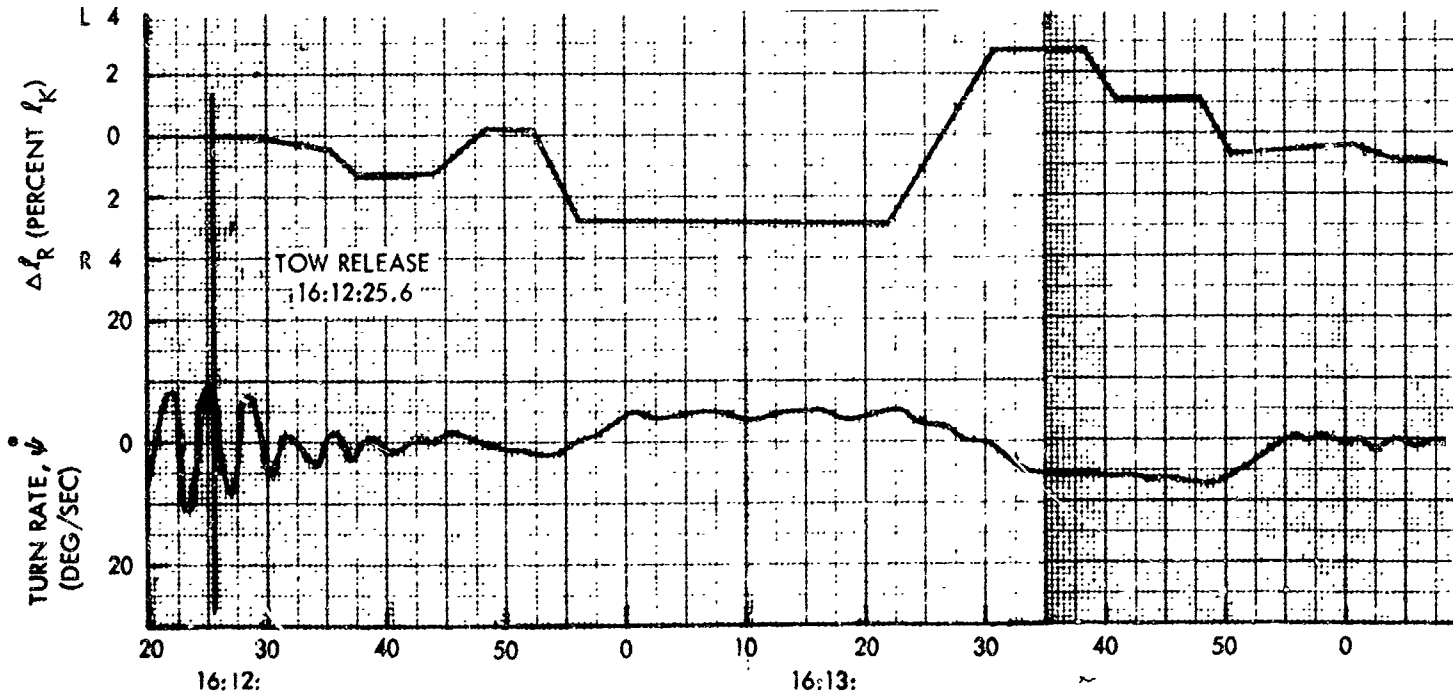

FOLDOUT FRAME 2

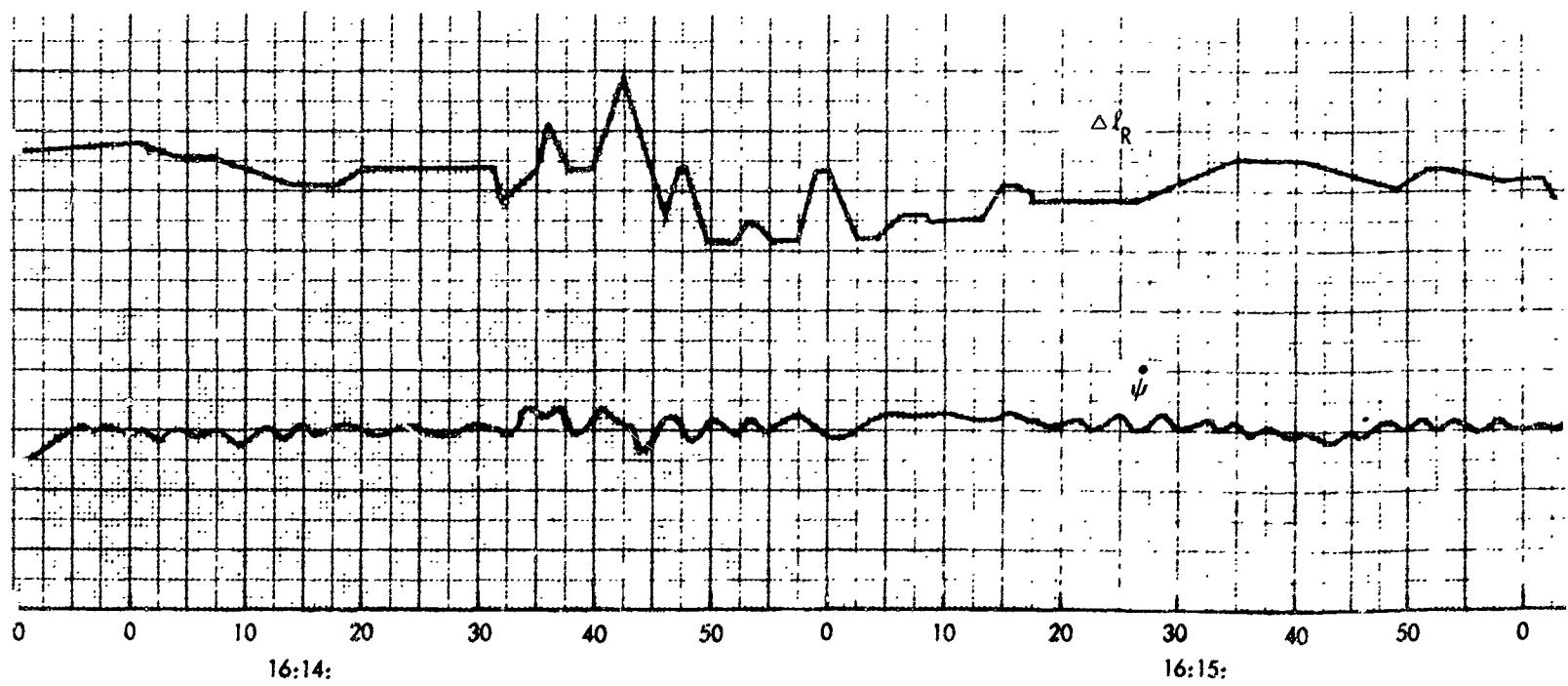

Figure

FOLDOUT FRAME 3

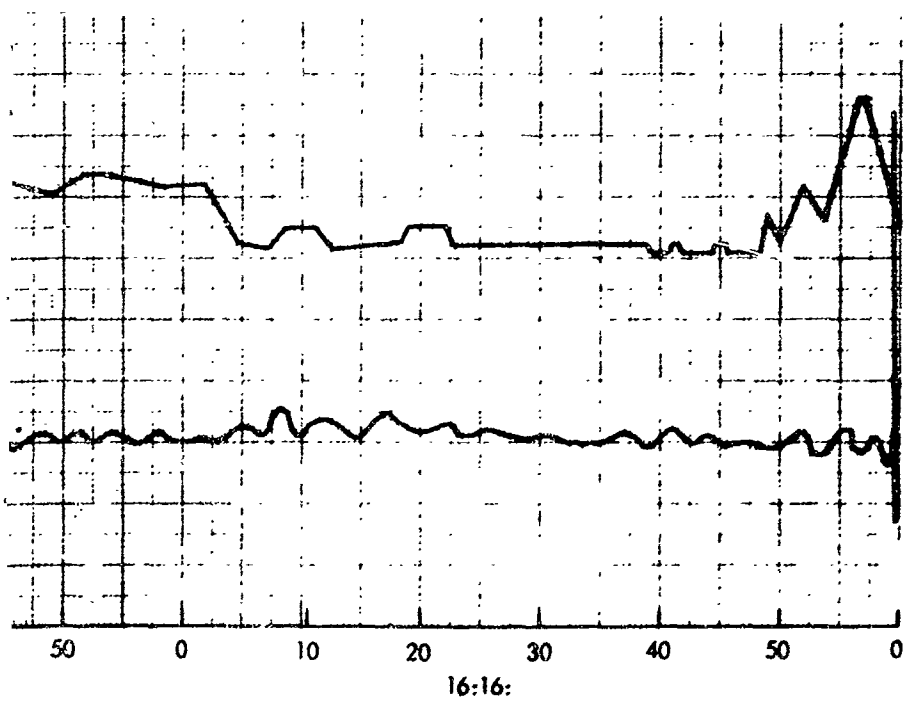

Figure 30. Flight 031 Time Histories (Sheet 2 of 2)

FOLDOUT FRAME 1

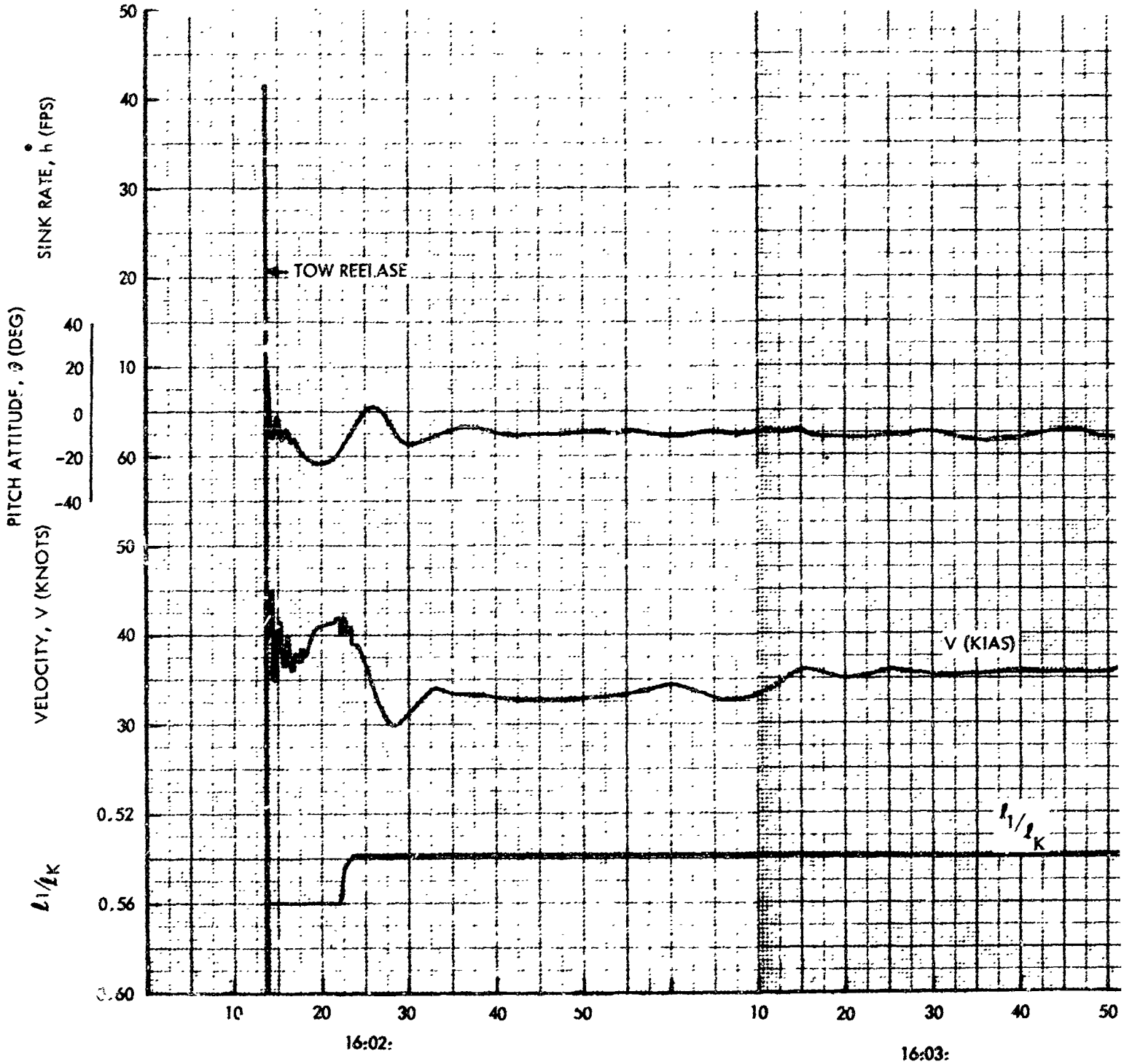

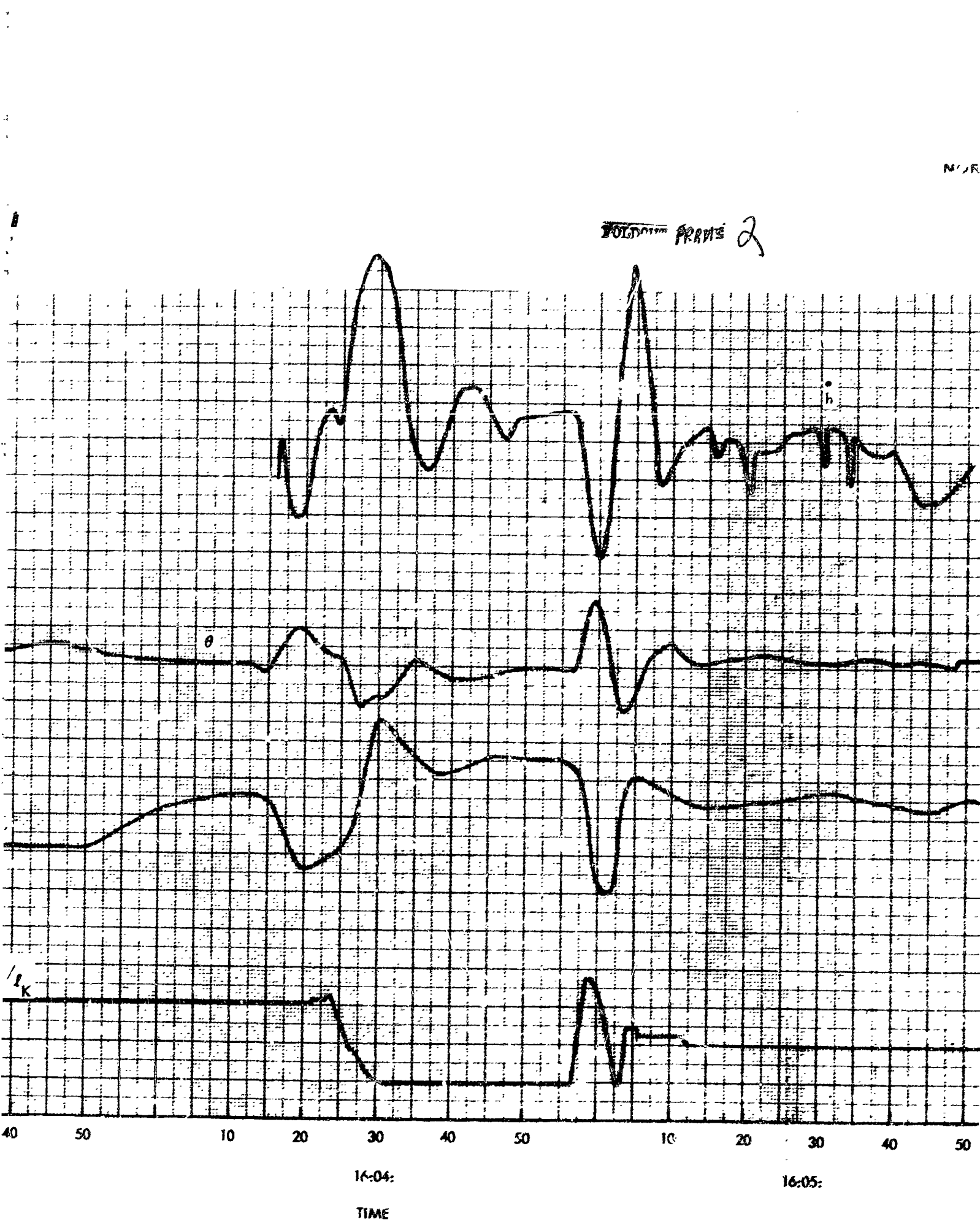
BOLDON PRAIRIE 2
ḣ
θ
/ℓK
40
50
10
20
30
40
50
10
20
30
40
50
16:04:
16:05:
TIME

FOLDOUT FRAME 2

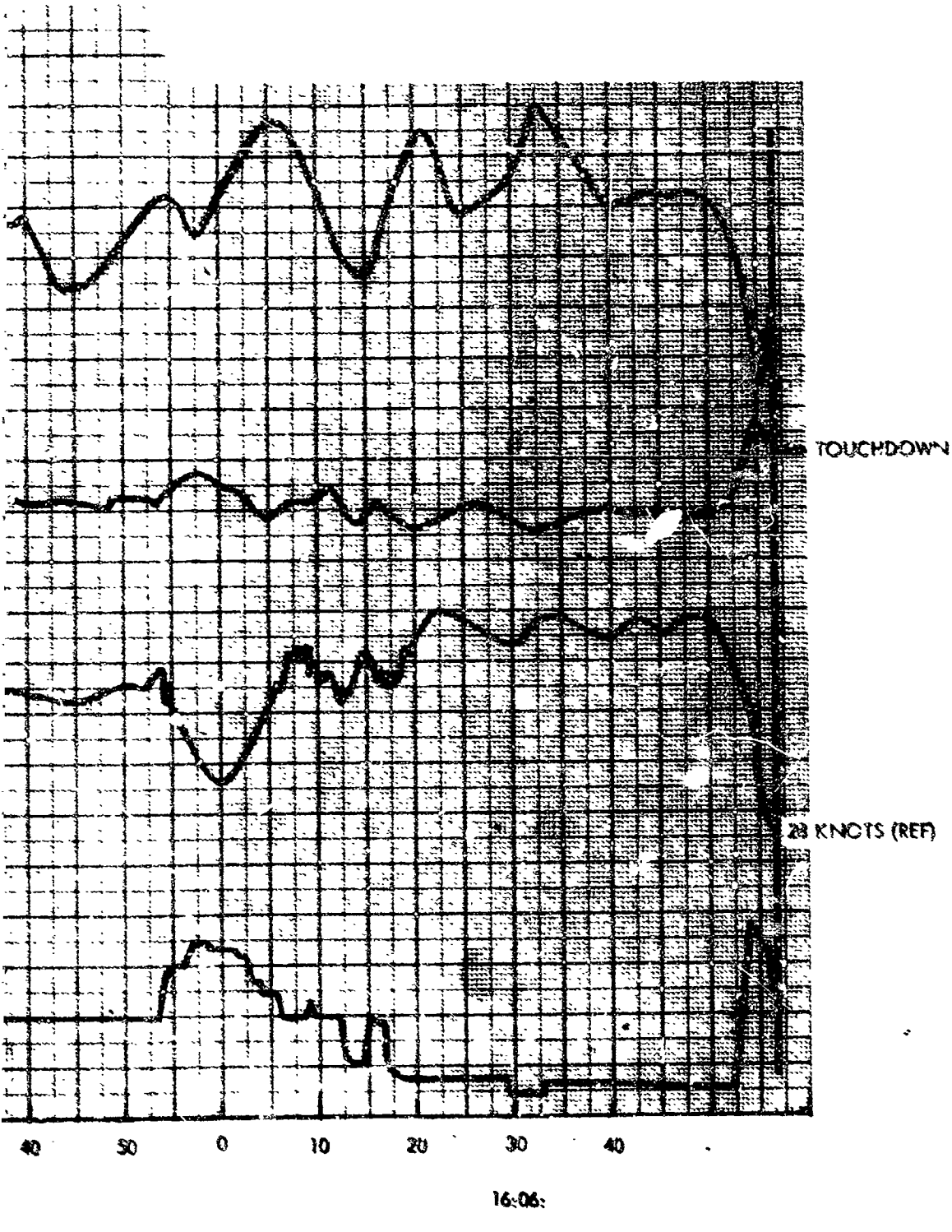

Figure 31. Flight 032 Time Histories (Sheet 1 of 2)

FOLDOUT FRAME

FOLDOUT FRAME

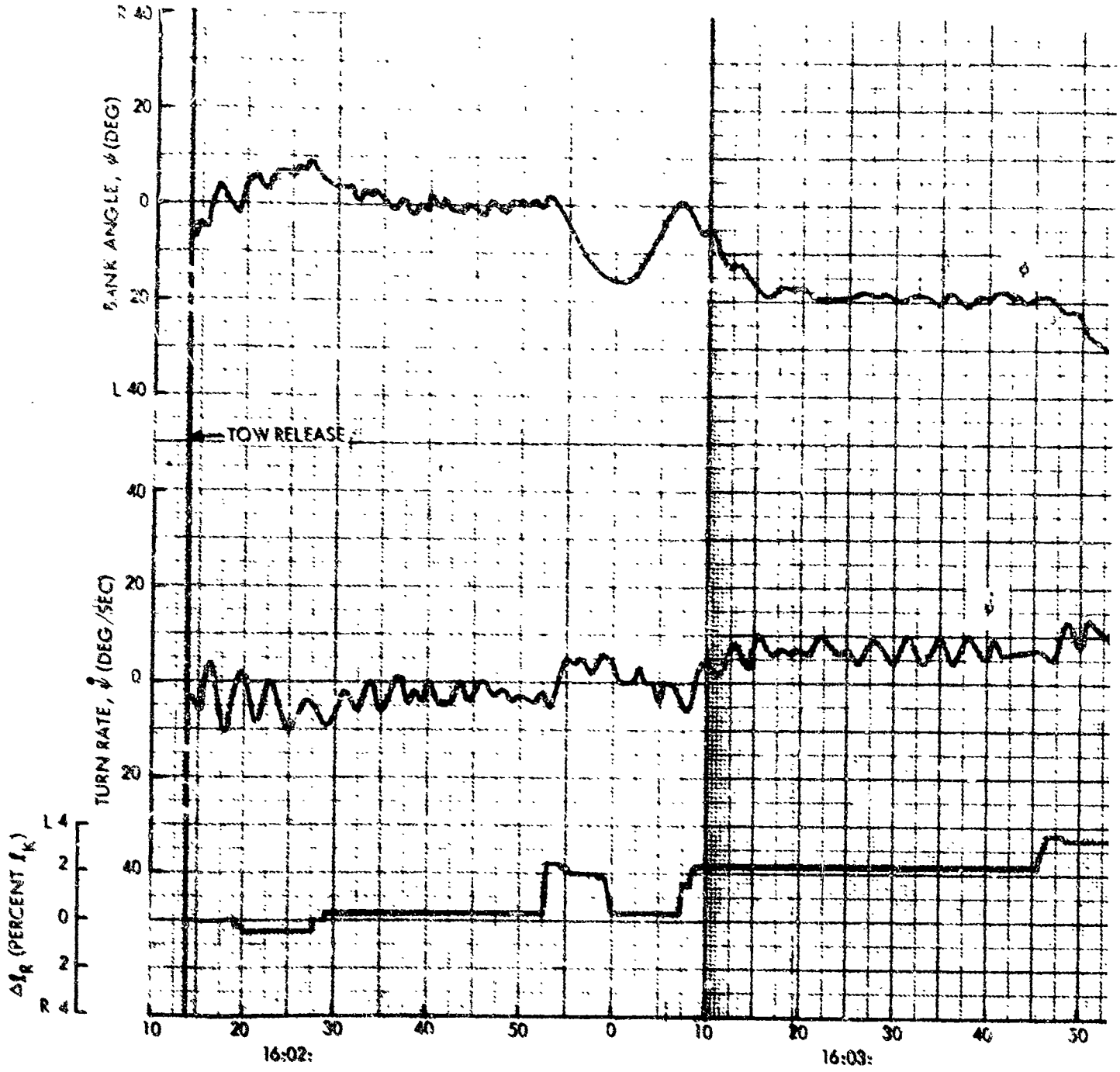

NORTH

FOLDOUT FRAME 2

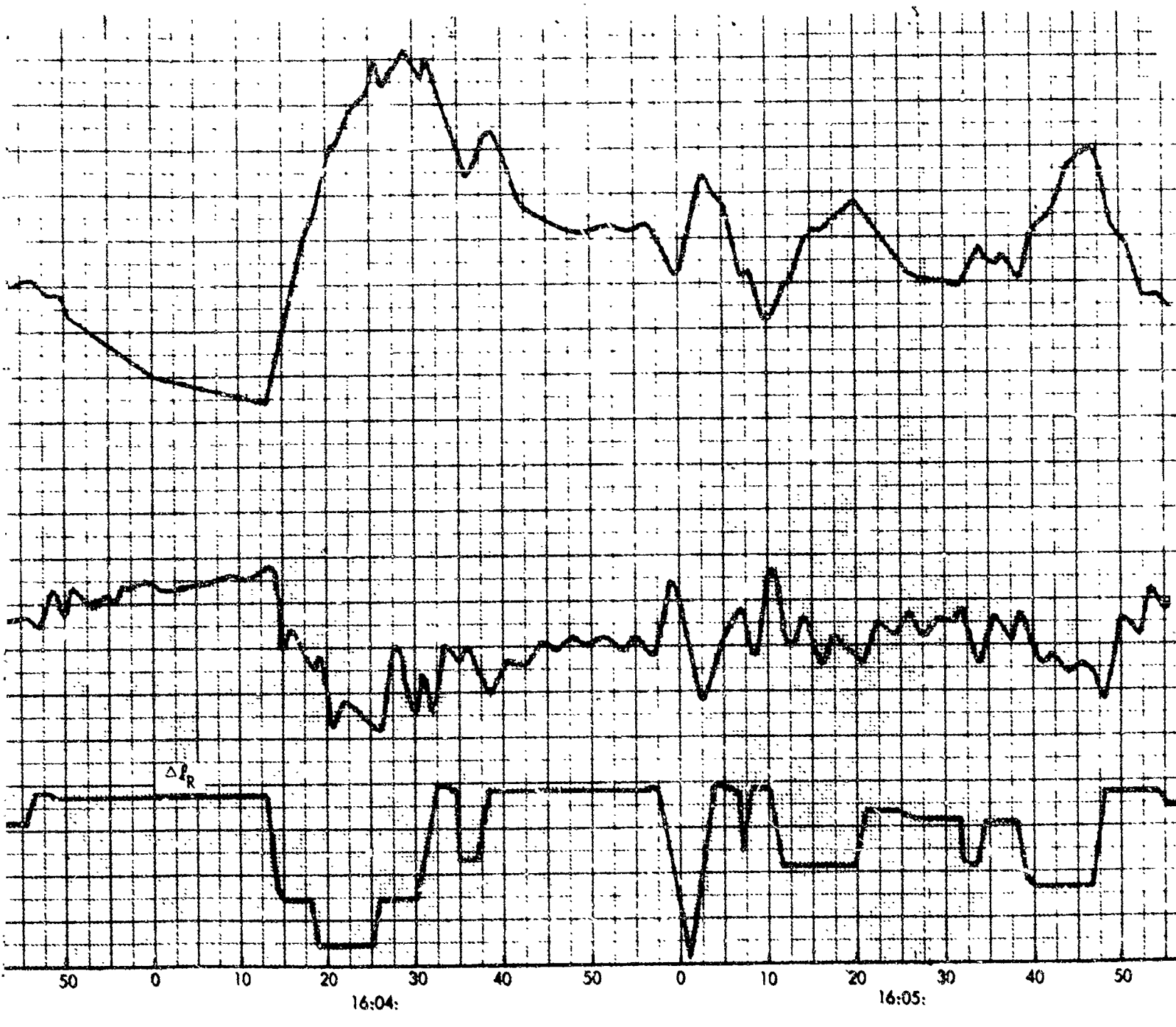

FOLDOUT FRAME 3

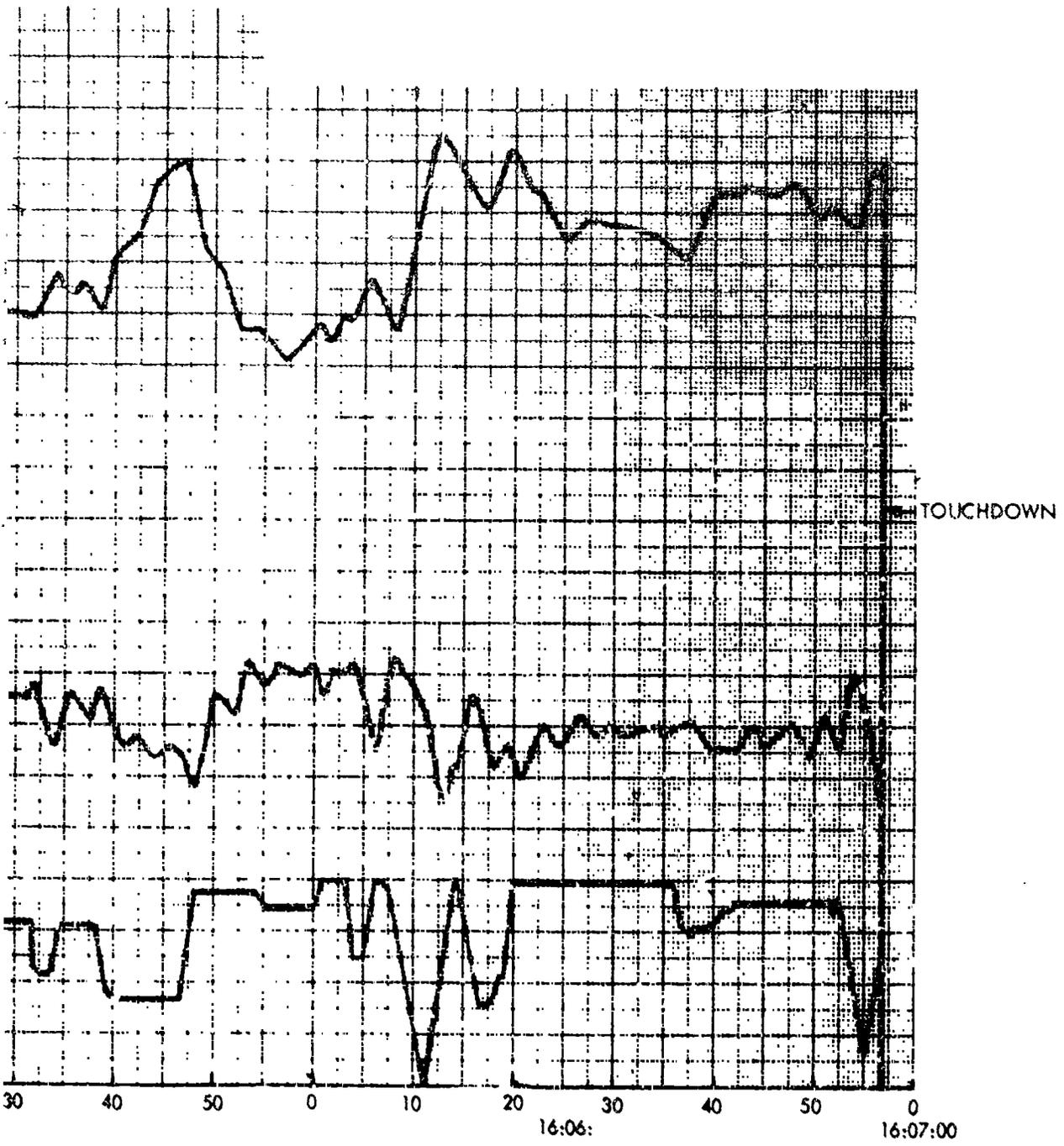

Figure 31. Flight 032 Time Histories (Sheet 2 of 2)

FOLDOUT FRAME 1

FOLDOUT FRAME

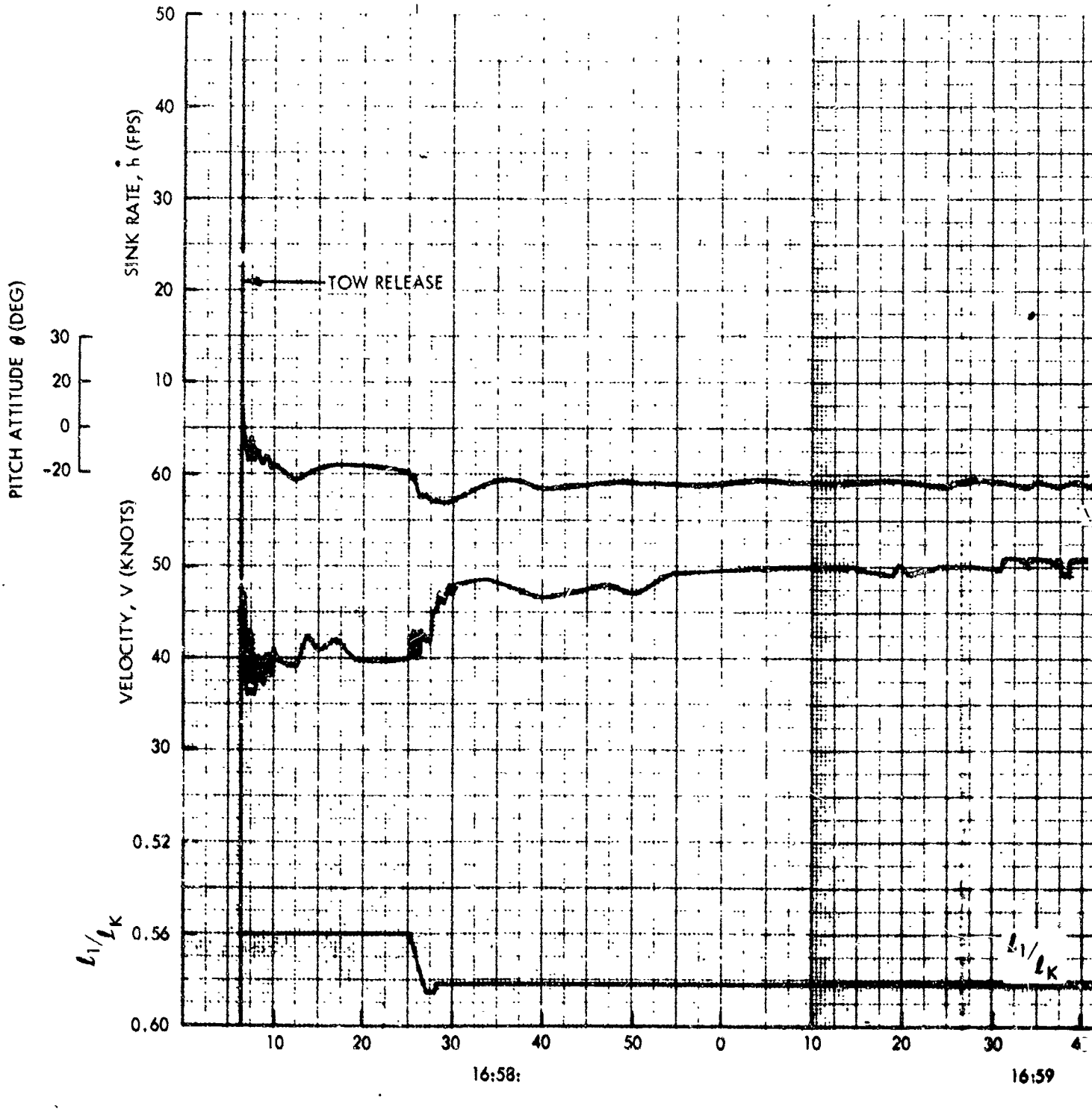

FRAME

FOLDOUT FRAME 2

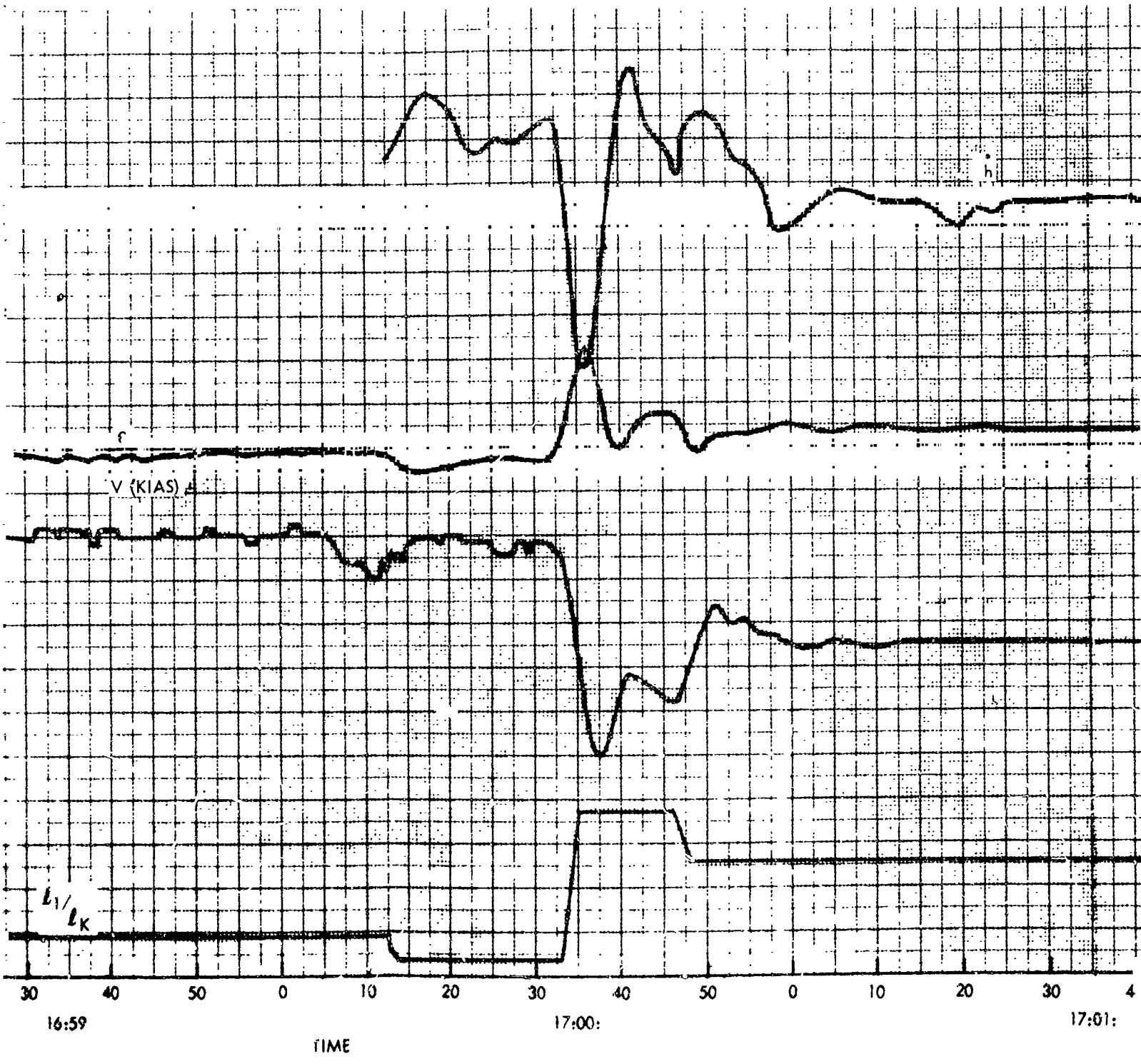

FOLDOUT FRAME 3

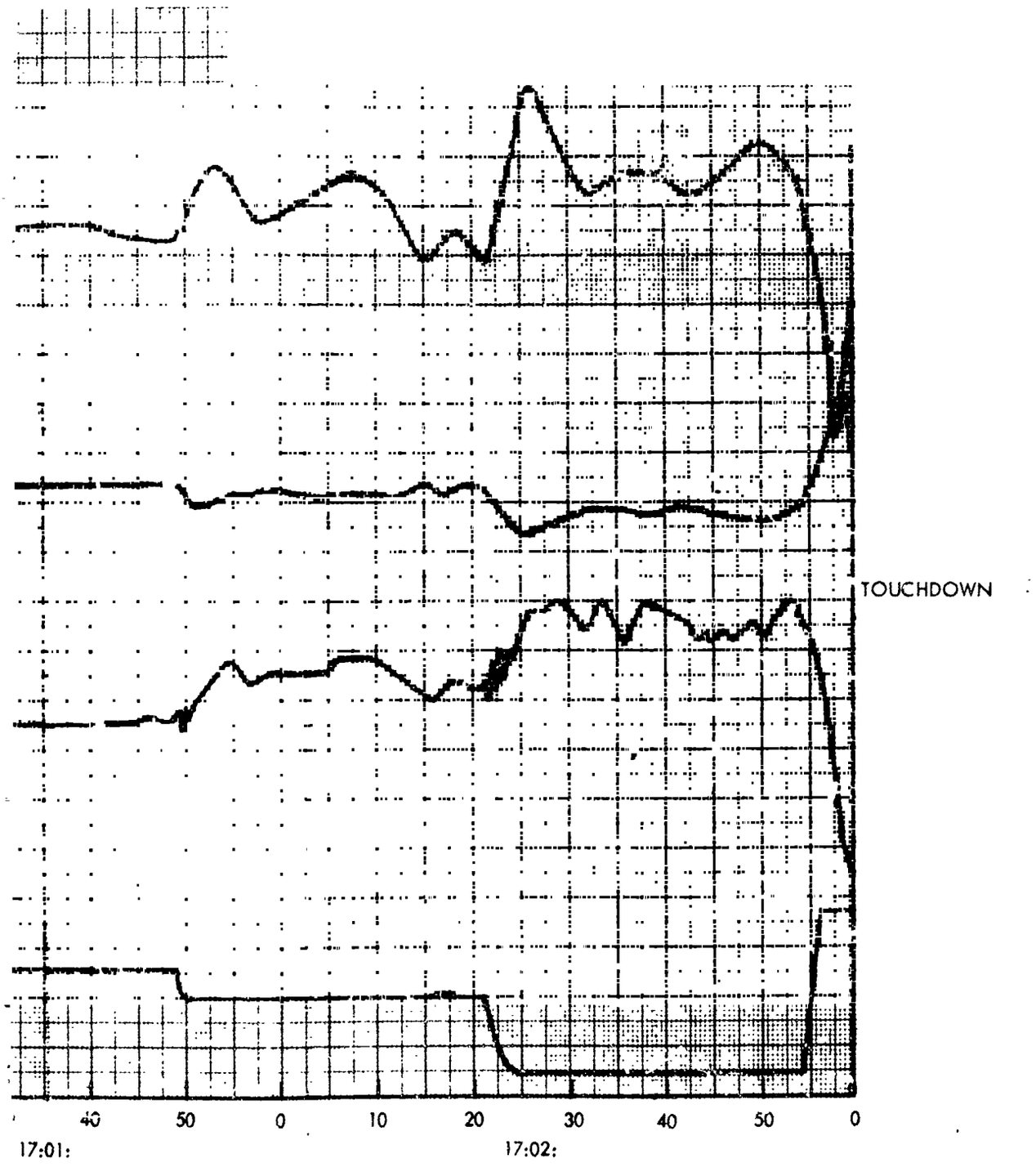

Figure 32. Flight 033 Time Histories (Sheet 1 of 2)

FOLDOUT FRAME

FOLDOUT FRAME

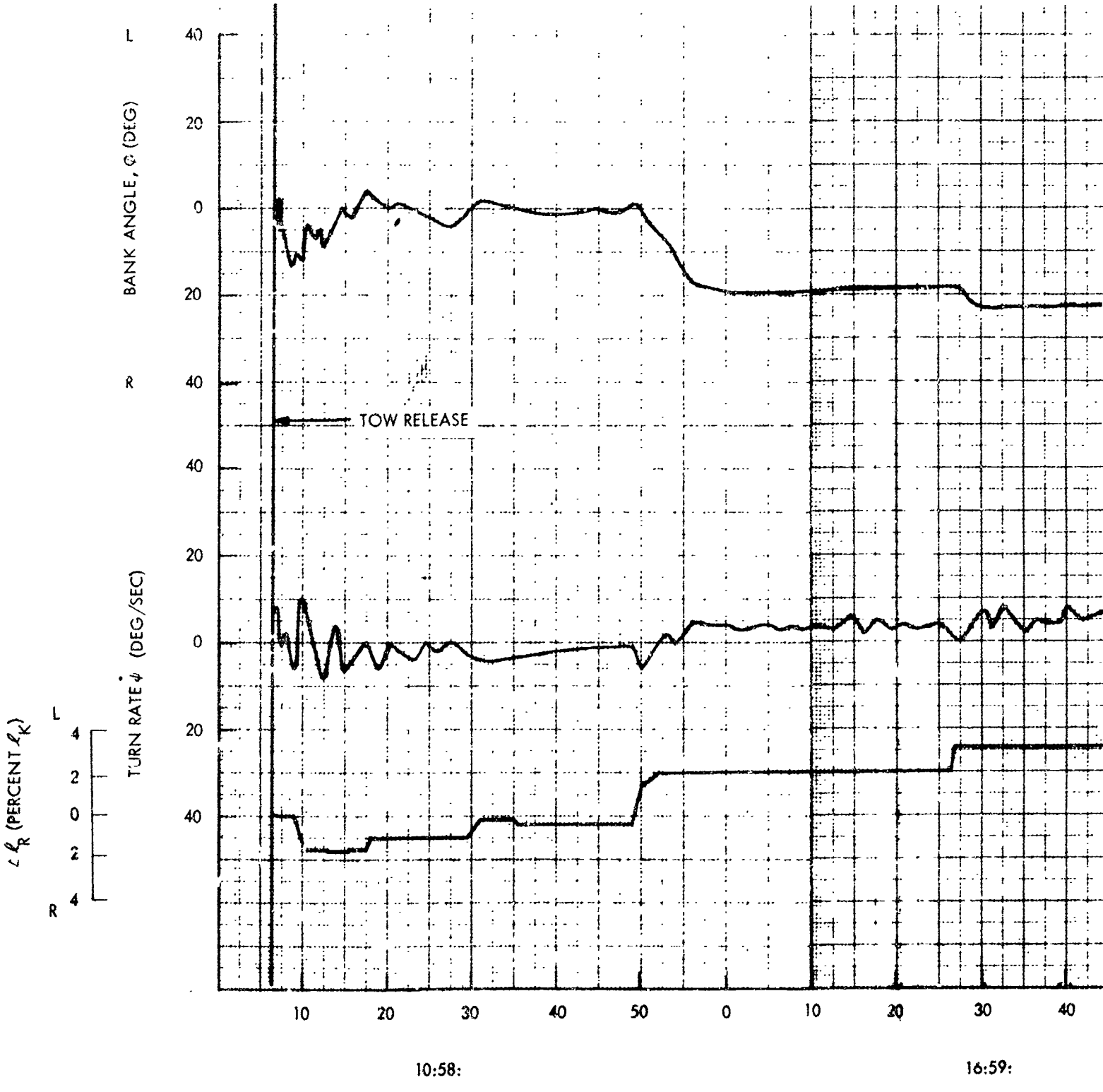

NOF

FOLDOUT FRAME 2

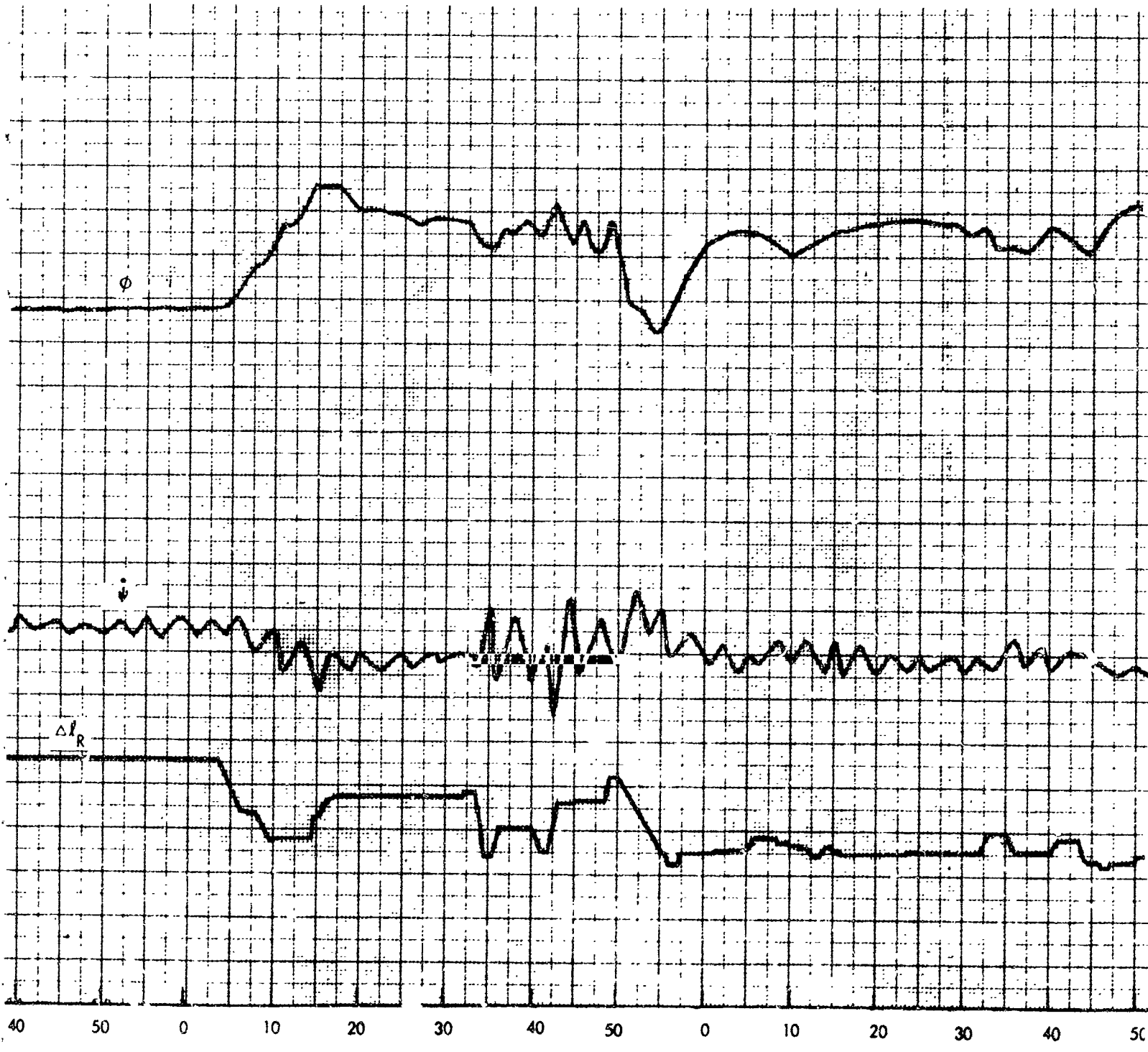

FOLDOUT FRAME 3

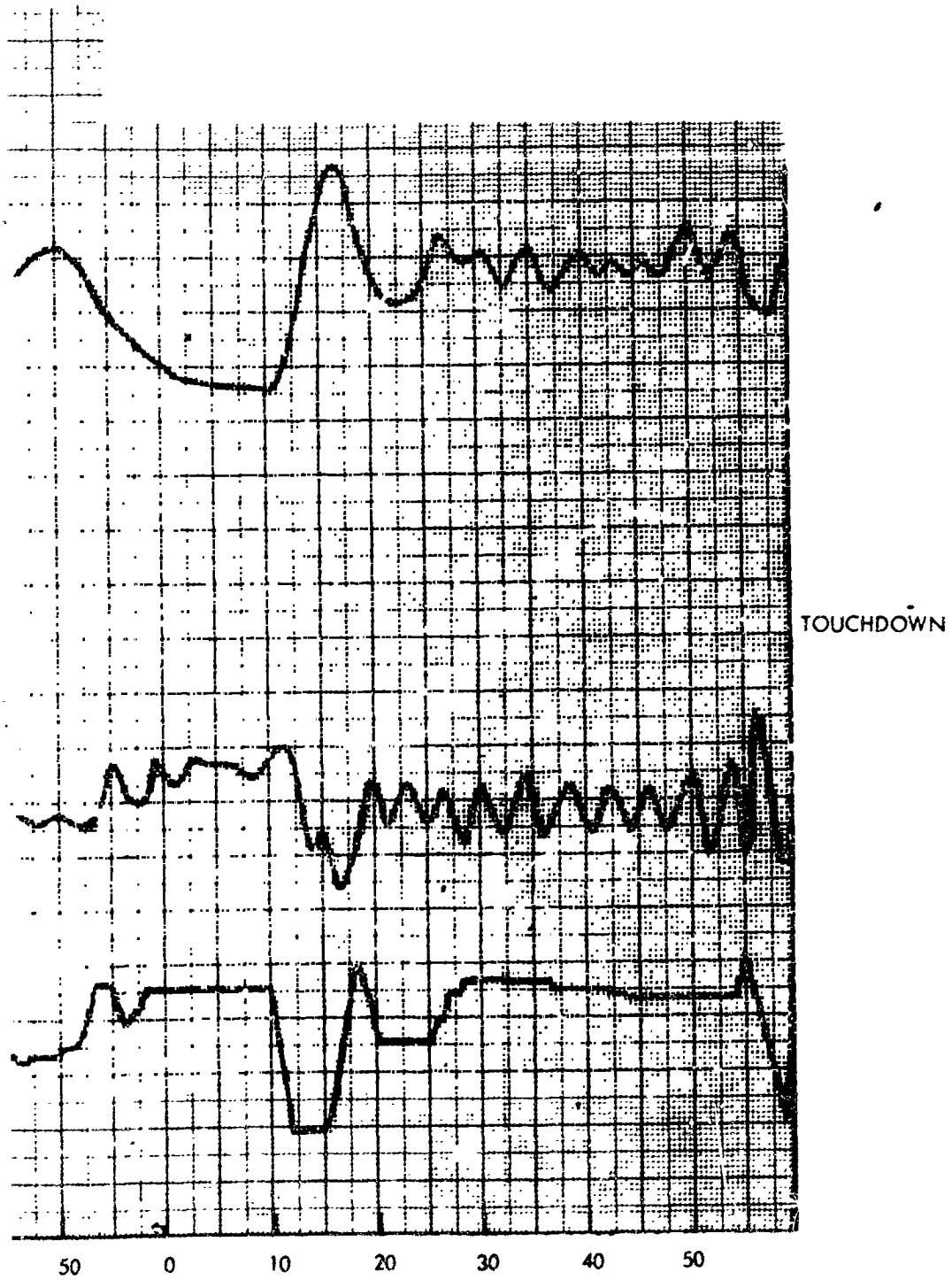

17:02:

Figure 32. Flight 033 Time Histories (Sheet 2 of 2)

data during preflare are unusual in that they do not achieve steady state. An inspection of the speeds and sink rates during landing preflares, when associated with the pitch and roll control line data, is indicative of the severe atmospheric disturbances at low altitudes during this test phase.

The data from the three phase test program tend to verify the data of SID 65-196 with regards to high-lobe sail performance and flare capabilities. Although a simulation was originally scheduled under this contract it was later deleted. Before the deletion, the equations of motion previously used were reviewed, and aerodynamic derivatives were calculated from data available at that time.

The amount of steady-state turn data obtained was relatively small. During Phase II, lateral control inputs were not held long enough to achieve steady-state flight. During Phase III, attitude gyros were available for only four flights. The data obtained are presented in Figure 33.

It can be seen from the plots of bank angle (ϕ) and turn rate ($\dot{\psi}$) that the maximum control effectiveness is at a pitch trim setting of $\ell_1/\ell_k = 0.56$. During Flight 028, turns were made at pitch settings of $0.53\,\ell_1/\ell_k$ with control effectiveness very low. Turns were made at $0.58\,\ell_1/\ell_k$ during Flight 033, and control effectiveness was less than expected. At the preflare pitch setting of $0.59\,\ell_1/\ell_k$, both the data and the test pilots indicate the turn control effectiveness to be low.

FLARE PERFORMANCE

A summary of significant parameters of all TTV flares is presented in Table 8. All the altitude and sink rate data presented in this enclosure were obtained from the on-board radar altimeter with the exception of Flight 005 where motion pictures were used. The following is a description of all TTV flares by flights:

Flight 005

This was the first radio-command TTV flight under this contract. The radar altimeter locked on the nose gear; hence, no audio tone was available for flare indication. The ground pilot flared the vehicle high, resulting in a minimum sink rate of approximately 16 fps at some altitude above the ground. The vehicle impacted at a sink rate of approximately 30 ft/sec. The minimum sink rate was high, since the maximum pitch-up command was only $\ell_1/\ell_k = \pm 0.54$.

Flight 014

On this flight, the second radio command flight, when the pilot pulled back on the stick he also pushed the flare button. The two signals cancelled each other, resulting in no flare.

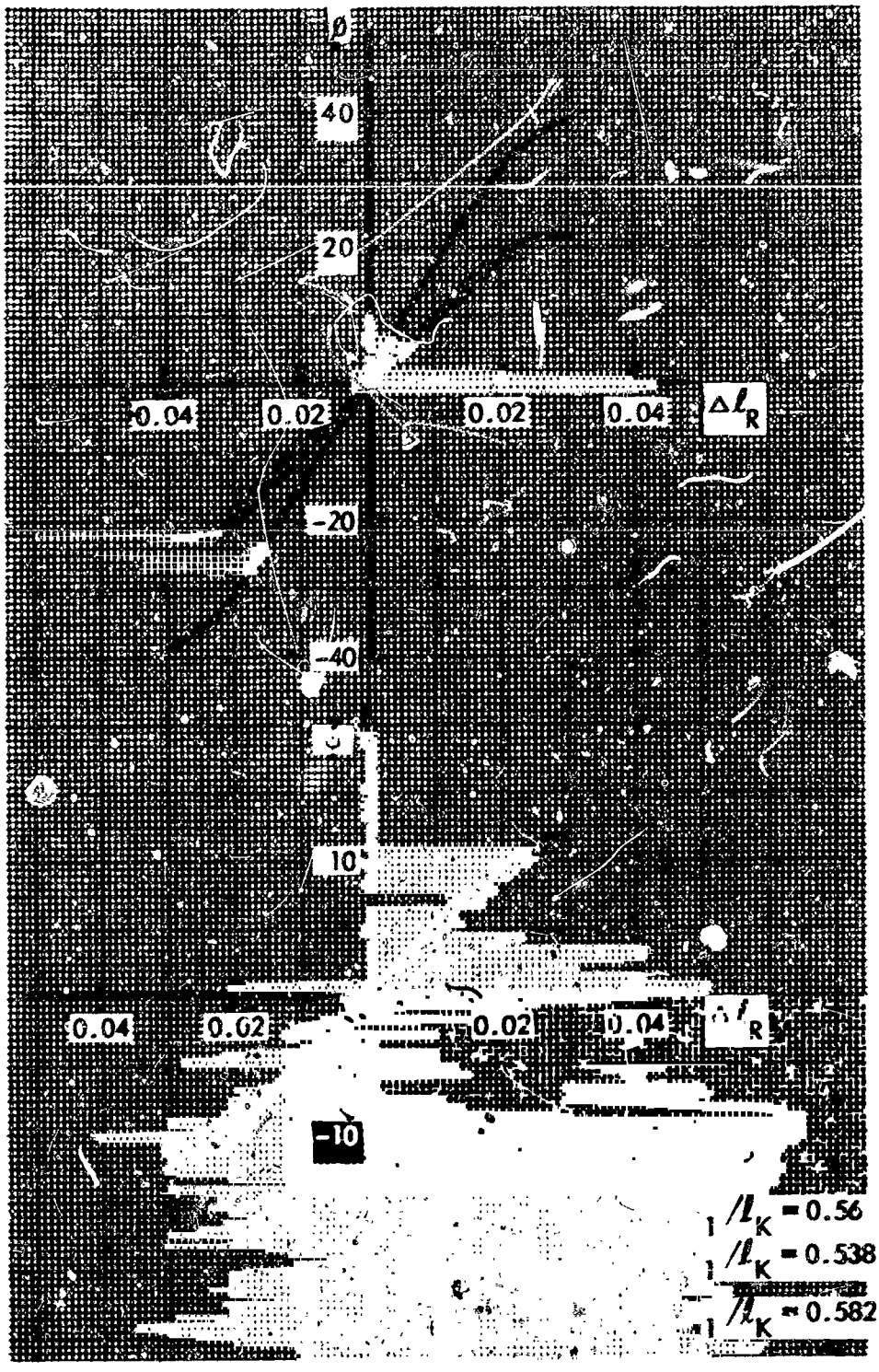

Figure 33. Steady-State Turn Data

Table 8. Summary of Tow Test Vehicle Flares

Flight	$\dot{h}_i$ (ft/sec)	$\dot{h}_{min}$ (ft/sec)	$\Delta\dot{h}_{td}$ (ft/sec)	Δh_{min} (ft)	Δh_{td} (ft)	V_i (knots)	l_l/l_k (Preflare)
005	NA	≈16.0	≈30.0	NA	NA	NA	0.590
014	38.0	38.0	38.0				0.595
020	34.5	9.5	11.0	103	110	48.5	0.595
020A	34.5	7.0		94		48.5	0.590
021	38.5	13.0	13.0	112	112	45.0	0.590
021A	29.5	15.0		105		48.5	0.590
022	36.5	13.0	13.0	111	111	47.0	0.585
023	33.0	8.0	19.0	89	111	48.5	0.565
024	28.0	6.0	28.5	67	108	51.5	0.590
024A	37.5	9.0		110		48.5	0.590
025	35.4	11.5	11.5	110	110	45.0	0.590
025A	34.0	15.0		130		47.5	0.588
026	32.0	10.5	21.0	88	116	48.0	0.588
026A	30.0	15.0		75		40.5	0.560
027	37.0	6.0	10.0	83	95	50.0	0.590
027A	35.0	9.5		86		47.0	0.580
028	38.0	9.0	9.0	103	103	51.5	0.589
029	35.0	6.0	15.0	85	100	50.0	0.592
029A	34.0	10.5		85		47.0	0.573
030	32.5	14.0	14.0	85	85	50 0	0.590
031	29.5	25.0	25.0	124	124	47.0	
031A	36.0	16.0		87		48.0	0.570
032	29.0	12.5	19.5	75	98	47.5	0.589
032A	34.5	14.5		90		47.5	0.582
033	32.5	7.0	18.0	72	92	48.5	0.590
033A	37.0	9.0		93		49.0	0.592

$\dot{h}_i$ = sink rate, preflare
$\dot{h}_{td}$ = sink rate, touchdown
V_i = velocity, preflare
l_l/l_k = line length to keel length

Flight 020

Due to a late preflare, steady-state conditions were not achieved at flare initiation. The preflare sink rate being somewhat lower than steady state resulted in reaching a minimum sink rate before touchdown. Figure 34 presents the significant parameters for this flare. The flare in the air on Flight 020 is presented in Figure 35. It can be seen that steady-state conditions were achieved for this flare. The preflare pitch line setting was 0.584, resulting in the preflare sink speed of 34.5 ft/sec. At the present time, the only logical explanation for the relatively short Δh between flare initiation and minimum sink rate is that of a head shear or gust. This would also explain the unusually low minimum sink rate obtained.

Flight 021

Figure 36 presents data for the touchdown flare. Due to lateral maneuvers during preflare, steady-state conditions were not achieved resulting in a velocity of 45 knots and a sink rate of 38.5 ft/sec at flare initiation. The higher sink rate and lower than nominal velocity resulted in a greater altitude span needed to reach minimum sink rate. The flare in the air on this flight was initiated after a sharp roll maneuver, which resulted in a decrease in sink rate at flare initiation. The effect of the roll transient on the flare maneuver resulted in a minimum sink rate of only 15 ft/sec, as shown in Figure 37.

Flight 022

Figure 38 presents the data from the flare on this flight. Preflare was late, and the pitch line setting in preflare was only 0.585. As can be seen from Figure 38, Sheet 1, the vehicle was still in a transient state at flare initiation. This transient condition resulted in a larger than normal altitude differential between flare initiation and minimum sink rate.

Flight 023

Figure 39 presents the data from the flare in this flight. Due to the preflare pitch line setting of only 0.585, a late preflare initiation and possibly a shear or gust, the vehicle was in a transient oscillating condition other than nominal while the velocity was approximately nominal. These conditions resulted reaching a minimum sink rate of 8 ft/sec, 22 feet above the ground. The touchdown sink rate was 19 ft/sec.

Flight 024

It can be seen from Figure 40 that the vehicle encountered a head gust or shear approximately four seconds before flare initiation. The airspeed

FOLDOUT FRAME 1

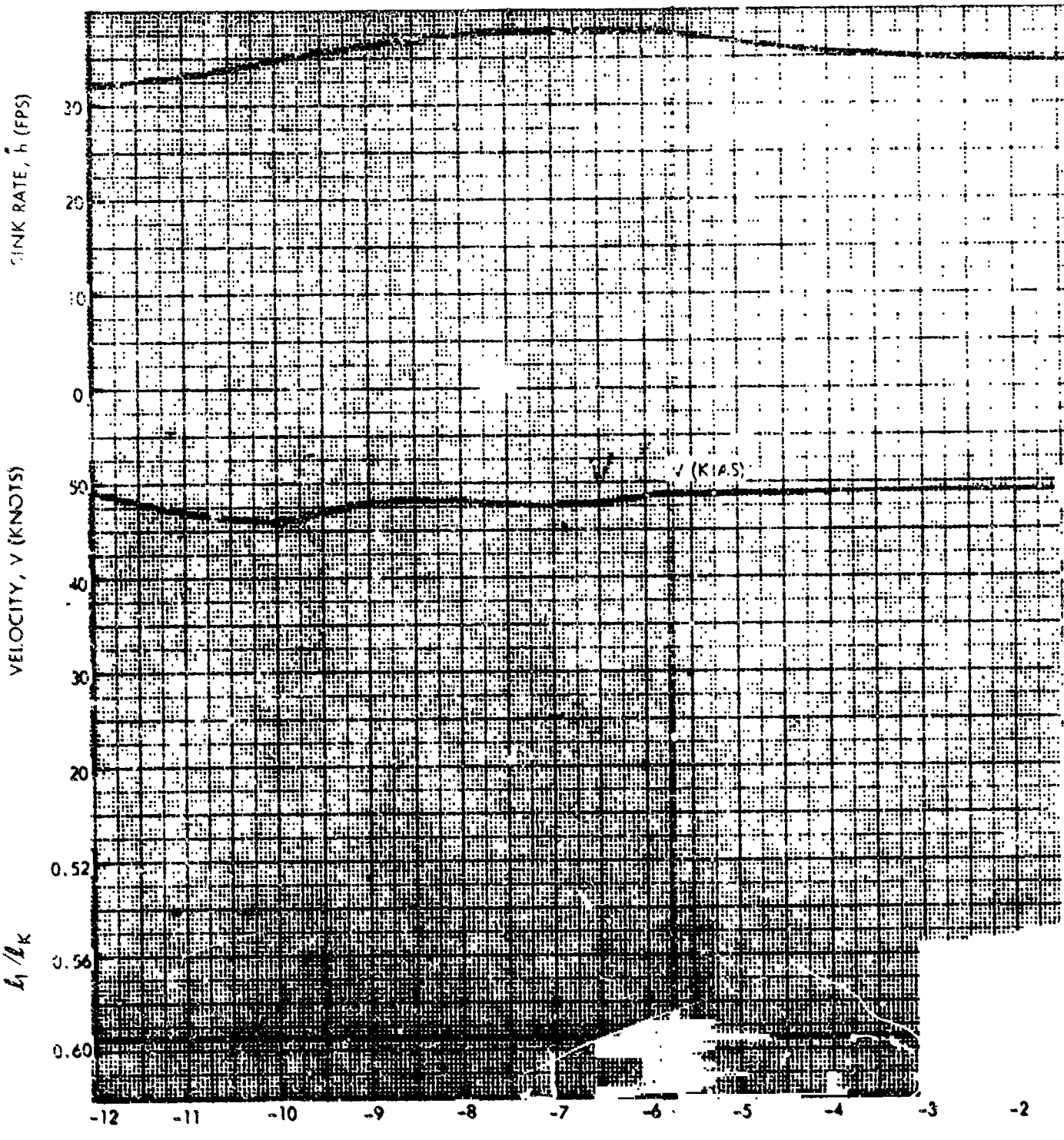

Figu

FOLDOUT FRAME 2

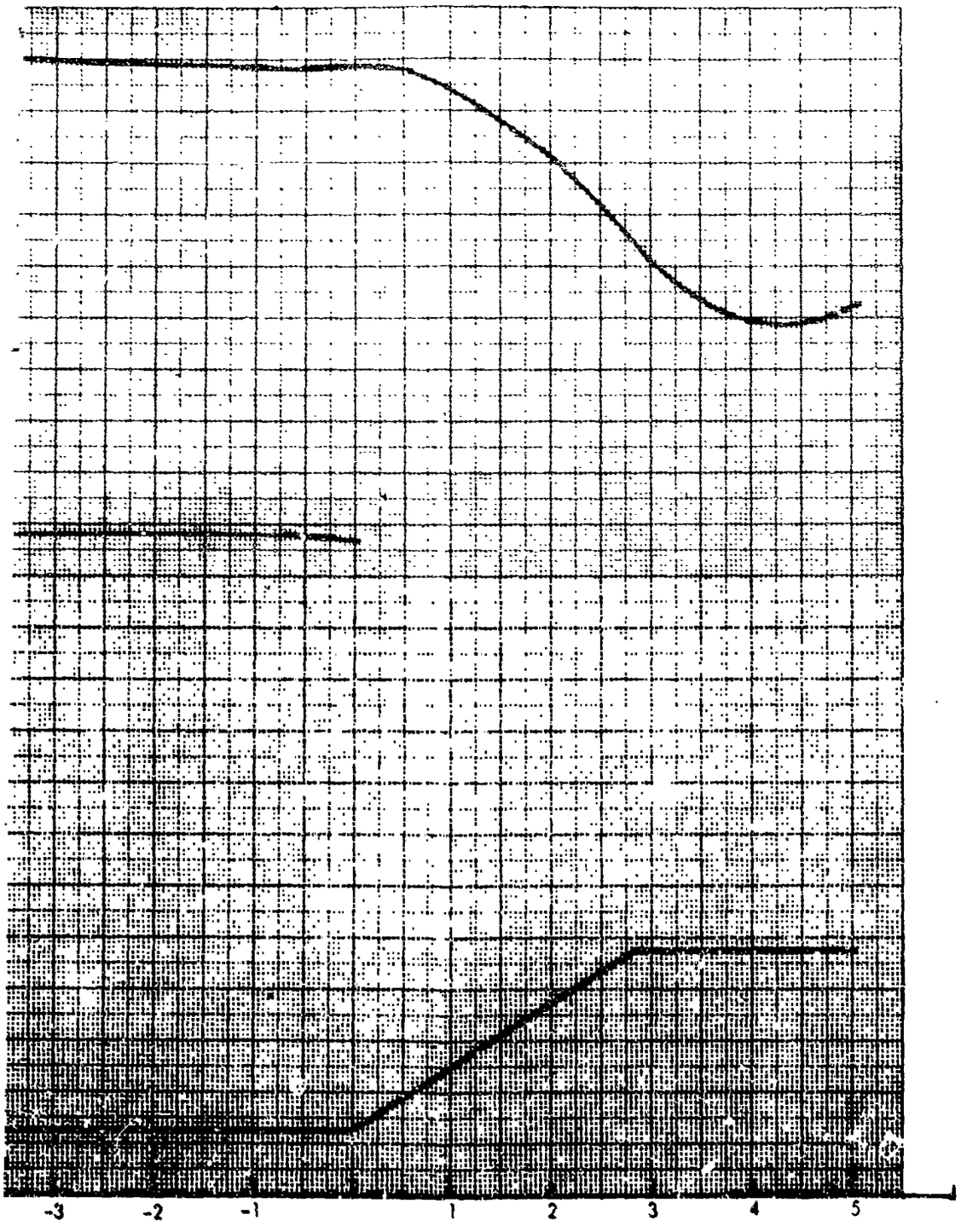

TIATION (SEC)

Figure 34. Flight 020 Touchdown Flare (Sheet 1 of 2)

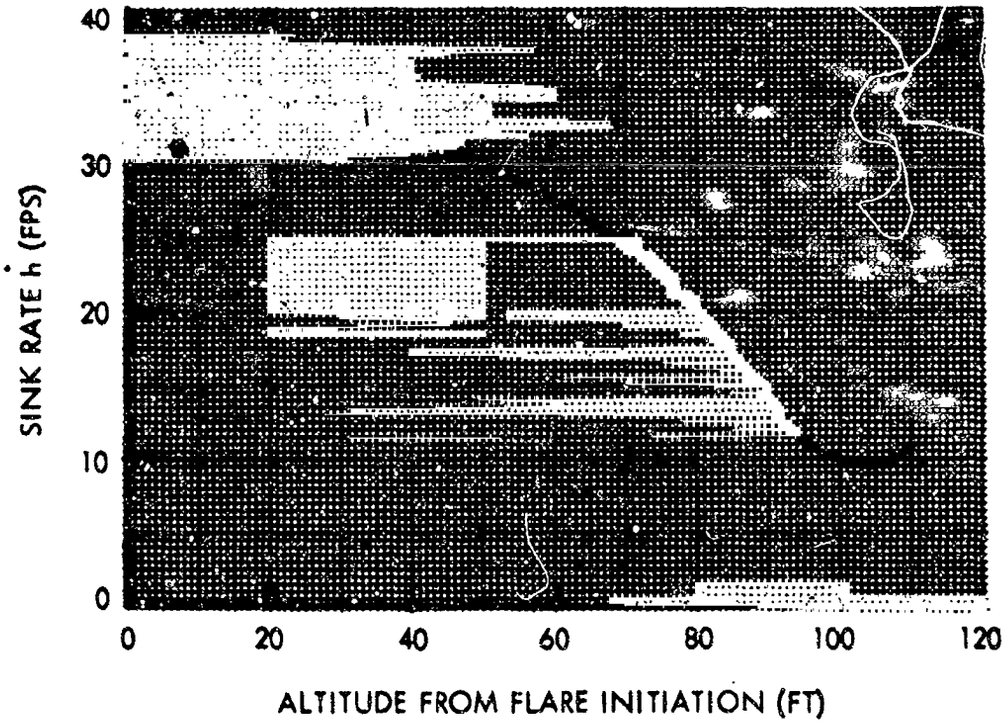

Figure 34. Flight 020 Touchdown Flare (Sheet 2 of 2)

FOLDOUT FRAME /

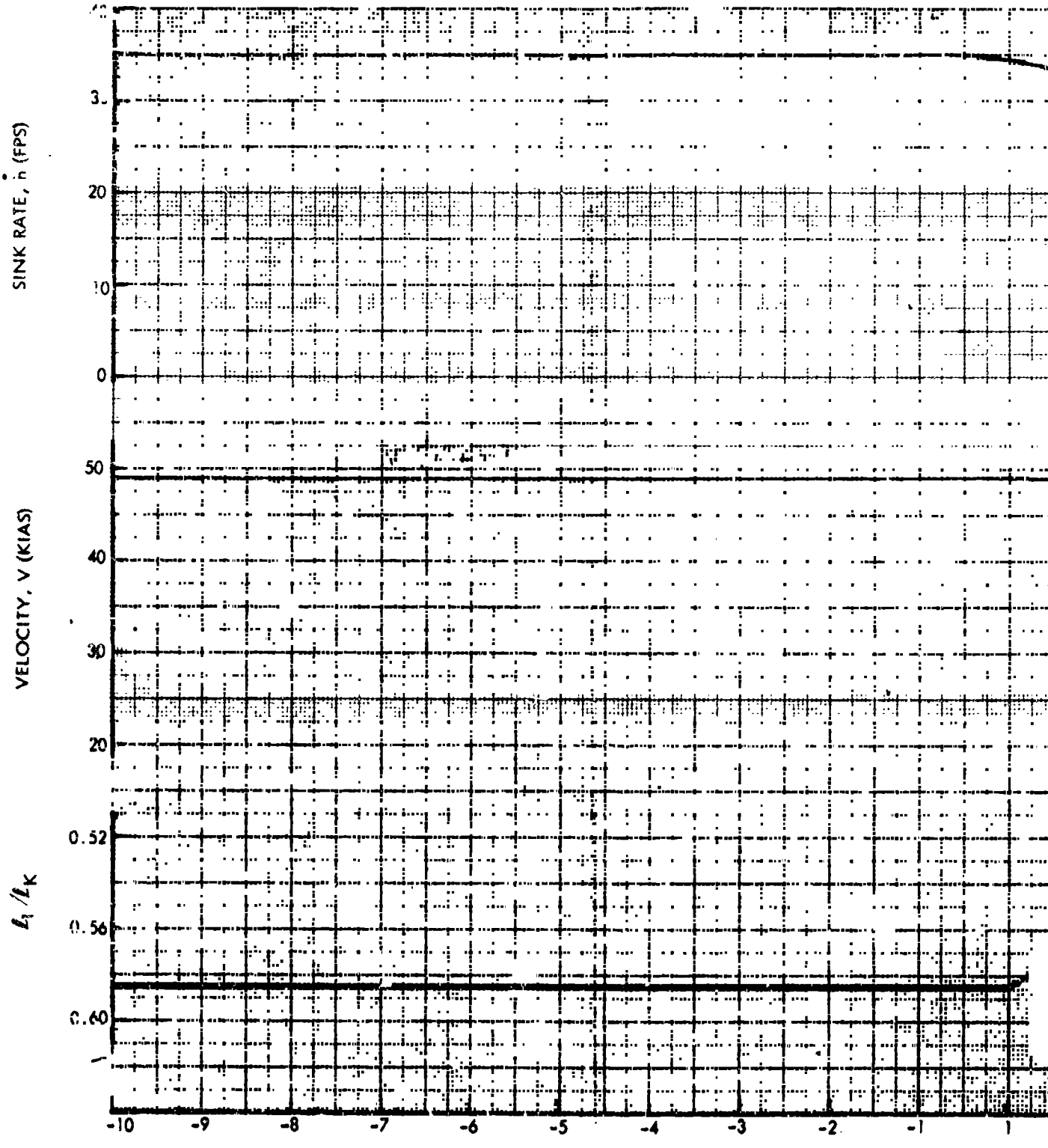

Figure 35.

FOLDOUT FRAME 2

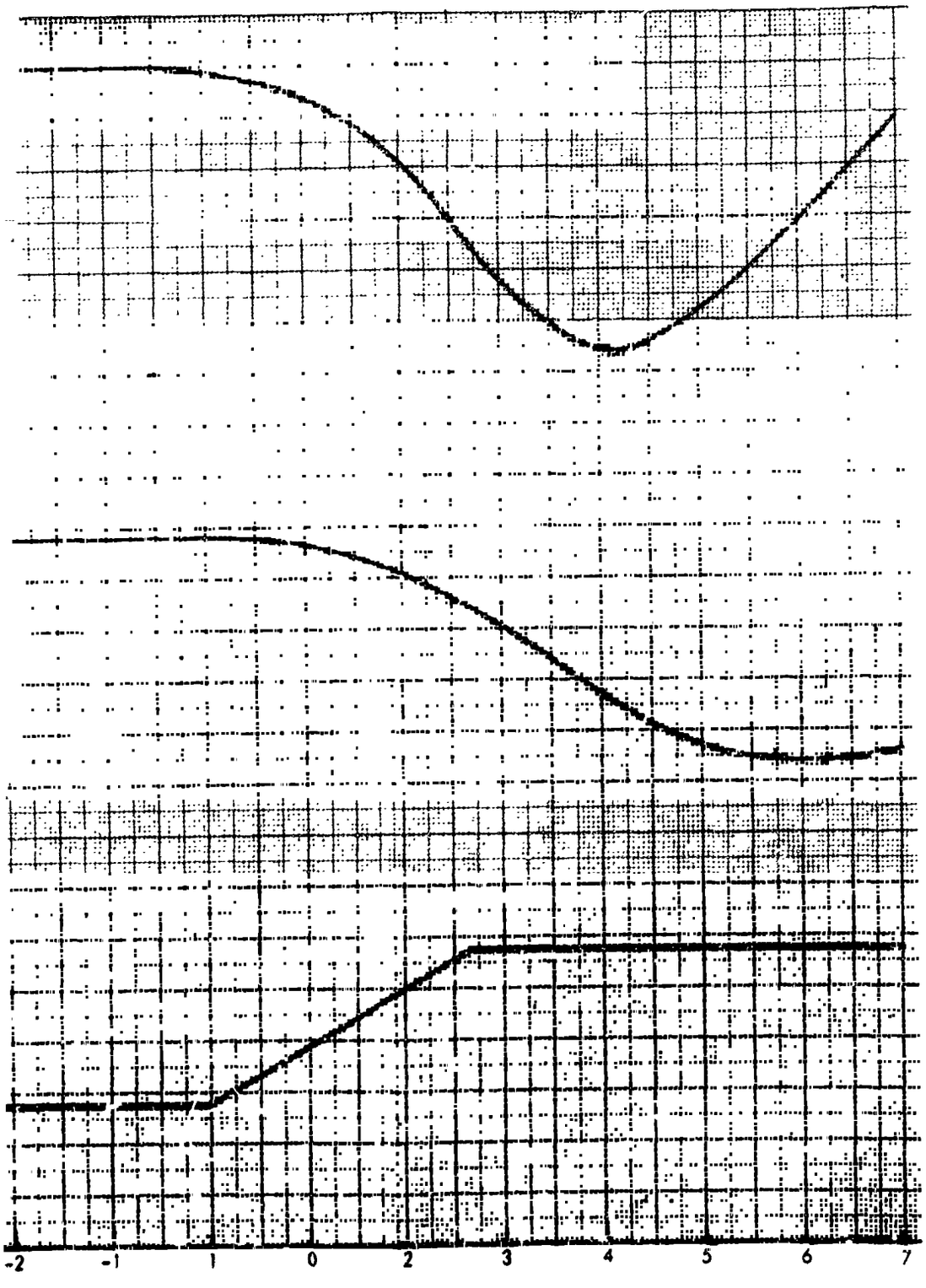

Figure 35. Flight 020 Flare at Altitude (Sheet 1 of 2)

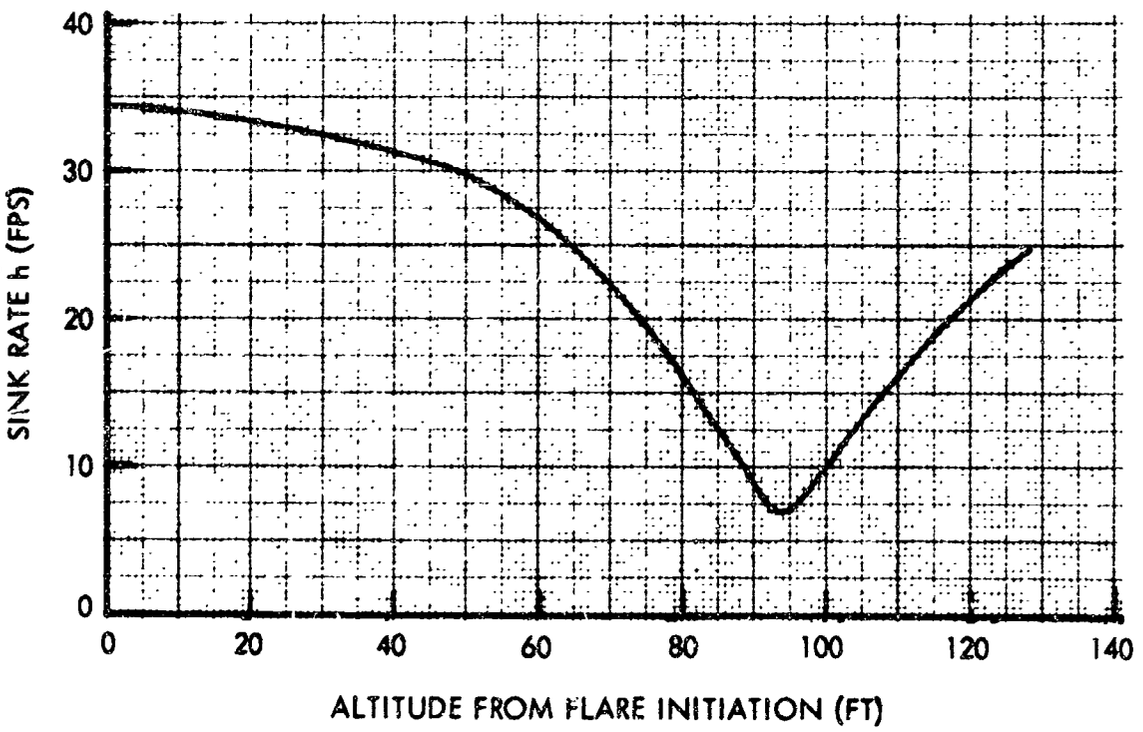

Figure 35. Flight 020 Flare at Altitude (Sheet 2 of 2)

FOLDOUT FRAME 1

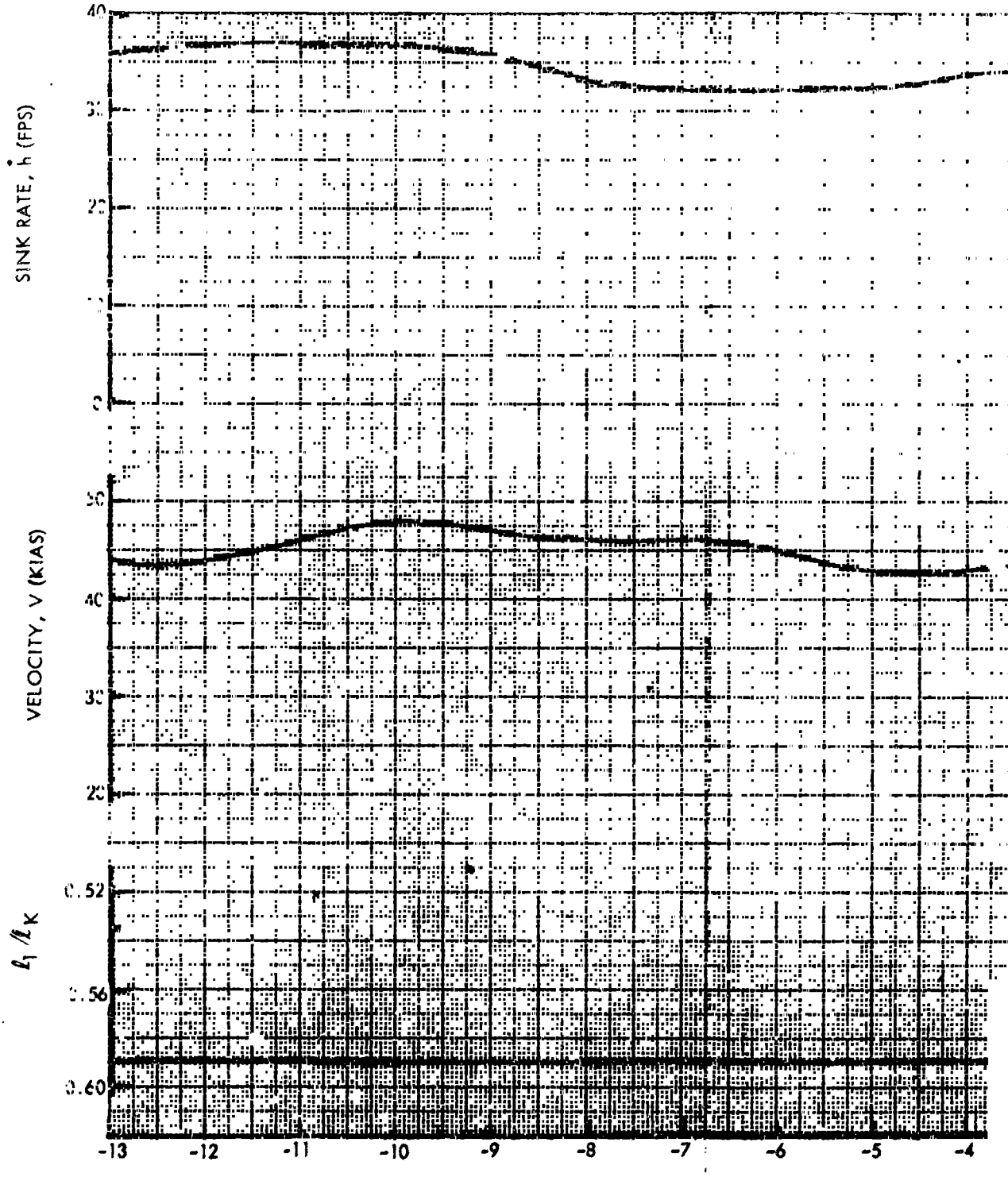

FOLDOUT FRAME 2

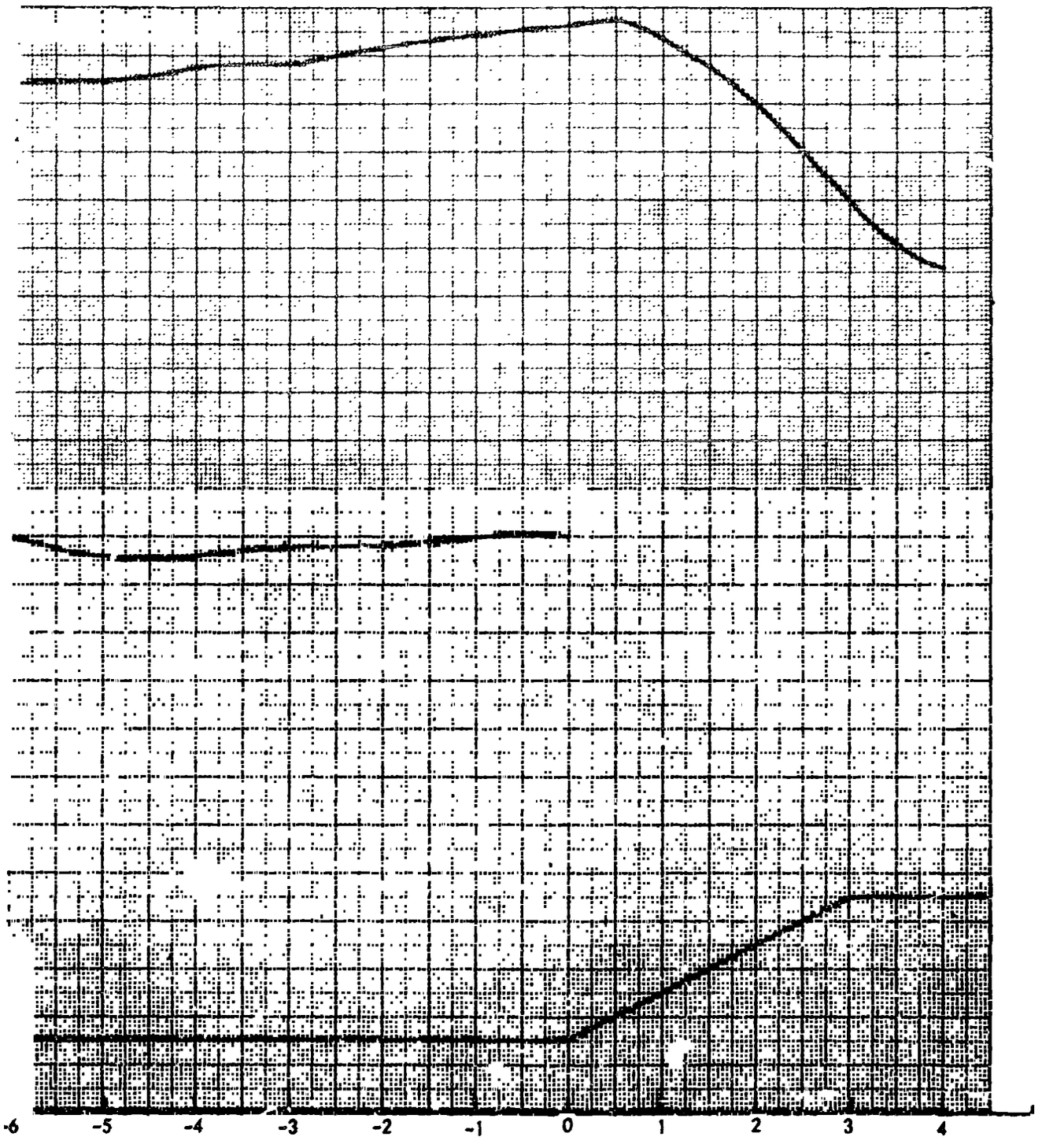

Figure 36. Flight 021 Touchdown Flare (Sheet 1 of 2)

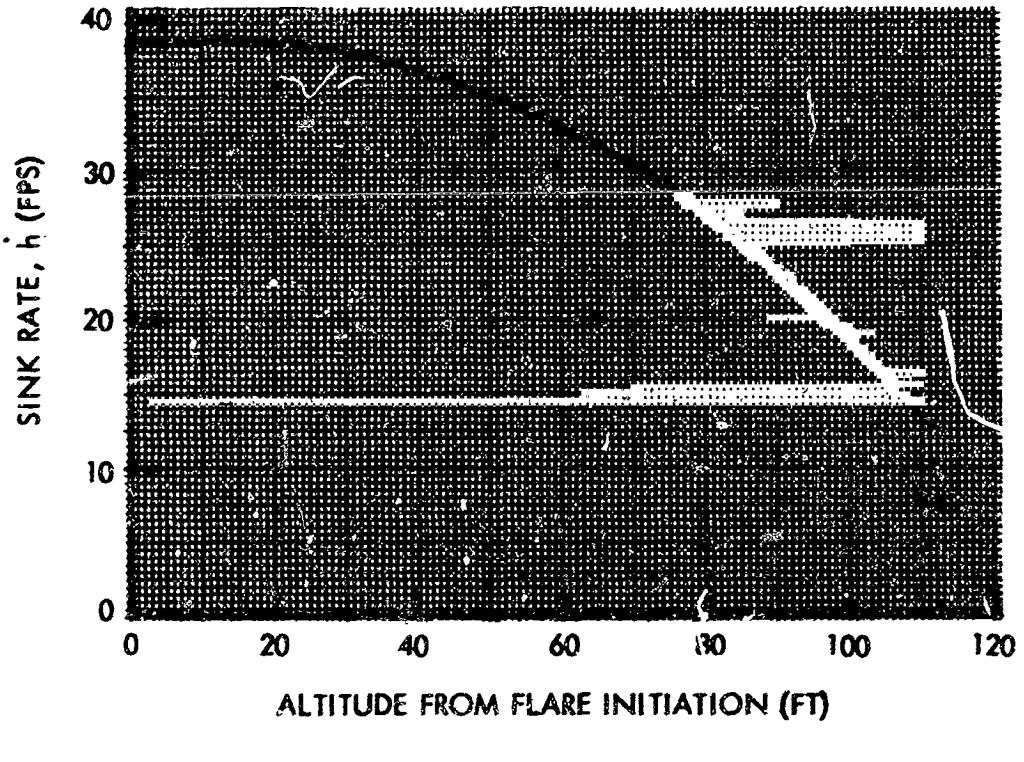

Figure 36. Flight 021 Touchdown Flare (Sheet 2 of 2)

FOLDOUT FRAME 1

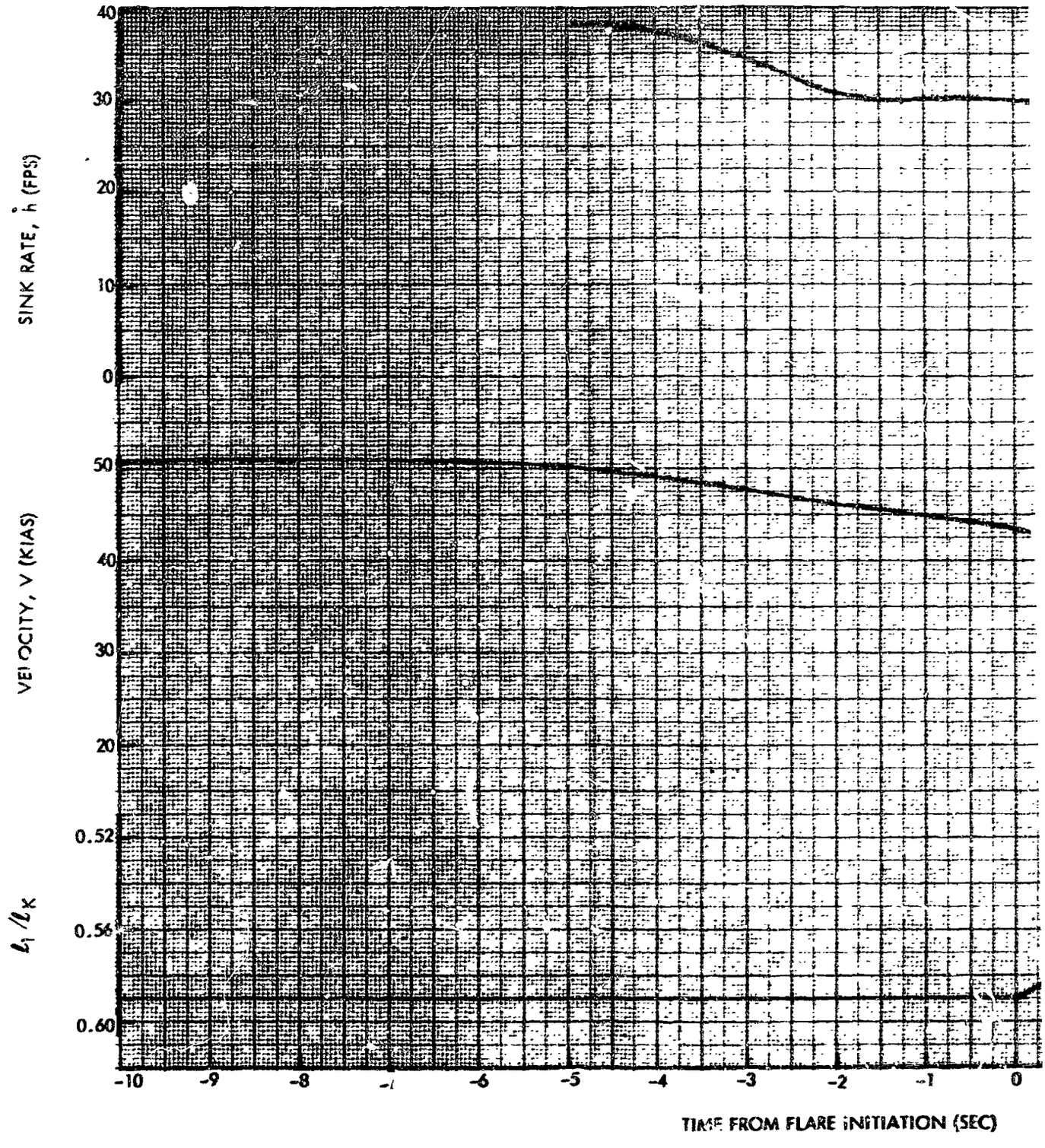

Figure 37.

FOLDOUT FRAME 2

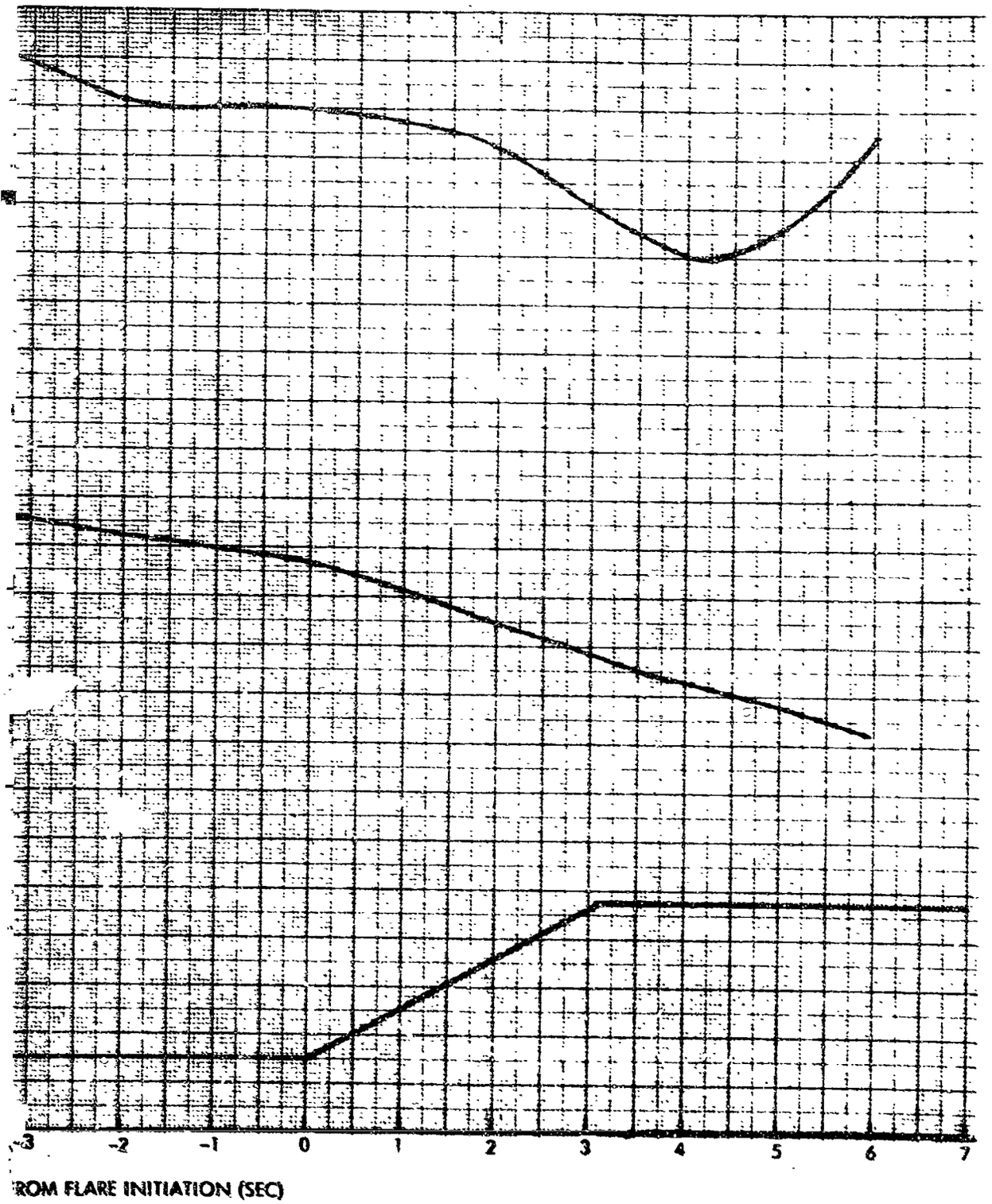

Figure 37. Flight 021 Flare at Altitude (Sheet 1 of 2)

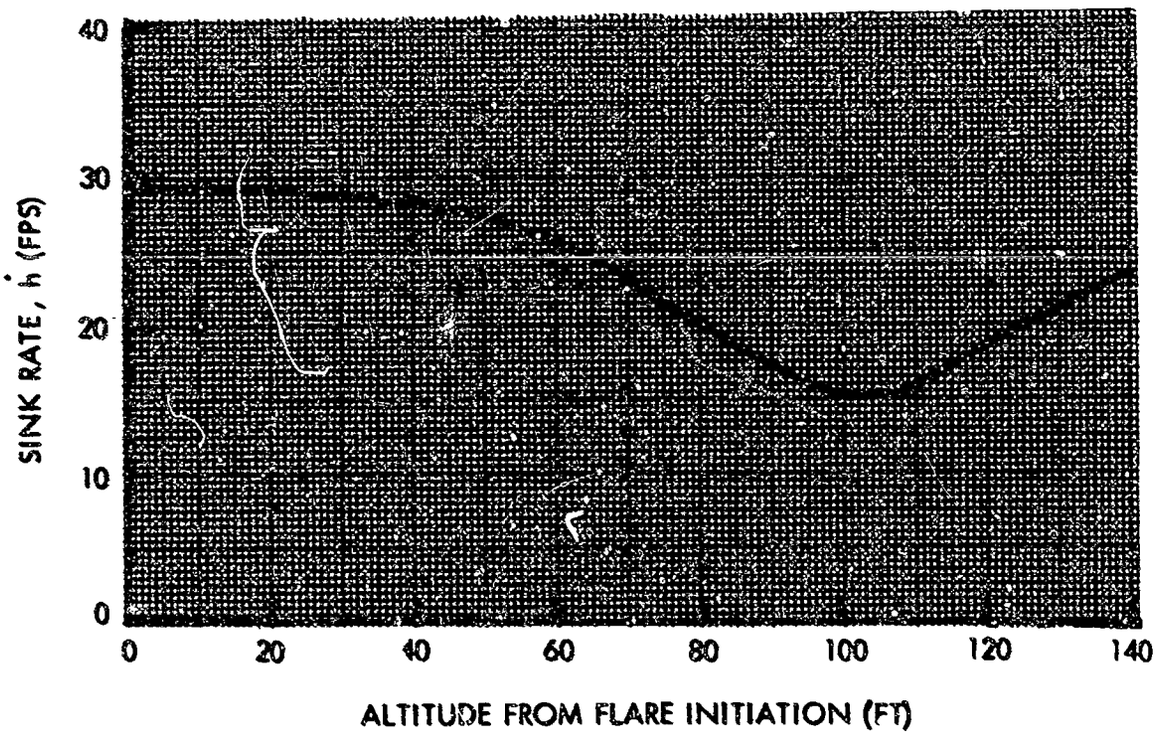

Figure 37. Flight 021 Flare at Altitude (Sheet 2 of 2)

PRECEDING PAGE BLANK NOT FILMED.

FOLDOUT FRAME

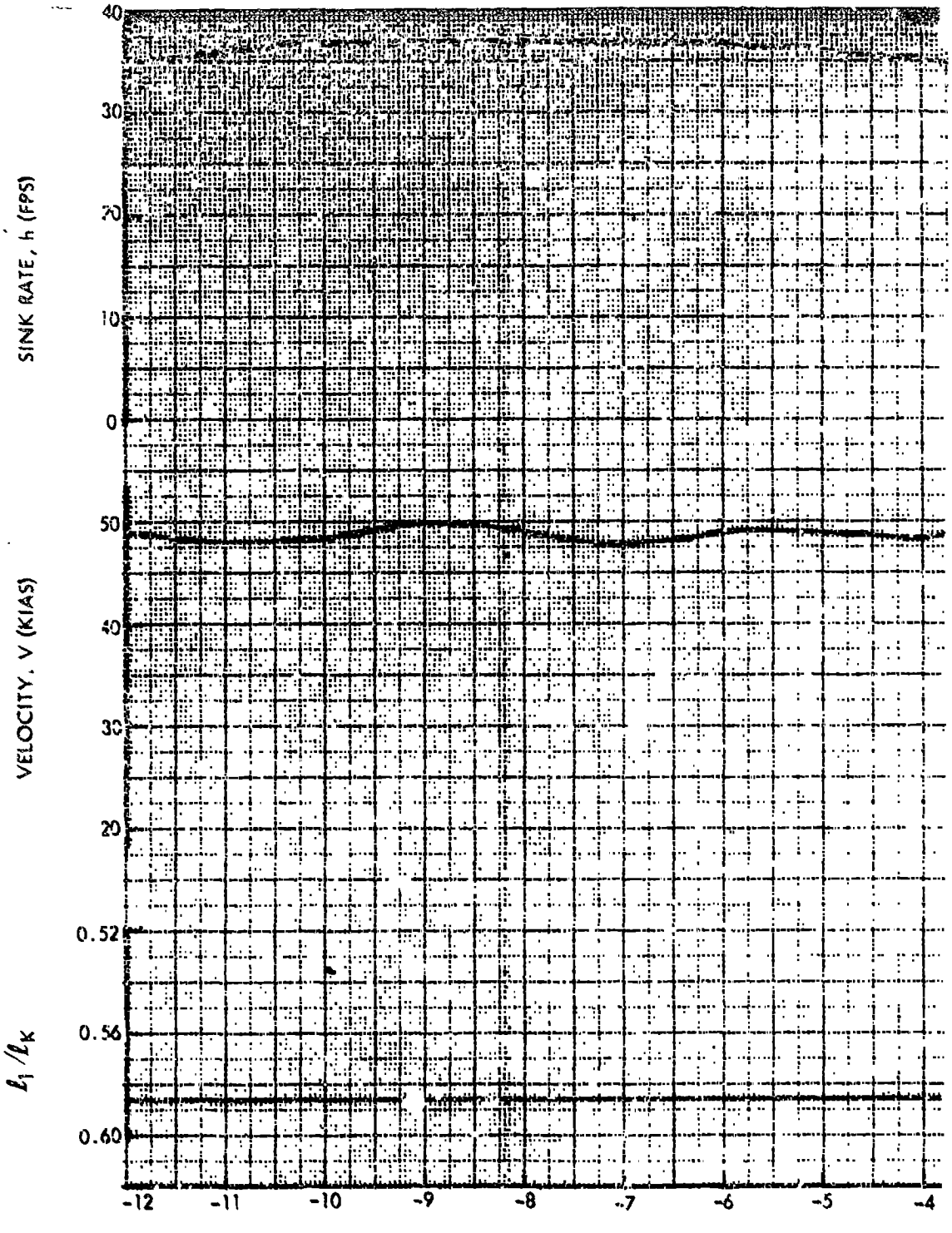

Fig

FOLDOUT FRAME 2

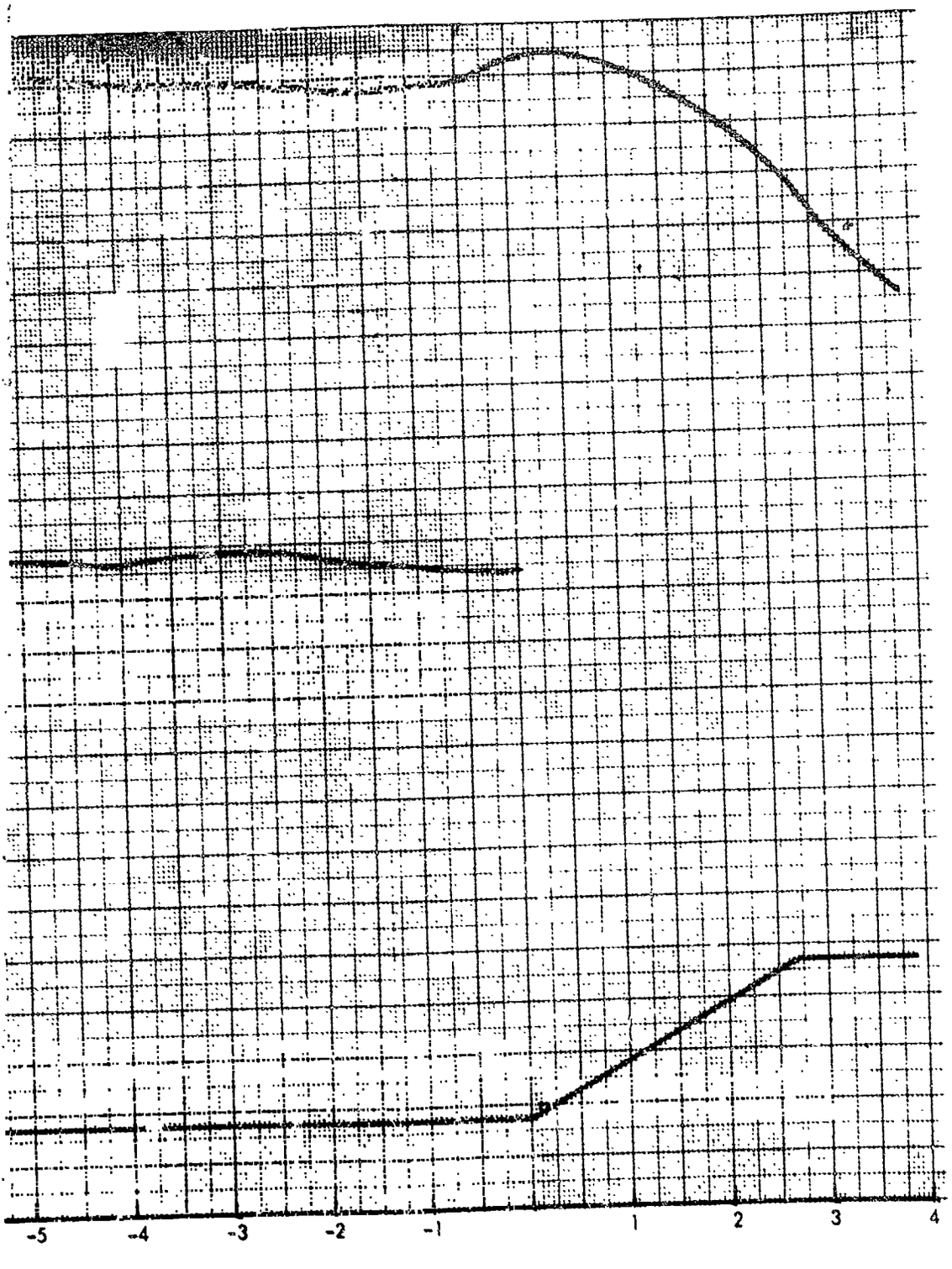

Figure 38. Flight 022 Touchdown Flare (Sheet 1 of 2)

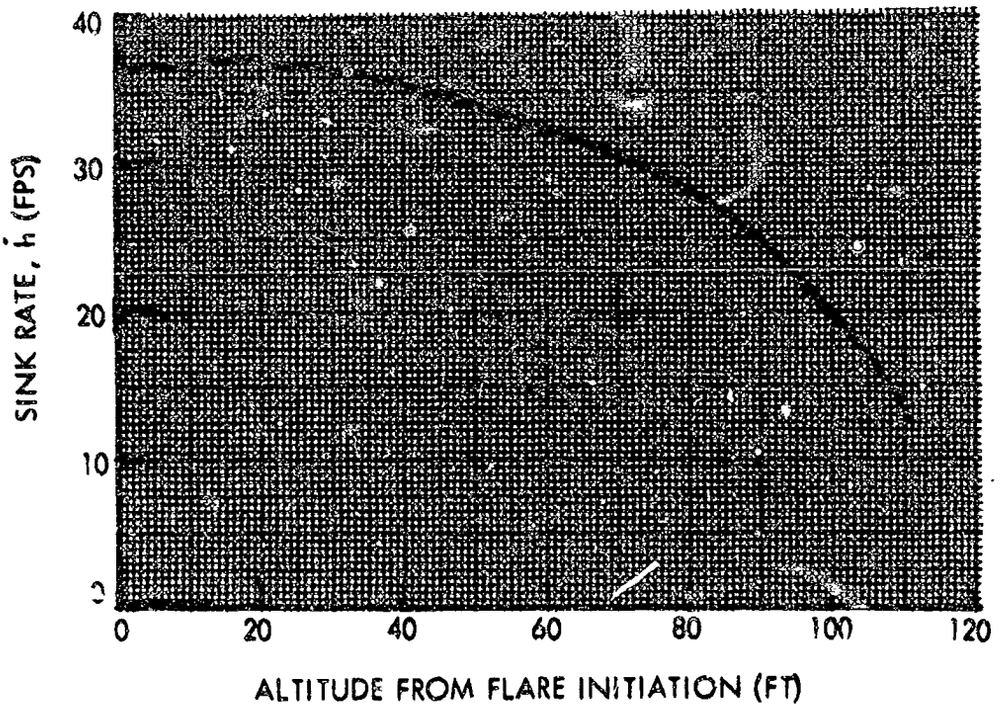

Figure 38. Flight 022 Touchdown Flare (Sheet 2 of 2)

FOLDOUT FR. 1

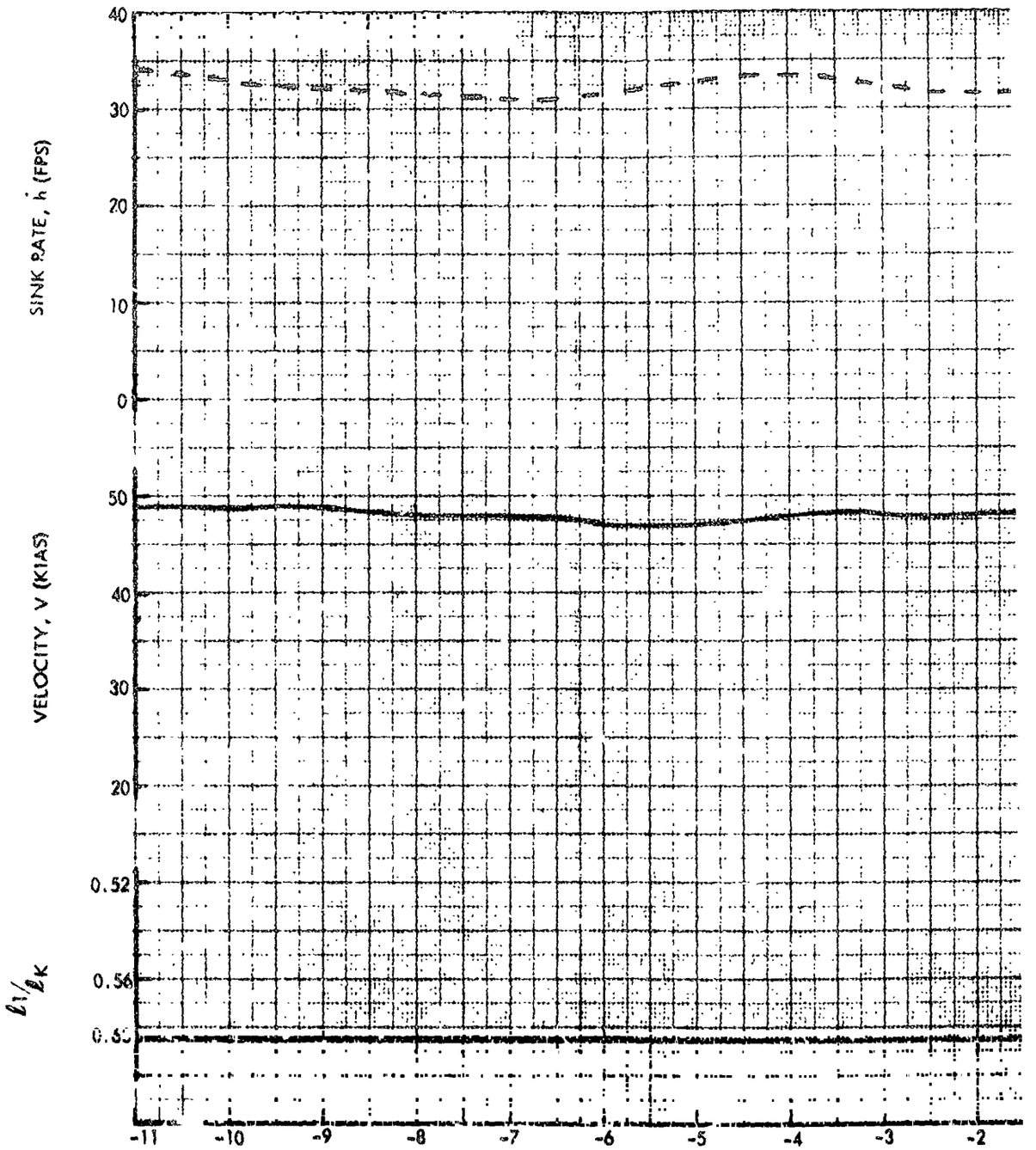

Figu

FOLDOUT FRAME 2

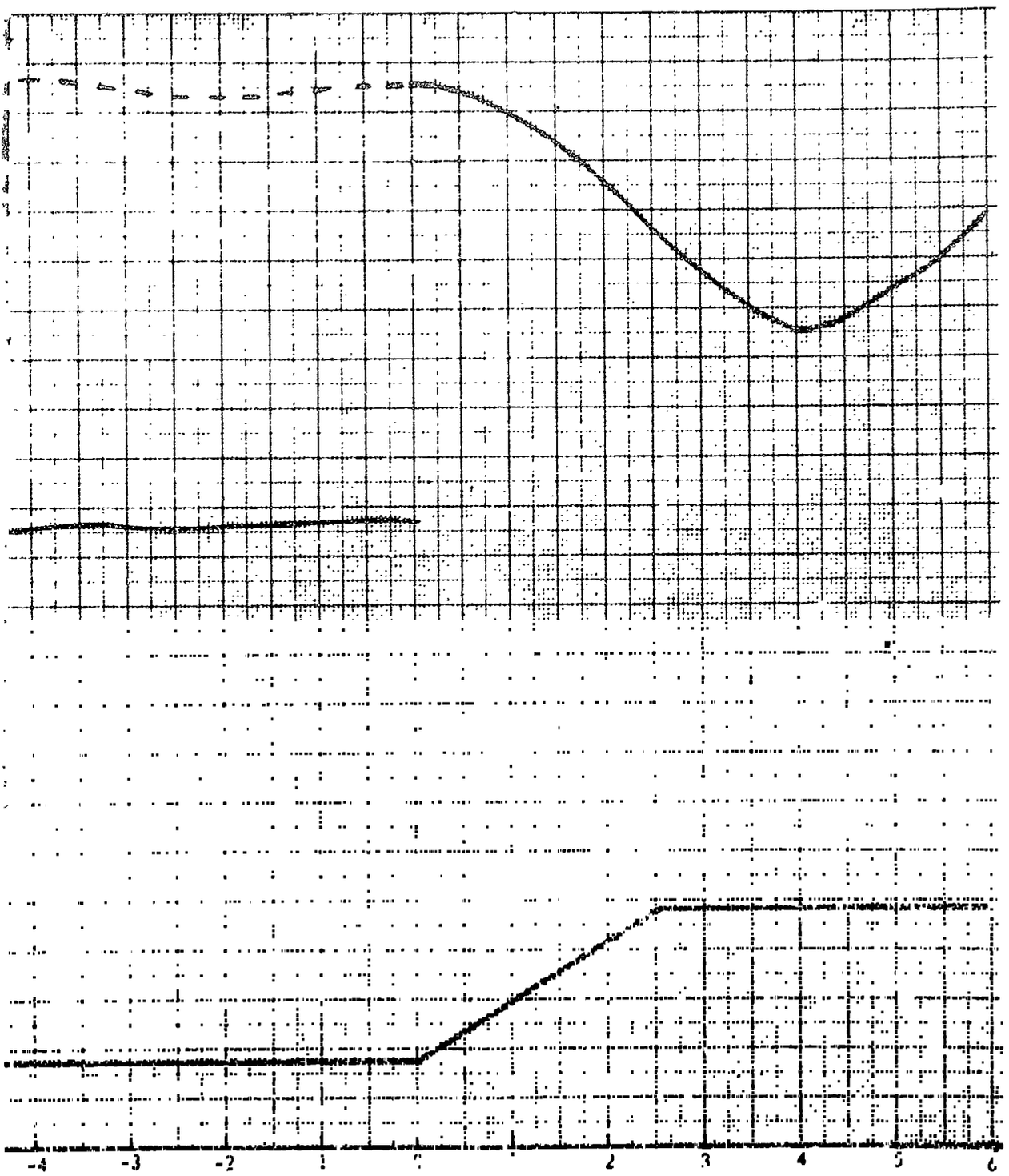

IME FROM FLARE INITIATION (SEC)

Figure 39. Flight 023 Touchdown Flare (Sheet 1 of 2)

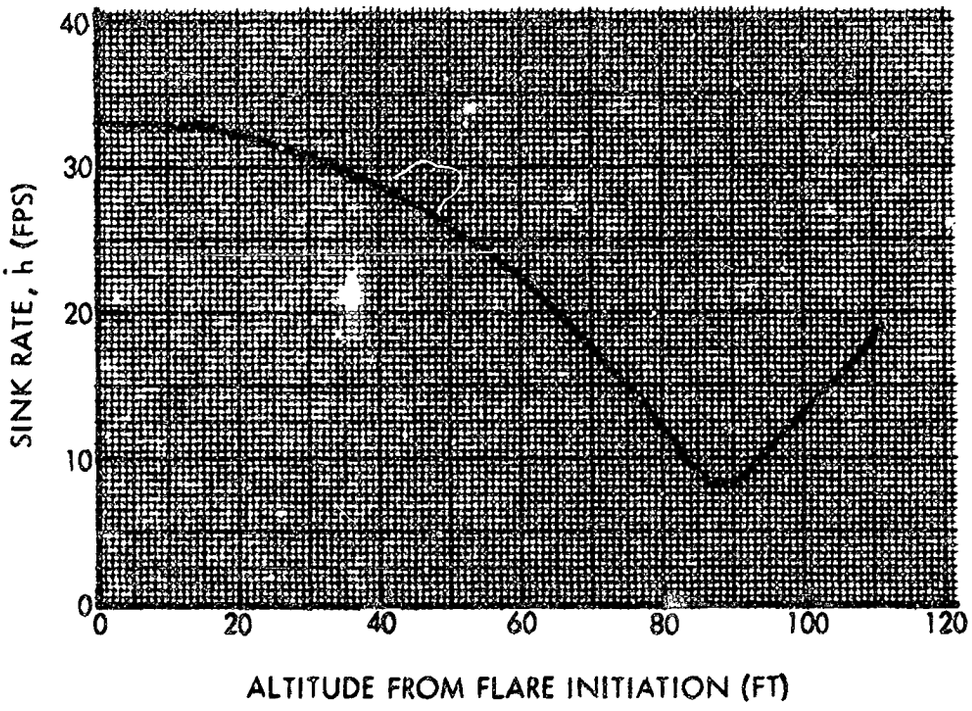

Figure 39. Flight 023 Touchdown Flare (Sheet 2 of 2)

FOLDOUT FRAME /

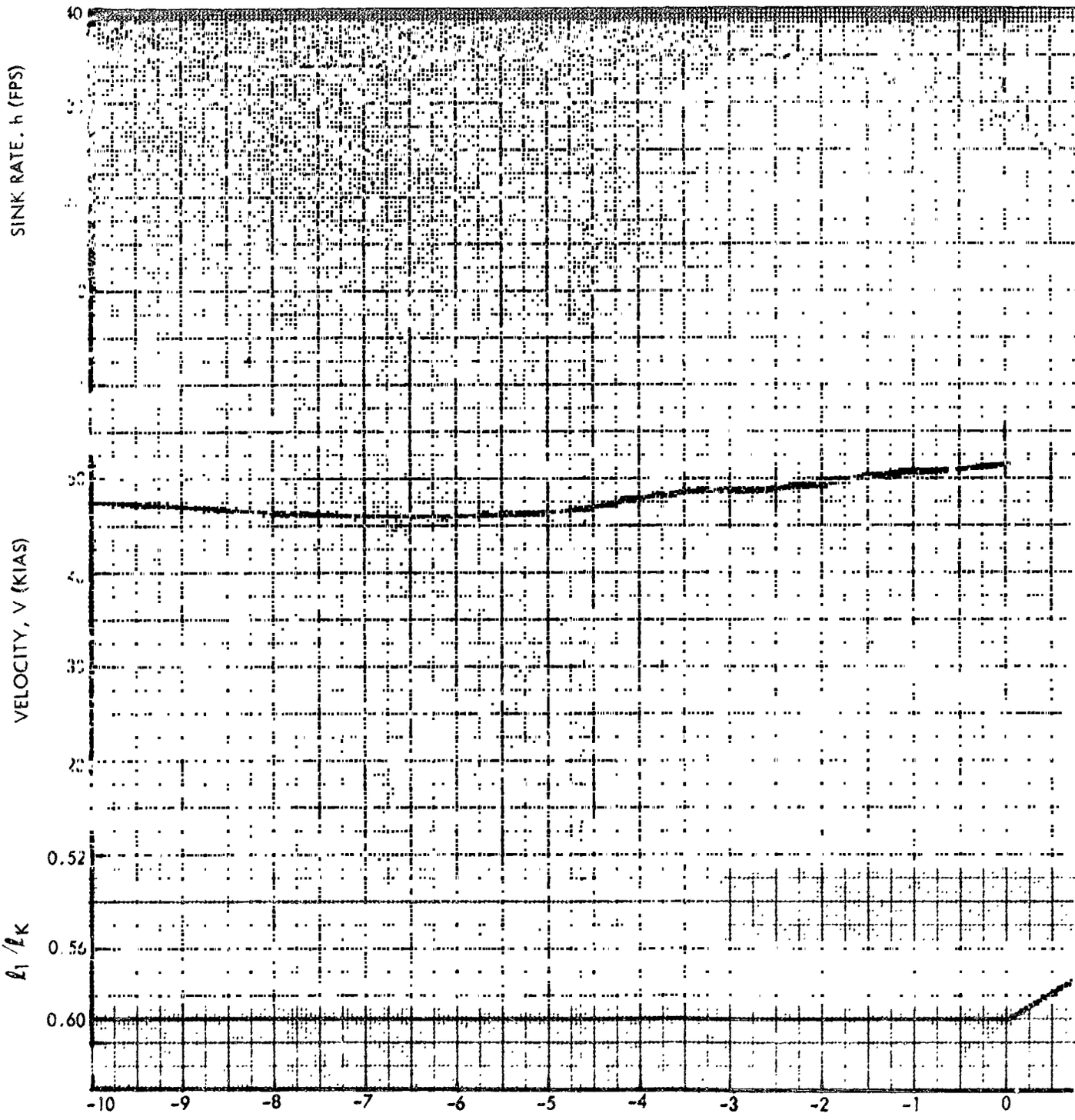

Figure

FOLDOUT FRAME 2

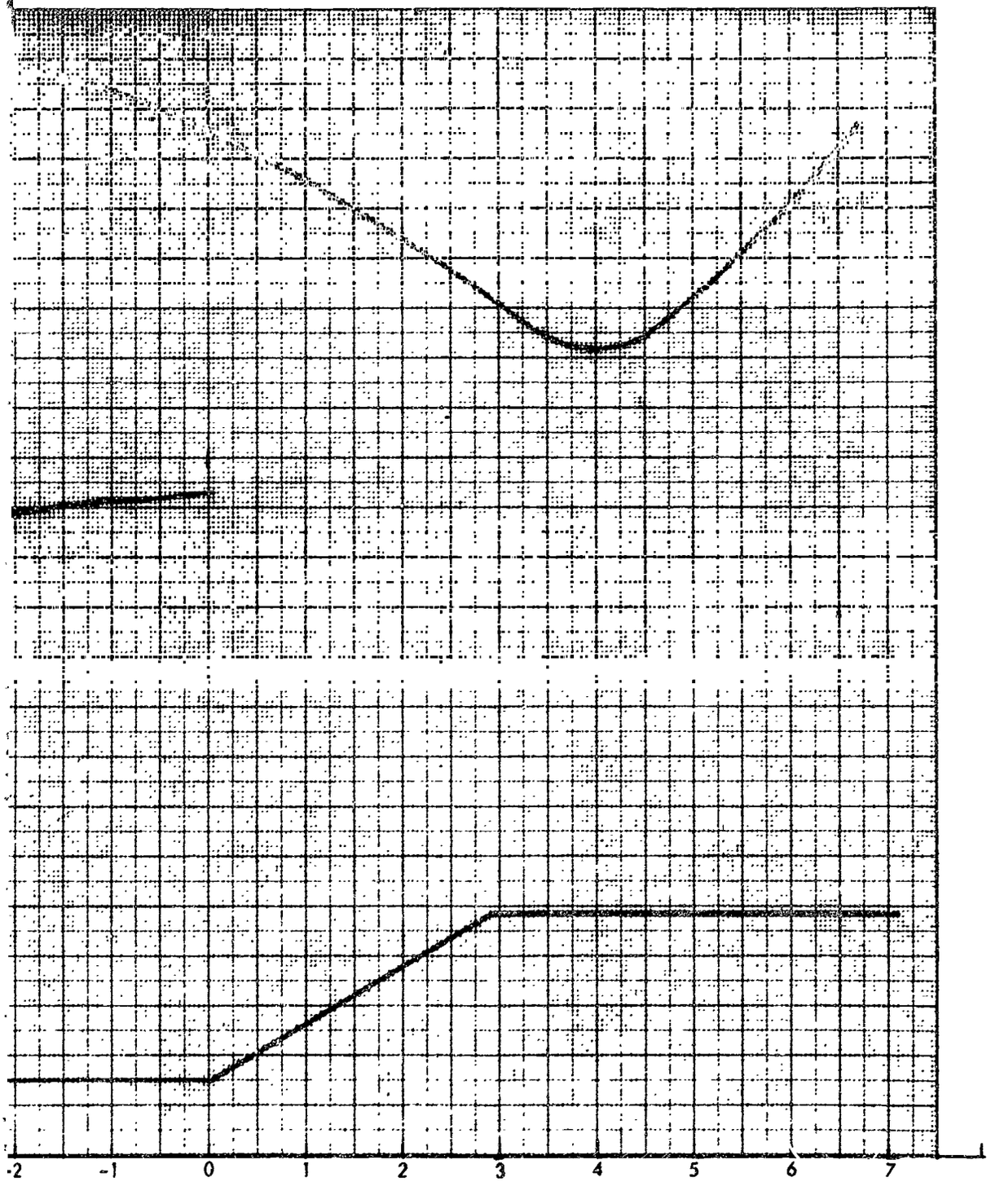

Figure 40. Flight 024 Touchdown Flare (Sheet 1 of 2)

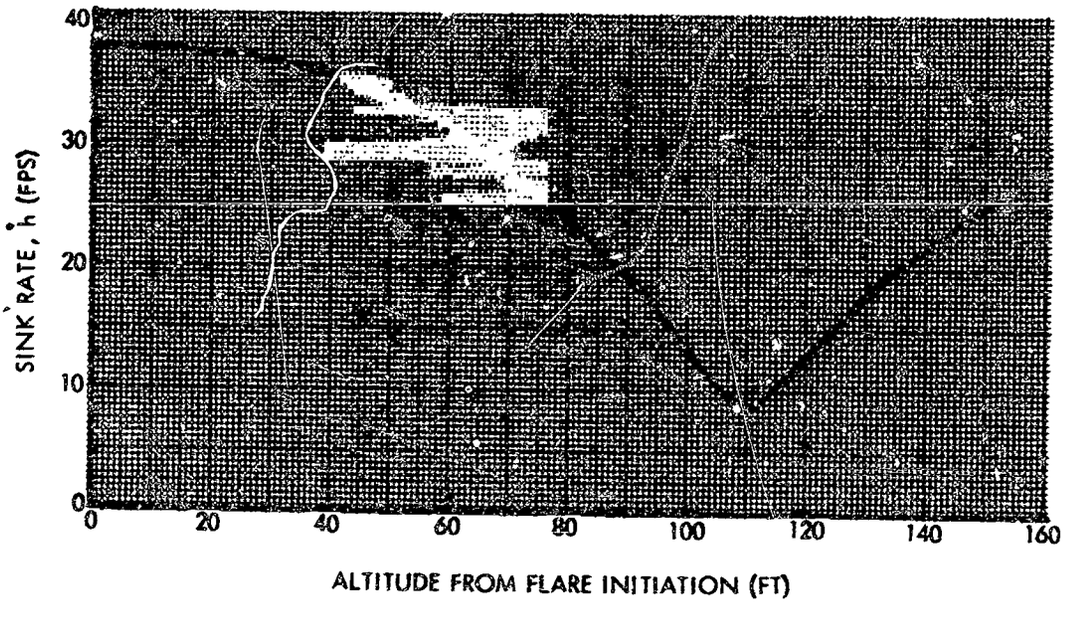

Figure 40. Flight 024 Touchdown Flare (Sheet 2 of 2)

increased 3 to 5 knots, the sink rate decreased 8 ft/sec and the vehicle pitched up 6 degrees due to the gust. The high energy and low sink rate at flare initiation resulted in reaching minimum sink rate 41 feet above the ground and a touchdown sink rate of 28.5 ft/sec. The flare in the air shown in Figure 41 is essentially a nominal flare. The preflare conditions at flare initiation are those normally expected. The altitude difference from flare initiation to that at minimum sink rate was also as expected.

Flight 025

It appears from Figure 42 that a fair amount of turbulence was encountered during preflare on this flight. Due to this turbulence, the vehicle was in a transient condition at flare initiation. The lower velocity (45 knots) at flare initiation resulted in a minimum sink rate at touchdown of only 11.5 ft/sec. During this flight, a two-step flare was performed at altitude. Due to this maneuver, the minimum sink rate was only 15 ft/sec, 130 feet after flare initiation. This flare is presented in Figure 43. A flare from ℓ_1/ℓ_k = 0.56 to 0.525 was also completed on this flight; however, since this flare was above 5000 feet, the radar altimeter was not functioning, and the only source of data is Nike radar. The quality of the data was poor, and the minimum sink rate was only approximately 15±4 ft/sec. The Δh to minimum sink rate was approximately 84 feet.

Flight 026

During this flight there was one flare performed at altitude. This flare from ℓ_1/ℓ_k = 0.56, is presented in Figure 44. It can be seen from these enclosures that the vehicle was close to steady state. The minimum sink rate achieved was 15 ft/sec, with a Δh from flare initiation of 75 feet. The touchdown flare for this flight is presented in Figure 45. It can be seen from Figure 45, Sheet 1, that the vehicle was in a transitory condition at flare initiation. The combination of this condition and the forward stick motion of the pilot after flare resulted in a minimum sink rate of 10.5 ft/sec, 25 feet above the ground.

Flight 027

Figure 46 presents the flare performed at altitude. Due to a late preflare, steady-state conditions were not achieved at flare initiation, and a slightly lower than expected minimum sink rate resulted. The touchdown flare is presented in Figure 47. Again, steady-state conditions were not achieved as a result of a late preflare and atmospheric perturbation. The high preflare velocity resulted in a minimum sink of 6 ft/sec.

FOLDOUT FRAME 1

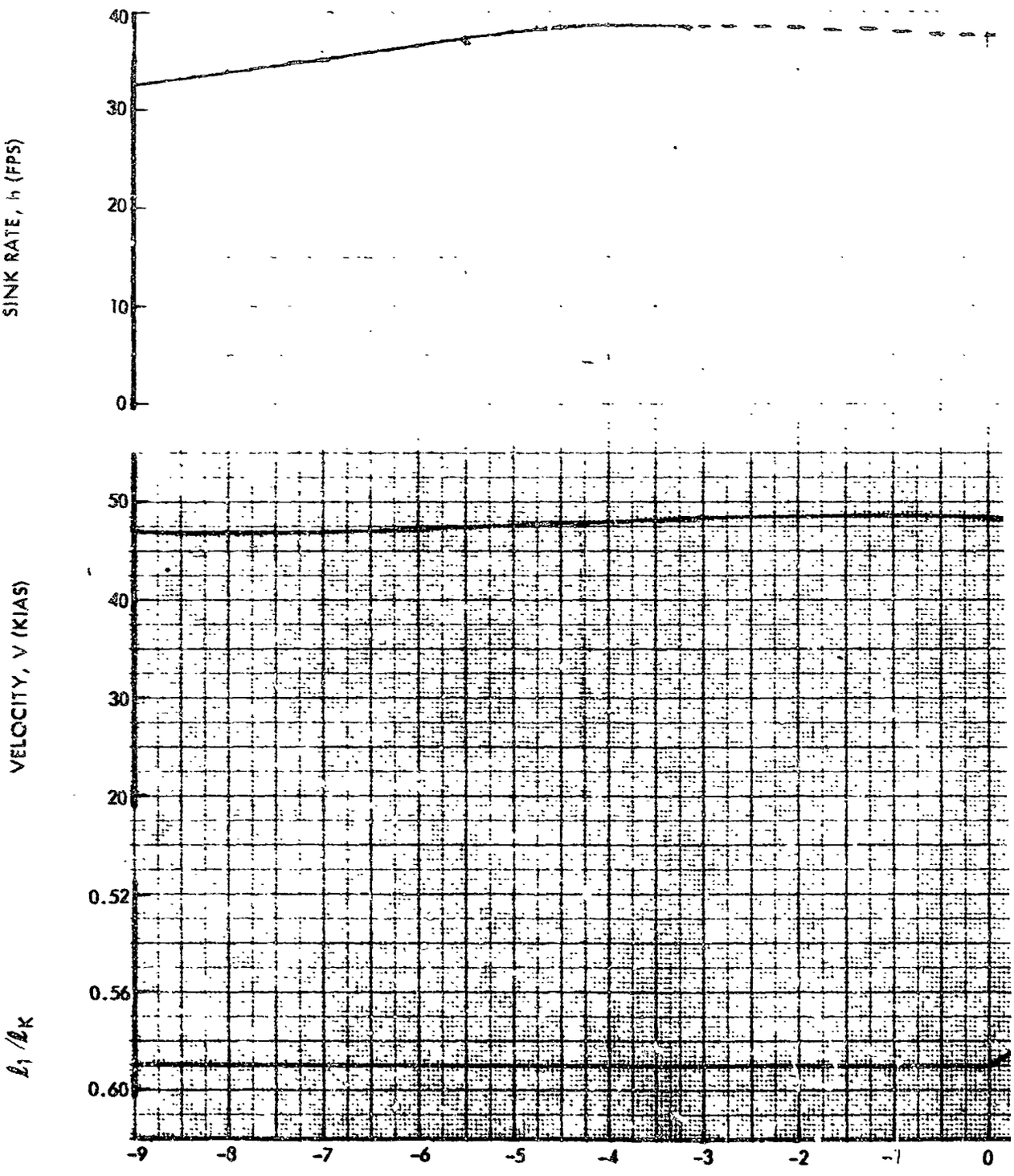

Fig

FOLDOUT FRAME 2

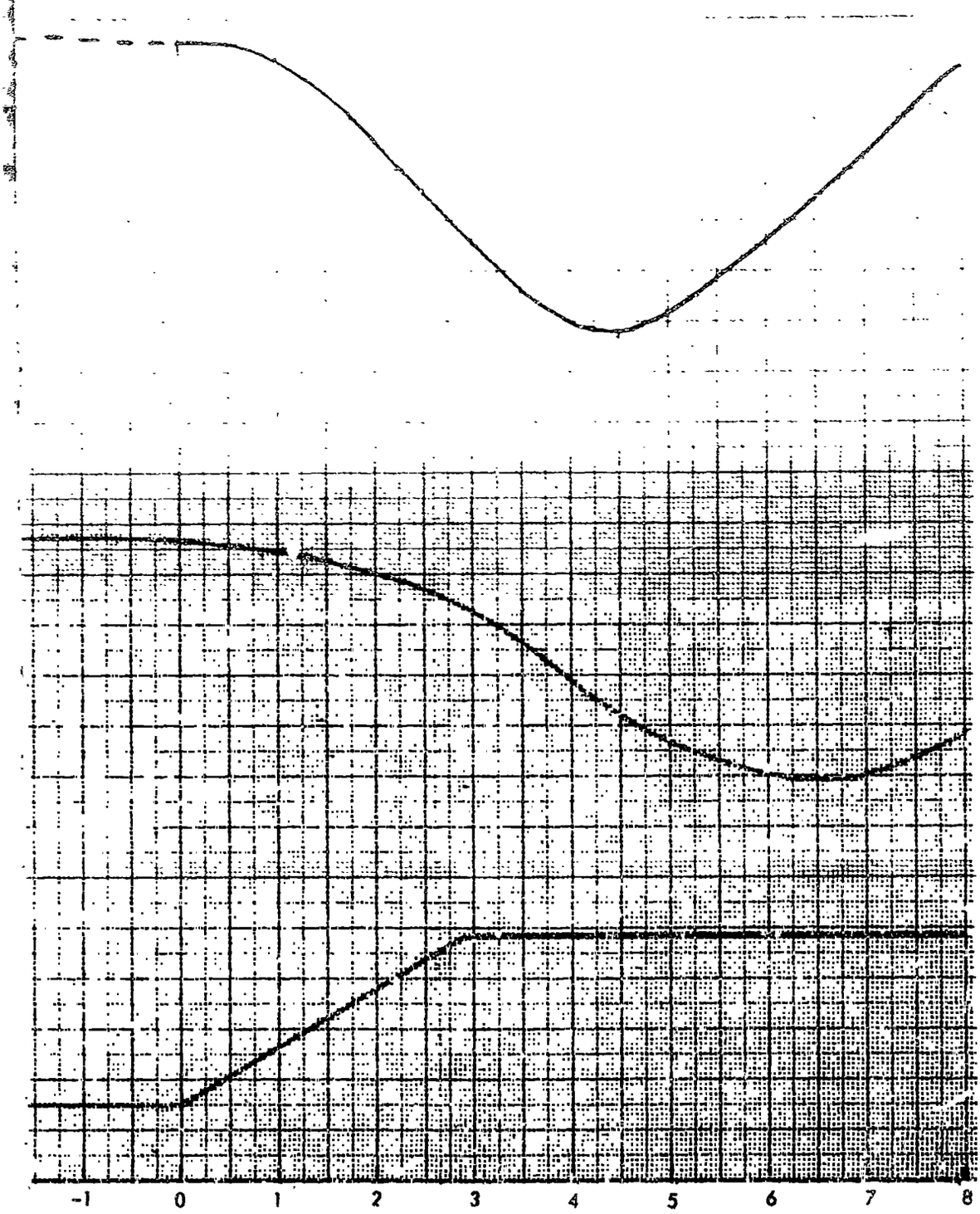

ITIATION (SEC)

Figure 41. Flight 024 Flare at Altitude (Sheet 1 of 2)

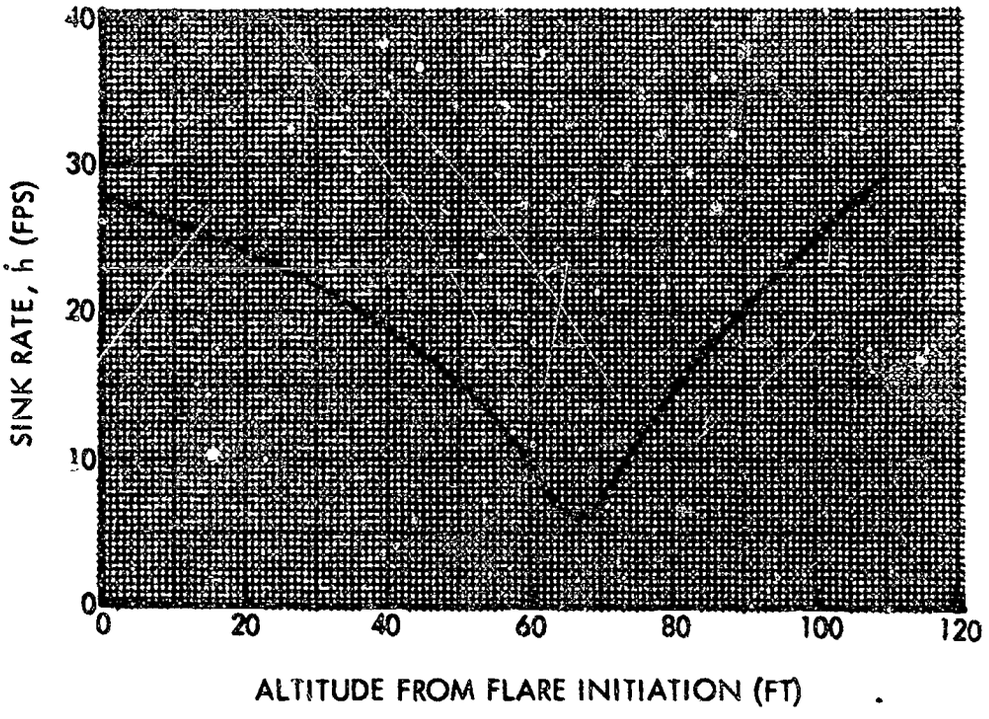

Figure 41. Flight 024 Flare at Altitude (Sheet 2 of 2)

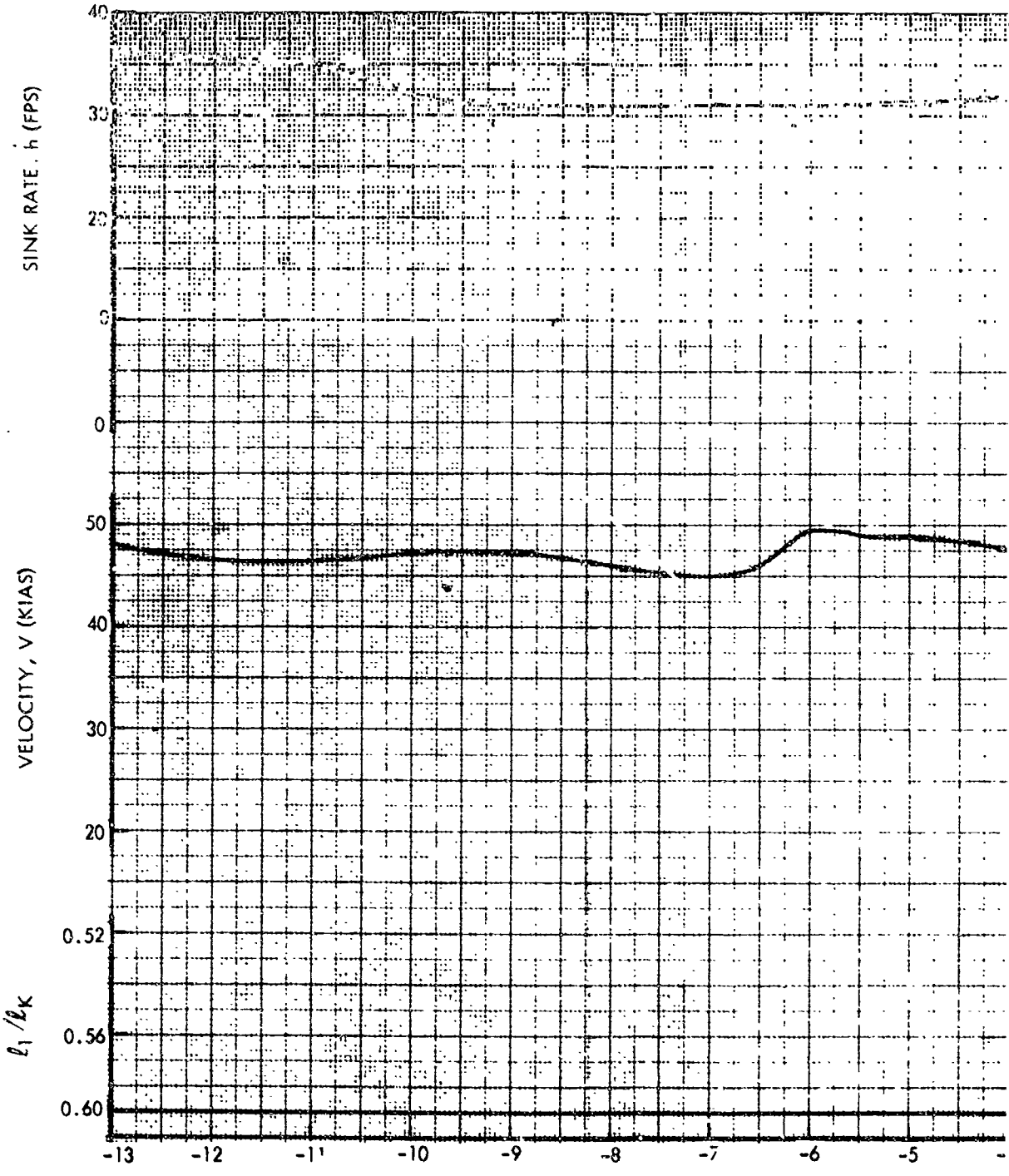

FOLDOUT FRAME 2

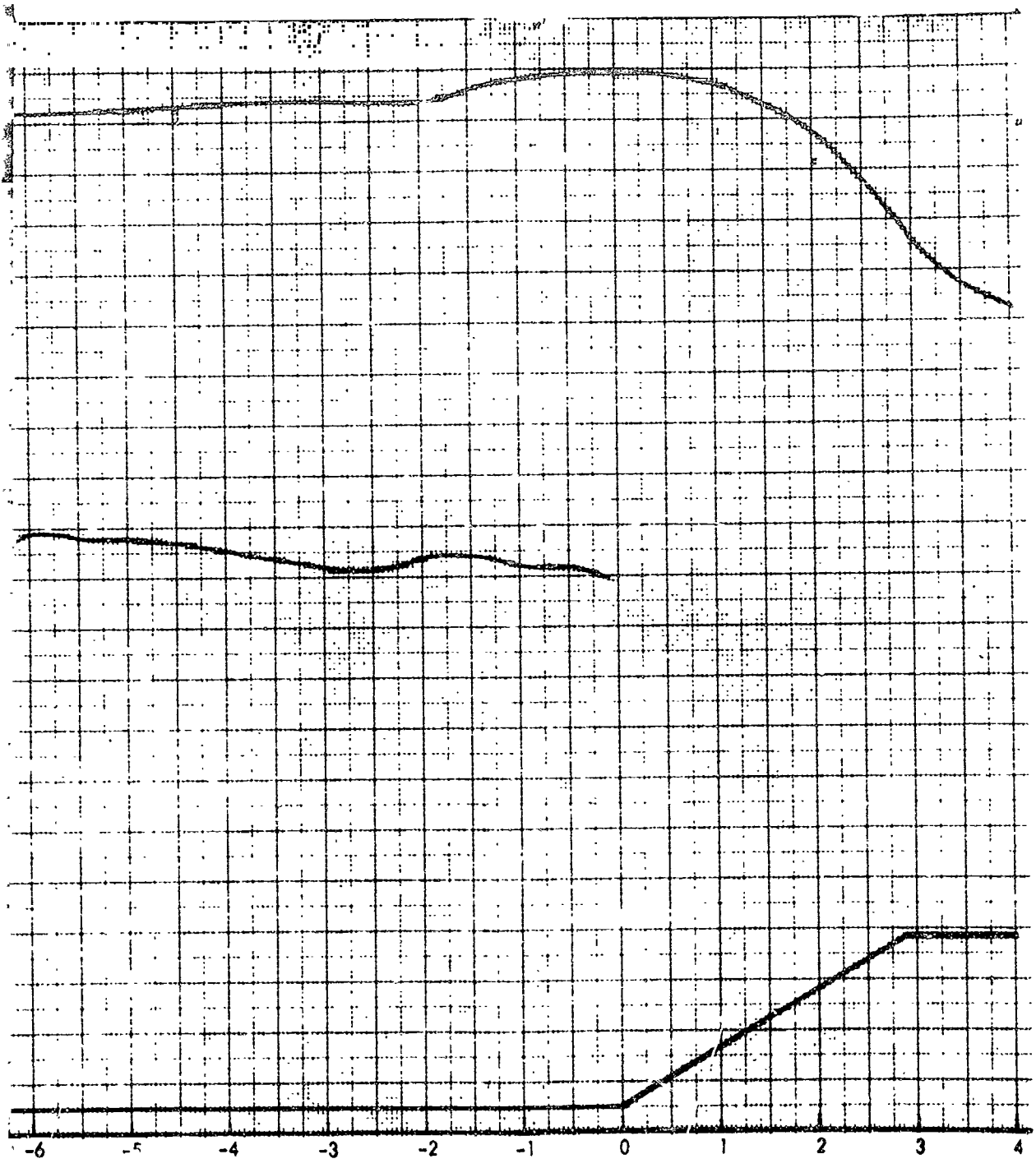

Figure 42. Flight 025 Touchdown Flare (Sheet 1 of 2)

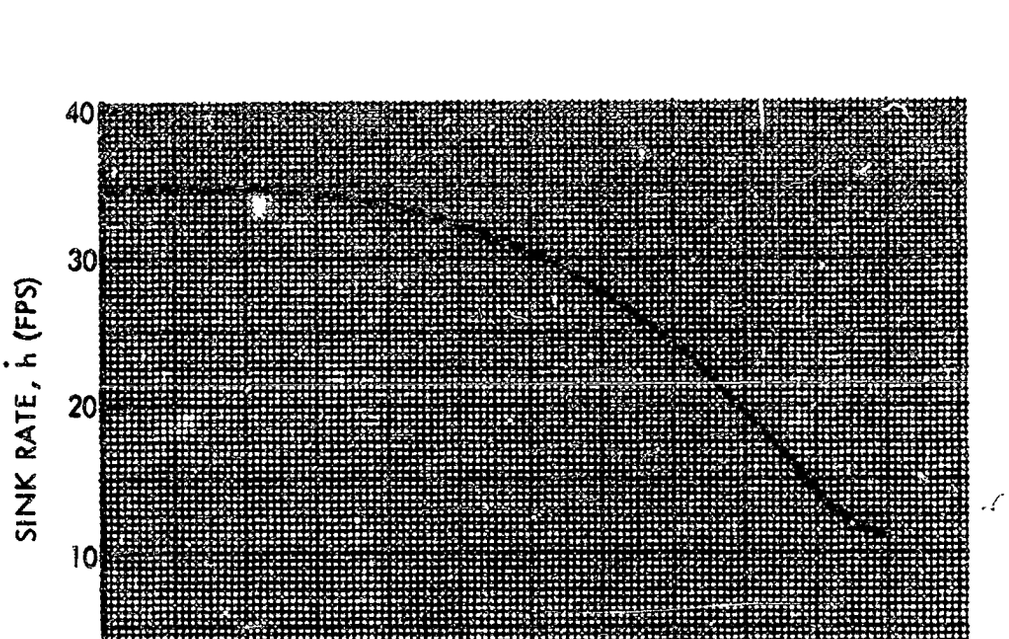

Figure 42. Flight 025 Touchdown Flare (Sheet 2 of 2)

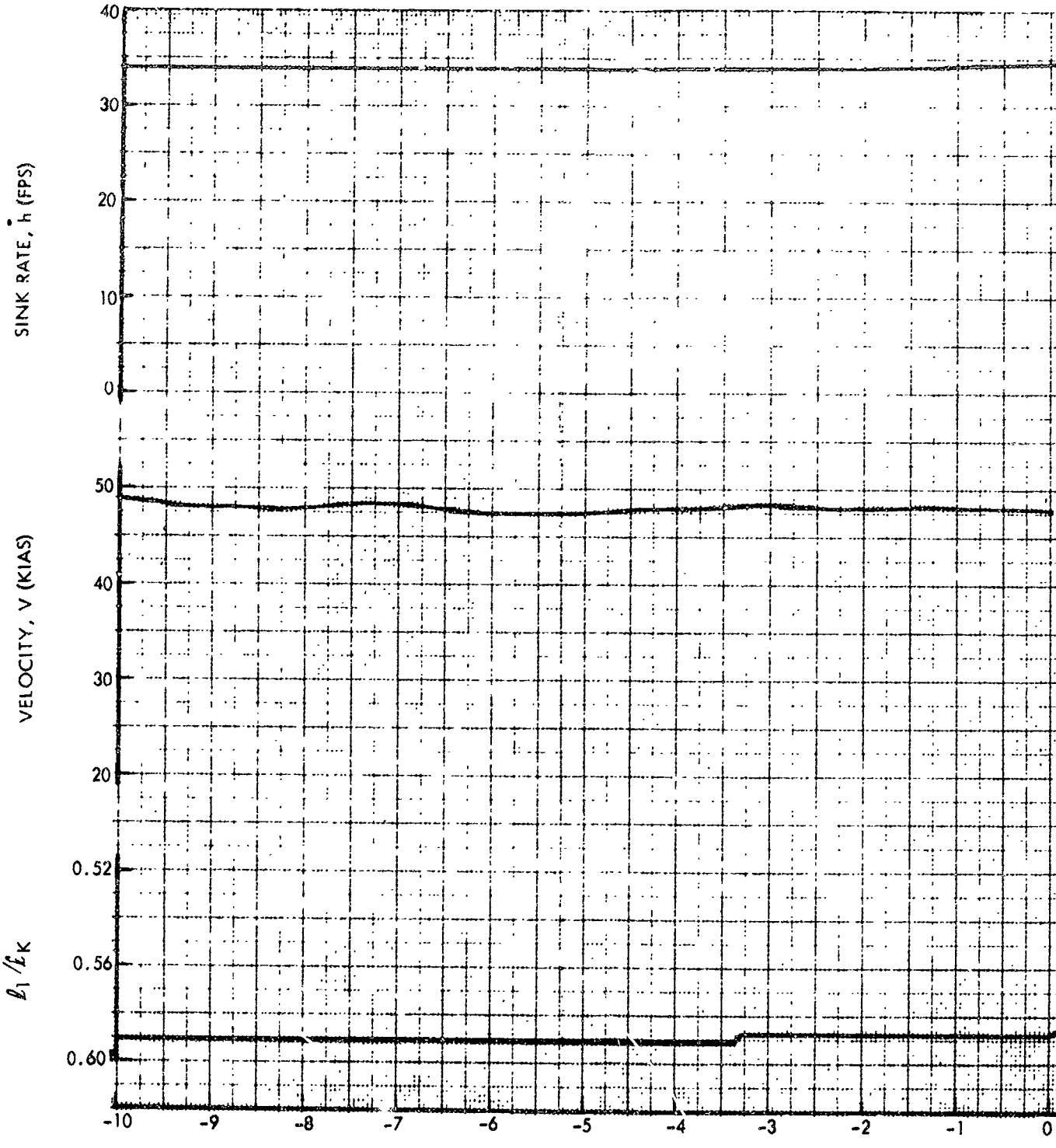

Figure 4

FOLDOUT FRAME 2

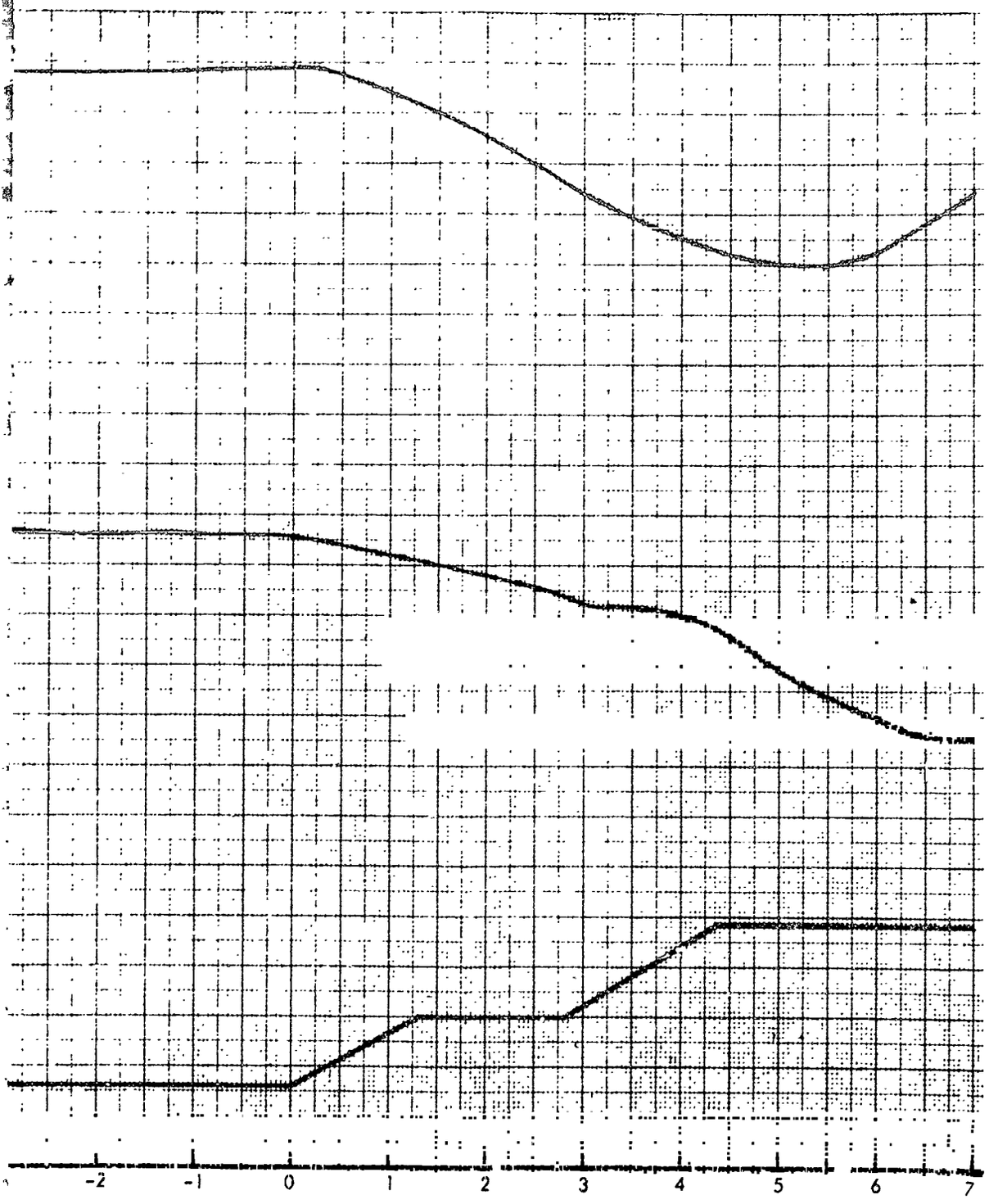

NITIATION (SEC) Figure 43. Flight 025 Flare at Altitude (Sheet 1 of 2)

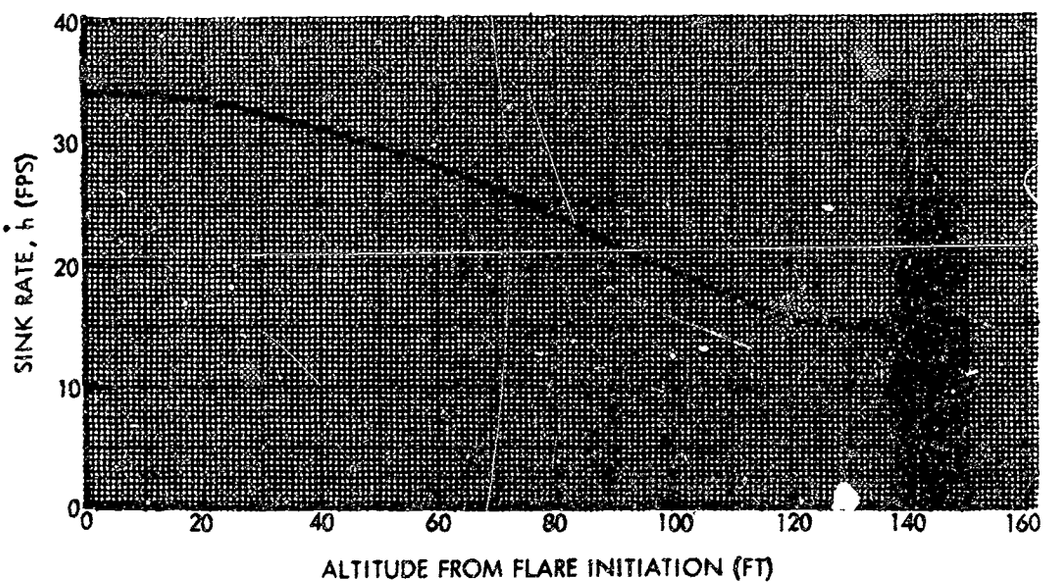

Figure 43. Flight 025 Flare at Altitude (Sheet 2 of 2)

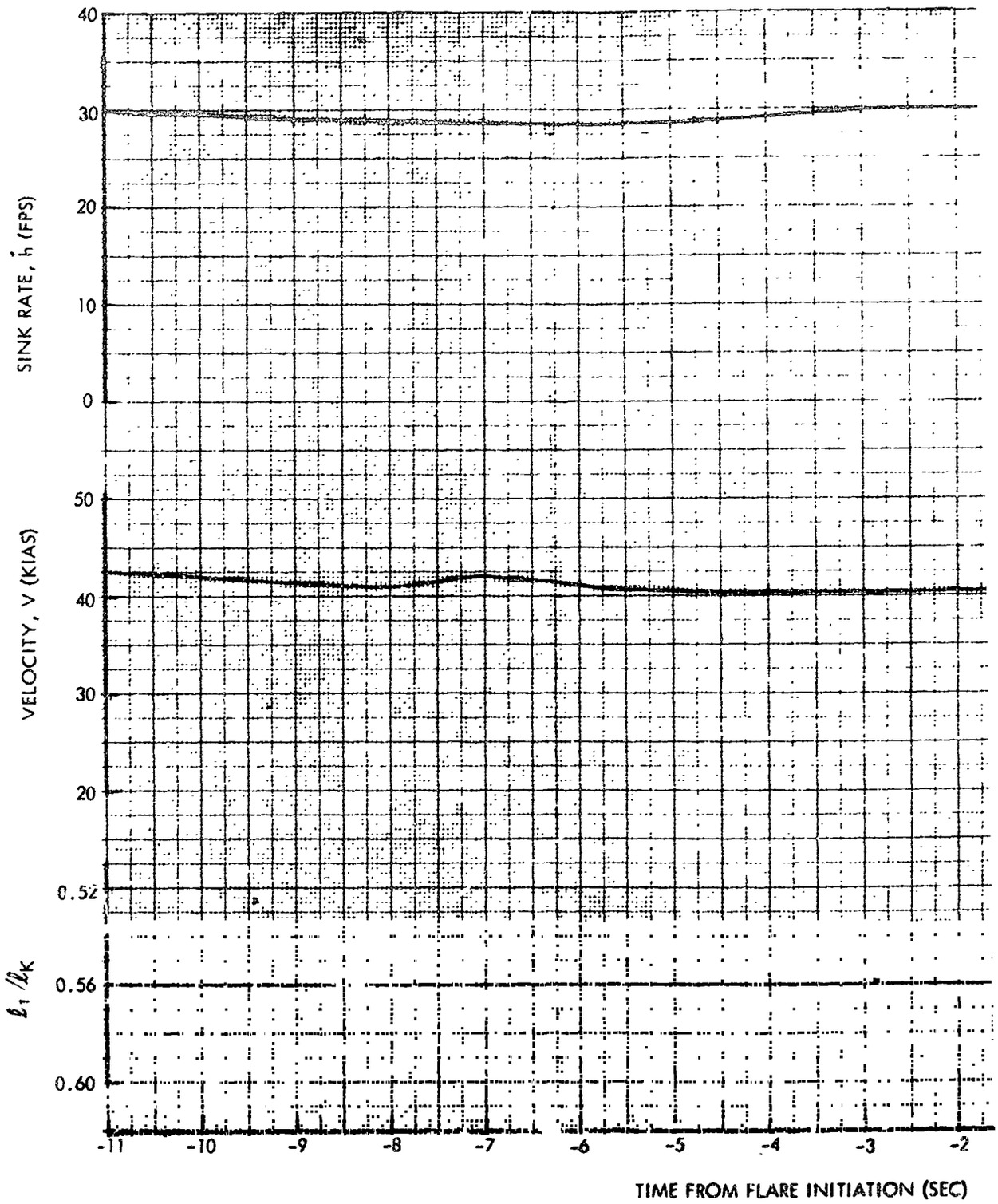

Figu

FOLDOUT FRAME 2

Figure 44. Flight 026 Flare at Altitude (Sheet 1 of 2)

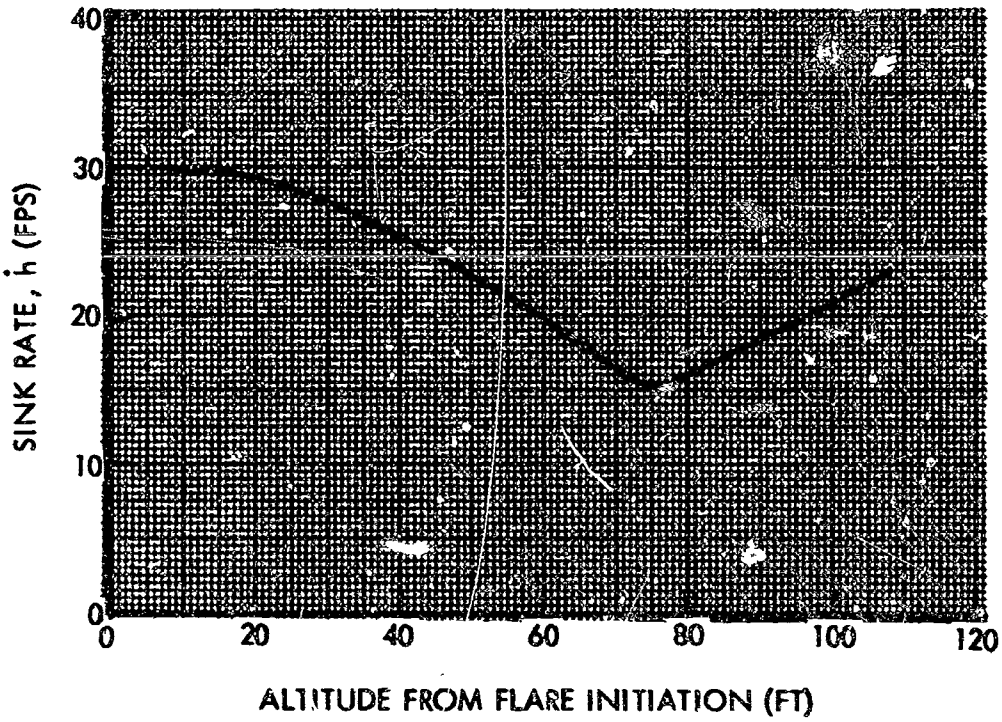

Figure 44. *Flight 026* **Flare at Altitude (Sheet 2 of 2)**

FOLDOUT FRAME 1

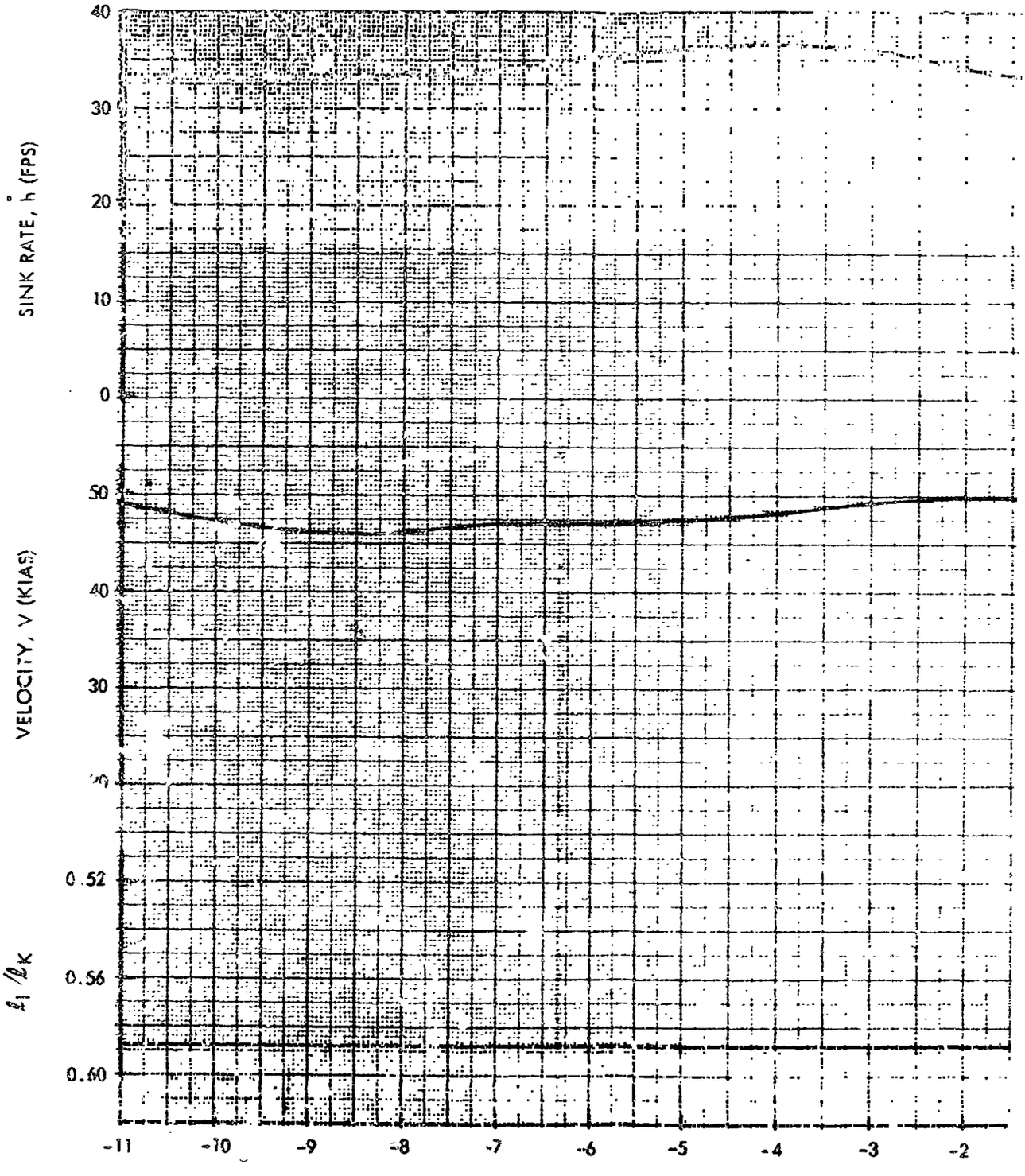

Figur

FOLDOUT FRAME 2

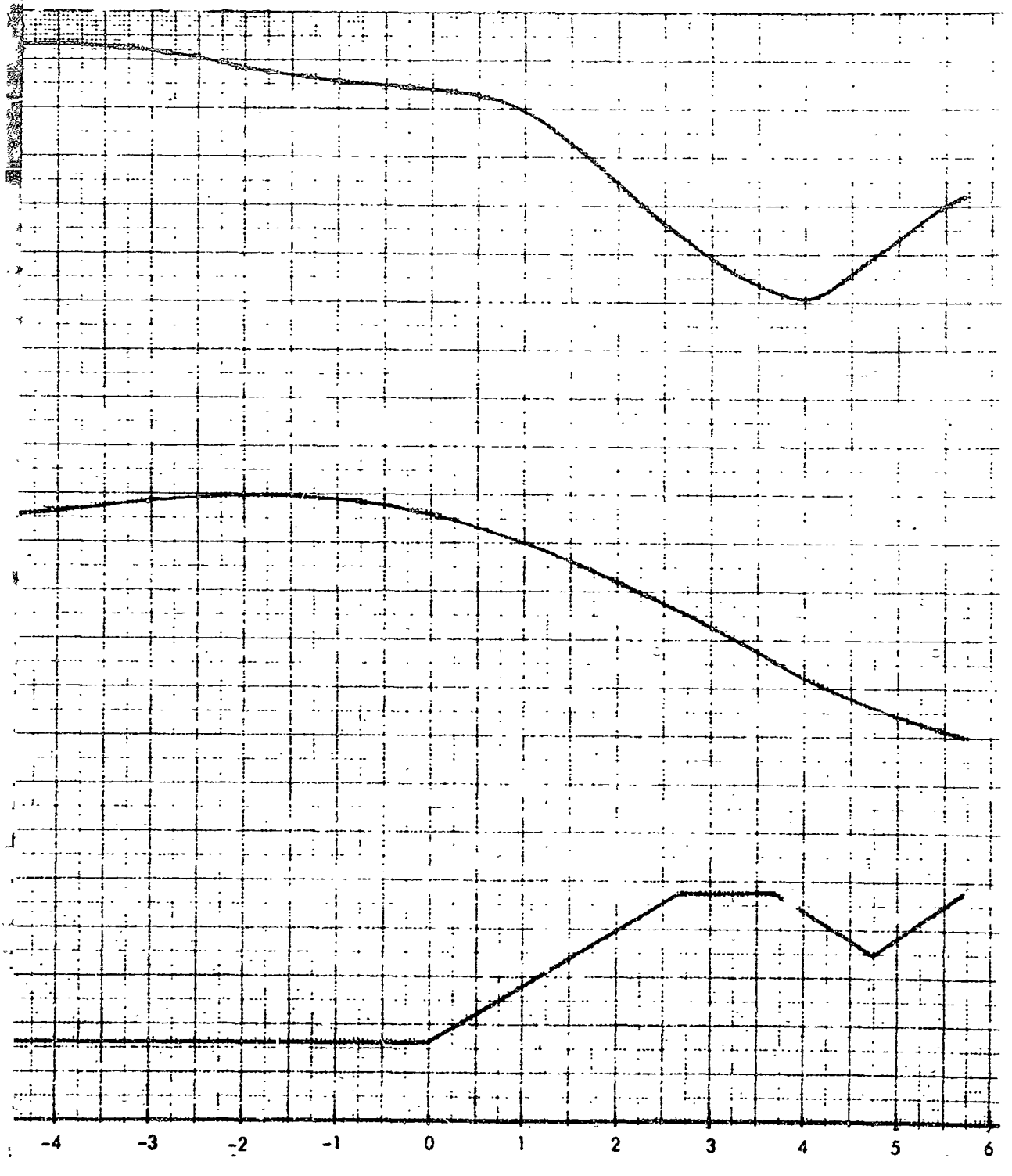

Figure 45. Flight 026 Touchdown Flare (Sheet 1 of 2)

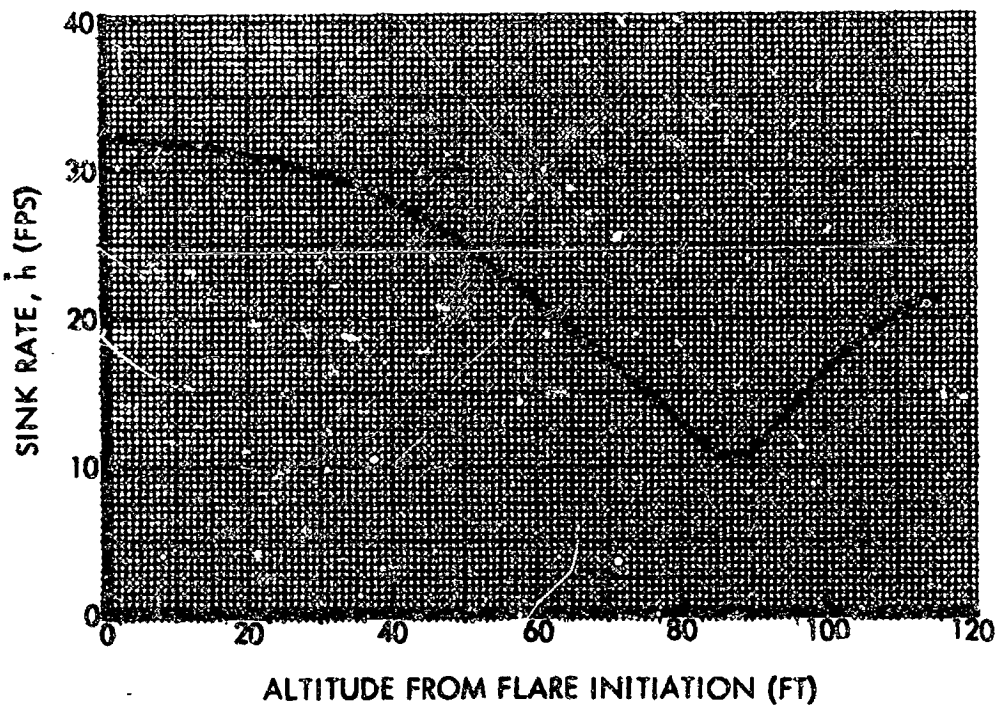

Figure 45. Flight 026 Touchdown Flare (Sheet 2 of 2)

FOLDOUT FRAME 1

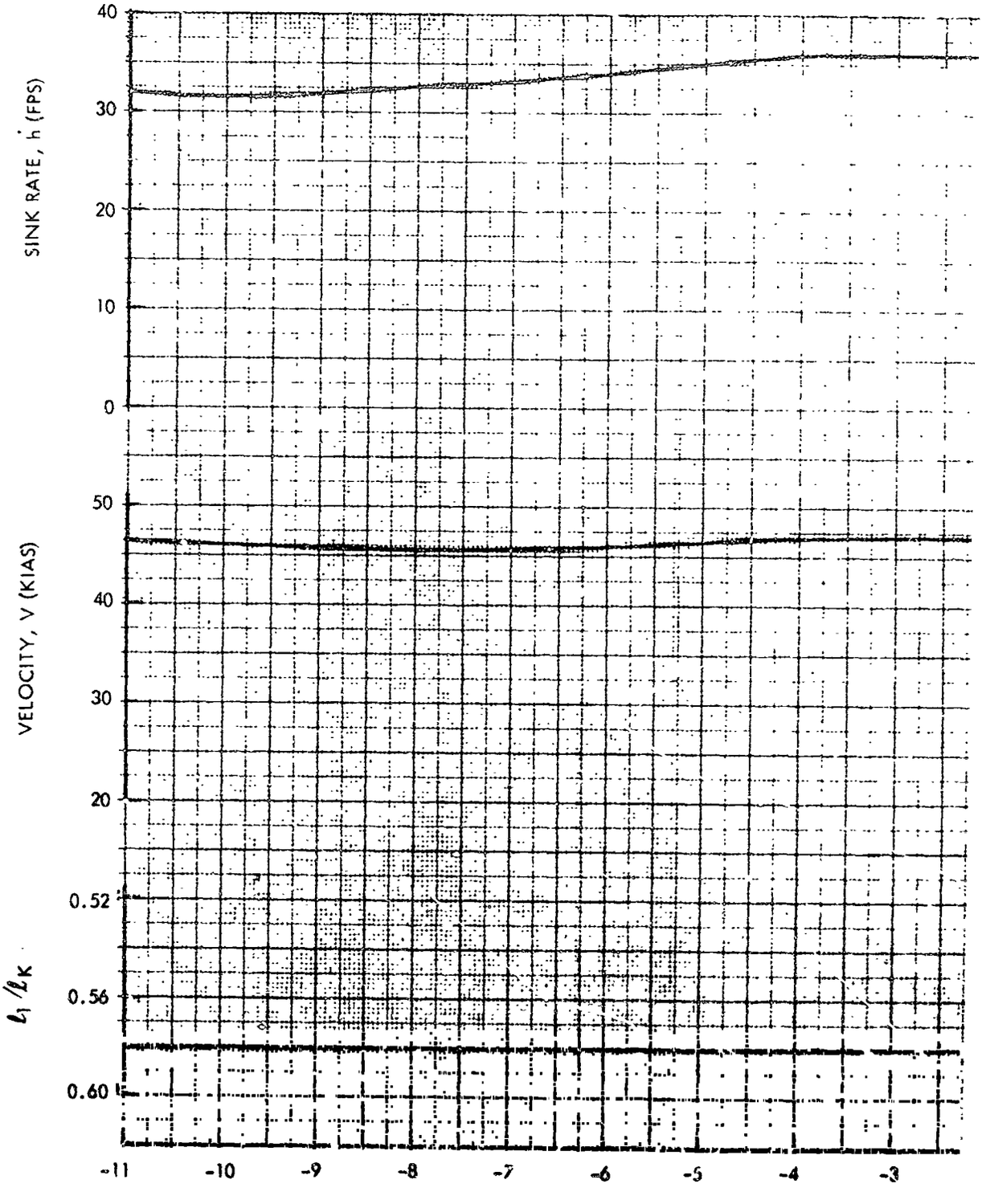

FOLDOUT FRAME 2

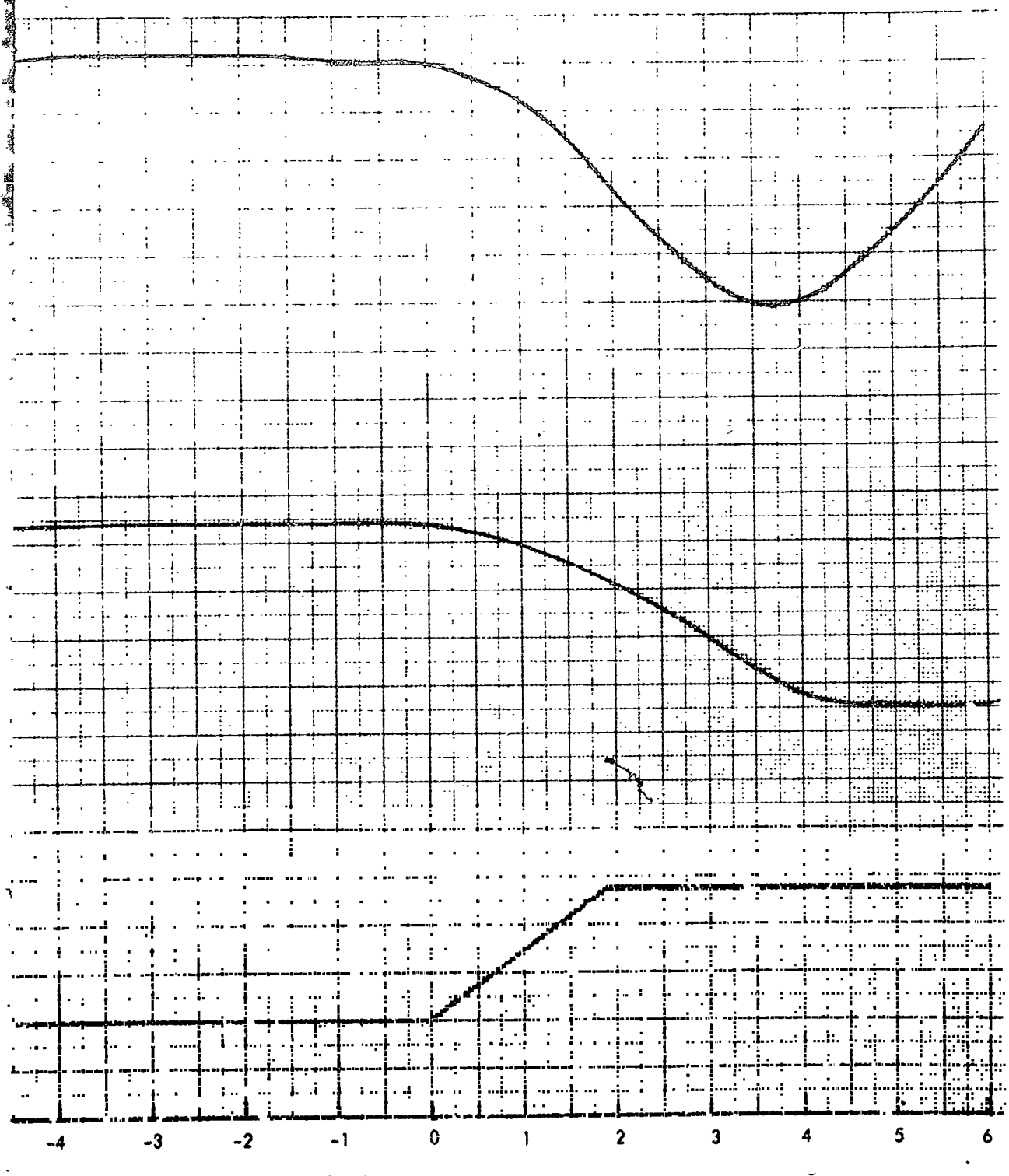

Figure 46. Flight 027 Flare at Altitude (Sheet 1 of 2)

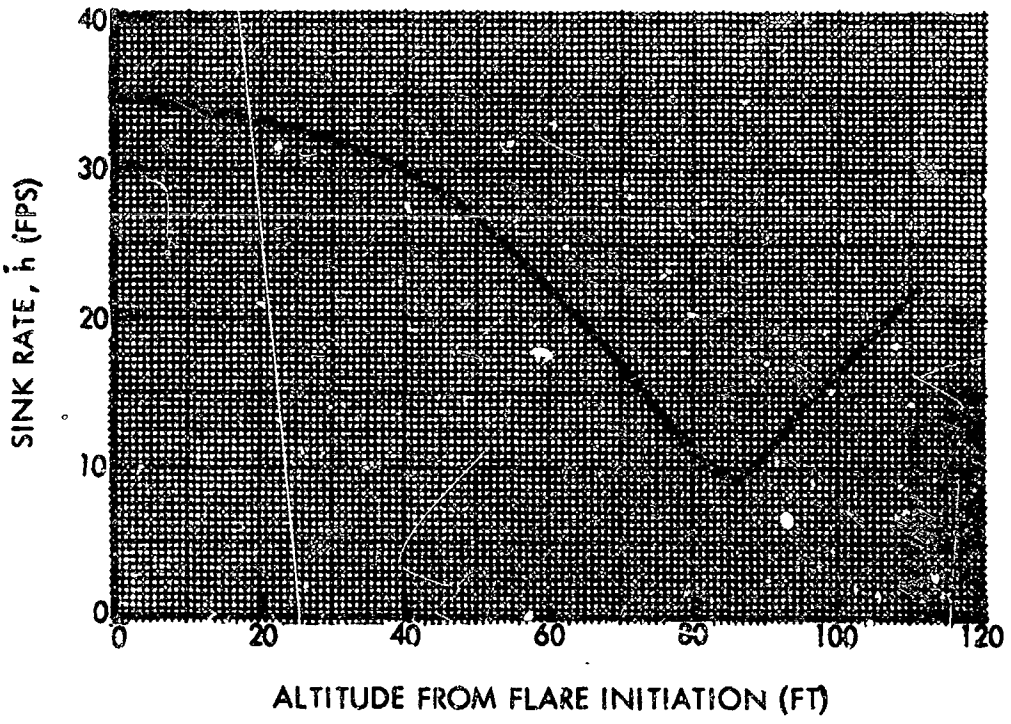

Figure 46. Flight 027 Flare at Altitude (Sheet 2 of 2)

FOLDOUT FRAME 1

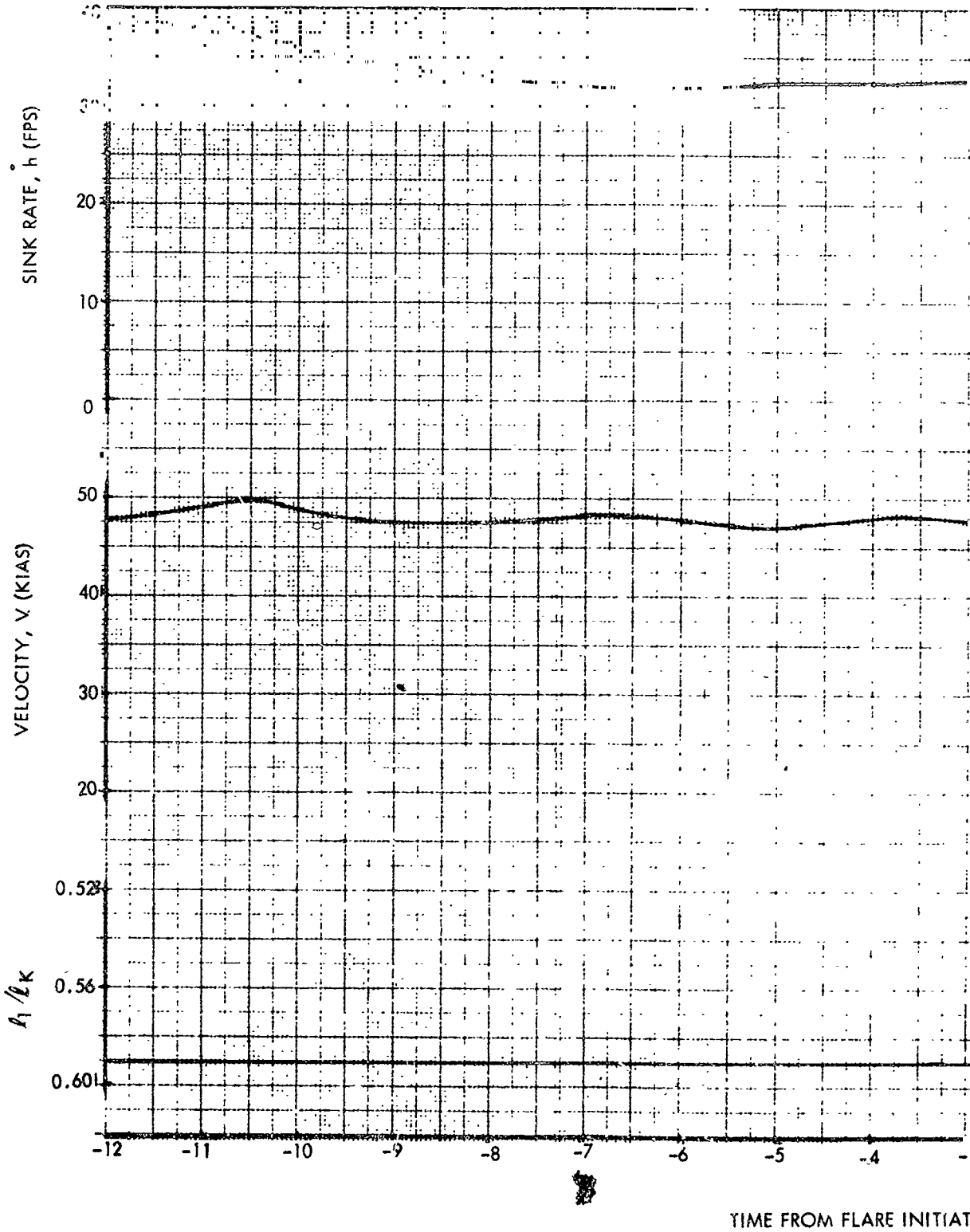

TIME FROM FLARE INITIAT

Fi

FOLDOUT FRAME 2

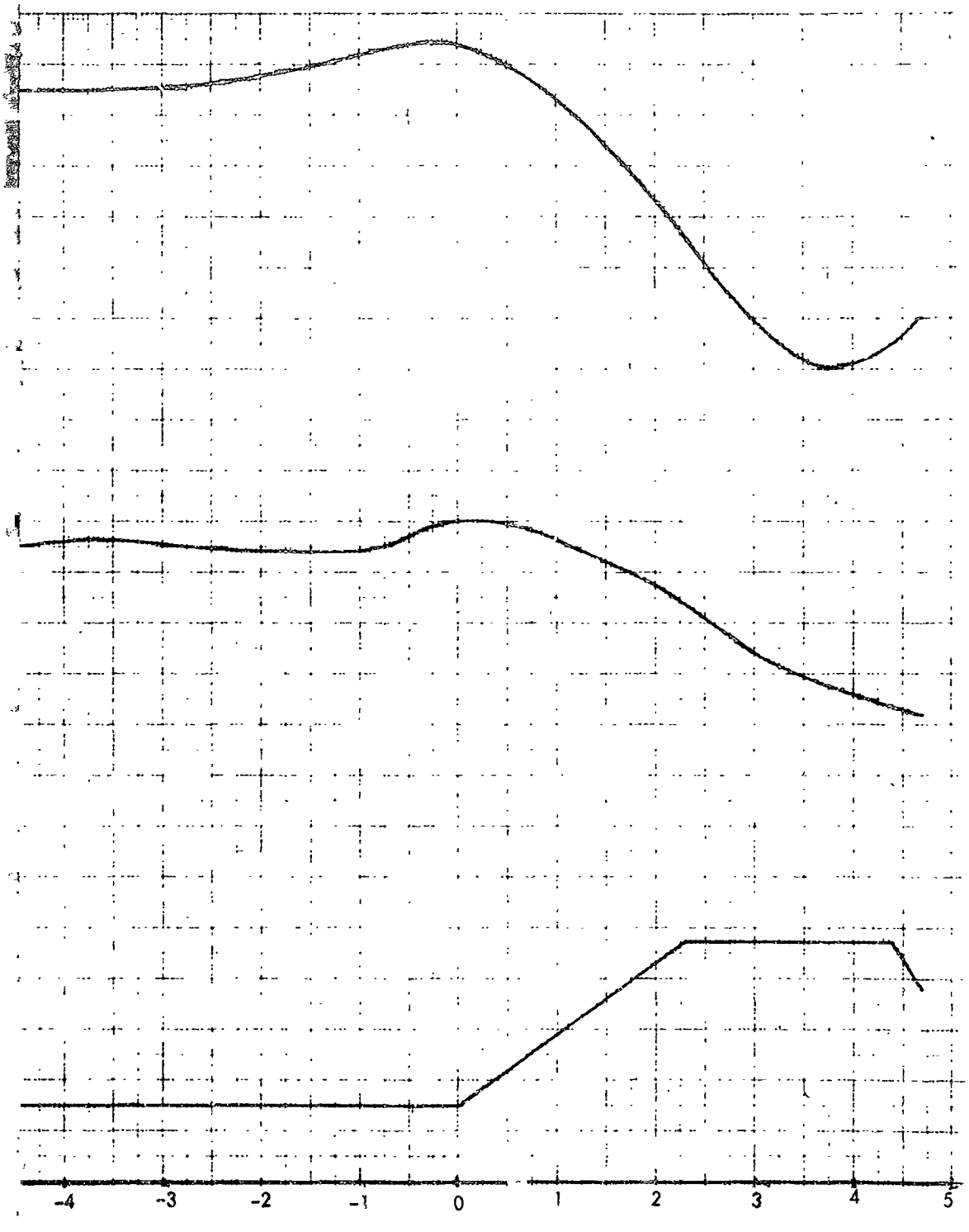

FLARE INITIATION (SEC)

Figure 47. Flight 027 Touchdown Flare (Sheet 1 of 2)

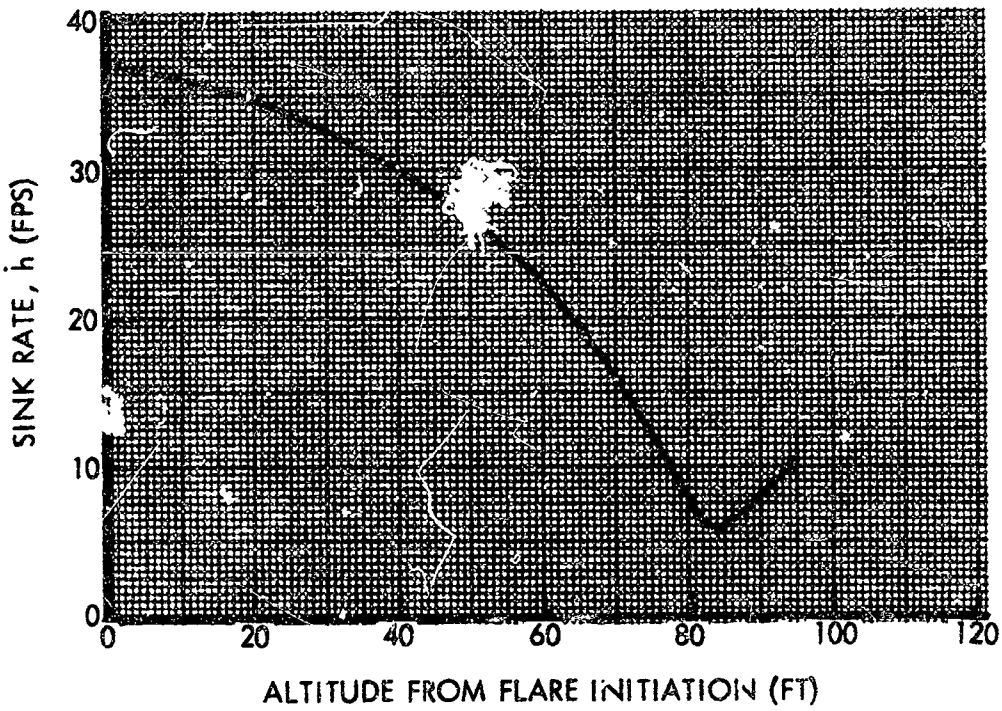

Figure 47. Flight 027 Touchdown Flare (Sheet 2 of 2)

Flight 028

The touchdown flare for this flight is presented in Figure 48. It can be seen that steady-state conditions were achieved on this flight. The flare probably would have been low had the pilot pulled the control stick all the way back.

Flight 029

The flare at altitude is presented in Figure 49. This flare was performed from $\ell_1/\ell_k = 0.572$. Again, the vehicle was in a transitory condition due to a late preflare. On the touchdown flare shown in Figure 50, the preflare was initiated from the $\ell_1/\ell_k = 0.55$ in one step to $\ell_1/\ell_k = 0.59$, causing an unusually large transient. This transient, coupled with atmospheric perturbations, resulted in highly unsteady conditions at flare initiation as evidenced by the sink-rate time history. The resultant flare was high. This condition was aggravated by the failure of the pilot to hold the control stick back.

Flight 030

The touchdown flare for this flight is presented in Figure 51. On this flight the atmospheric perturbations are highly evident in the velocity trace. This flare was performed late, at 85 feet, resulting in a minimum sink rate of 14 ft/sec.

Flight 031

The flare at altitude on this flight was performed from $\ell_1/\ell_k = 0.57$ and is presented in Figure 52. The velocity and sink-rate time histories indicate relatively steady-state conditions at flare initiation. The minimum sink rate was 14 ft/sec. The touchdown maneuver is presented in Figure 53. During preflare, the vehicle encountered some turbulence, apparently causing the pilot to change his pitch setting. These pitch maneuvers during preflare aggravated the transients. At 125 feet above ground level, the chase pilot called, "flare." The pilot apparently reacted to this erroneous cue and pulled the stick back to $\ell_1/\ell_k = 0.54$ before realizing he was high. The pilot offered no explanation for the other pitch maneuvers. The resulting impact sink rate was 25 ft/sec.

Flight 032

The flare at altitude for this flight was from $\ell_1/\ell_k = 0.582$ and is presented in Figure 54. The minimum sink rate was 14.5 ft/sec, which was slightly higher than expected. This may have been due to the forward

FOLDOUT FRAME 1

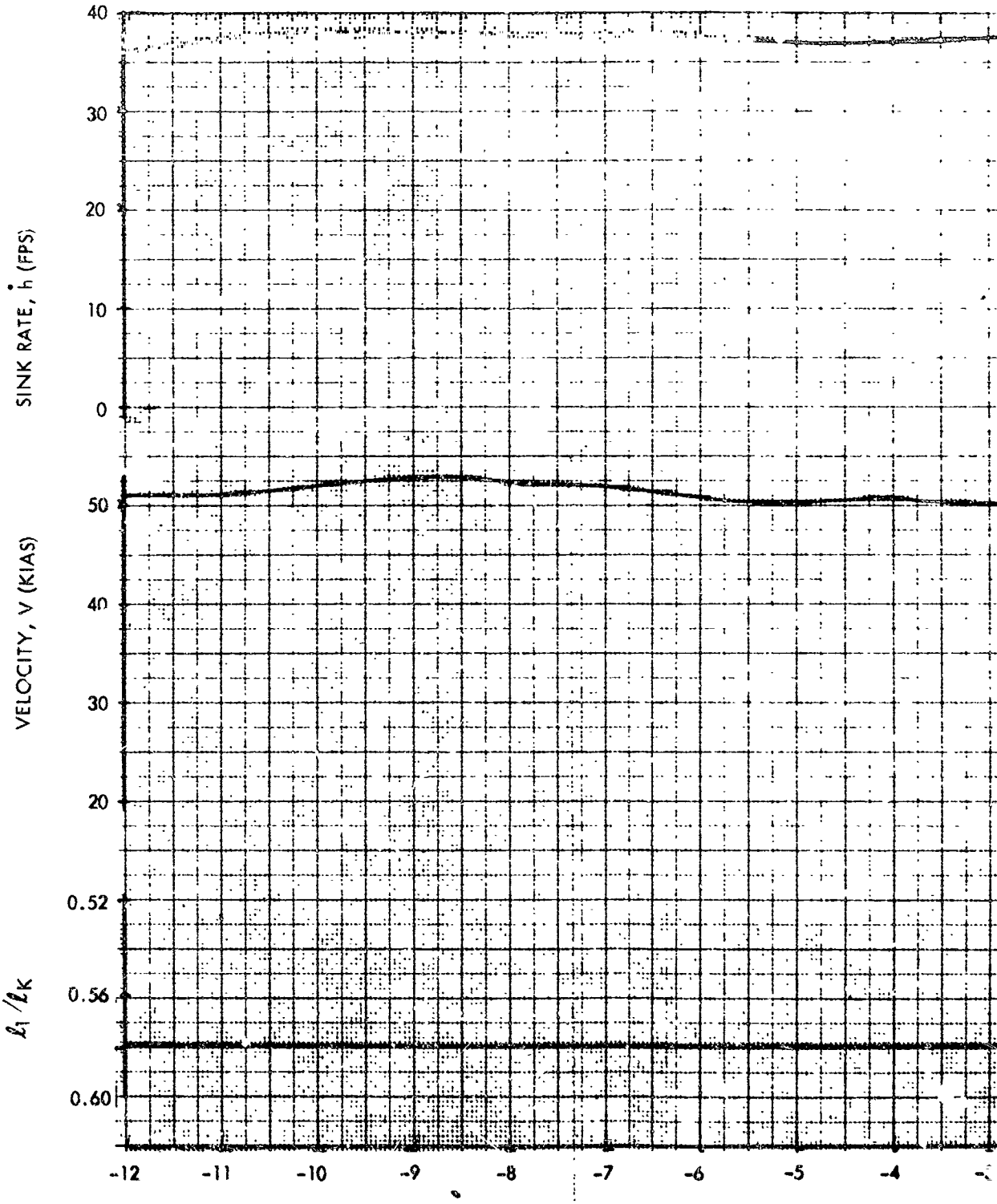

Fi

FOLDOUT FRAME 2

Figure 48. Flight 028 Touchdown Flare (Sheet 1 of 2)

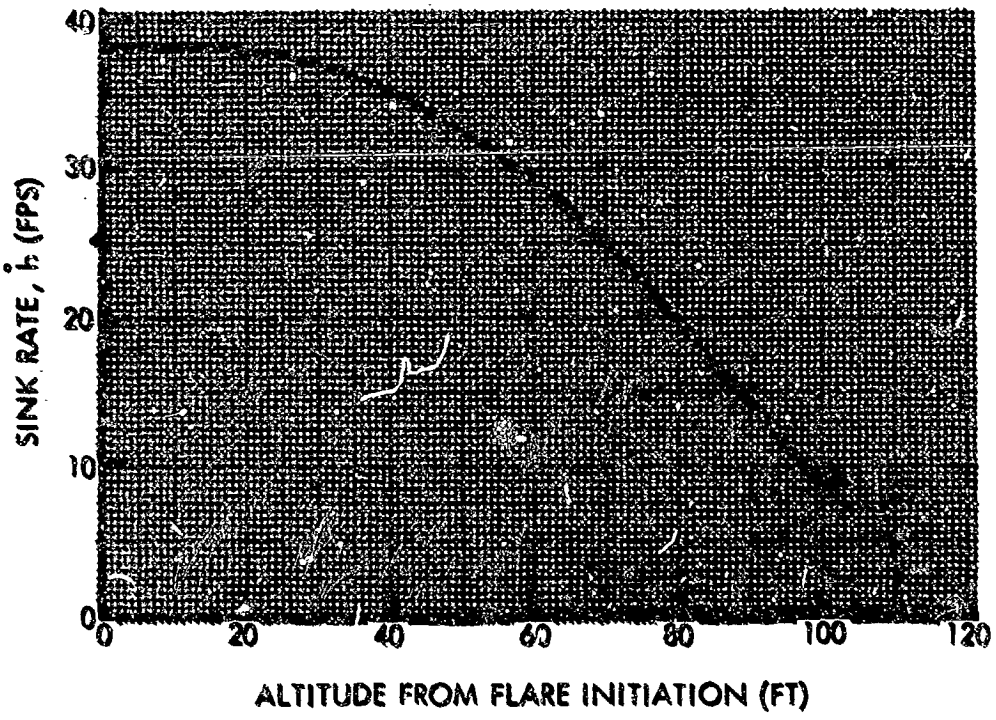

Figure 48. Flight 028 Touchdown Flare (Sheet 2 of 2)

FOLDOUT FRAME 1

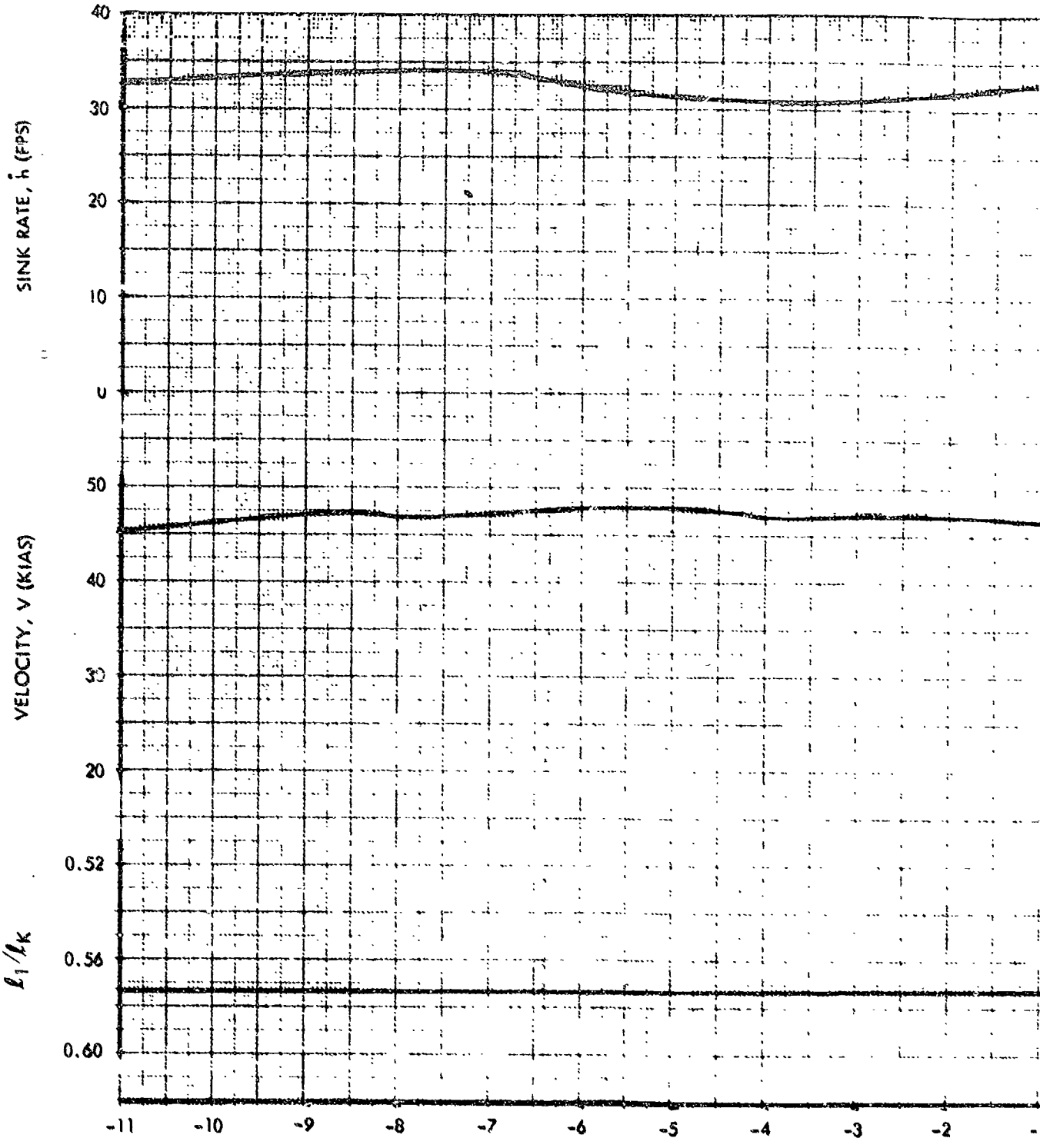

Figure 49

FOLDOUT FRAME 2

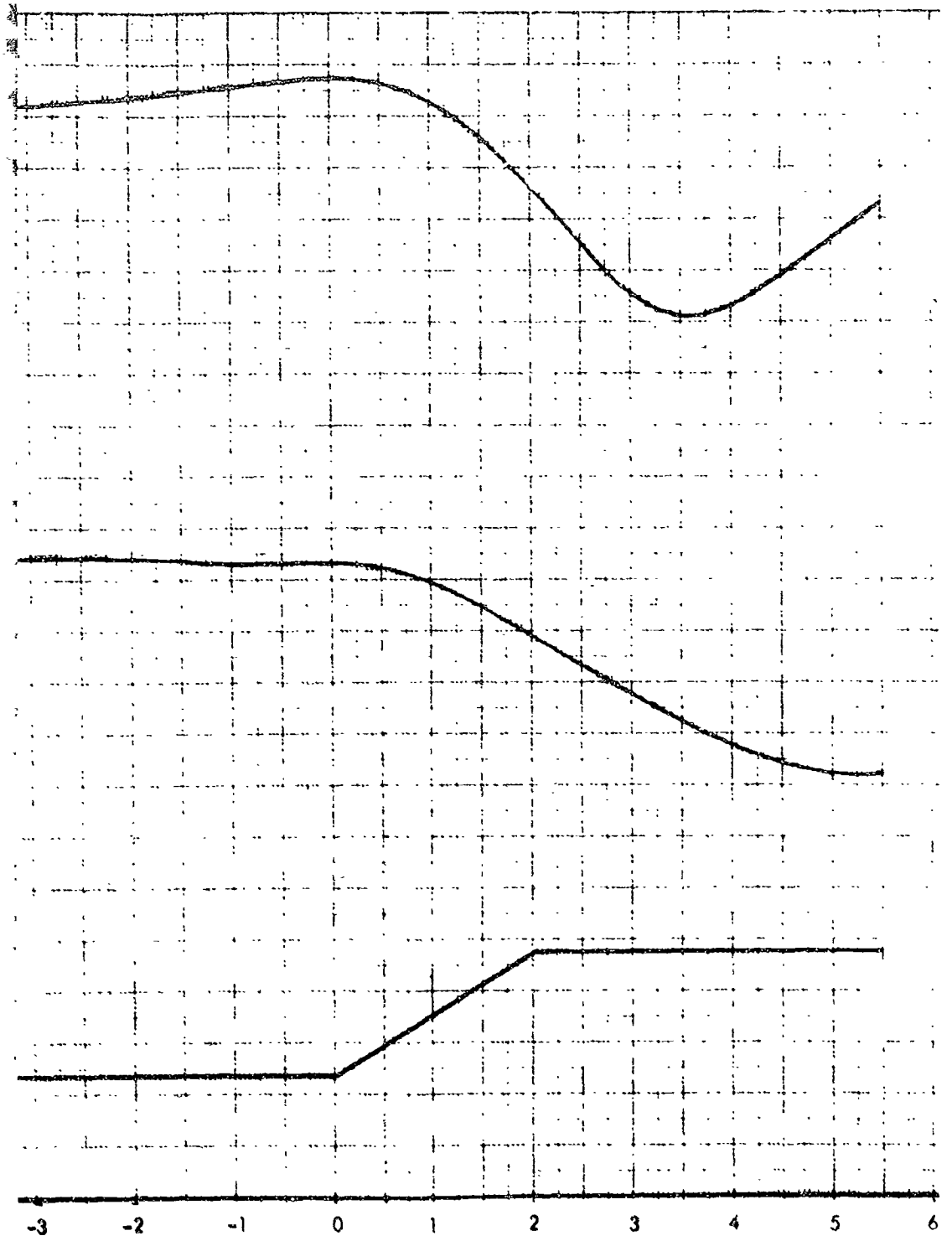

Figure 49. Flight 029 Flare at Altitude (Sheet 1 of 2)

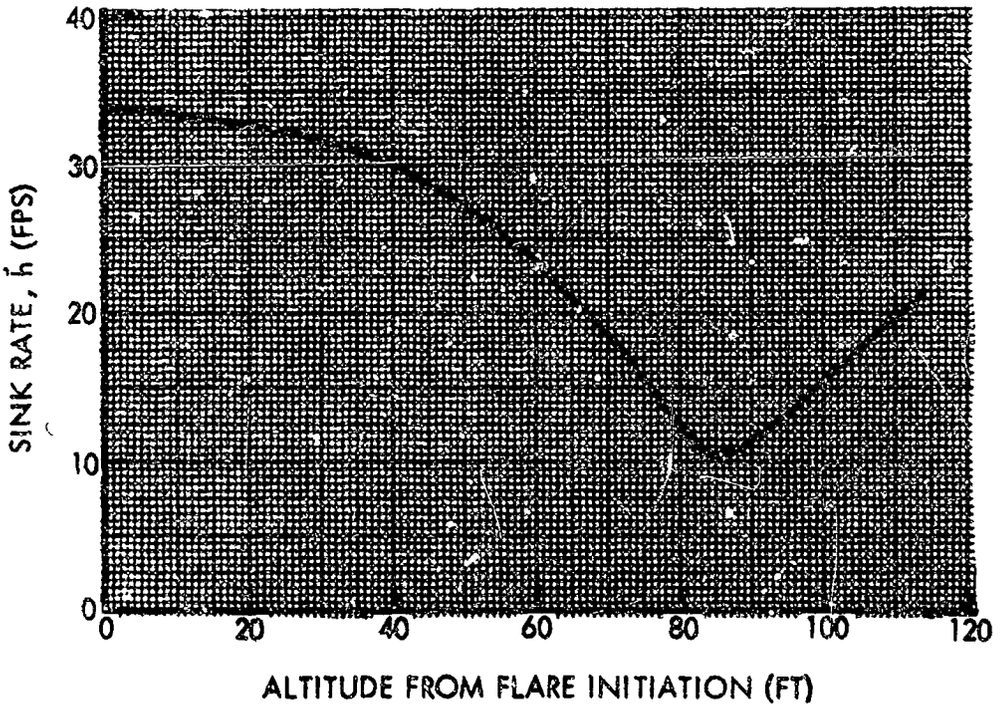

Figure 49. Flight 029 Flare at Altitude (Sheet 2 of 3)

FOLDOUT FRAME //

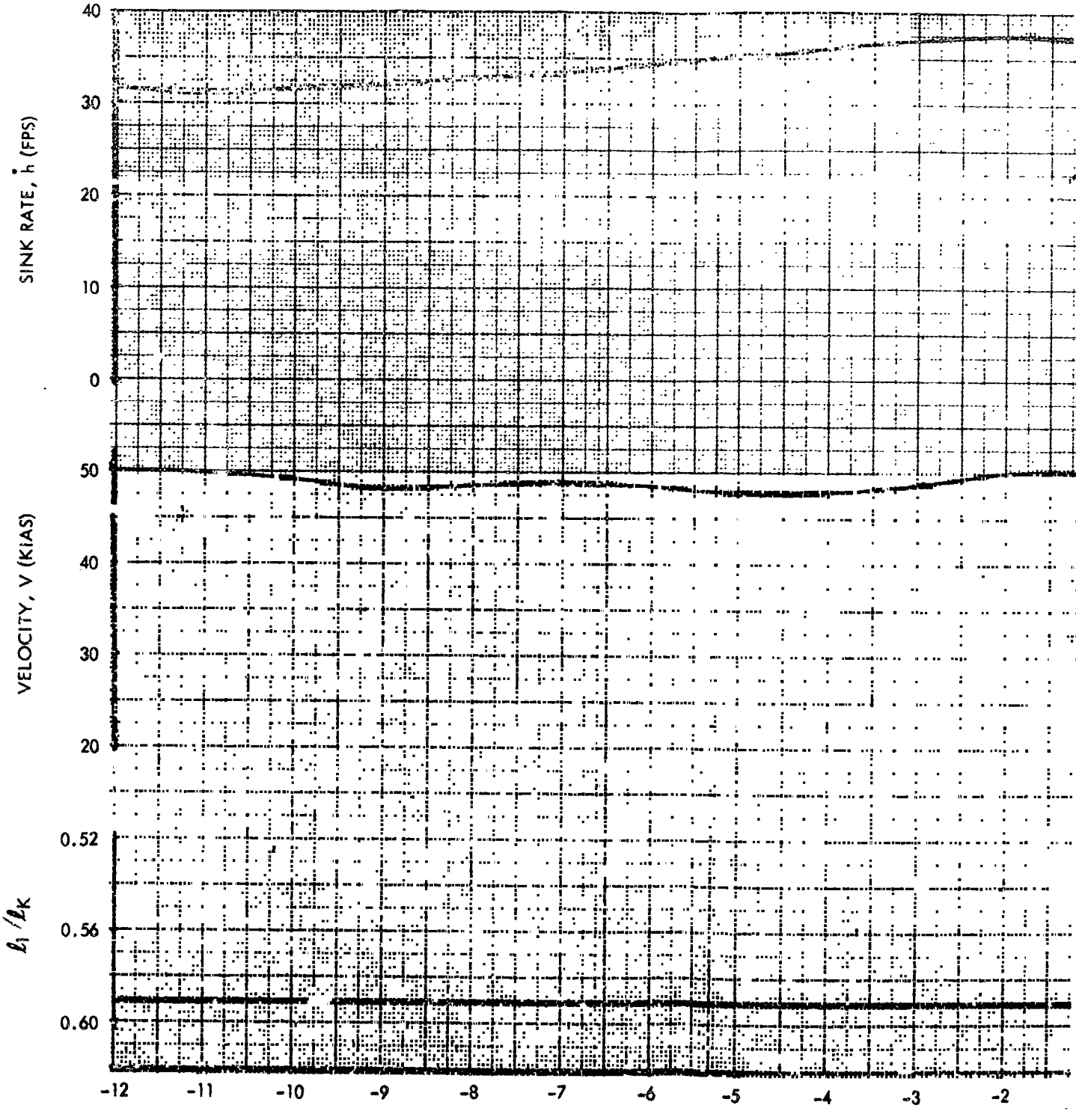

Figure

FOLDOUT FRAME 2

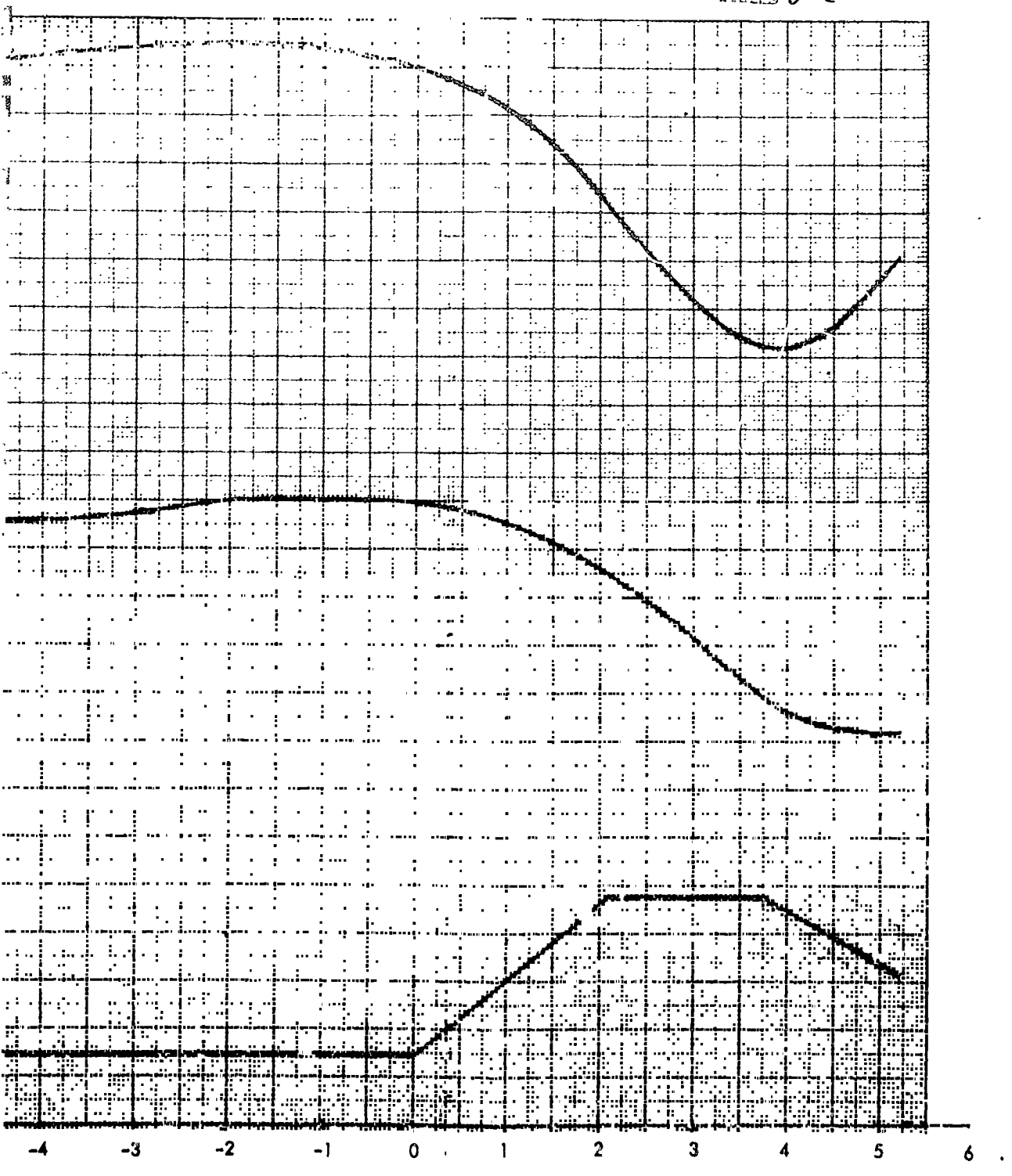

Figure 50. Flight 029 Touchdown Flare (Sheet 1 of 2)

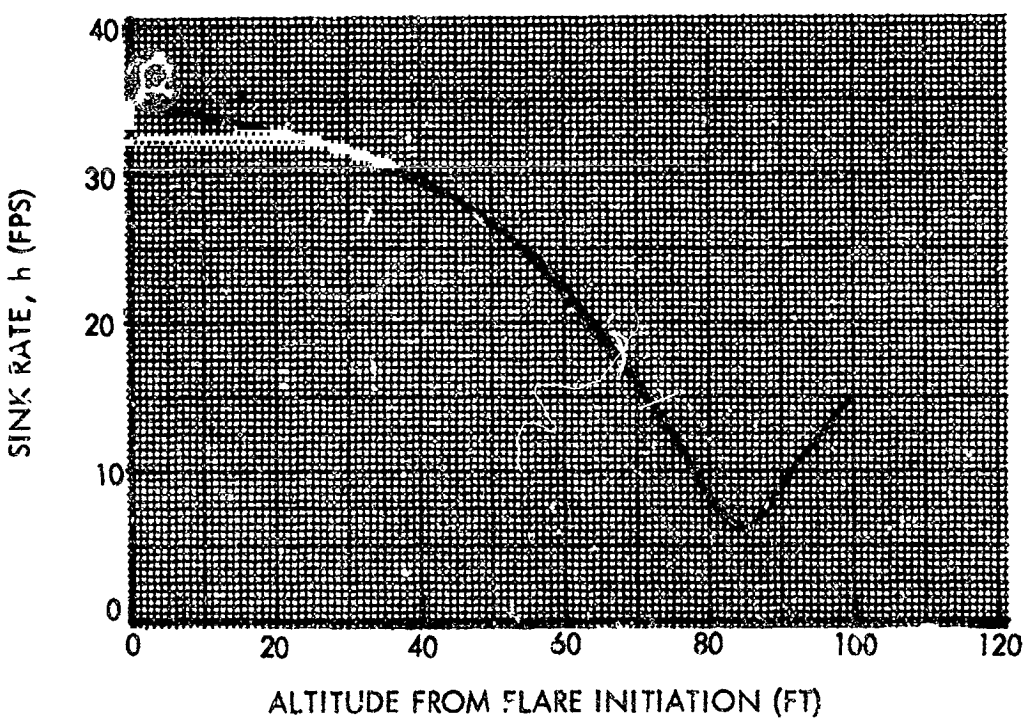

Figure 50. Flight 029 Touchdown Flare (Sheet 2 of 2)

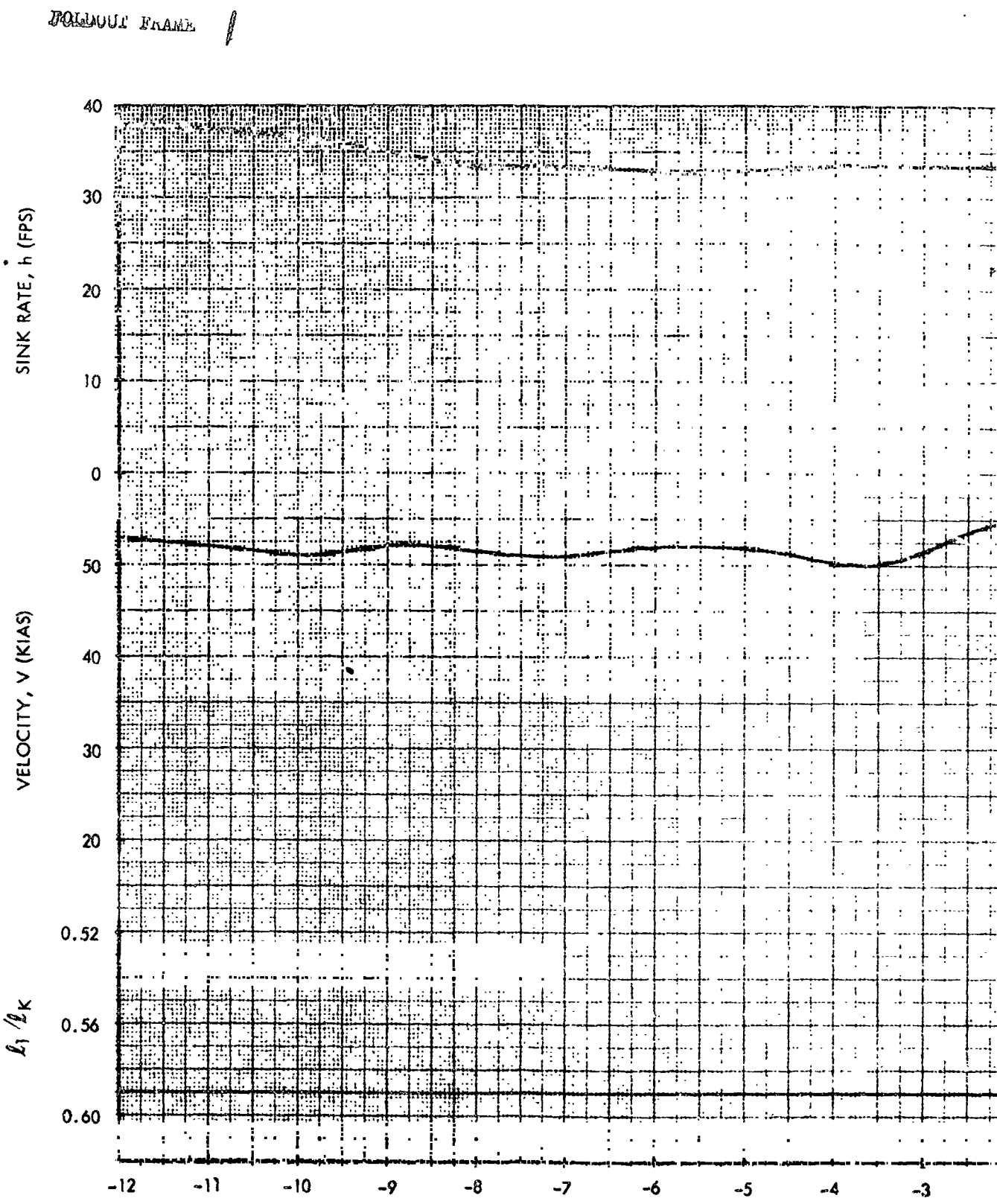

Figure 51. Fligl

FOLDOUT FRAME 2

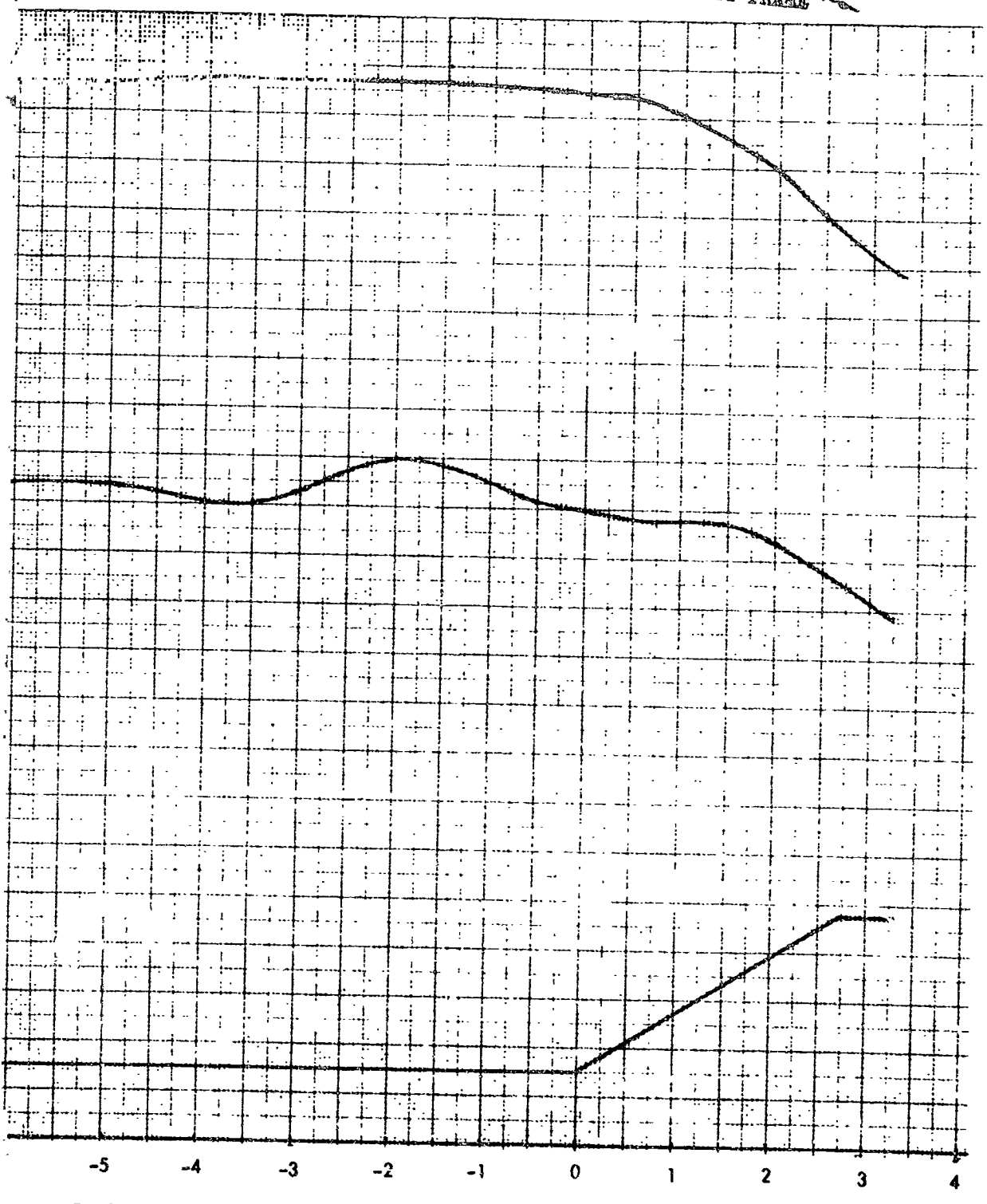

Figure 51. Flight 030 Touchdown Flare (Sheet 1 of 2)

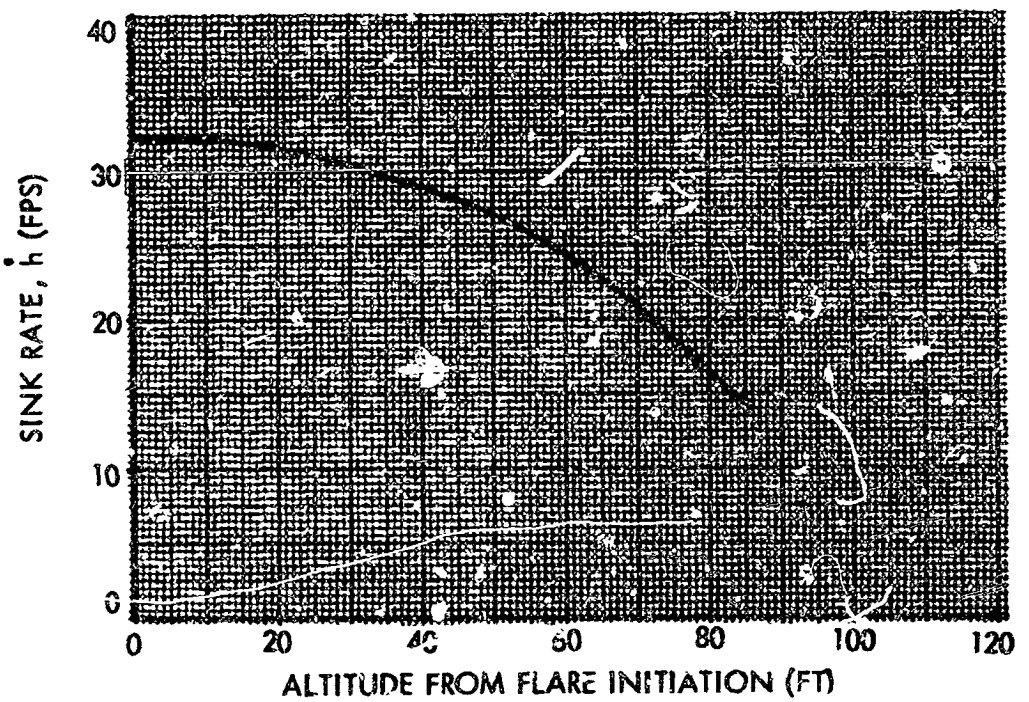

Figure 51. Flight 030 Touchdown Flare (Sheet 2 of 2)

FOLDOUT FRAME 1

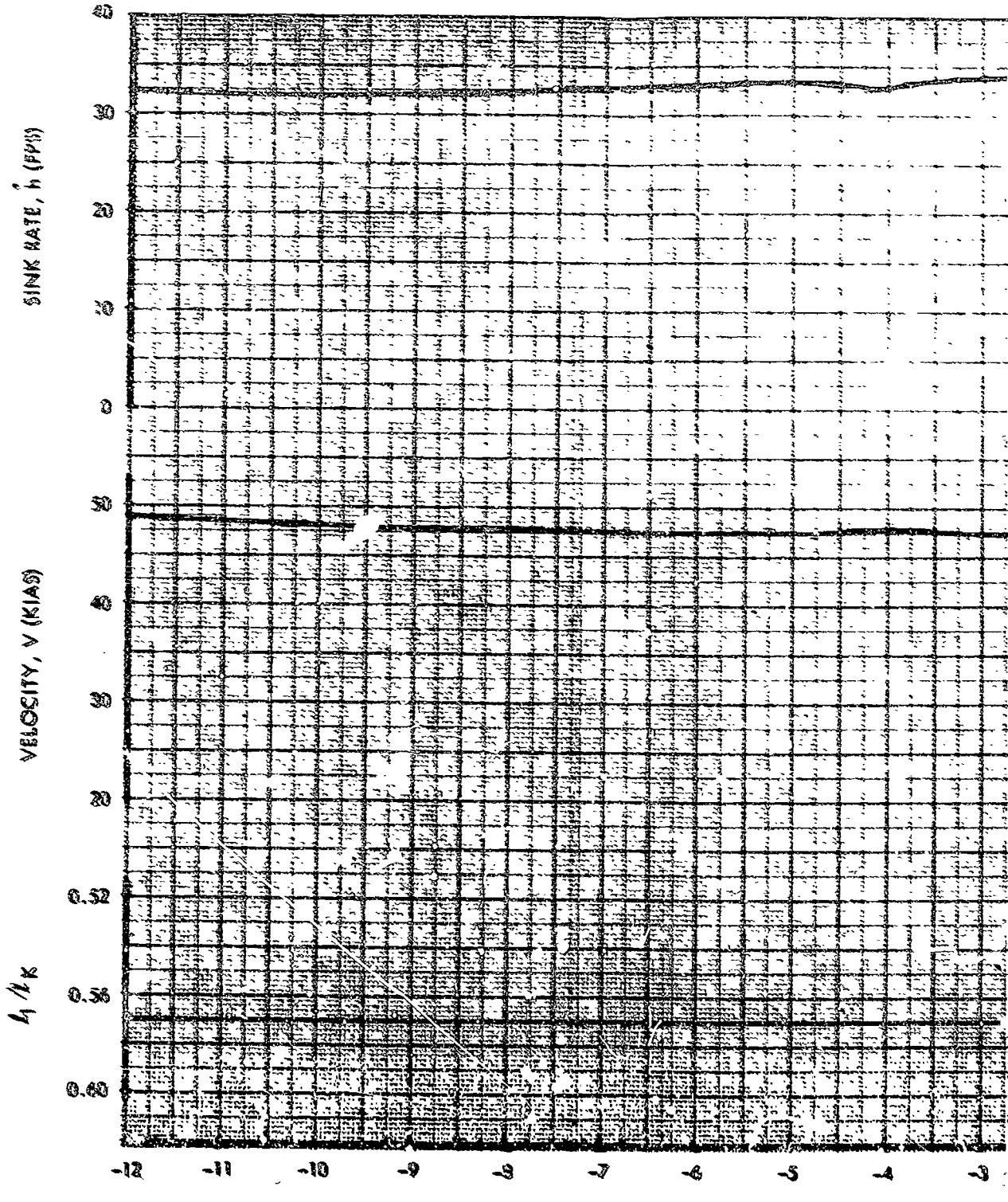

Figu

FOLDOUT FRAME 2

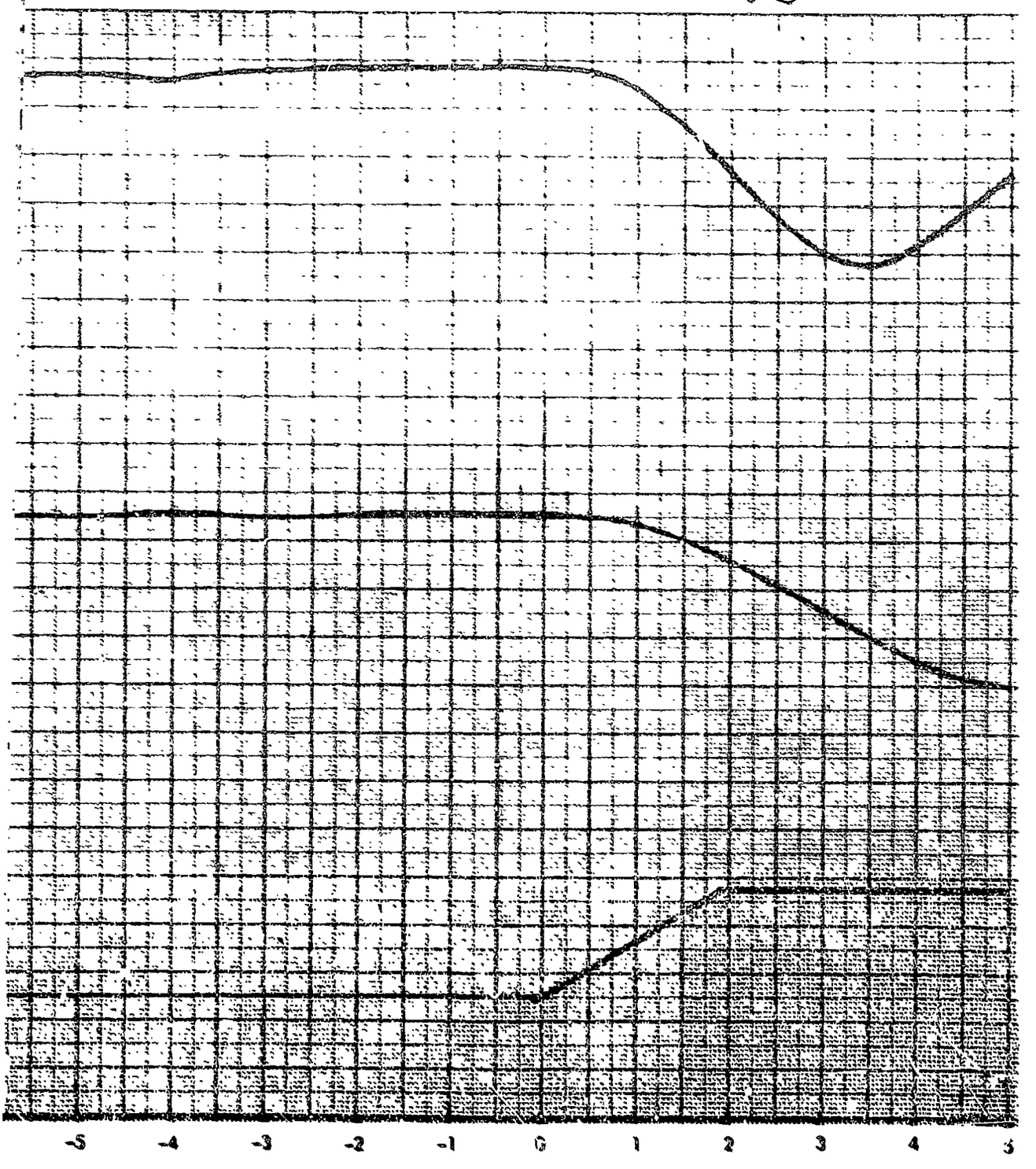

Figure 52. Flight 031 Flare at Altitude (Sheet 1 of 2)

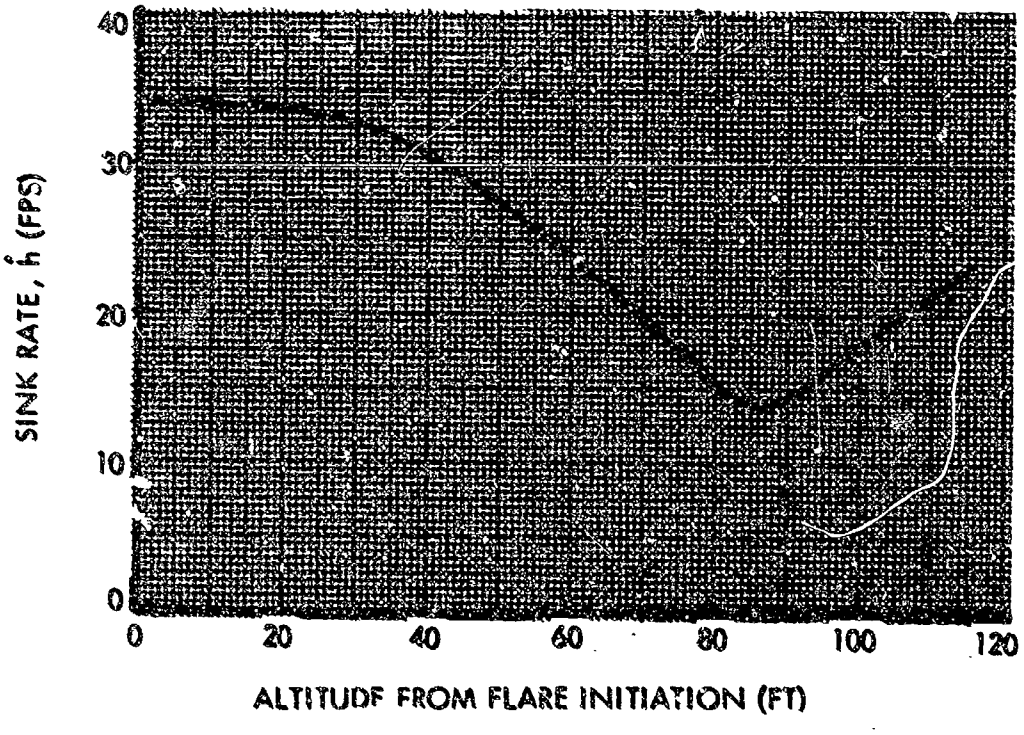

Figure 52 Flight 031 Flare at Altitude (Sheet 2 of 2)

FOLDOUT FRAME 1

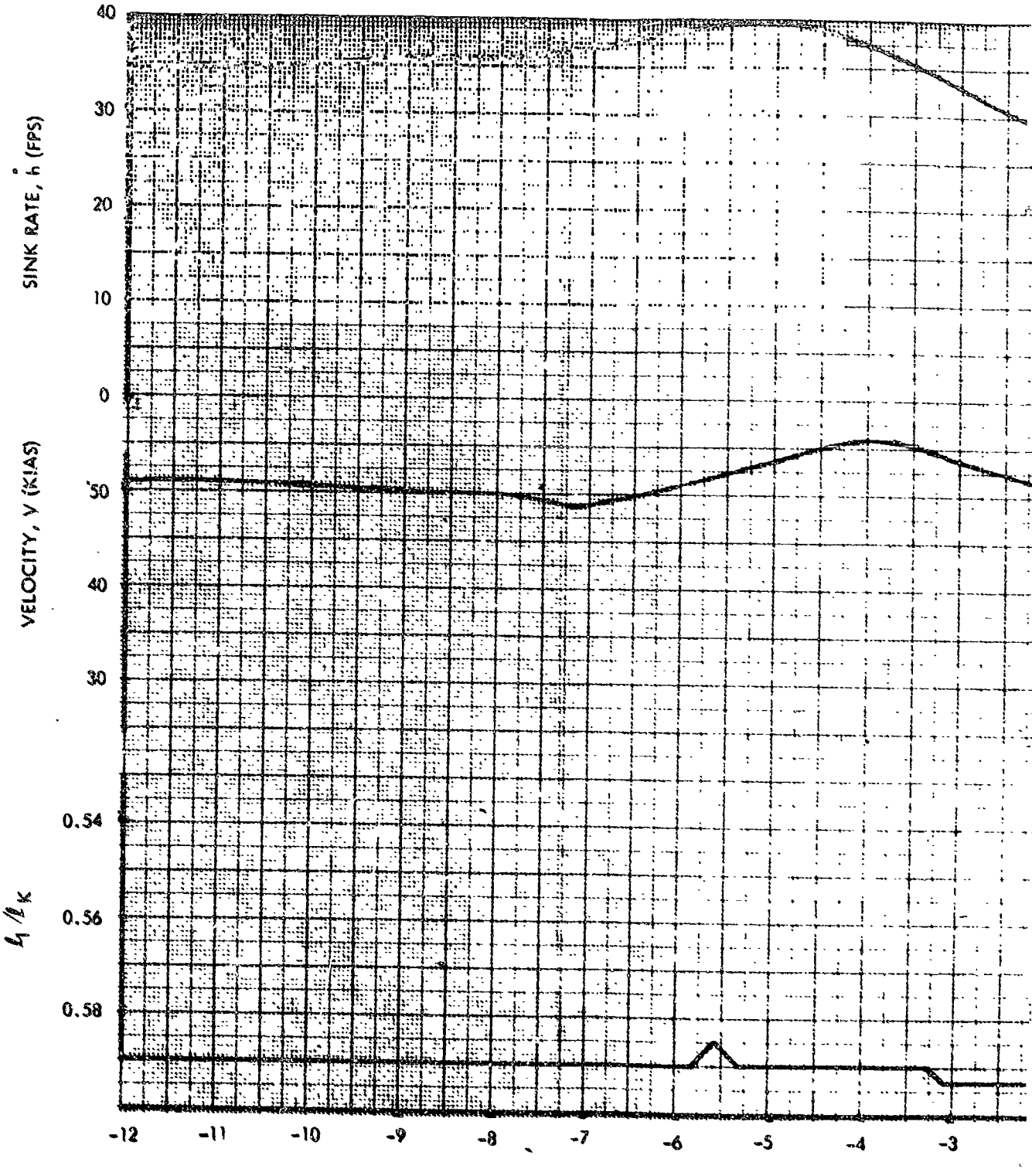

Figure 5

FOLDOUT FRAME 2

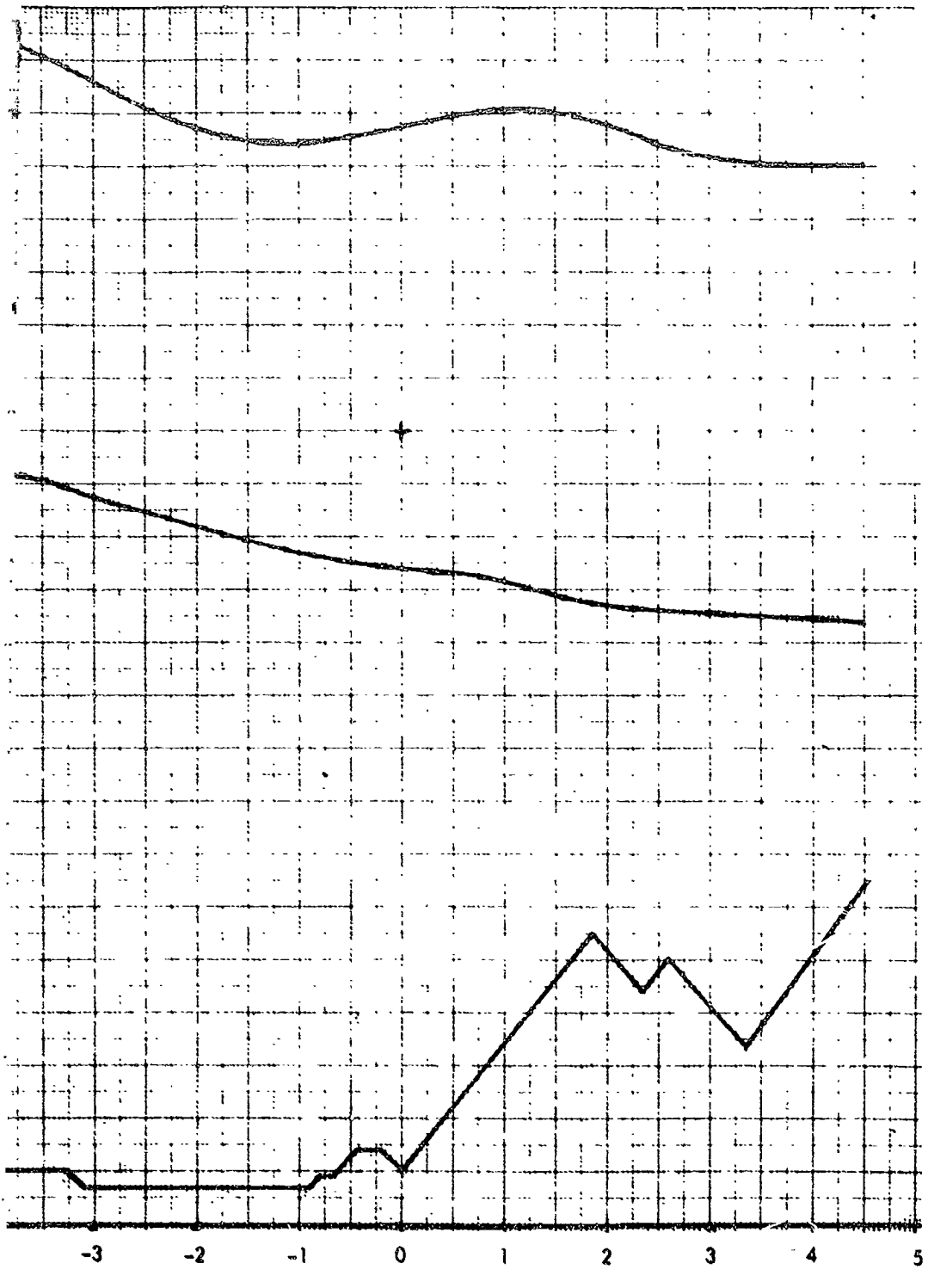

Figure 53. Flight 031 Touchdown Flare (Sheet 1 of 2)

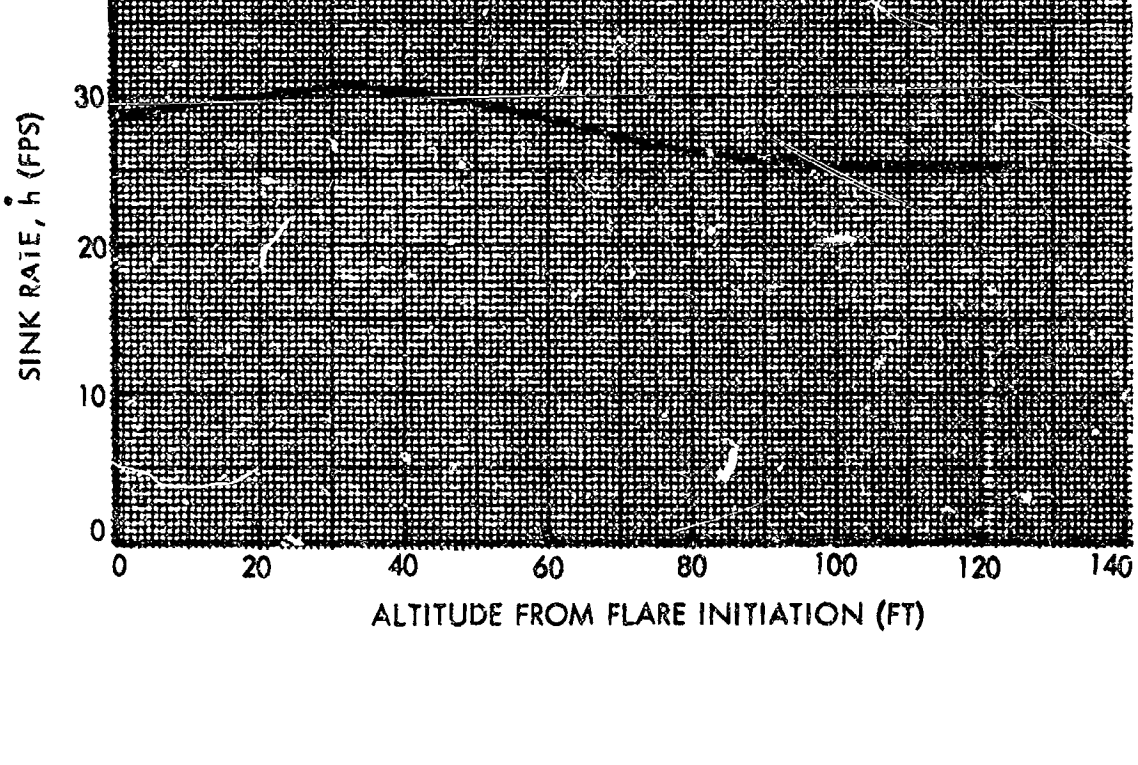

Figure 53. Flight 031 Touchdown Flare (Sheet 2 of 2)

PRECEDING PAGE BLANK NOT FILMED.

FOLDOUT FRAME 1

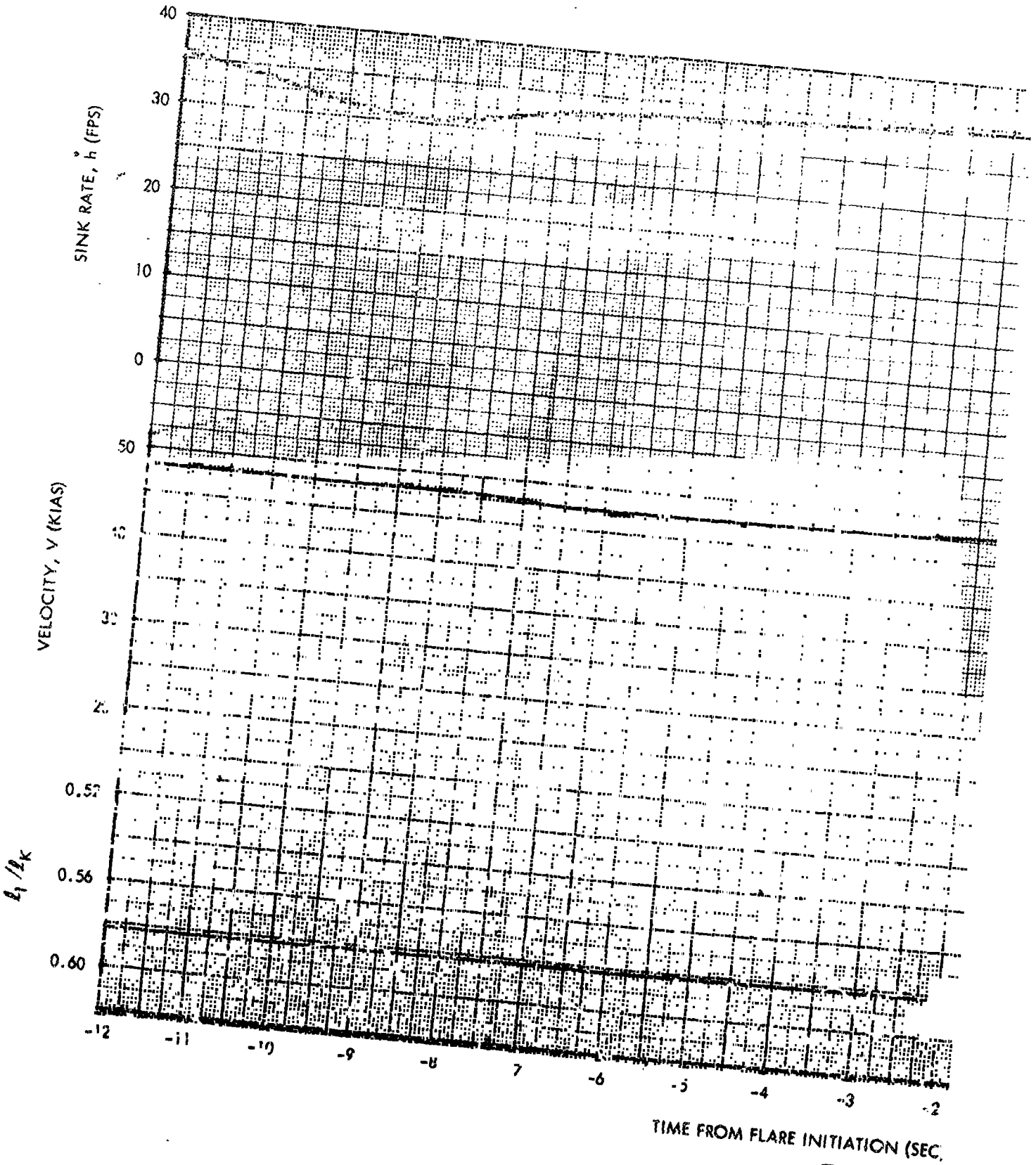

Figure 54.

FOLDOUT FRAME 2

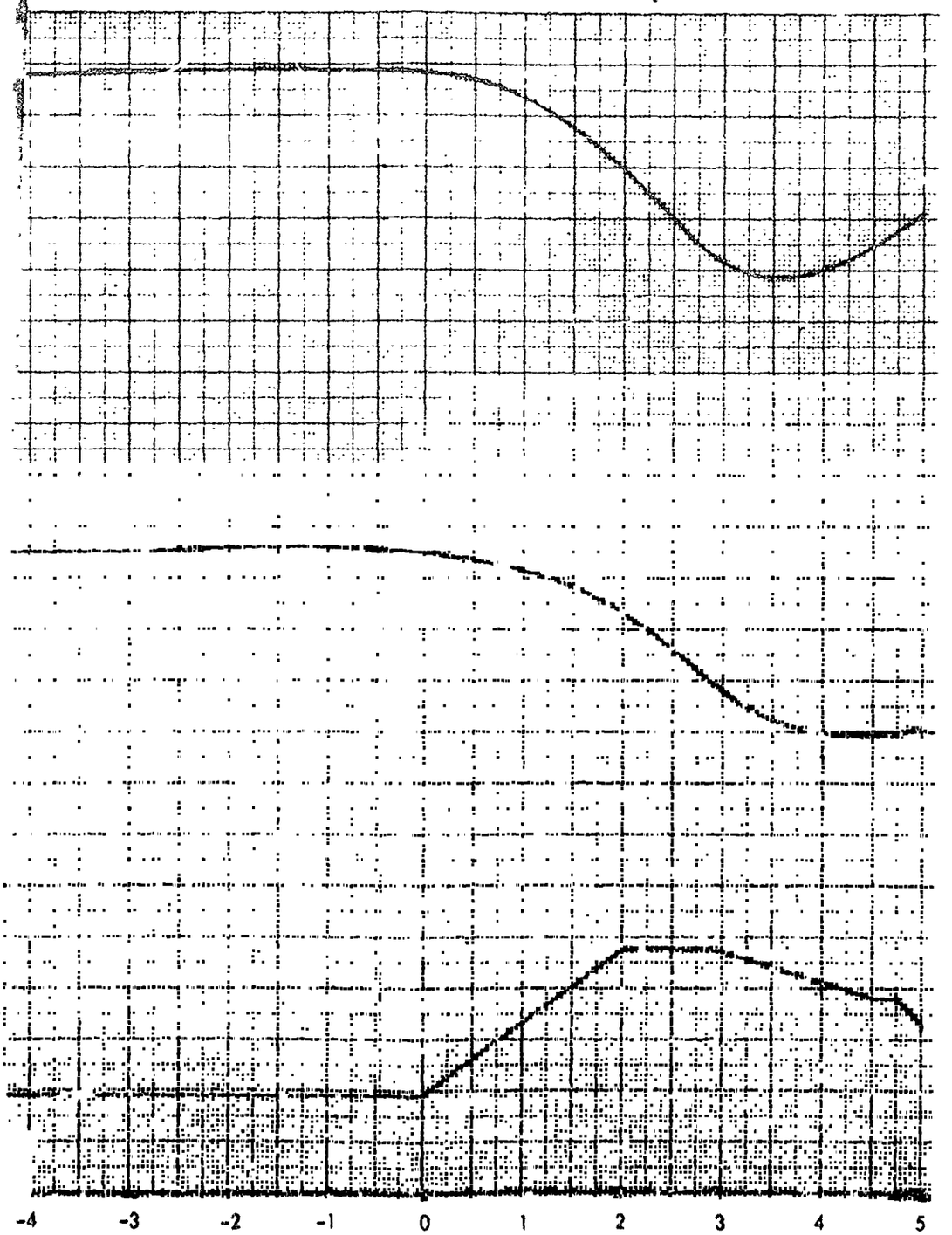

Figure 54. Flight 032 Flare at Altitude (Sheet 1 of 2)

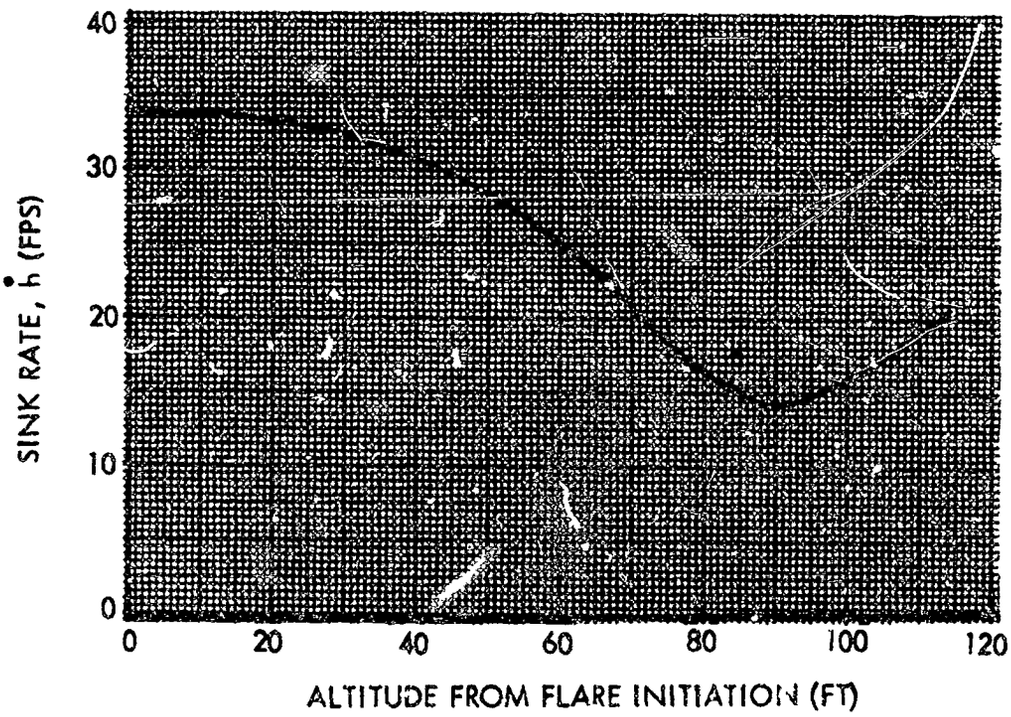

Figure 54. Flight 032 Flare at Altitude (Sheet 2 of 2)

stick motion during flare. Figure 55 presents the touchdown flare. This flare was high and had a minimum sink rate of only 12.5 ft/sec. This was due primarily to the fact that the pilot didn't hold the stick back during flare.

Flight 033

The flare at altitude in this flight was performed from $\ell_1/\ell_k = 0.59$, and is presented in Figure 56. This was done to check the ability of the pilot to flare using the trim control. The touchdown flare is presented in Figure 57. It can be seen from the time history of the sink rate and airspeed that the vehicle encountered unstable winds during preflare. These unsteady conditions resulted in a high flare.

In Figures 34 through 43 it may be noted that occasionally the sink rate is dashed. This was done to denote an estimated curve, since the sink rate amplifier had saturated and the data shifted. In these figures, the airspeed is not presented after flare initiation on touchdown flares, because the normal acceleration is on the same telemetry channel and replaces airspeed at this time.

During Phase III (Flights 026 through 033, there was an inversion layer over the lakebed for all flights. A flare was shot through this layer to observe the smoke and determine wind direction in the layer. The two days this was done the smoke took the form of a "Z"; the general effect of this inversion layer was high flares. A plot of initial velocity (knots) divided by initial sink rate ft/sec versus Δh from flare initiation to minimum sink rate is presented in Figure 58. This plot presents all flares that were performed from a preflare $\ell_1/\ell_k = 0.59$. It appears from this plot that the flare performance of vehicle 002 in Phase III is comparable to that of both vehicles during Phase II. Vehicle 001 in Phase III, which had a pitch line rate 3 ft/sec faster than vehicle 2, appears to flare slightly faster, approximately 5 to 10 feet.

A plot of percent of touchdown flares below any given touchdown sink rate versus sink rate is plotted in Figure 59. It can be seen that approximately 50 percent of the flights were below the gear limit of 17.5 ft/sec. The slope of this curve would have been considerably steeper had the weather conditions been ideal.

All Phase II flares are plotted in Figure 60. Phase III touchdown and at altitude flares are presented in Figures 61 and 62, respectively. These composite plots were made for easy comparison of all flare data in the $h - \Delta h$ phase.

FOLDOUT FRAME 1

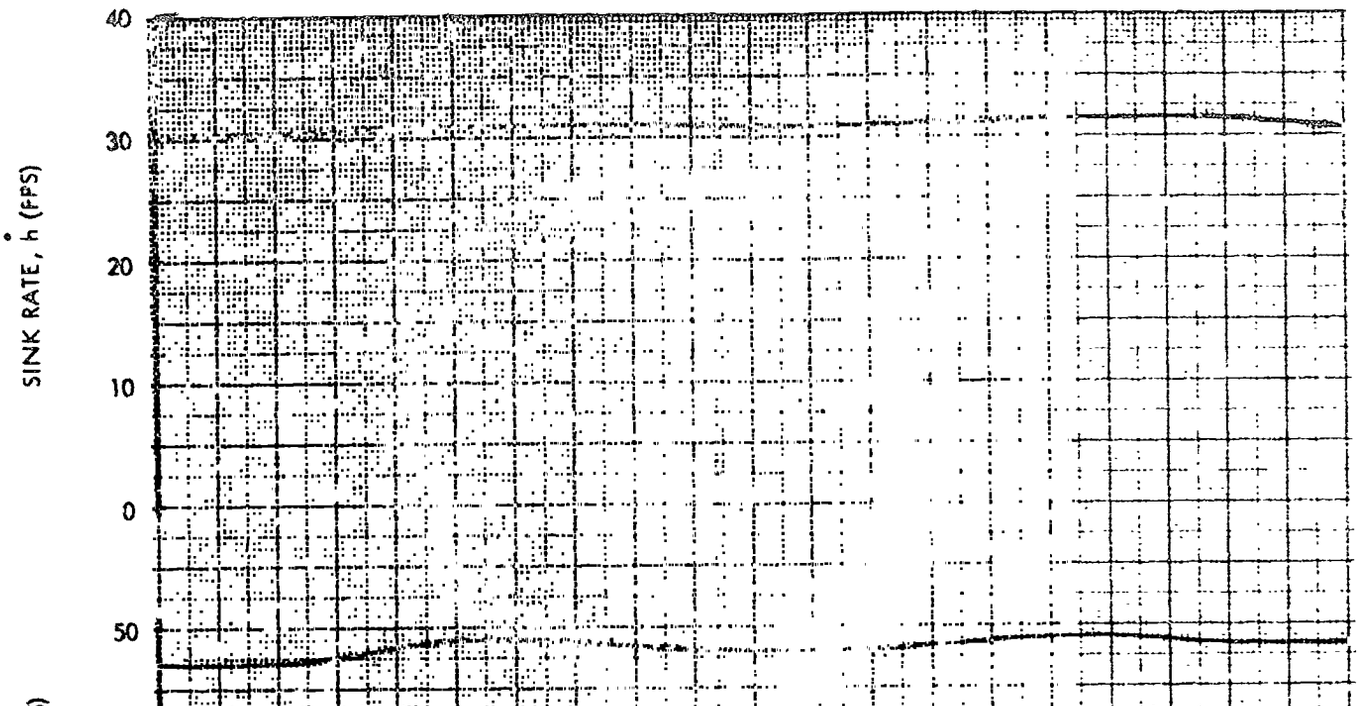

Figure 55.

FOLDOUT FRAME 2

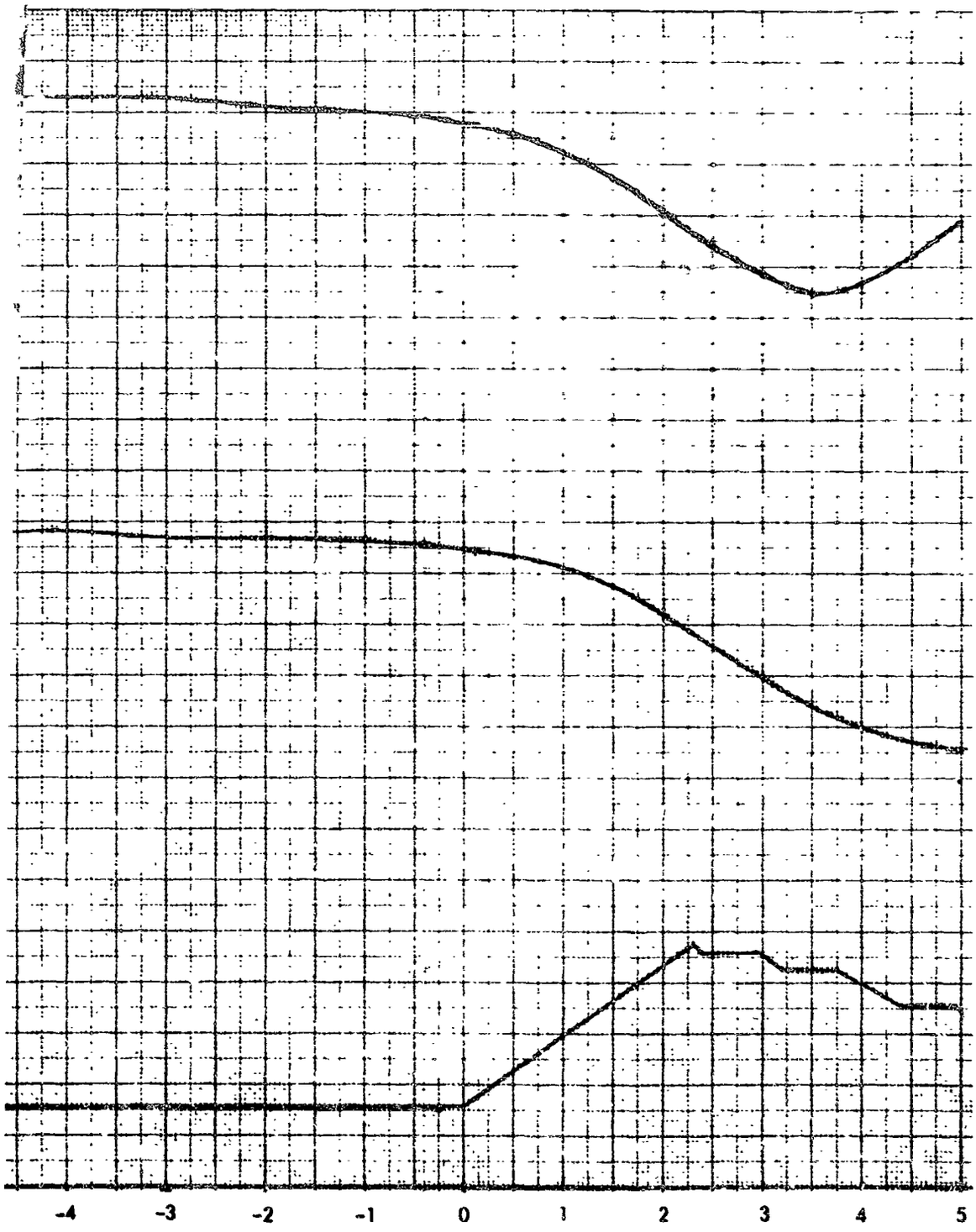

FROM FLARE INITIATION (SEC)

Figure 55. Flight 032 Touchdown Flare (Sheet 1 of 2)

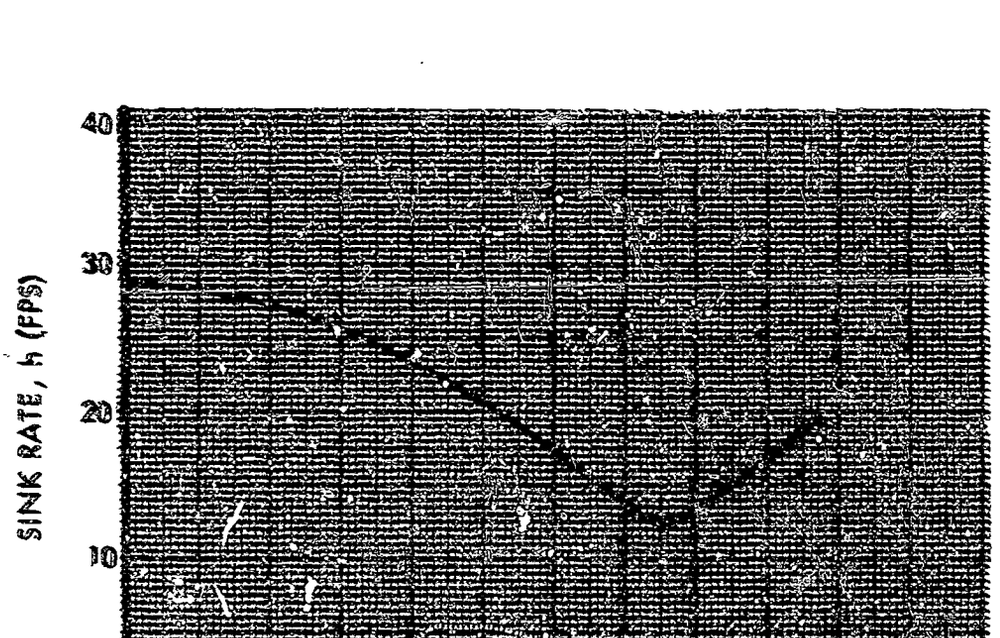

Figure 55. Flight 032 Touchdown Flare (Sheet 2 of 2)

...CEDING PAGE BLANK NOT FILMED.

FALLOUT Frame 1

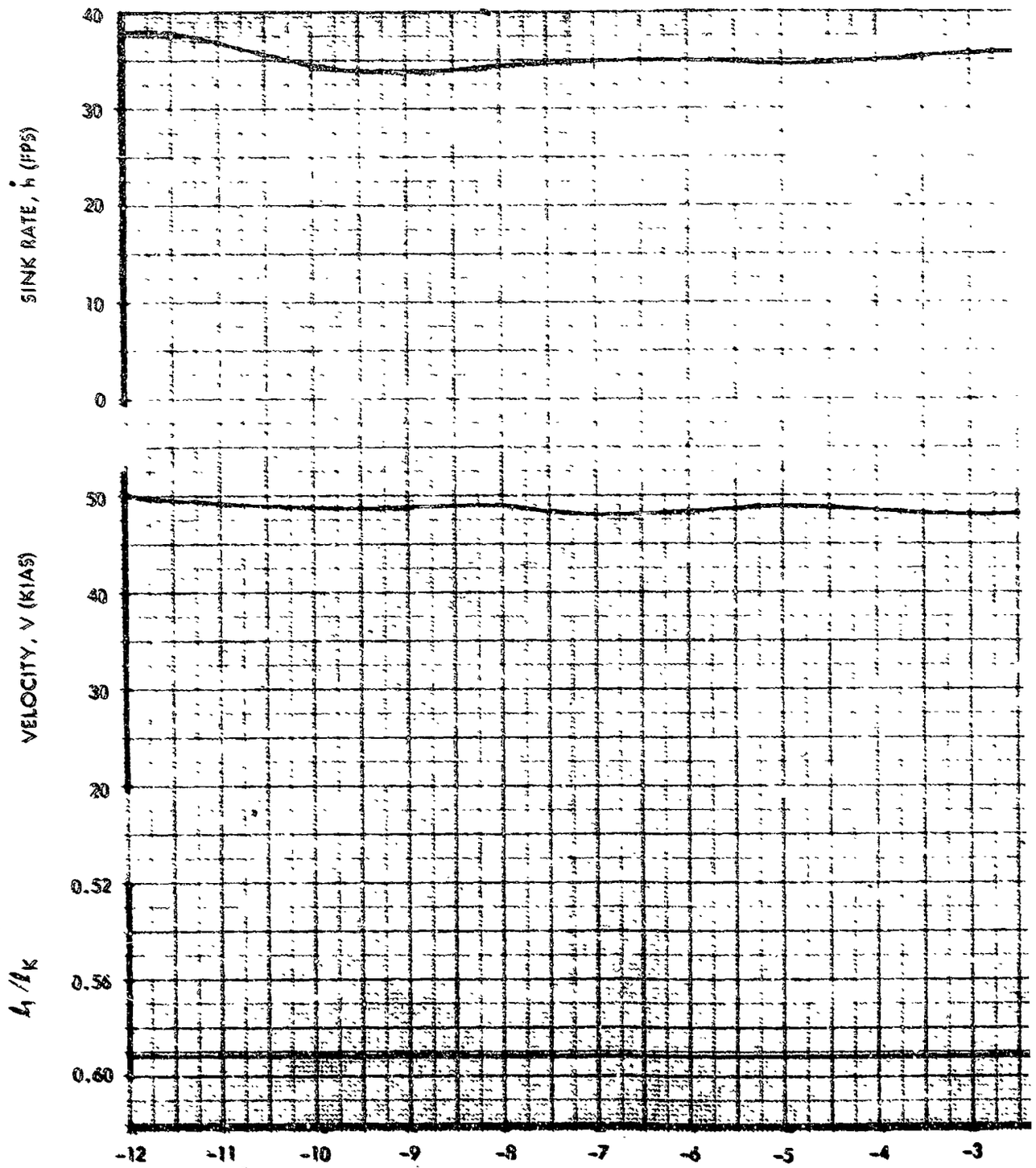

Figure

FOLDOUT FRAME 2

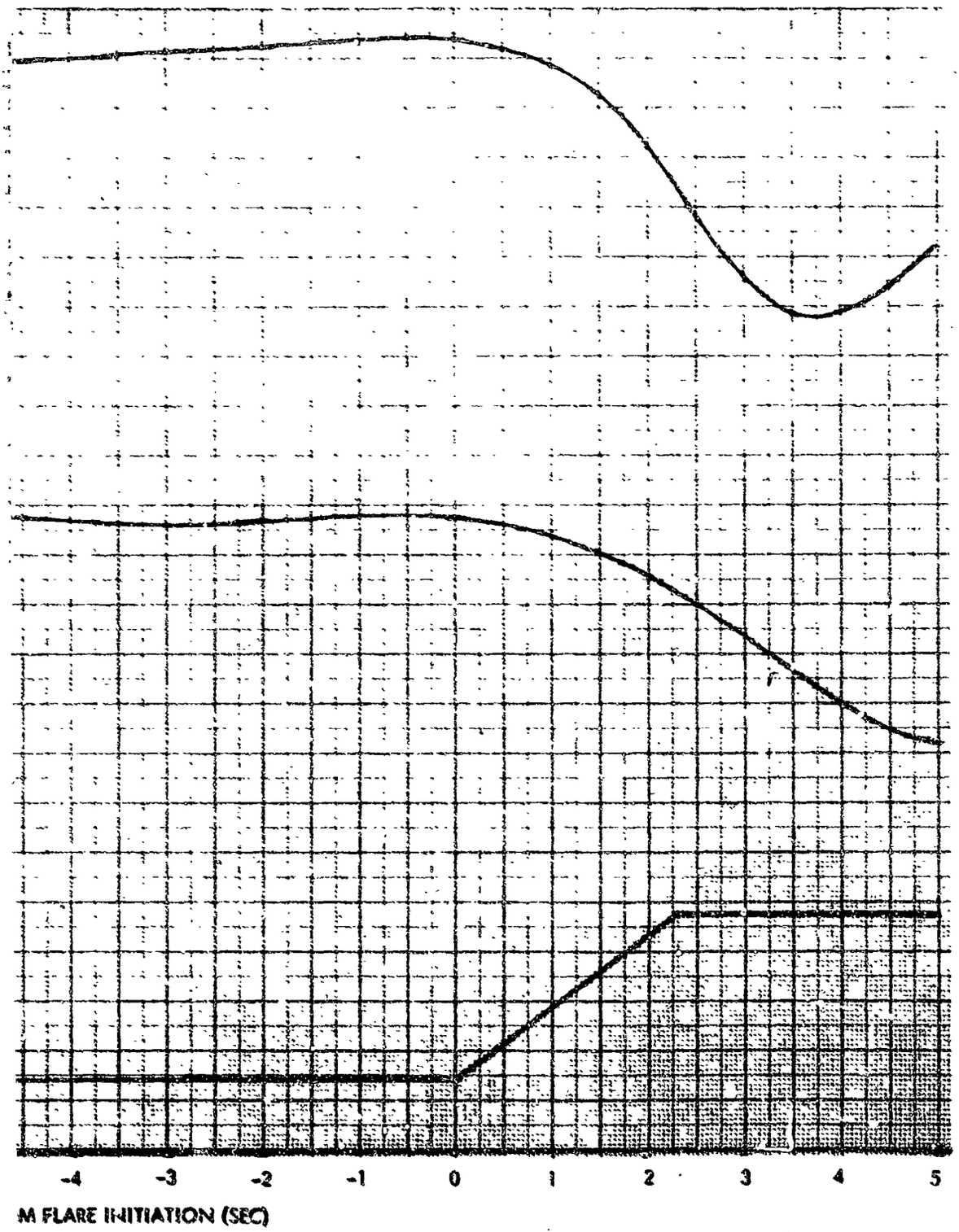

Figure 56. Flight 033 Flare at Altitude (Sheet 1 of 2)

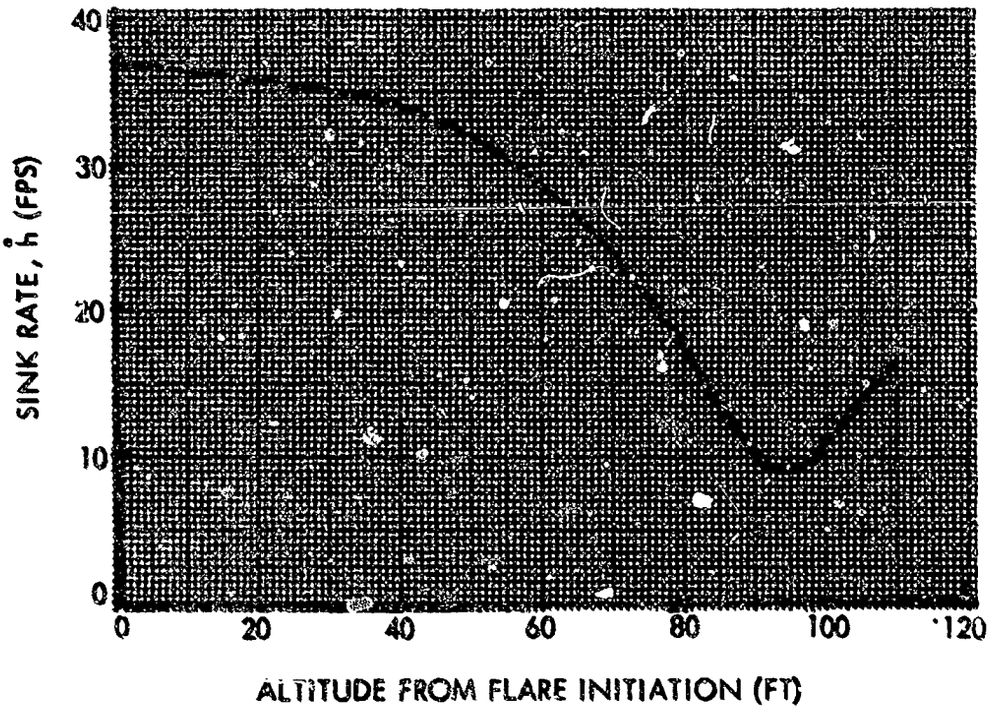

Figure 56. Flight 033 Flare at Altitude (Sheet 2 of 2)

FOLDOUT FRAME 1

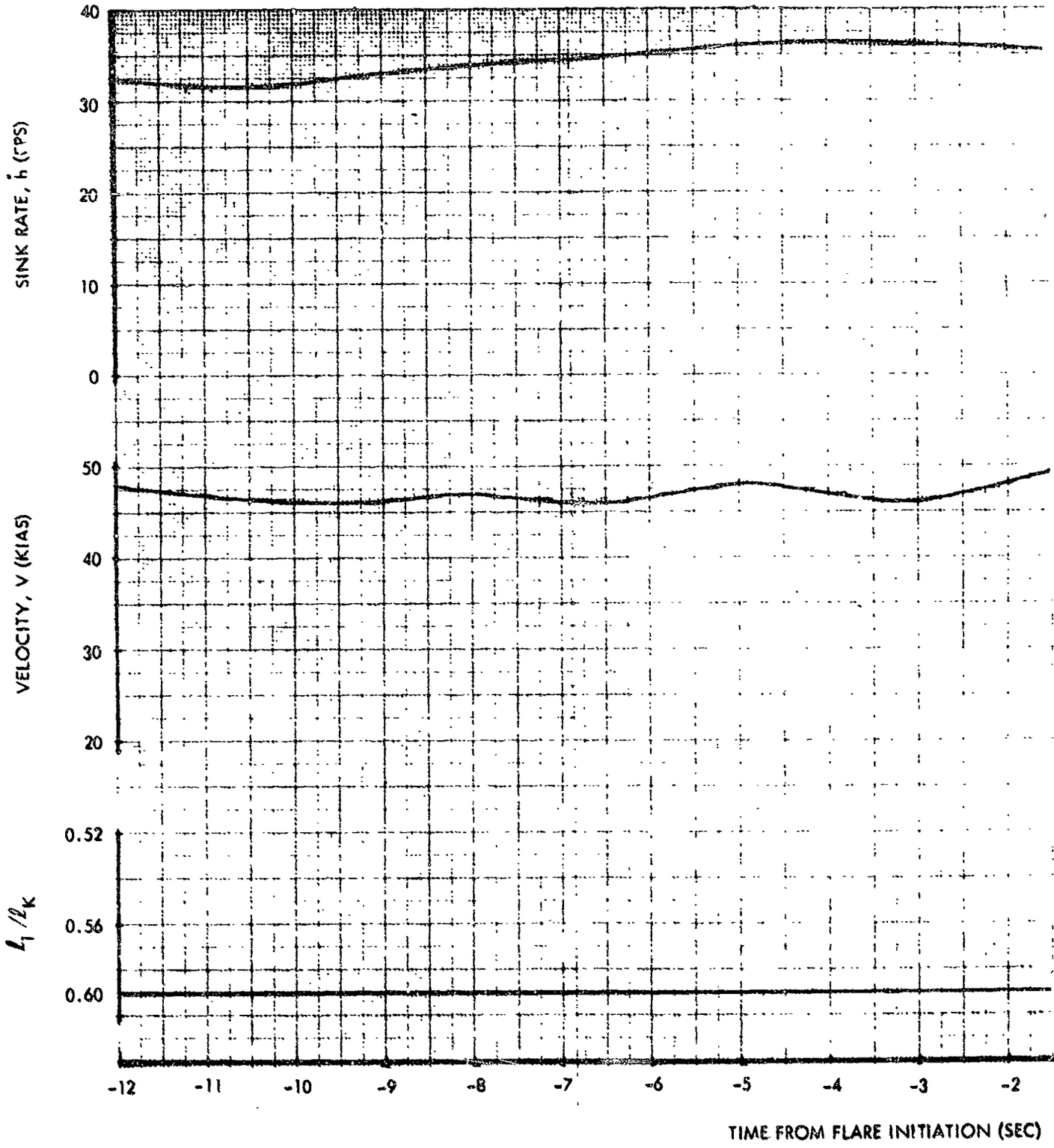

Figure 57.

FOLDOUT FRAME 2

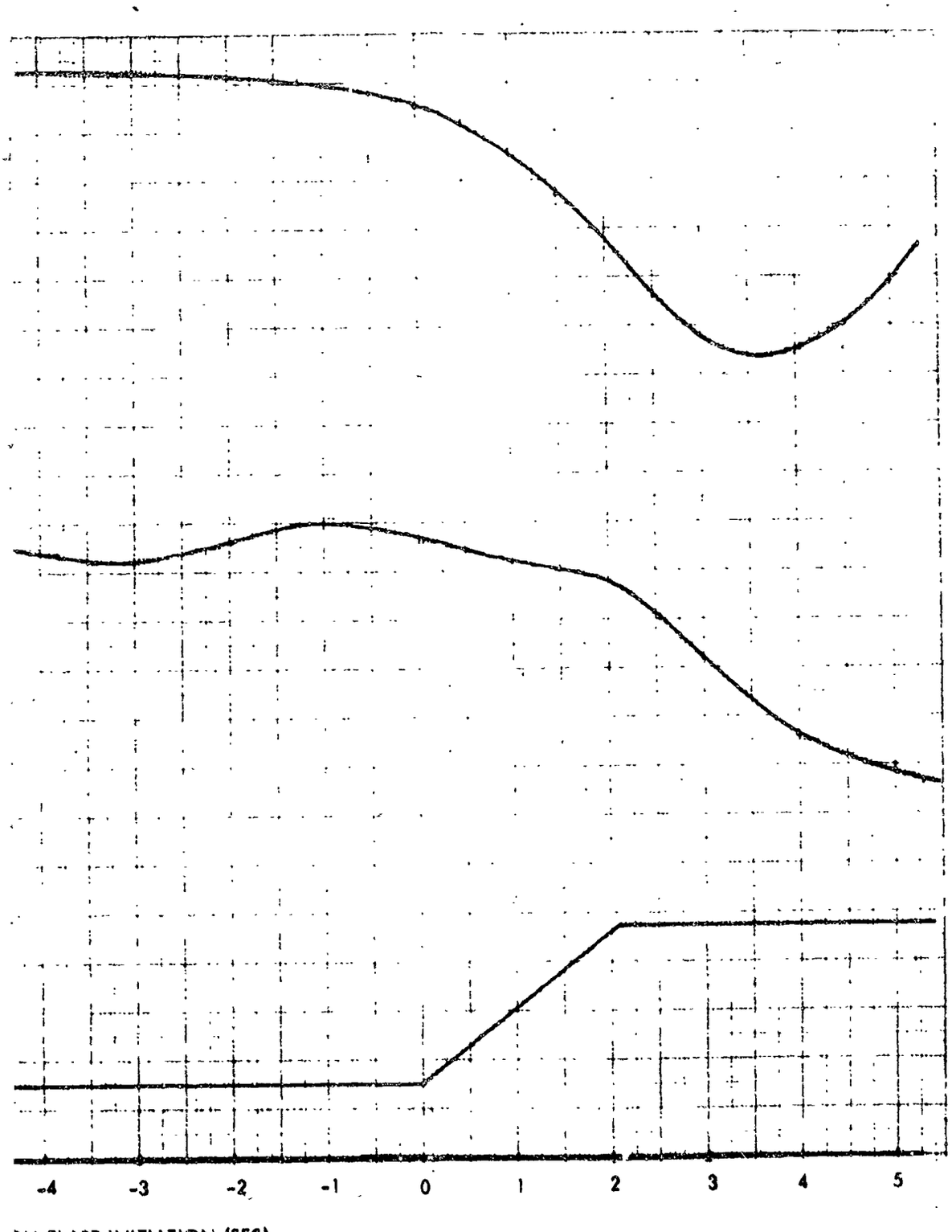

Figure 57. Flight 033 Touchdown Flare (Sheet 1 of 2)

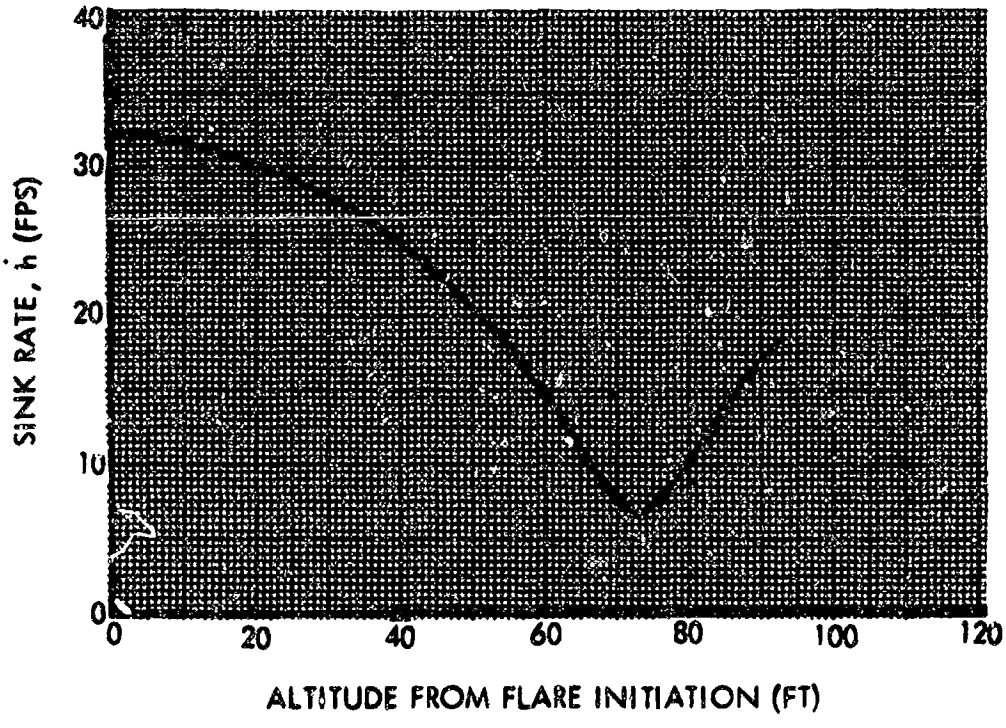

Figure 57. Flight 033 Touchdown Flare (Sheet 2 of 2)

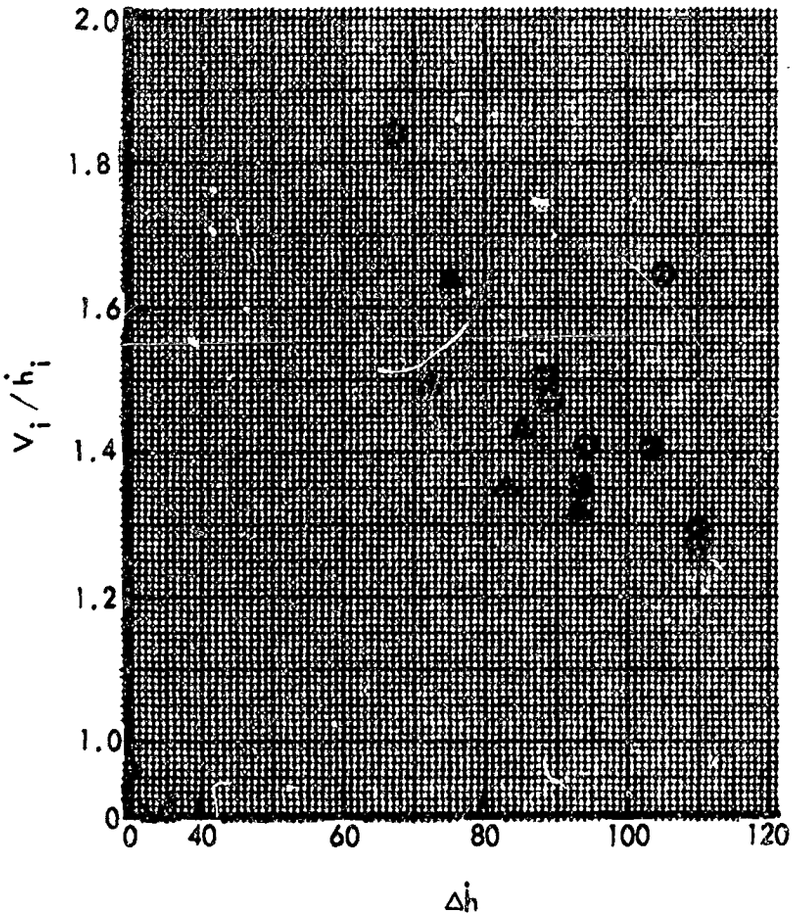

Figure 58. Effect of Preflare Speed and Sink Rate on Flare Altitude

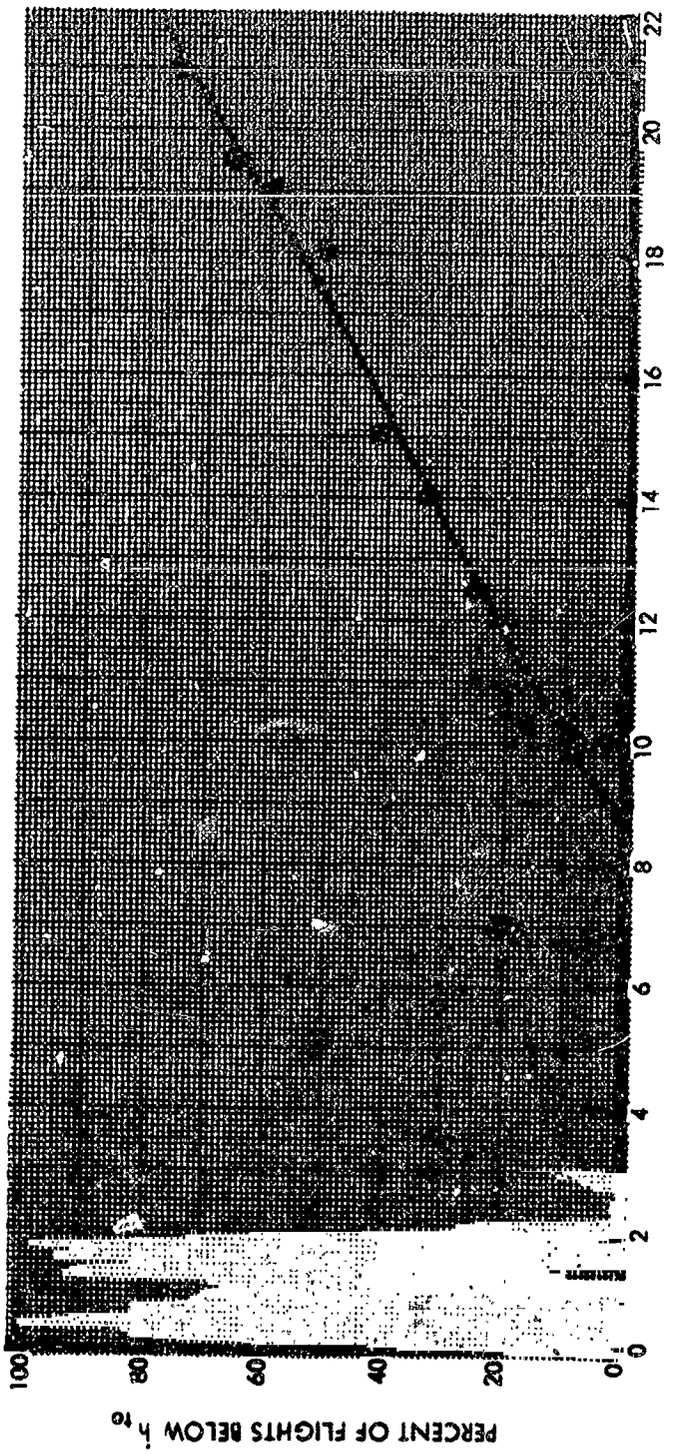

Figure 59. Evaluation of Flare Capability

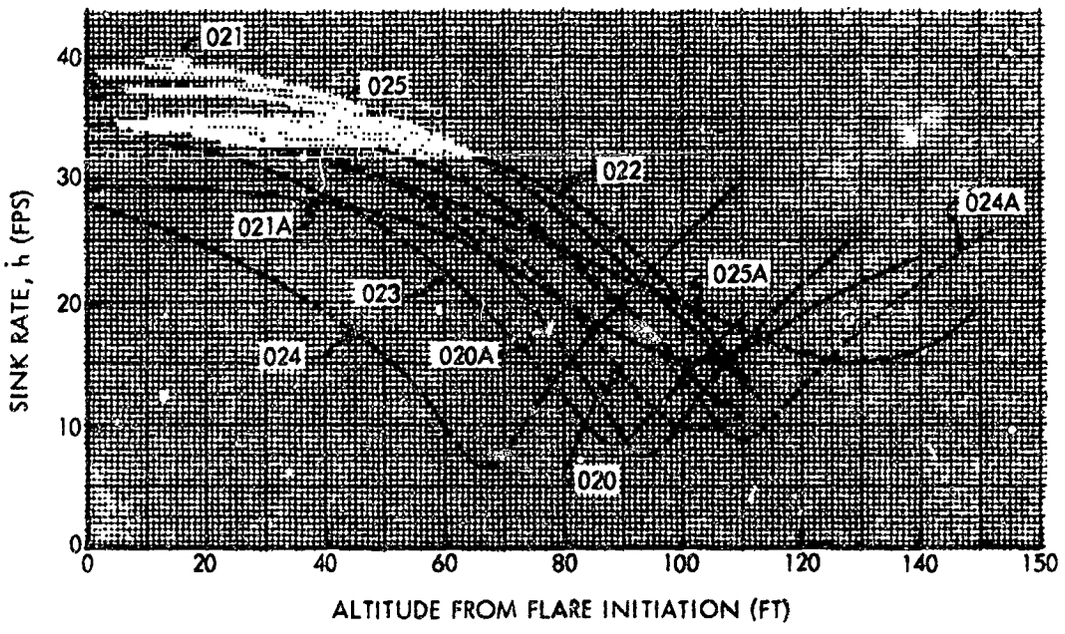

Figure 60. Composite of Phase II Flares

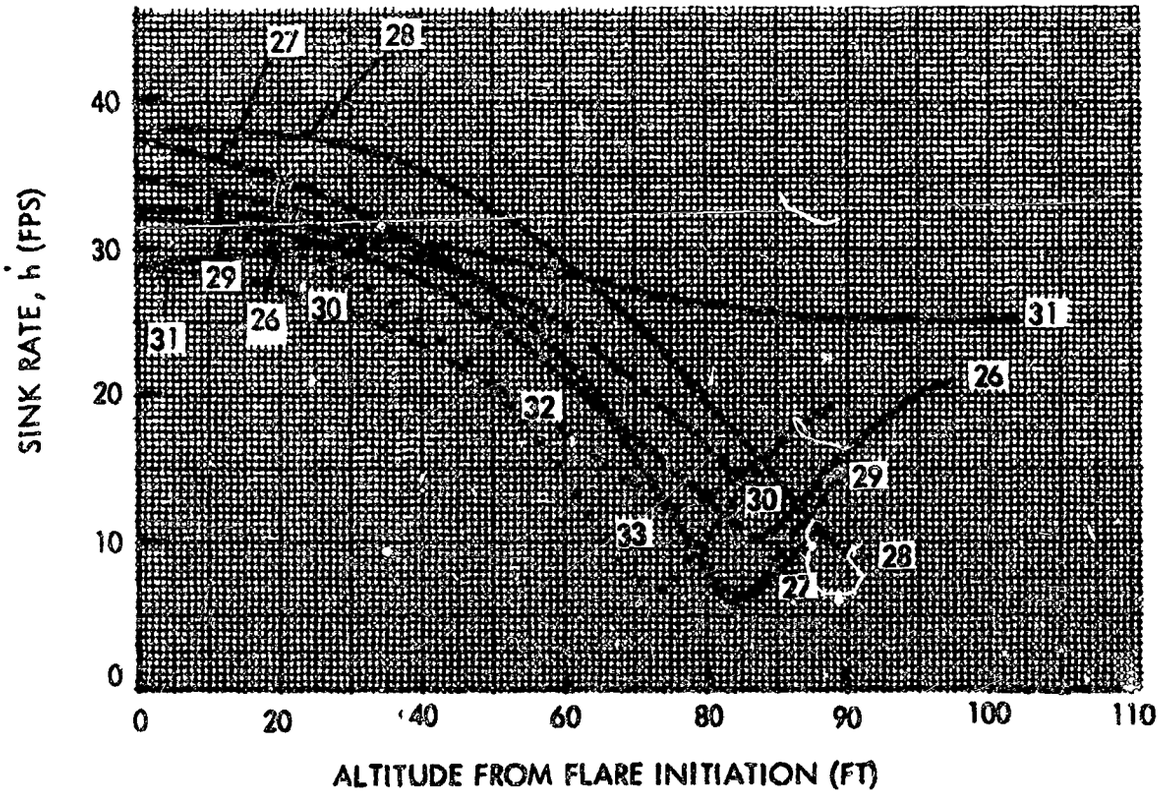

Figure 61. Composite of Phase III Touchdown Flares

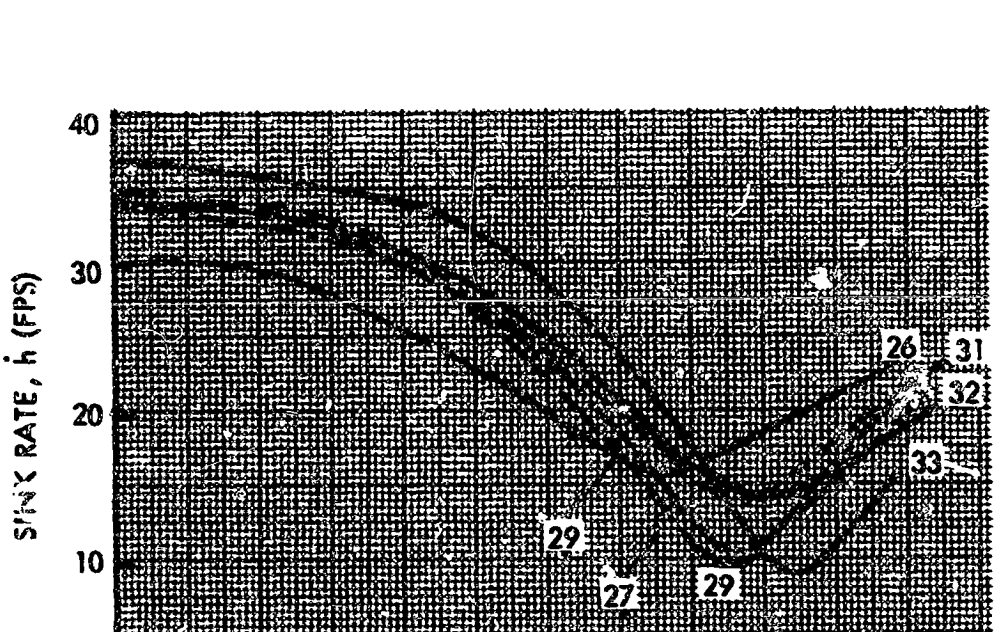

Figure 62. Composite of Phase III Flares at Altitude

PROGRAM PILOTS' REVIEW

The twelve manned flights of the Paraglider flight test program were flown to demonstrate the feasibility of the Paraglider concept. These flights were flown by the two program pilots, who obtained both qualitative and quantitative data to complete a basic evaluation of system stability and control, flight performance, landing capability, and navigation. The scope of the maneuvers performed during the flights encompassed the full range of both lateral and longitudinal control, utilizing both the Gemini hand controller and the trim controls. Maneuvers included stabilized straight and turning flight, inflight flares, reversals, and landings.

The system proved to have strong positive stability about all axes with good damping, returning to trim rapidly from turbulence created by the chase aircraft, and when released from the tow helicopter, in a strong lateral directional oscillation. Steep turns (40-degree bank) revealed no wind-up tendencies; nor was there any pitch-up or tuck revealed over the pitch control range. Stalls or in-flight flares initiated from neutral trim (maximum L/D) to full nose-down trim exhibited positive recovery in every instance. A lateral trim shift with pitch change, evident throughout the program, resulted from indeterminate assymetry of the rubberized wing.

Control response in both pitch and roll is positive, smooth, and immediate, and the system exhibits no perceptible adverse yaw or sideslip. The system, wing, cables, and capsule, flies as a rigid body with no apparent cable slackening during in-flight maneuvers, including steep turns, stalls, and recoveries.

Adequate lateral and pitch control capability existed for all maneuvers flown. Control rates laterally were satisfactory at seven in./sec, though safely flown as low as four in./sec on one flight. Pitch control rates of seven, nine, and twelve in./sec were flown with the higher rates being preferred. Control inputs can be effected with either the Gemini hand controller or the trim controls which are preferable for sustained control input and provide smoother control application. The Gemini hand controller is adequate; however, due to higher than optimum breakout forces of this unit there was a tendency to over control. The system demonstrates excellent maneuverability in flight and can be banked to forty degrees for tight and rapid turns of a radius less than two hundred fifty feet.

The landing of the system is undoubtedly the maneuver requiring technique and skill. The system was flown and landed twelve times during the

test program and demonstrated an expected susceptibility to wind shears and gusts with its wing loading of eight pounds per square foot. The landings made were both above and below the landing specification of 17-1/2 ft/sec, being as low as 10 and as high as 26 ft/sec.

The critical point on landing is flare initiation. Ideally, to accomplish a successful landing below the gear limit of 17-1/2 ft/sec, this point must be correctly determined within plus or minus 20 feet assuming speed and sink rate are correct - no wind shears. Flares were accomplished with a single movement of the hand controller to the aft stop and holding it there through touchdown, though on some landings the control was inadvertantly moved from the stop prior to touchdown while putting in lateral control to compensate for roll during flare.

Two methods have been used by the program test pilots for flare initiation. Initially, the pilots flared on a predetermined altitude as indicated by a radar altimeter. This method was abandoned as it meant the pilots eyes were inside the cockpit at a critical time, and for the majority of flights the pilots looked outside and flared on an audio tone received at the correct flare altitude. This method has several advantages in that the pilot gains experience in perceiving the correct altitude and can compensate for audio failure and attitude changes due to shears or gust conditions.

Ideally, the pilot should be able to land consistently and safely with no cues. The program pilots feel that, given a nominal amount of training, they could visually determine the correct flare altitude within the allowable range and also recognize gust and shear conditions large enough to have a significant effect on landing.

Further landing investigation included in-flight flares initiated from multiple nose-down trim settings in an attempt to determine if the preflare now used for landing (11-in. nose-down pitch trim) can be reduced resulting in slower preflare speeds, lower preflare sink rates, lower and easier to judge flare altitude, and a more normal approach attitude.

Precision landings were demonstrated as no problem with the excellent system maneuverability, providing a pilot can reach a satisfactory low-key position.

Three flights were flown with the capsule ballasted to a two-man configuration and no significant difference was noted during flight or landing. Due to this short duration of flights, navigation consisted of simply checking the VOR and DME with local stations demonstrating satisfactory operation. Navigation with a two-man crew using standard operational navaids appears to present no problem and the use of Nike radar indicates radar vectoring would indeed be feasible.

The Gemini capsule port is considerably smaller than the canopy on the tow test vehicle; however, experience with the Gemini capsule and flying the Paraglider indicates to the program pilots that this would present no large problem during flight or landing with adequate training.

In summation, the Paraglider test program has shown the system to be stable, responsive, and very maneuverable, displaying adequate control in all in-flight maneuvers and landings. The system was flown and landed twelve times, and though landing data and several above-specification landings indicate that the system would require further landing tests to become operational, it can be said that concept is feasible for a landing system with which a trained astronaut could consistently make a safe land landing. The system has definite potential, and as a result of this basic flight program, a number of recommendations are made for further sophistication of the system.

These include:

1. Conduct further investigation of flare techniques, flare altitude, preflare pitch line settings and pitch cable rate on flare performances

2. Investigate the performance of the "T"-sail wing and other promising sophistications of the Paraglider wing

3. Investigate the ability of the pilot to land the capsule safely and consistently with no cues other than visual perception of the landing area

4. Establish a simulator program for pilot training on flare and landing

5. Higher capsule release altitudes should be obtained and investigated making navigation and radar control a prime test item

6. Investigate the open loop command system after first increasing the control centering and enlarging the electrical null band

7. Conduct an in-flight evaluation of Gemini port visibility for flight and landing

D. F. McCusker
Senior Engineering Test Pilot

CONCLUSIONS

The performance capability of the Paraglider wing and vehicle combination was demonstrated. Control response of the combination was excellent.

Capability of landing at a predetermined point was demonstrated.

The critical point in making a safe landing is the flare initiation point. This capability was sufficiently demonstrated in that a large majority of the flights attained a reasonable touchdown sink rate even though atmospheric conditions caused varying flight parameters at or near the time of flare initiation.

The flight control system, pneumatic actuator, and PCE, have shown the capability to operate for long periods of time under flight loads wit.. little or no trouble.

RECOMMENDATIONS

The Paraglider landing system development has progressed to a point in which there is complete confidence in attaining complete operational capability for spacecraft recovery.

To attain this operational capability, the following recommendations are made:

- Further testing using the full-scale test vehicle for deployment sequence and refinement
- A continuation of the recently completed tow test vehicle manned flights
- A program to refine and optimize the Paraglider wing configuration
- The development of a suitable simulator for pilot training.

PAGES 20 + 21 BLANK NOT FILMED